THE USE OF MOLLUSCAN SHELL BIOGEOCHEMISTRY IN ENVIRONMENTAL RECONSTRUCTION

LYNDA MITCHELL B.A.(HONS)

Thesis prepared for the degree of PhD
Department of Geology and Applied Geology
University of Glasgow

November 1994

ProQuest LLC.
789 East Eisenhower Parkway
P.O. Box 1346
Ann Arbor, MI 48106 – 1346

DECLARATION

The material presented in this thesis summarizes the results of three years of independent research carried out in the Department of Geology and Applied Geology of the University of Glasgow under the supervision of Dr Gordon B. Curry.
This thesis is entirely my own work and any published or unpublished results of other researchers have been given full acknowledgement in the text.

Lynda Mitchell

CO-AUTHORS DECLARATION

We certify that Lynda Mitchell has written this thesis and the papers contained within it herself and has received only help and advice of a general nature as would be expected in the course of normal PhD supervision.

Gordon B. Curry

Anthony E. Fallick

ABSTRACT

Stable carbon and oxygen isotope analysis of fast growing carbonate shells of fossil molluscs from the Plio-Pleistocene of New Zealand and Recent species from Scotland has revealed a high degree of isotopic variability and a strong correlation between $\delta^{13}C$ and $\delta^{18}O$ in each case. This phenomenon may be due to kinetic isotope effects which are inherent in fast growing shells or areas of shell. If this is the case then equilibrium isotope partitioning may not have had time to occur before the completion of calcite precipitation. Kinetic effects would favour the lighter isotopes of both carbon and oxygen; it is therefore the highest $\delta^{13}C$ and $\delta^{18}O$ values that are most likely to reflect equilibrium with the environment. Very small carbonate particles often give particularly low $\delta^{13}C$ and $\delta^{18}O$ values. These results have implications for the use of isotopic data in environmental reconstruction based on fast growing shells and may also be applicable to other carbonate precipitating organisms.

Stable isotope analysis of a series of fossil and recent mollusc shells from interglacial shell beds near Wanganui, New Zealand, yielded interglacial palaeotemperatures spanning the past 3.6 million years. The results indicate a cooling of about 10°C at about 1 My from earlier warm interglacial temperatures (15-20°C) to cooler interglacial temperatures (5-10°C) which have lasted to the present. This event coincides with a positive excursion in the strontium isotope ratio of seawater indicating greater erosional input to the ocean and with a significant molluscan extinction event in New Zealand. These changes may all be associated with a well documented change in the dominant global climatic cycle from 41 ky periodicity to 100 ky periodicity which occurred at about this time.

Stable oxygen and carbon isotope profiles and intracrystalline amino acid profiles (free and total) were determined for the New Zealand giant Pliocene oyster *Crassostrea ingens* by sampling annual growth increments along a sagittal section. These profiles reflect both ontogenetic and environmental change over the life-time of the oyster (approximately 20 years). $\delta^{18}O$ increases gradually from the umbo towards the shell margin, levelling off about half way along the shell. The $\delta^{13}C$ profile shows an initial sharp increase at the umbo, and then gradually decreases towards the shell margin. The amino acid profile reveals a gradual decrease in

abundance from the umbo to the shell margin, indicative of a progressive increase in the relative amounts of inorganic carbonate to protein over the life of the oyster, that may also be a consequence of decreasing growth rate.

Amino acid analysis was carried out on intracrystalline organic material from fossil and recent mollusc shells from South Wanganui Basin, New Zealand, ranging in age from 3.6 My to Recent. The absolute abundance of amino acids is highly variable but shows a gradual decline through time due to diagenetic effects. The proportion of peptide-bound amino acids decreases with time, and there is a corresponding increase in free amino acids as proteins are broken down by natural hydrolysis. By 0.5 My, most amino acids are free, after which there is a general decrease in most individual amino acids, presumably because they decay or become incorporated into predominantly insoluble geopolymers. Alanine is a notable exception, increasing in older samples because it is a common by-product of the breakdown of other amino acids. Amino acid data from different species and from shell beds of different ages were compared using multivariate statistical techniques. The results indicate that, despite the effects of diagenesis, the original biochemical distinction between different groups of molluscs (i.e. different proteins within the shell) survives for at least 3.6 My, and may be detectable in older specimens provided sufficient original amino acids remain.

Individual intracrystalline amino acids from *Pecten maximus* shells from the west coast of Scotland were separated by hplc (high pressure liquid chromatography) for carbon isotope analysis. The aim was to recover individual amino acids that had not been derivatized. However, the results do not show good separation at high sensitivity. Glycine in particular is spread across the whole range of retention times and is mixed with many of the other amino acids. Many of the peaks overlap. Some amino acids show two or more peaks. Separation of underivatized amino acids by hplc can therefore be problematical.
Carbon isotope analysis of bacterially produced standard amino acid samples shows significant variation in $\delta^{13}C$ between different individual amino acids. This may reflect different environments of production or may reflect biological fractionation effects.

CONTENTS

Chapter 1 Introduction

1.1 Format of Thesis 1
1.2 Molluscs as Environmental Indicators 3
1.3 Biomineralization in Mollusc Shells 4
1.4 Intercrystalline and Intracrystalline Organic Matter 5
1.5 Types of Intracrystalline Biomolecules 5
1.6 Proteins, Peptides and Amino Acids 6

Chapter 2 The Geology of South Wanganui Basin, New Zealand

2.1 Introduction 11
2.2 The Waitotaran Stage 13
2.3 The Nukumaruan Stage 15
2.4 The Castlecliffian Stage 16
2.5 The Haweran Stage 19

Chapter 3 Methods

3.1 Selection and Preparation of Shells 21
3.1.1 Selection of Specimens 21
3.1.2 Cleaning the Shells 21
3.2 Preparation of Carbonate Samples 23
3.2.1 Producing powdered carbonate samples 23
3.2.2 Separating different sized powder fractions 23
3.2.3 Removing intercrystalline organic matter 24
3.3 Extraction of Intracrystalline Biomolecules 25
3.3.1 Releasing the intracrystalline biomolecules 25
3.3.2 Removal of insoluble residues 27
3.3.3 Filtration and concentration 27
3.4 Separation of amino acids by hplc 28
3.4.1 Protein and peptide hydrolysis 28
3.4.2 The hplc system 28
3.5 Amino Acid Analysis 31

3.6 Stable Isotope Analysis 32
3.6.1 Introduction 32
3.6.2 $\delta^{13}C$ and $\delta^{18}O$ of Shell Carbonates 33
3.6.3 $\delta^{13}C$ of Intracrystalline Biomolecules 34

Chapter 4 Stable Carbon and Oxygen Isotope Compositions of Mollusc Shells from Britain and New Zealand

4.1 Abstract 35
4.2 Introduction 35
4.3 Methods 37
4.4 Results 40
4.5 Discussion 47
4.6 Conclusions 51
4.7 Appendix: Data Table 54

Chapter 5 Evidence for a Pleistocene Interglacial Cooling (~1 My) from Molluscan Faunas of New Zealand

5.1 Abstract 56
5.2 Introduction 56
5.3 Method 58
5.4 Results and Discussion 62
5.5 Conclusions 68
5.6 Appendices: Data Tables and Species Lists 69

Chapter 6 Stable Isotope and Amino Acid Profiles of the New Zealand Giant Pliocene Oyster *Crassostrea ingens*

6.1 Abstract 85
6.2 Introduction 86
6.3 Method 87
6.3.1 Collection and Sampling Techniques 87
6.3.2 Stable Oxygen and Carbon Analysis 87
6.3.3 Amino Acid Analysis 89

6.4 Results 90
6.4.1 Stable Isotope Profiles 90
6.4.2 Amino Acid Profiles 90
6.5 Discussion 103
6.6 Conclusions 108
6.7 Appendix: Data Tables 109

Chapter 7 Diagenesis and Survival of Intracrystalline Amino Acids in Fossil and Recent Mollusc Shells from Britain and New Zealand

7.1 Abstract 115
7.2 Introduction 116
7.3 Method 117
7.4 Changes in Amino Acid Compositions through Time 121
7.5 Taxonomic Implications 129
7.6 Conclusions 137
7.7 Appendix: Data Tables 138

Chapter 8 Separation of Individual Amino Acids for Stable Carbon Isotope Analysis

8.1 Abstract 144
8.2 Introduction 144
8.3 Method 146
8.4 Results 148
8.5 Discussion 151
8.6 Conclusions 152

Chapter 9 Discussion and Conclusions

9.1 Summary of results 154
9.2 Suggestions for further work 156

ACKNOWLEDGEMENTS

This project was funded by NERC grant GT4/91/GS/49 and the Department of Geology and Applied Geology, University of Glasgow, and was completed under the supervision of Dr G. B. Curry. I would also like to thank Dr A. E. Fallick at the Stable Isotope Laboratory, Scottish Universities Research and Reactor Centre, East Kilbride, for his considerable help and advice. Dr Maggie Cusack and Dr Ken Johnson gave advice on biochemistry and statistical taxonomy.

The technical staff at the Department particularly R. Morrison, S. Miller, D. Turner, D. McLean, M. McLeod and J. Kavenagh and also the technical staff at SURRC were of invaluable assistance throughout the project. Dr A. Ansell from Oban Marine Laboratory provided specimens collected from the west coast of Scotland.

In New Zealand, I would like to thank Prof R. Sibson, Prof. D. Campbell and Dr D. Lee at Otago University Geology Department in Dunedin, Dr K. Probert at Portobello Marine Lab and Dr A. Beu at DSIR Wellington for help and advice during fieldwork. I would particularly like to thank Dr H. Campbell for his generosity and hosptitality while I was in New Zealand.

Finally I would like to thank my friends in the Geology Department particularly Andy, Dave, Sarah, Robbie and Mark without all of whom life would not have been nearly so much fun.

CHAPTER 1

INTRODUCTION

1.1 Format of Thesis

The thesis consists mainly of five papers forming chapters 4 through to 8. Introducing these, this first chapter is followed by two other short chapters. Chapter 2 describes the geology of the field area from which the shell samples were collected during two field excursions to New Zealand in late 1991 and early 1993. The stratigraphy of the shell beds is considered in some detail as it is important to know the age of each shell sample as accurately as possible. Chapter 3 is a detailed account of all the practical methods used during the course of the research.

Chapter 4 investigates the use of stable carbon and oxygen isotope analysis of shell carbonates for environmental reconstruction by measuring the variation in $\delta^{13}C$ and $\delta^{18}O$ within single specimens of several large mollusc shell species. The variation within each specimen is found to be significant and a strong correlation is found between $\delta^{13}C$ and $\delta^{18}O$ which may be due to kinetic isotope effects inherent in fast growing shells. Care must be taken, therefore, in using stable isotope analysis of fast growing carbonates for environmental reconstruction. This chapter has been accepted for publication by the journal *Palaeogeography, Palaeoclimatology, Palaeoecology.*

In chapter 5, stable oxygen isotope ratios from a series of fossil and recent shell samples from interglacial shell beds in a sequence of shallow marine sediments from near Wanganui, New Zealand, yielded interglacial palaeotemperatures spanning the past 3.6 million years. A significant cooling of about 10°C is found at about 1 My which may be related to a well documented change in the dominant climatic cycle from 41ky to 100ky. A study of the molluscan assemblages from each shellbed also reveals a significant molluscan extinction event which occurs simultaneously with the change in temperature at about 1 My. An altered version of this chapter is to be submitted to the journal *Geology* or *Nature.*

Chapter 6 investigates both the stable isotope and intracrystalline amino acid profiles of a single large specimen of the New Zealand giant Pliocene oyster *Crassostrea ingens*. The carbon, oxygen and amino acid profiles are compared and are related to both ontogenetic and environmental changes over the life time of the oyster (about 20 years). Changes over this time scale are mostly attributed to effects caused by the change in growth rate from a rapidly growing juvenile to a slow growing, sexually mature adult. This chapter has been submitted for publication to the journal *Lethaia* and is at present in review.

In Chapter 7 the intracrystalline amino acid contents of a series of whole shell samples from a variety of species of various ages between 3.6 My and the present are investigated and the results related to amino acid diagenesis reactions, the burial environment and taxonomy. The results show that most intracrystalline proteins are hydrolysed within the first 0.5 My of burial. Most individual amino acids show a gradual decline as they break down to other compounds. There is an increase in alanine, a common reaction product of other amino acid reactions. It is found that diagenesis reactions are similar in all samples and therefore taxonomic groupings obtained from the multivariate statistical analysis of intracrystalline amino acid assemblages are relatively unaffected as long as there is enough original amino acid remaining to give a taxonomic signal. This chapter has been submitted to the journal *Palaeontology* for publication and is at present in review.

Chapter 8 concerns the separation of individual underivatized amino acids from shell carbonates for carbon isotope analysis, and considers the factors which control the carbon isotope signature of biogenic organic molecules, which may be environmentally or thermodynamically controlled. Standard bacterially produced amino acid samples are analysed and the results from different individual amino acids compared. This chapter leads on to further work which is beyond the scope of this thesis.

Finally, there is a concluding chapter in which all the results from the preceding five chapters are brought together, summarized and discussed, and suggestions are made for further work.

1.2 Molluscs as Environmental Indicators

Mollusc shells have been chosen as the main tool for environmental analysis in this study. Mollusc shells are ideal for use as environmental indicators: they cover a long time range, and they are very abundant in a range of habitats. Different mollusc shell assemblages occupy different types of habitat. Many are depth- or sediment-type specific. Often the position, orientation and state of preservation of fossil mollusc shells can yield valuable information about the environment in which they lived. Stable oxygen isotope analysis of the calcium carbonate shells can be used to compile detailed palaeotemperature data. Carbon isotope analysis can yeild information on primary productivity. Mollusc shells also contain abundant intracrystalline organic molecules. These have been preserved since crystallization of the shell carbonate and represent a valuable and as yet little studied source of potential environmental and taxonomic information.

Mollusc shells throughout the fossil record have been extensively used for environmental reconstruction, for example by comparison with similar recent species (eg. Beu, 1972) and by stable isotope analysis of the shell carbonate (eg Stevens and Vella, 1981; Muhs and Kyser, 1987; Rollins et al., 1987; Romanek and Grossman, 1989) or of preserved organic molecules (Risk, 1991). Stable oxygen isotope profiles of individual mollusc shells have been used to determine ecological and palaeoenvironmental information (Krantz et al., 1987), for age determination (Dare and Deith, 1991) and to determine changing shell growth characteristics through ontogeny (Romanek and Grossman, 1989). Single mollusc shell specimens have been seen to exhibit cycles in oxygen isotope values which correspond to annual and seasonal temperature cycles (Williams et al., 1981; Jones et al., 1983). An excellent correspondence has been seen between annual $\delta^{18}O$ cycles and annual internal growth increments (Krantz et al., 1987), showing that faster growth may occur during warm conditions. The shell of the mollusc contains a wealth of environmental information waiting to be uncovered. In order to understand how such information becomes incorporated into the shell, it is necessary to understand something about how the shell forms.

1.3 Biomineralization in Mollusc Shells

Biomineralization is the process whereby minerals are laid down or precipitated by living tissues. The number of different biominerals known to exist in nature may exceed sixty, distributed widely within all five kingdoms, and calcium minerals constitute about half of all the known biominerals (Lowenstam and Weiner, 1989).

The most common biomineral in mollusc shells is calcium carbonate. The mollusc shell consists mainly of a layered structure of calcium carbonate in the form of calcite, aragonite or both. However, molluscs are known to synthesize over twenty different biominerals for up to seventeen different functions (Lowenstam and Weiner, 1989). The biominerals include both crystalline materials and amorphous forms of substances such as fluorite, calcium carbonate, calcium phosphate, calcium pyrophosphate and silica. Obvious functions include protective shells, buoyancy devices, trap doors and egg shells.

The molluscan tissue primarily responsible for the shell formation is the mantle, a thin sheet lining the inner surface of the shell (fig 1.1). It is composed of two closely spaced epithelia separated by connective tissue. The cells of the outer mantle epithelium synthesize and secrete macromolecules including acidic glycoprotiens and proteoglycans. These macromolecules self-assemble to form a matrix or framework within and around which calcium carbonate is precipitated. The organic matrix macromolecules control crystal nucleation and growth by acting as substrates for calcium carbonate precipitation (Lowenstam and Weiner, 1989).

The cells of the outer mantle epithelium are also involved in the active pumping of chosen ions into the mineralizing compartment or extrapallial space. The fluid thus produced within the extrapallial space is known as the extracytoplasmic calcifying fluid (ECF). The calcium carbonate of the shell is precipitated from calcium and carbonate ions in the ECF (Lowenstam and Weiner, 1989).

1.4 Intercrystalline and Intracrystalline Organic Matter

The mollusc shell has an typical organic content of 0.01-5% (Hare and Abelson 1965). The organic material is in the form of envelopes surrounding each calcium carbonate crystal (intercrystalline biomolecules) and also as a matrix permeating the crystals (intracrystalline biomolecules). The intercrystalline fraction may easily be lost, contaminated or replaced by molecules from permeating groundwaters or surrounding sediment through time. It is therefore unlikely that the original composition of intercrystalline organic matter will be preserved. The intracrystalline organic material, however, is trapped and will remain in a closed system until decrystallization (Curry et al., 1991b). If any reactions occur then the reaction products will remain.

1.5 Types of Intracrystalline Biomolecules

The intracrystalline organic matter in mollusc shells consists mainly of protein but it also contains small amounts of lipids, carbohydrates and other molecules (Lowenstam and Weiner, 1989). Similarly, brachiopod shells have been shown to contain abundant protein (Curry et al., 1991; Walton, 1992), also lipids (Curry et al., 1991), carbohydrates (Collins et al., 1991) and alcohols (Clegg, 1993). Protein, the most abundant type of intracrystalline biomolecule, is also the most complex and interesting due to its composition of chains of different amino acids, the sequence of which is determined by the unique genetic make-up of the individual organism. Analysis of intracrystalline biomolecules in this study will therefore concentrate solely on proteins, and their constituent peptides and amino acids.

1.6 Proteins, Peptides and Amino Acids

Proteins are large polymeric molecules consisting of chains of monomers, amino acids, linked by peptide bonds. The peptide bonds readily break down by hydrolysis reactions due to heat or pressure, breaking the proteins into smaller peptide molecules (shorter chains) or single amino acids (fig 1.2). Intracrystalline proteins in fossils are often partly or wholly disintegrated into single amino acids. Walton (1992) showed that in shells older than about 0.5 My, up to 80% of brachiopod intracrystalline amino acids were in the free state. It is therefore much easier and more useful to analyse bulk individual amino acids in fossils than to try to find and sequence a pristine protein.

There are some twenty commonly found proteinogenic amino acids which together form the building blocks of the proteins of all living species (fig 1.3). Commonly used three letter abbreviations for these amino acids are shown in table 1.1. Each amino acid contains a basic amino group and an acidic carboxyl group and thus may exhibit amphoteric properties. Amino acids may be classified as neutral, basic or acidic according to the number of amino and carboxyl groups they contain. Commonest are the neutral compounds which contain an equal number of amino and carboxyl groups (usually one of each).The basic or acidic compounds contain an extra amino or carboxyl group respectively. With the exception of glycine, amino acids contain a chiral centre and can exist in two optically active forms (enantiomers), L- amino acids and D- amino acids, which are mirror images of each other and will rotate a beam of plane polarized light in opposite directions. Amino acids produced in biological systems consist entirely of L- amino acids. Laboratory or non biological synthesis, however, usually produces optically inactive racemates (mixtures containing equal numbers of each enantiomer). Amino acids from biological systems can slowly revert to optically inactive racemates through time (Schroeder and Bada 1976). The rates of amino acid racemization reactions in fossil shells have been used for purposes of geochronology and amino acid stratigraphy (eg. Hare and Abelson, 1968; Belknap and Wehmiller, 1980; Pillans, 1983).

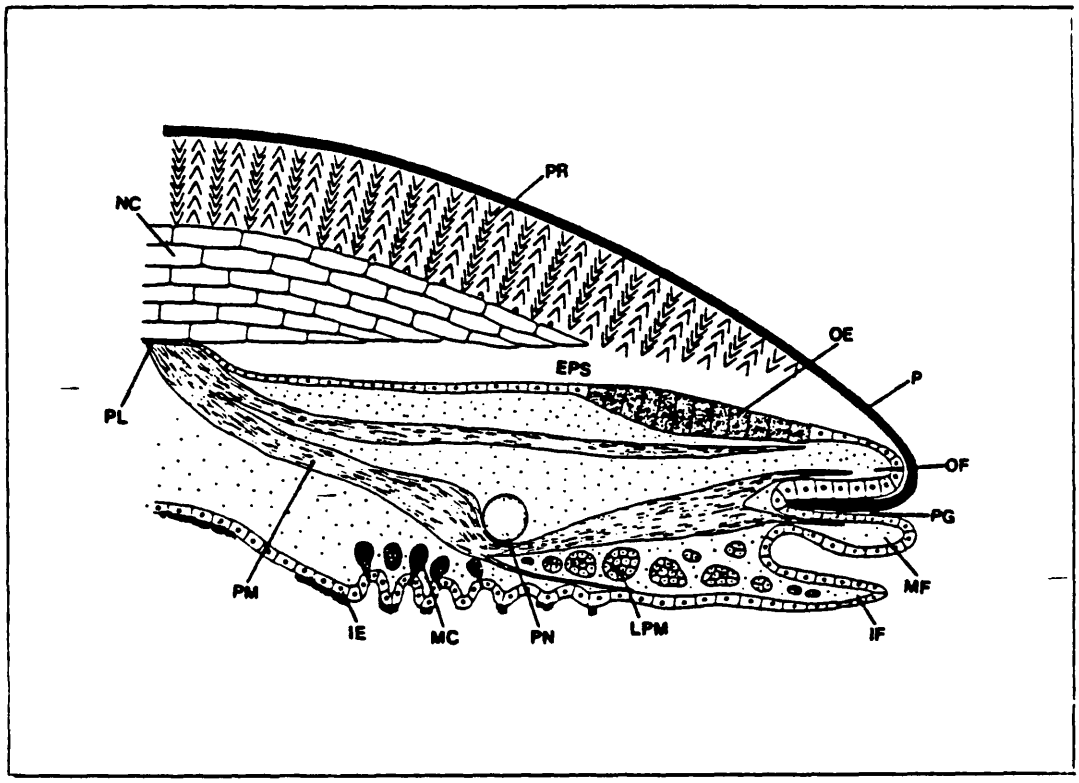

Figure 1.1 Radial section of the mantle edge of a bivalve to show the relationship between the shell and mantle. (Not drawn to scale.) EPS, extrapallial space; IE, inner epithelium; IF, inner fold; LPM, longitudinal pallial muscle; MC, mucous cell; MF, middle fold; NC, nacreous shell layer; OE, outer epithelium; OF, outer fold; P, periostracum; PG, periostracal groove; PL, pallial line; PM, pallial muscle; PN, pallial nerve; PR, prismatic shell layer. From Simkiss and Wilbur, 1979.

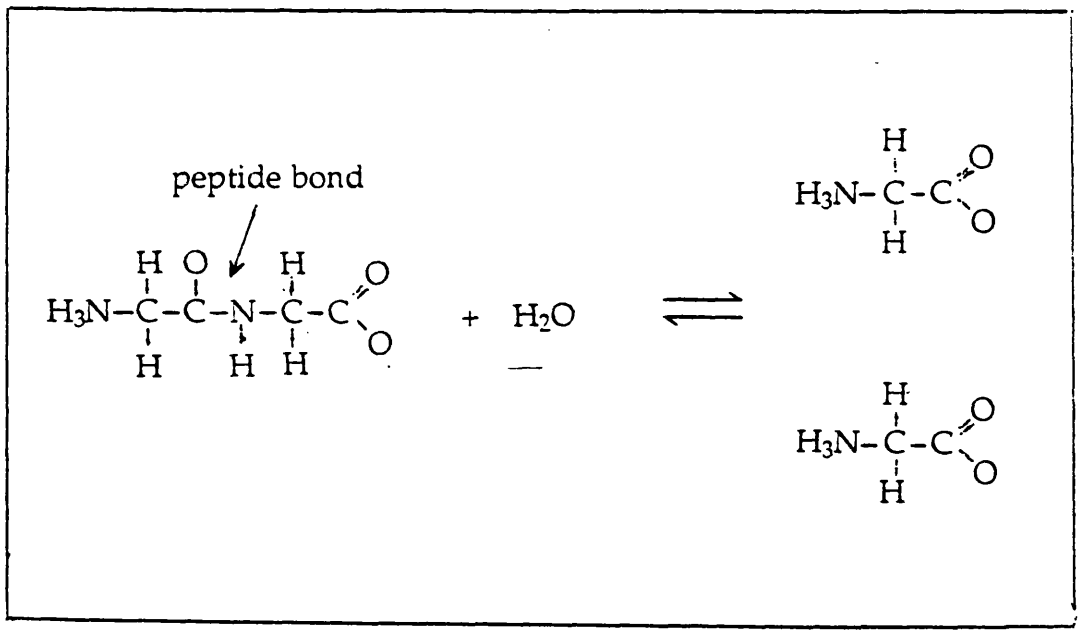

Fig. 1.2 Breaking of the peptide bond by hydrolysis

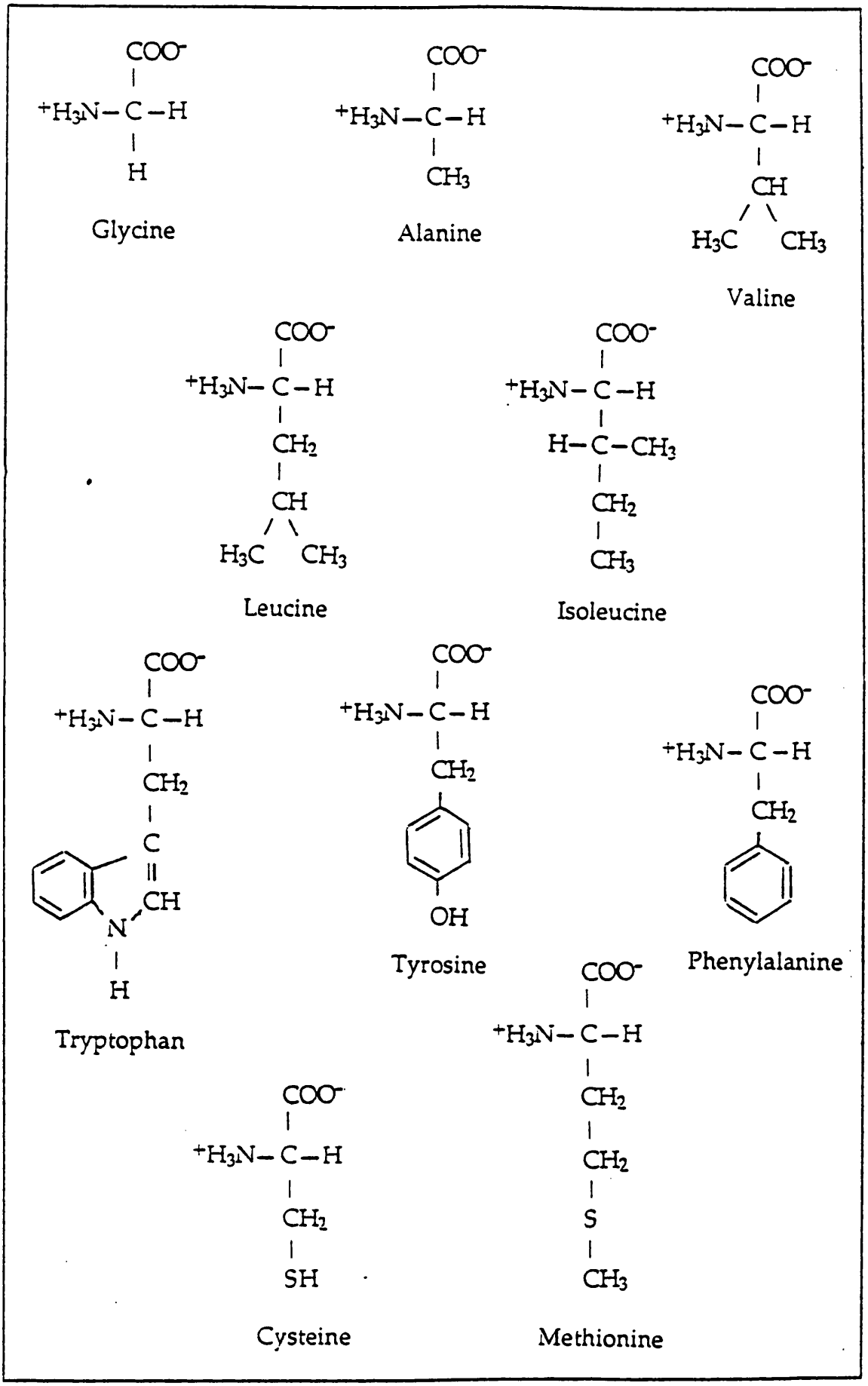

Fig. 1.3 20 Common Proteinogenic Amino Acids

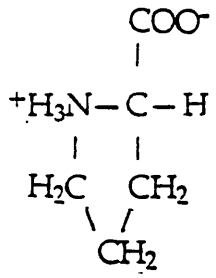

Proline

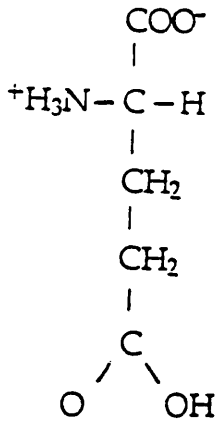

Glutamic Acid

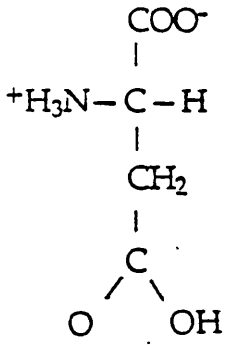

Aspartic Acid

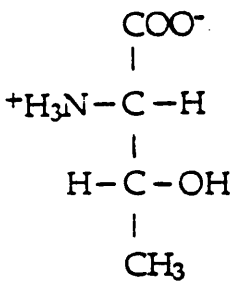

Threonine

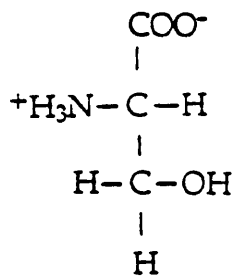

Serine

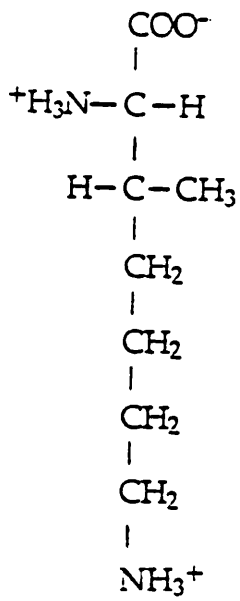

Lysine

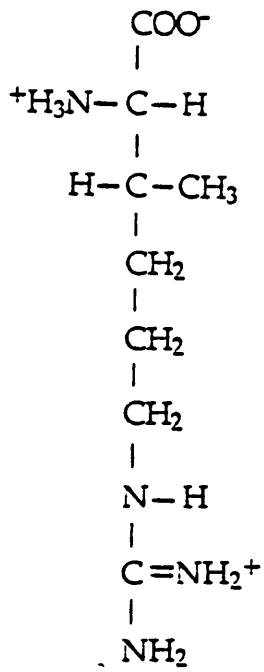

Arginine

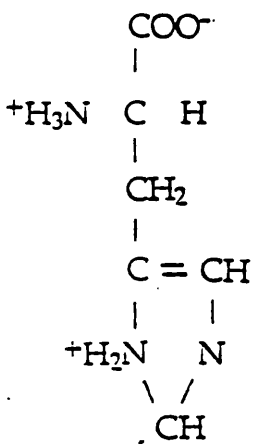

Histidine

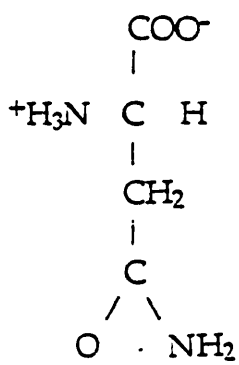

Asparagine

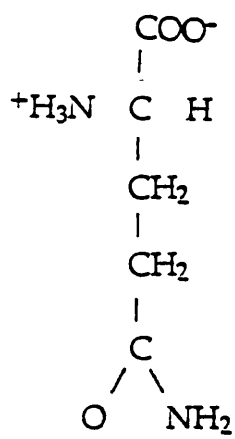

Glutamine

Amino acid	*Three-letter abbreviation*
Alanine	Ala
Arginine	Arg
Asparagine	Asn
Aspartic acid	Asp
Asparagine or aspartic acid	Asx
Cysteine	Cys
Glutamine	Gln
Glutamic acid	Glu
Glutamine or glutamic acid	Glx
Glycine	Gly
Histidine	His
Isoleucine	Ile
Leucine	Leu
Lysine	Lys
Methionine	Met
Phenylalanine	Phe
Proline	Pro
Serine	Ser
Threonine	Thr
Tryptophan	Trp
Tyrosine	Tyr
Valine	Val

Table 1.1 Three letter abbreviations for amino acids

CHAPTER 2

THE GEOLOGY OF SOUTH WANGANUI BASIN, NEW ZEALAND

2.1 Introduction

New Zealand offers some of the most complete and detailed sequences of late Pliocene to late Pleistocene marine rocks exposed on land anywhere in the world (Beu et al., 1987). The South Wanganui Basin, located in the south west of North Island (fig. 2.1), contains a sequence of shallow marine sediments spanning a period from about 3.6 million years ago to the present day (Fleming, 1953). Due to sea level fluctuations, most of the sequence was deposited during intergacials, forming a series of disconformity bounded cyclothems (Fleming, 1953; Abbott and Carter, 1991).
The basin is a half-graben containing up to 4000 m of sediments, and has developed by a combination of progressive subsidence and onlap to the south with emergence and offlap in the north (Anderton 1981). The sediments show gentle regional dips towards a depocentre 20 km south of Wanganui and are cut by NE-NNE trending faults generally downthrown towards the basin (Anderton, 1981). The sediments have been uplifted to the East due to activity on the Pacific/Indo-Australasian plate boundary resulting in excellent exposure in coastal cliffs, road and river cuttings. A geological map of the area showing the locations of fossil collection is shown in fig. 2.2. The fossil molluscan faunas are closely related to modern molluscan faunas occurring around the coasts of New Zealand, which were collected from the various locations shown in fig. 2.3.

Cenozoic sediments in New Zealand are often characterized by a long series of distinct molluscan faunas which correspond to recognized stages or groups of stages (Beu and Maxwell, 1990). The changing faunas are characterized by several factors, including the gradual stepwise extinction of warm water taxa (Beu 1987), the evolution of many long lineages and the arrival of new species as planktonic larvae in ocean currents (Beu and Maxwell, 1990). Much of the stratigraphy of the Wanganui Series was therefore originally based on

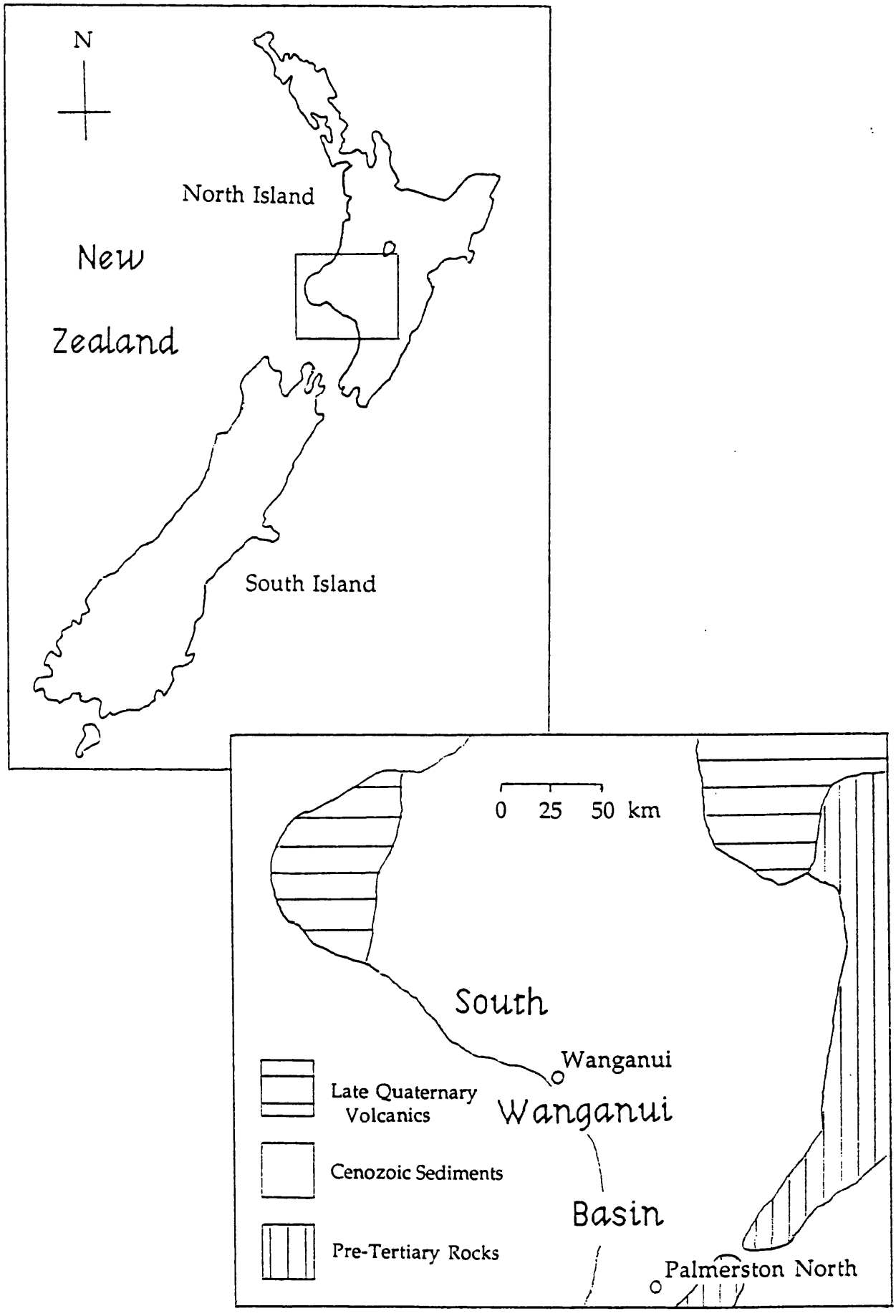

Fig. 2.1 Location Map of the South Wanganui Basin

molluscan assemblages (Fleming, 1953). The ages of many beds have now been accurately determined by a variety of other means, including fission-track dating of zircon and glass in tephras (Seward, 1976; Boellstorff and Te Punga, 1977; Pillans and Kohn, 1981; Pillans, 1990), amino acid racemization dating (Pillans and Kohn, 1981; Pillans, 1983), palaeomagnetism (Pillans and Wright, 1990; Turner and Kamp, 1990) and oxygen isotope analysis (Stevens and Vella, 1981). The stratigraphy of the South Wanganui Basin is summarized in fig. 2.4. The sedimentology was described in great detail by Fleming (1953) and will be only briefly described here.

2.2 The Waitotaran Stage

The Waipipian Substage

The lowest bed, the Pepper shell sand, is a cemented concretionary shelly sandstone overlain by the thick estuarine sand layers of the Rangikura sandstone. The succeeding Waipipi Formation includes a basal conglomerate and four major shell beds separated by blue-grey silt and sand. The overlying Waverley Formation is a thick layer of massive blue-grey silts and sand.
The Waipipian Substage is characterized by a distinctive warm water fauna. The occurrence of the warm water foraminifera *Amphistegina*, and warm water molluscs such as *Crassostrea*, *Maoricardium* and *Isognomon* in the Waipipian shellbeds suggests that the mean annual sea temperature at these times was not below 20°C (Beu, 1972).

The Mangapanian Substage

The basal Mangapani Shell Conglomerate is followed by the thick, barren Paparangi Sandstone. Coarser, looser sand with shellbed members forms the Makokako Sand. The Wilkies Shellbed is a thin, persistent shellbed, also with a warm water molluscan fauna. Above lie beds containing sand, muddy sand and shellbed members (Te Rimu Sand, Parihauhau and Te Rimu Shellbeds) with faunas similar to that of the Wilkies Shellbed (Fleming, 1953).

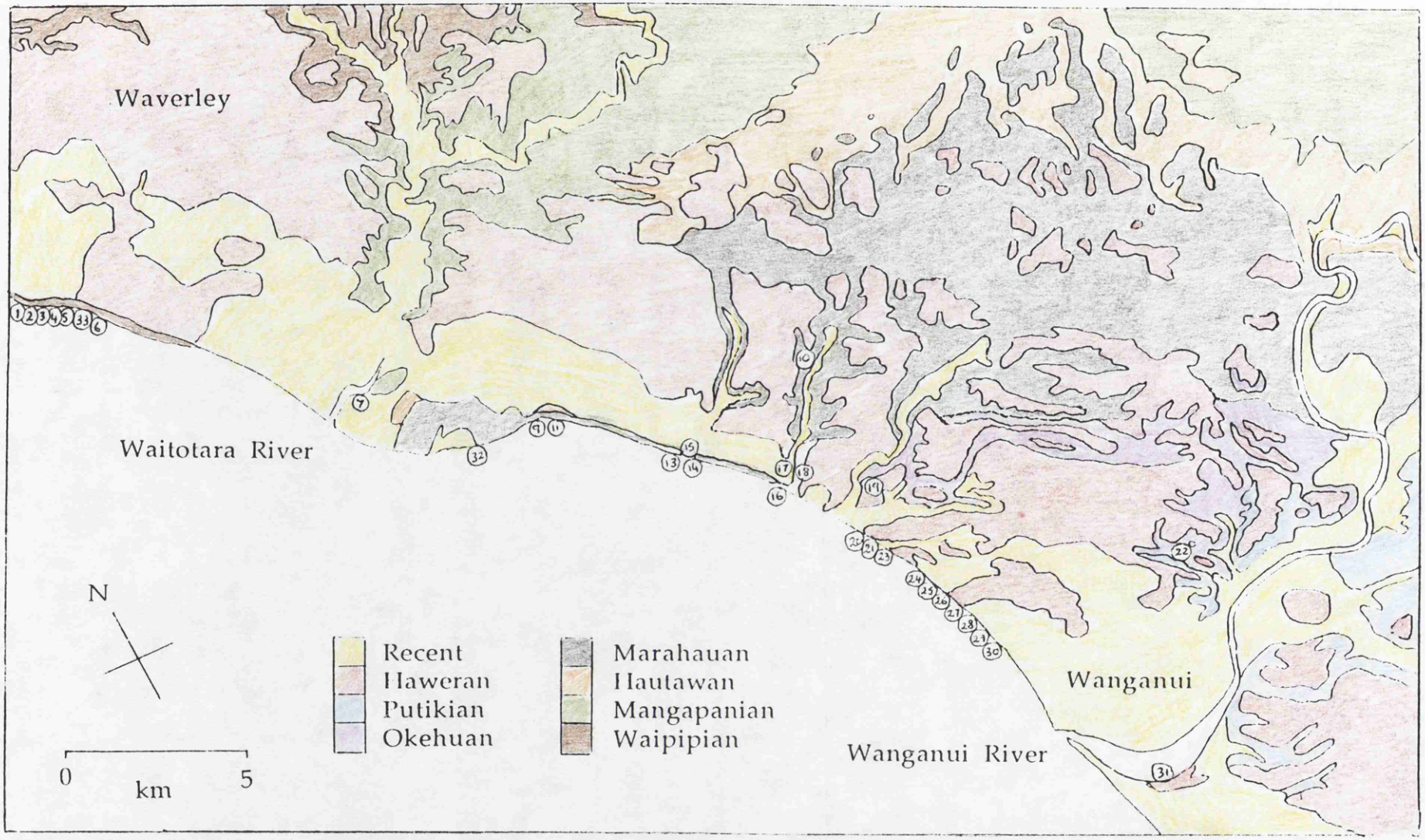

Fig. 2.2 Geological map of Wanganui (after Fleming, 1953)

Table 2.1 Grid references of fossil locations shown in fig. 2.2

LOCATION NO.	SHELLBED	GRID REF.	MAP*
1	Pepper Shell Sand	458 529	1
2	Rangikura Sandstone	460 527	1
3	Snapper Point Shellbed	466 542	1
4	Lower Waipipi Shellbed	471 524	1
5	Middle Waipipi Shellbed	475 523	1
6	Upper Waipipi Shellbed	483 520	1
7	Wilkie's Shellbed	556 498	2
8	Hautawa Shellbed	980 537	3
9	Nukumaru Limestone	625 482	2
10	Nukumaru Brown Sand	715 509	2
11	Nukumaru Brown Sand	628 483	2
12	Waipuru Shellbed	070 347	3
13	Pukekiwi Shell Sand	665 473	2
14	Mangahou Siltstone	670 472	2
15	Butler's Shell Conglomerate	667 473	2
16	Okehu Shell Grit	775 480	2
17	Okehu Shell Grit	707 457	2
18	Okehu Shell Grit	709 468	2
19	Kaimatira Pumice Sand	728 456	2
20	Lower Kai Iwi Siltstone	707 457	2
21	Omapu Shellbed	733 445	2
22	Kaikokapu Shell Grit	836 436	2
23	Kaikokapu Shell Grit	738 440	2
24	Kupe Formation	754 428	2
25	Upper Kai Iwi Siltstone	755 427	2
26	Tom's Conglomerate	760 424	2
27	Lower Castlecliff Shellbed	765 418	2
28	Tainui Shellbed	770 415	2
29	Shakespeare Cliff Sand	774 410	2
30	Upper Castlecliff Shellbed	775 408	2
31	Landguard Sand	833 368	2
32	Rapanui Formation	595 475	2
33	Rapanui Formation	480 521	1

*Maps

1. NZ Department of Survey and Land Information Sheet 260-Q22: Patea
2. NZ Department of Survey and Land Information Sheet 260-R22: Wanganui
3. NZ Department of Survey and Land Information Sheet 260-S22: Whangaehu

2.3 The Nukumaruan Stage

The Hautawan Substage

The basal formation of the Nukumaruan is by definition the Hautawa Shellbed (Fleming 1953). This muddy shelly sandstone contains both Mangapanian and Nukumaruan index fossils and from these is inferred to be about 2.4 My old (Beu et al., 1987). This shellbed shows the first faunal evidence for a significant cooling of the sea with the appearance of the subantarctic taxa *Chlamys patagonica delicatula* and *Jacquinotia edwardsii* (Fleming, 1944; Beu et al., 1977; Beu, 1984) coinciding with an increase in glaciation in the Northern Hemisphere.
Above this, the Kuranui Limestone is a coarse, pebbly, current bedded detrital shell limestone of variable thickness, overlain by the Tuha Sand, a sparsely fossiliferous blue-grey marine muddy sandstone.

The Marahauan Substage

Ash from within the loose, rusty, pebbly Ohingaiti Sand at the base of the Marahauan Substage yields a fission track date of 1.50 my (Pillans 1990). This is in good agreement with the estimate of Seward (1974) of 1.55 my for the base of the Marahauan Substage based on extrapolation from beds in the adjacent Rangitikei Valley sequence. Above the Ohingaiti Sand is the Nukumaru Limestone (Plate 2.1), a series of pebbly, shelly, coquina limestone layers, sometimes concretionary, indispersed by sand. This is overlain by the Mangamako Shellbed, at the base of the fossiliferous Nukumaru Brown Sand (Plate 2.3), and the Waipuru Shellbed, towards its top. The molluscan faunas from these beds indicate a recovery of sea temperatures after the cool Hautawan (Fleming, 1953).

At the top of the Nukumaruan, forming the upper part of the Marahauan Substage, the mostly non-marine Maxwell Group contains a very sparse fauna. The Tewkesbury Formation consists of blue-grey estuarine sand, silt and clay with occasional lenticular shellbeds. The molluscan faunas within the Tewkesbury Formation

are similar to those in the Nukumaruan Brown Sand. This is overlain by the Lower Maxwell Formation, a thick sequence of non-marine beds with lignite seams and soil bands. Ash within the Mangahou Siltstone, an estuarine tidal flat deposit, near the top of the Maxwell Group yields a fission track age of 1.26 my (Pillans, 1990). This is overlain by another non-marine sequence, the Upper Maxwell Formation (Fleming, 1953).

2.4 The Castlecliffian Stage

Okehuan Substage

The base of the Castlecliffian (Okehuan Substage) is marked by the base-Jaramillo magnetic reversal at 1.07 my (Turner and Kamp, 1990). The basal bed, the Butler's Shell Conglomerate, lies unconformably on the underlying Maxwell Group and consists of a coarse shallow water deposit of rolled and broken shells representing a return to marine conditions. This grades laterally into the Makirikiri Tuff, a white rhyolitic silt. Fission-track dating of pumice and ash in the Makirikiri Tuff have yielded ages of 1.06 and 1.04 my (Seward 1974).
The overlying Lower Okehu Siltstone is a thick layer of massive blue-grey silt with a prominent basal shell conglomerate. The top-Jaramillo magnetic reversal (0.99 my, Shackleton et al., 1990) occurs at the next bed, the Okehu Shell Grit (Turner and Kamp, 1990), a thin, coarse shell grit. This is succeeded by the Upper Okehu Siltstone, another thick sequence of blue-grey silt.
The overlying Kaimatira Pumice Sand Formation, a shelly sand with abundant pumice and tuff (Plate 2.4), contains the base Brunhes magnetic reversal (Turner and Kamp, 1990) dated at 0.78 my (Shackleton et al., 1990). Above this lie the Lower Kai-Iwi Siltstone, the Omapu Shellbed, the Lower Westmere Siltstone, the Kaikokapu Shell Grit and the Upper Westmere Siltstone. All these early Castlecliffian beds are characterized by a somewhat impoverished molluscan fauna after the extinction of many Nukumaruan genera (Fleming, 1953).

Pukikian Substage

The Kupe Formation at the base of the Putikian Substage consists of muddy sandstone and siltstone containing plentiful well preserved mollusc shells. Molluscan faunas had by now rediversified due partly to the arrival of new immigrant genera that may indicate a slight warming of the water to subtropical temperatures (Fleming, 1953).
The LAD (last appearance datum) of the calcareous nannofossil *Pseudoemiliana lacunosa* occurs in the overlying Upper Kai-Iwi Siltstone, a fine grained blue muddy siltstone (Beu and Edwards, 1984). This became extinct during isotope stage 12 in the deep sea 460 ka ago (Gartner, 1977; Thierstein et al., 1977). There is however, reason to suspect that the extinction may have occurred earlier in certain parts of the south west Pacific (Abbott and Carter, 1991). The Upper Kai-Iwi Siltstone is therefore at least 460 ka old.

The beds in the upper part of the Castlecliffian are characterized by a series of different molluscan faunas with different populations of the bivalve *Pecten* (Fleming, 1953). The basal conglomerate (Tom's Conglomerate) of the Seafield Sand, lies unconformably on the underlying Upper Kai-Iwi Siltstone. This is followed by the Lower Castlecliff Shellbed, a thin, persistent shelly muddy sandstone layer. Overlying this is the Pinnacle Sand, a sequence of interbedded sands and silty mudstones, and the Tainui Shellbed, a richly fossiliferous grey siltstone (Plate 2.2). Above this, the Shakespeare Cliff Siltstone, a massive blue-grey siltstone with scattered fossils of a quiet offshore environment, is followed by the Shakespeare Cliff Sand, a loose, current-bedded sand with lenticular shellbeds, representing an abrupt change back to shallow water. The overlying Upper Castlecliff Shellbed consists of a fine grained muddy sandstone containing abundant molluscs. Finally, the Karaka Siltstone is followed by the Mosstown Sand and the Putiki Shellbed, a shelly, muddy sandstone.

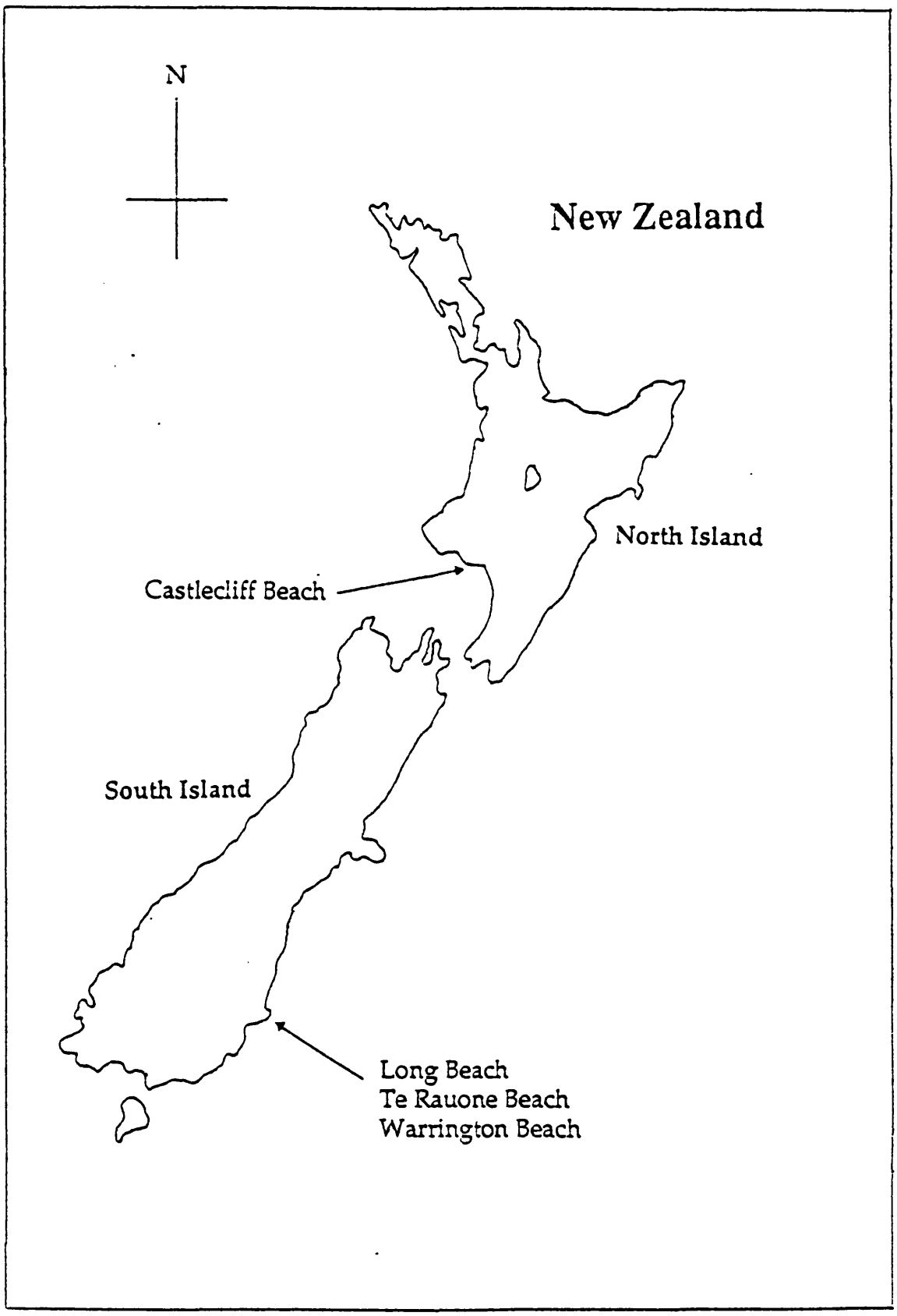

Fig. 2.3 Map showing locations of collection sites for recent molluscs

2.5 The Haweran Stage

Formerly a separate Series, the Haweran Stage was recognized as a new Stage in the Wanganui Series by Beu et al., 1987 on the basis of new correlations between marine sediments and terrace cover beds. The base of the Haweran Stage, the Landguard Formation, consists of interbedded micaceous sands, silts, shellbeds and pebble bands. It lies unconformably on the Rangitawa pumice at the top of the Castlecliffian Stage which yeilds fission track ages of around 370 ka (Seward, 1976; Boellstorff and Te Punga, 1977; Pillans and Kohn, 1981). This is therefore a maximum age for the base of the Hawera Stage. The beds above the Landguard Formation consist mainly of covering beds on marine and fluvial terraces. The youngest of the fossil shell beds in the sequence is the Rapanui Marine Sand. Samples from the Rapanui lignite which directly overlies this, yield an amino acid racemization date of 110 ka (Pillans, 1990). Based on pollen evidence, the lignite accumulated over a period of 10 000 years (Bussel 1988a). Pillans (1983) attributed the incision of the Rapanui wave cut platform, directly below the Rapanui Marine Sand, to a well documented high sea level event between 120 000 and 140 000 years ago. The Rapanui Marine Sand is therefore around 120 000 years old.

Stage	Substage	Formation	Thickness	Age (m.y.)
Haweran		Alluvium	?	
		Rapanui Formation	15m	0.12 - 0.14
		Brunswick Formation	20m	0.2 - 0.235
		Kaiatea Formation	50m	
		Landguard Formation	15m	
Castlecliffian	Putikian	Putiki Shellbed	1m	0.37 ± 0.05
		Mosstown Sand	20m	
		Karaka Siltstone	10m	
		Upper Castlecliff Shellbed	2m	
		Shakespeare Cliff Sand	12m	
		Shakespeare Cliff Siltstone	10m	
		Tainui Shellbed	6m	
		Pinnacle Sand	10m	
		Lower Castlecliff Shellbed	1m	
		Seafield Sand	20m	
		Upper Kai Iwi Siltstone	9m	
		Kupe Formation	5m	
	Okehuan	Upper Westmere Siltstone	18m	
		Kaikokapu Formation	15cm	
		Lower Westmere Siltstone	10m	
		Ophiomorpha Sand	1m	
		Omapu Shellbed	3m	
		Lower Kai Iwi Siltstone	20m	
		Kaimatira Pumice Sand	15m	0.78
		Upper Okehu Siltstone	6m	
		Okehu Shell Grit	8m	0.99
		Lower Okehu Siltstone	20m	
		Mowhanau Formation	1m	
		Ototoka Siltstone	3m	
		Butler's Shell Conglomerate	10m	1.07
Nukumaruan	Marahauan	Upper Maxwell Formation	30m	
		Mangahou Siltstone	5m	1.26 ± 0.17
		Middle Maxwell Formation	10m	
		Pukekiwi Shell Sand	8m	
		Lower Maxwell Formation	25m	
		Tewkesbury Formation	30m	
		Waipuru Shellbed	4m	
		Nukumaru Brown Sand	30m	
		Mangamako Shellbed	15m	
		Nukumaru Limestone	180m	
		Ohingaiti Sand	10m	1.5 ± 0.21
	Hautawan	Undifferentiated Formations	60m	
		Kuranui Limestone	7m	
		Hautawa Shellbed	3m	2.4
Waitotaran	Mangapanian	Te Rama Shellbed	} 80m	
		Parihauhau Shellbed		
		Te Rimu Sand		
		Wilkies Shellbed	10m	
		Makokako Sand	70m	
		Mangaweka Mudstone	} 250m	
		Paparangi Sandstone		
		Mangapani Shell Conglomerate		
	Waipipian	Waverley Formation	70m	
		Upper Waipipi Shellbed	} 55m	
		Middle Waipipi Shellbed		
		Lower Waipipi Shellbed		
		Snapper Point Shellbed		
		Rangikura Sandstone	50m	
		Pepper Shell Sand	?	

Fig 2.4 Stratigraphy of the Wanganui Series. Approximate thicknesses after Fleming (1953) and Abbott and Carter (1991). Dates from Pillans (1990), Beu et al. (1987) and Turner and Kamp (1990).

Plate 2.1 Nukumaru Limestone, coastal section

Plate 2.2 Tainui Shellbed, coastal section

Plate 2.3 Nukumaru Brown Sand, Great Northwestern Road

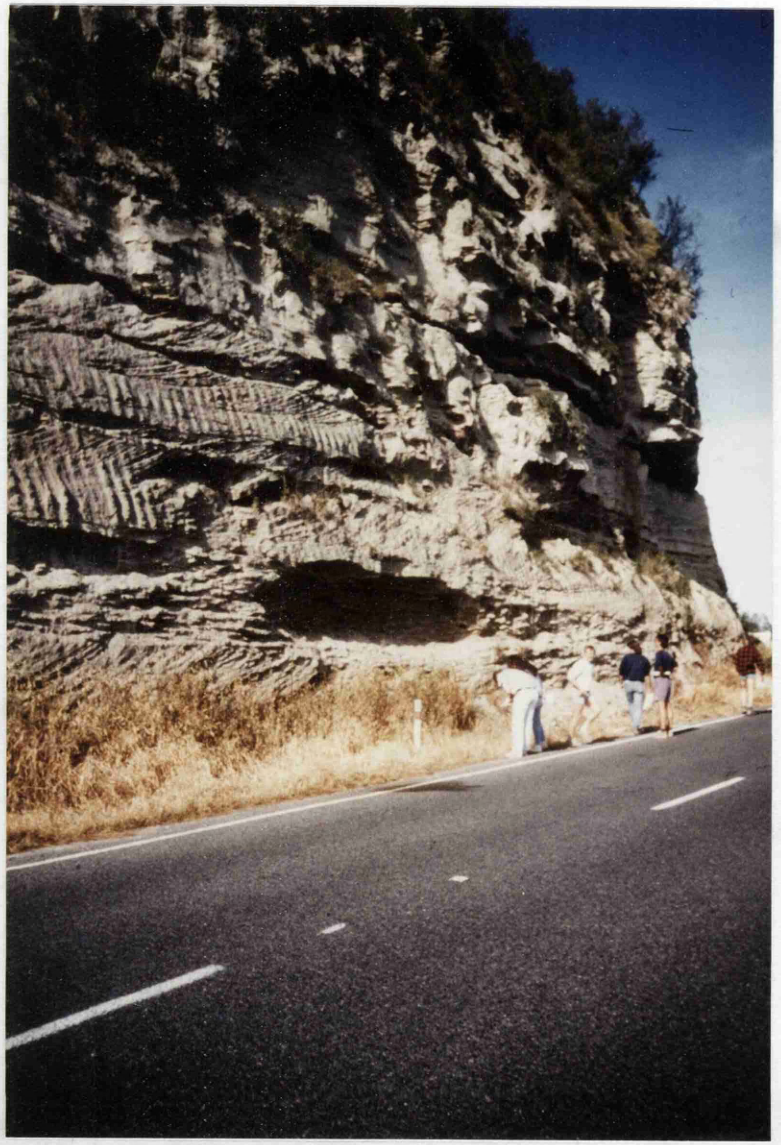

Plate 2.4 Kaimatira Pumice Sand, Wanganui River Road

CHAPTER 3: METHODS

3.1 Selection and Preparation of Shells

3.1.1 Selection of specimens

Intracrystalline biomolecules are obtained from within the crystal matrix of the shell where they have been trapped, protected from interaction with the external environment, since the time of crystallization. It is therefore important to ensure that the crystals of the shell are preserved in their original state and that no recrystallization has occurred, as this could result in the loss or replacement of some or all of the intracrystalline biomolecules present in the shell. Calcium carbonate recrystallization could also result in isotopic re-setting thus changing the isotopic signature of the shell from its original value.
Therefore, during collection, only the best preserved specimens were selected for analysis. Heavily encrusted or bored specimens were discarded. Specimens of each species were examined by SEM (scanning electron microscope) for signs of damage or alteration (appendix 3.1).
Mollusc shells may consist of the relatively stable form of calcium carbonate, low magnesium calcite, or of the less stable form, aragonite, or a mixture of both. Shells made of aragonite may revert to low magnesium calcite over time, a process involving recrystallization and the loss of biomolecules. The calcium carbonate composition of each species was determined using XRD (X Ray diffraction) analysis (fig. 3.1). The composition of fossil species was where possible compared to the composition of living relatives. Where possible the fossil species were selected which were composed mostly or entirely of stable low magnesium calcite.

3.1.2 Cleaning the shells

The shell surface was scrubbed and scraped to remove sediment and algae. The periostracum and ligament, if present, were removed. The surface layer of the shell, if very dirty, was etched away using 2N hydrochloric acid. The shells were washed in water, then soaked in an aqueous solution of bleach for at least 2 hours to remove any remaining organic molecules from the surface by oxidation. Finally the shells were washed thoroughly in clean Milli Ro water and left to air dry.

Fig. 3.1 XRD traces showing a calcium carbonate composition of
a) calcite and b) aragonite

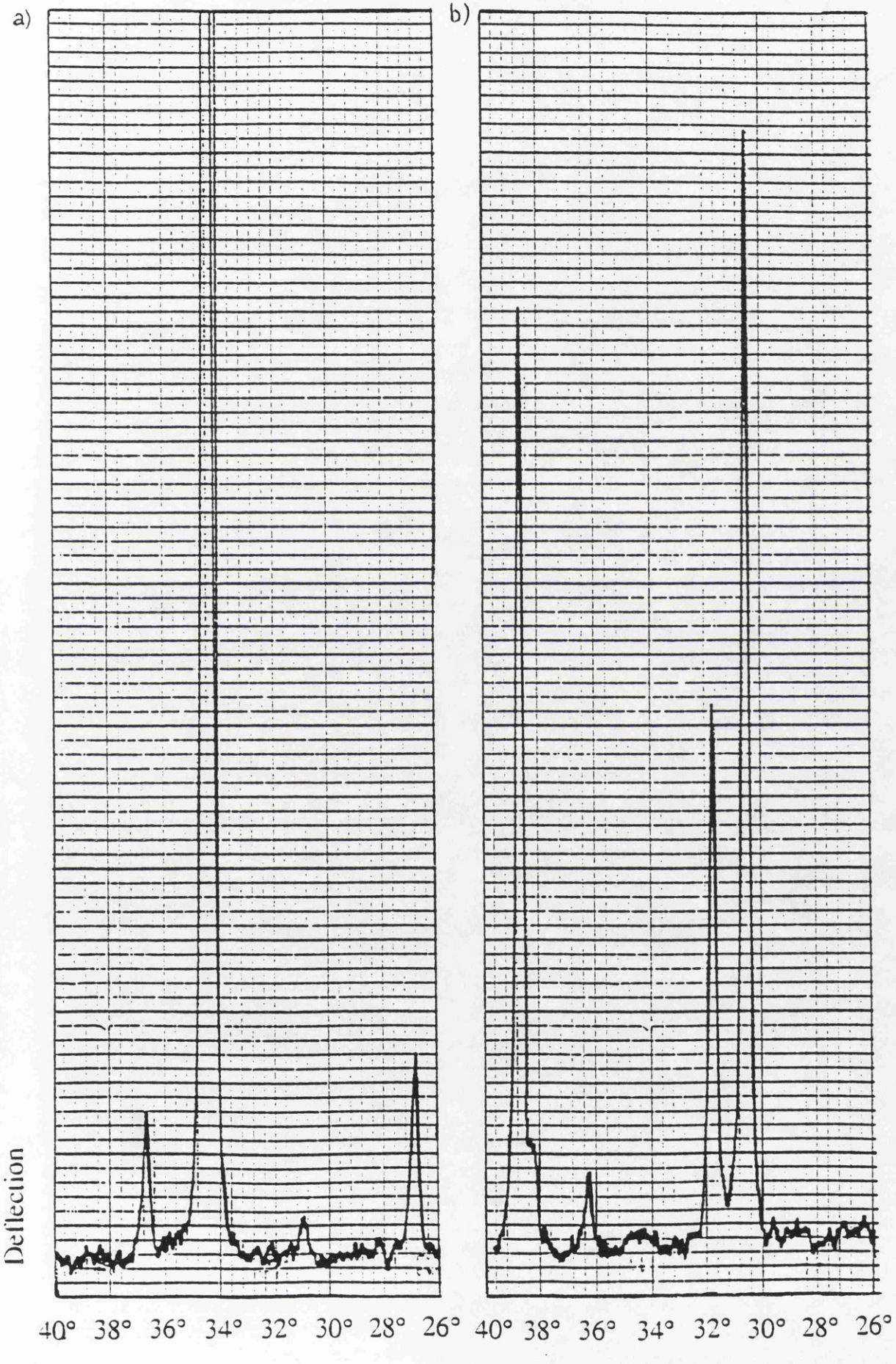

3.2 Preparation of Carbonate Samples

3.2.1. Producing powdered carbonate samples

a) Tema and crushing machine

The shells were first smashed and crushed by hand, using a pestle and mortar for smaller specimens and a large hammer for the more robust species. Each sample consisted of a well preserved shell or number of shells of the same species, age and locality. Particularly large samples were needed for the extraction of intracrystalline biomolecules for separation, and up to a kilogram of shell material was processed in these cases. The crushed samples were ground to a fine powder by an agate Tema or a metal drum crushing machine.

b) Drilled samples

Small carbonate samples were obtained using a dentist's drill with a narrow rotating tip of diameter 0.5 or 1.0 mm. This method could be used to produce many small powdered carbonate samples relatively quickly. The sample size produced by this method was typically approximately 20 mg. These small samples were ideal for stable isotope analysis and for dissolution for amino acid analysis.

3.2.2. Separating different sized powder fractions

Following suggestions that the isotopic composition may be affected by particle size (Fritz and Fontes, 1966), some of the crushed carbonate from certain species was divided into ten different powder size fractions between 0 and 150 μm (table 3.1) for isotope analysis. Size fractions were separated using firstly a series of mesh sieves (Krumbein and Pettijohn, 1961; Folk, 1974; Buller and McManus, 1979). The finest particles below the smallest sieve mesh of 32 μm were then separated by means of sedimentation rates in water (Jackson, 1979).

Table 3.1: Carbonate powder size fractions for isotopic analysis

Fraction	Separation method	Particle size (μm)
1	sieve	125-150
2	sieve	106-125
3	sieve	90-106
4	sieve	75-90
5	sieve	63-75
6	sieve	32-63
7	sedimentation	15-32
8	sedimentation	10-15
9	sedimentation	5-10
10	sedimentation	< 5

3.2.3. Removing intercrystalline organic matter

a) bleaching

Large powdered carbonate samples were soaked in 10 % bleach solution for at least 12 hours to remove all intercrystalline organic molecules by oxidation. Bleach was then removed by repeated washing of the powdered samples in clean Milli Q water and centrifugation. Wet samples were frozen and lyopholized to a dry powder.

b) plasma ashing

Small carbonate samples for isotopic analysis which had not been treated in bleach were placed in a plasma asher for at least one hour in order to remove intercrystalline organic matter. This method, though much quicker and easier than bleaching, would not work for larger samples as it would require oxygen plasma penetrating the entire sample in order for the organic matter to be completely oxidised. Amino acid analysis (section 3.5) of samples processed by the two methods were compared to confirm that the results achieved were equivalent.

3.3 Extraction of Intracrystalline Biomolecules

3.3.1. Releasing the intracrystalline biomolecules

In order to release the intracrystalline biomolecules from the crystal matrix it is necessary to dissolve away the calcium carbonate within which they are trapped. Two different methods were tried as follows:

a) hydrochloric acid
Separation of the intracrystalline organic matter was first attempted by dissolving the calcium carbonate powder completely in 12N hydrochloric acid, thus quickly liberating the intracrystalline organic molecules into solution. The hydrochloric acid was removed by lyophilising in the presence of a solid NaOH trap in order to reduce the acidity. The concentrated hydrochloric acid was diluted with water several times during lyopholisation to ensure its complete removal. The resulting dry residue, however, consisted largely of a precipitate of calcium chloride, within which the organic molecules were buried. The total dry weight of organic matter therefore could not be measured unless the calcium chloride could be removed. This proved to be a problem as hydrolysis had resulted in the breakdown of the organic matter into small molecules which could not be removed from the calcium chloride by filtration.
A solution of 2N hydrochloric acid has been shown to leave protein molecules intact (Walton 1992). This can easily be verified by dissolving a recent sample of, for example, *Pecten maximus* in 2N HCl and analysing it using the amino acid analyser (section 3.5). Virtually no free amino acids are found (fig. 3.2), whereas if an identical sample is deliberately hydrolysed using 6N HCl, abundant proteinogenic amino acids are produced in the free state (fig. 3.3). If 2N HCl is used, therefore, the proteins are not hydrolysed and can be filtered and concentrated (section 3.3.3). However, it was found that the hydrochloric acid caused damage to the filtration system due to corrosion. The method was abandoned for large samples which required filtration but hydrochloric acid continued to be used extensively for the quick dissolution of small samples for amino acid analysis (section 3.5).

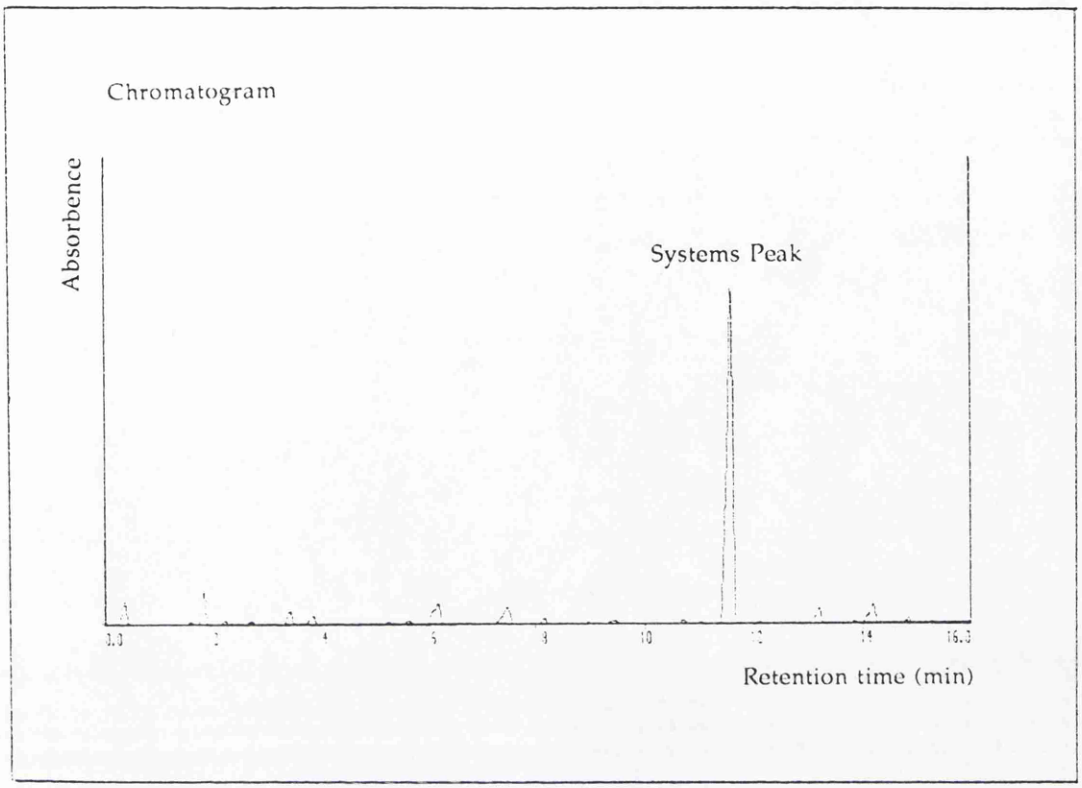

Fig. 3.2 Free amino acids from a recent *Pecten maximus* shell.

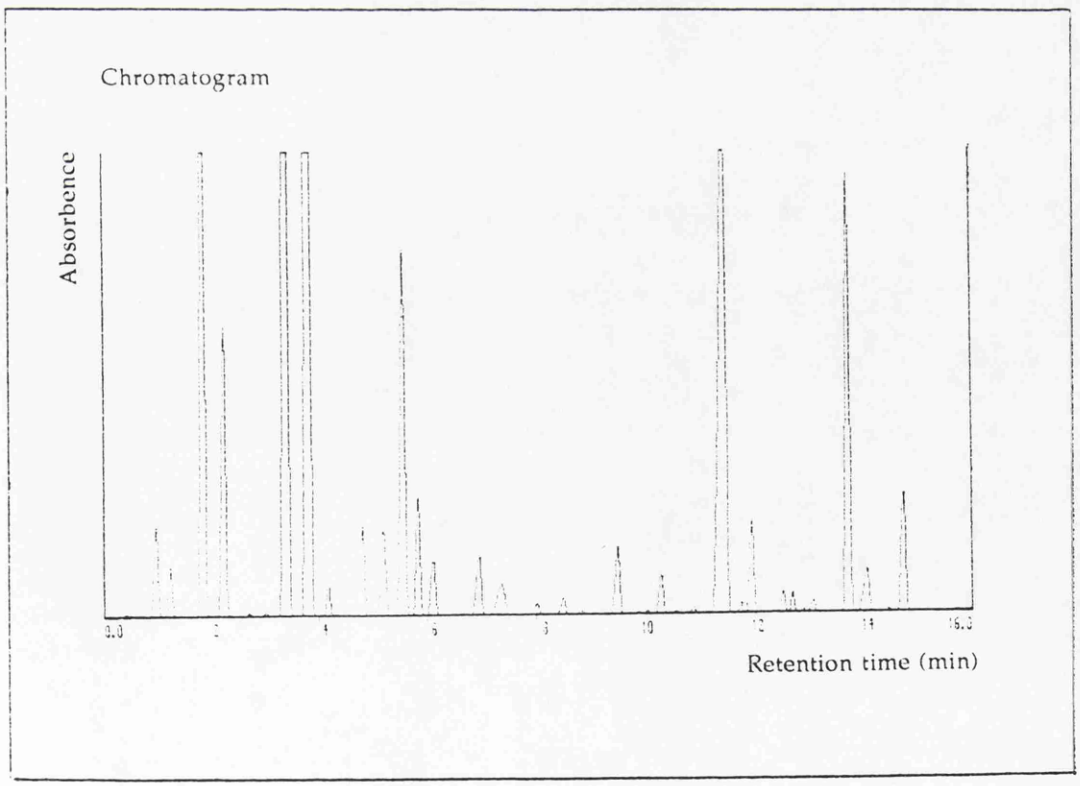

Fig. 3.3 Free amino acids from a recent *Pecten maximus* shell, after protein hydrolysis using 6N HCl

b) ethylene diamino tetra acetic acid (EDTA).
This method was used instead of using hydrochloric acid for dissolving large shell samples in order to obtain proteins by means of filtration. This method was used only for recent shell samples, the fossil shells having lost most or all of their proteins through natural hydrolysis (Walton 1992). Using this method, enough protein could be obtained to yield sufficient quantities of individual amino acids for subsequent geochemical analysis.
An aqueous solution of 20 % EDTA is prepared by adding EDTA slowly to a small amount of NaOH solution in clean Milli Q water. When the EDTA stops dissolving more water is added (and a little more NaOH may be necessary). The EDTA may take several days of stirring to dissolve completely. The resulting EDTA solution (pH 8) was used to dissolve the powdered shell by chelation of the calcium ions at a ratio of 23 ml/gram. The powdered shell dissolves slowly and may take several days of constant stirring to dissolve completely.

3.3.2. Removal of insoluble residues

When demineralization is complete, there is often a small residue of insoluble material which must be removed before filtration and concentration of the sample. In order to do this the solution is centrifuged for 20 minutes at 4000 revolutions/min. The insoluble residues were kept and stored in the freezer for future analysis.

3.3.3. Filtration and concentration

A Millipore Minitan tangential flow filtration system with 10 kDa cutoff filters was used to remove the EDTA solution and concentrate up the solution of soluble organic molecules. Using this system it was possible to reduce the solution to approximately 30 ml of organic molecules in water. Samples were then further concentrated to approximately 1 ml using an Amicon minicon B15 concentrator and stored in the freezer.

3.4 Separation of amino acids by high pressure liquid chromatography (HPLC)

3.4.1 Protein and peptide hydrolysis

In order for amino acids to be separated, identified and collected from a sample containing proteins and peptides, the amino acids must be freed by hydrolysis of the peptide bonds. This can be done in many ways. The method used here is as follows.
The filtered and concentrated sample was placed in a sterile glass tube. This was placed in a glass hydrolysis bottle containing a small amount of 6N hydrochloric acid (fig 3.4). The hydrolysis bottle was then sealed and placed in an oven at 165 degrees centigrade for at least one hour, enabling the sample to be hydrolysed by the hot acid vapour rising from the bottom of the hydrolysis bottle. The sample was then freeze dried to remove traces of HCl and redissolved in clean Milli Q water ready to be injected into the HPLC system.

3.4.2 The HPLC system

The HPLC system consists of several parts (fig 3.5). The sample enters the HPLC by injection as a liquid phase at the injector. As the sample is injected it is transported by a moving stream of a mixture of two buffer solutions to the column. The column is a narrow tube containing a bed of small particles or beads. The beads have apolar surface properties which cause them to bind to the hydrophobic parts of molecules. The proportions of the two buffer solutions are gradually changed until the polarity of the buffers weakens. As the interaction between the beads and a particular type of molecule diminishes, that type of molecule is released. The sample mixture is therefore separated as a result of different components adhering to the beads to different extents. Hence the sample is separated into various zones of components within the column. These migrate through the bed of particles and eventually pass out of the column to a detector. The detector monitors the eluate by means of UV absorbtion at selected wavelengths. The detector is connected to a recording device which records a peak or deflection each time a band of components passes out of the column. The collection of peaks so produced comprises the chromatogram. Individual peaks are

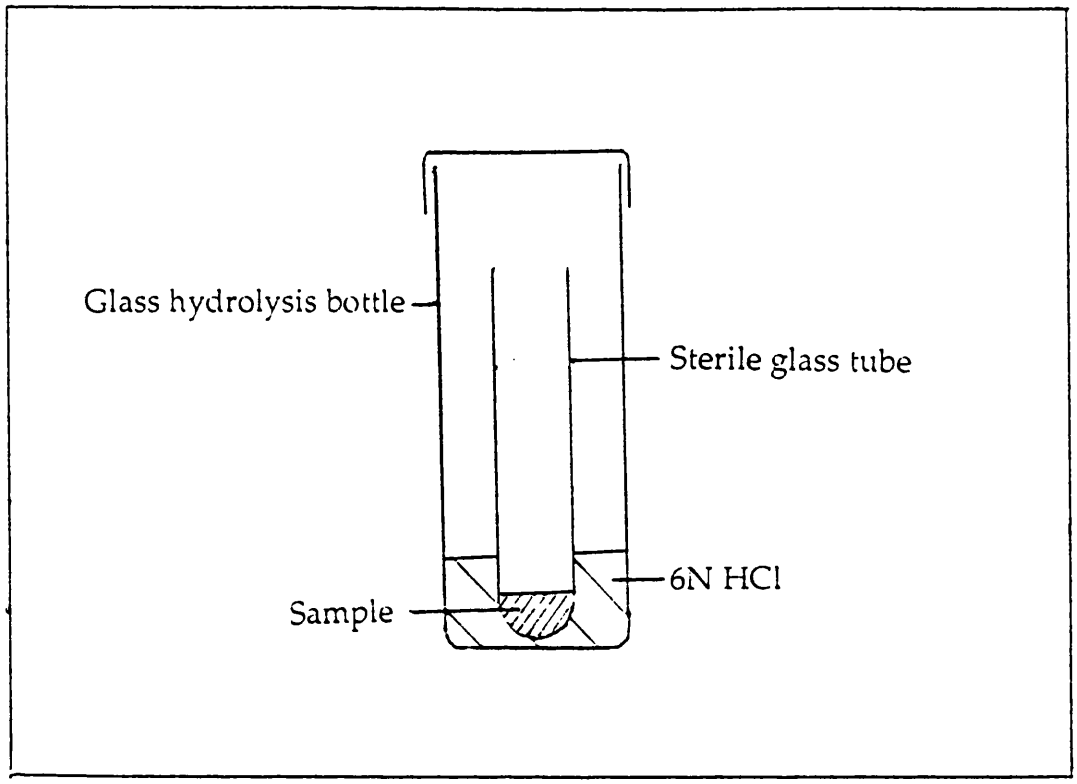

Fig. 3.4 Manual hydrolysis of the filtered and concentrated sample of intracrystalline biomolecules using 6N HCl.

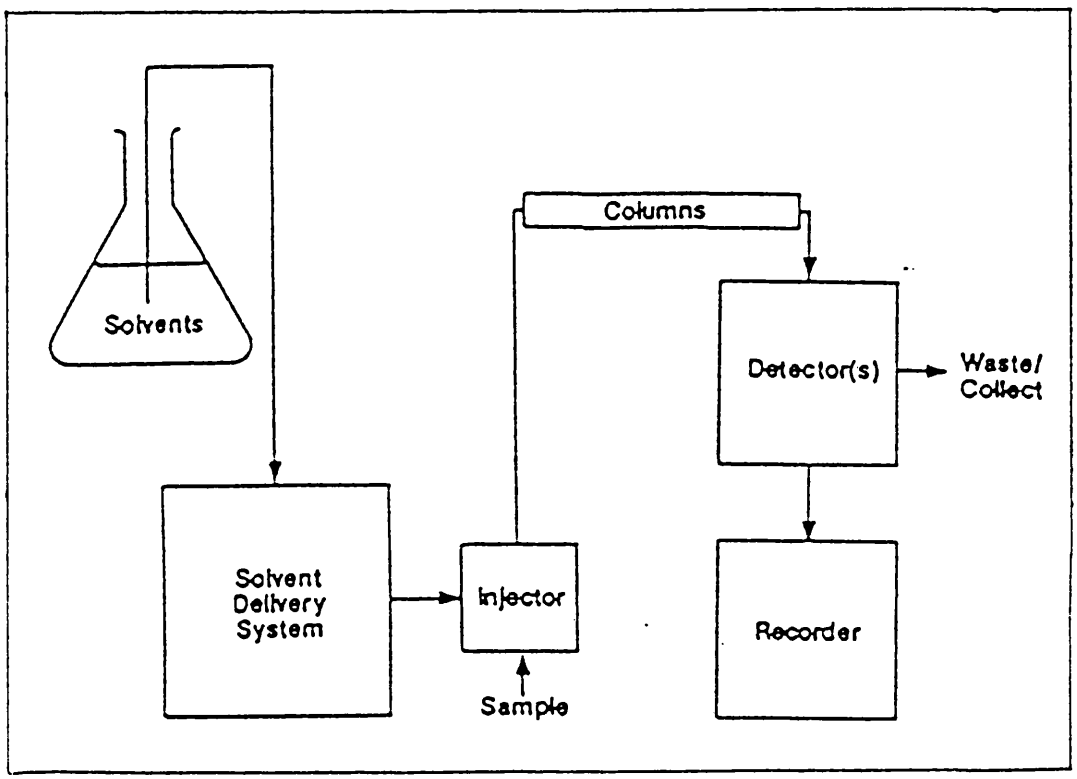

Fig. 3.5 The hplc system.

characterised and identified by means of their retention time, the time taken for the sample component to move through the column to the detector. After passing through the detector the fractionated sample is automatically collected in a series of eppendorf tubes, the number and frequency of which are controlled.

Intracrystalline mollusc shell extracts and prepared samples of mixed standard Sigma L-amino acids (Kit No. LAA-21) were fractionated using a Jones Chromatography Spherisorb amino 5μ column (25cm length, 4.6 mm inside diameter). The buffer solutions used as mobile phases were: A: 10mM potassium phosphate, pH 4.3; B: acetonitrile/ water in a ratio of 100: 14. ABI hplc grade acetonitrile and milli-Q water were used in all buffer solutions. The solutions were degassed either by ultrasonication prior to use or by helium gas sparging during chromatography. The following elution program was used: 5% solvent A and 95% solvent B for 20 min; 30% solvent A and 70% solvent B for 7 min; 50% solvent A and 50% solvent B for 3 min (table 3.2). The flow rate was 1ml / min. The eluate was monitored by UV absorbtion at frequencies of 254 nm. The fractionated eluate was collected in eppendorf tubes at intervals of 30 seconds (i.e. giving 60 samples per 30 minute run; each sample consisting of 0.5 ml of solution). The contents of the tubes were then analysed using an Applied Biosystems 420H system (Dupont et al., 1989) (section 3.5).

Table 3.2 Elution program for Jones Chromatography Spherisorb amino 5μ column

Time (min)	Flow (ml/min)	%A	%B
0	1	5	95
5	1	5	95
20	1	30	70
27	1	50	50
30	1	5	95

3.5 Amino Acid Analysis

Amino acid analysis was carried out using an Applied Biosystems 420H amino acid analyser. If the amino acids to be analysed are not free, i.e. if they are present as parts of proteins or peptides then the sample must be hydrolysed in order to break the peptide bonds and release the amino acids so that they can be detected. This can be done either manually as described in section 3.4.1 or it can be done automatically by the amino acid analyser as follows. The sample is introduced to the sample frit as an aqueous or acidic solution. The hydrolysis head clamps over the sample frit forming a sealed chamber. The sample is surrounded by argon gas in order to dry it and also in order to provide an inert atmosphere in which hydrolysis will take place. The sample is heated to 165°C and hydrolysed using 6N hydrochloric acid vapour. After 75 minutes the temperature decreases, the acid vapour is removed and the sample is dried again with argon.

The sample is then ready for individual amino acids to be separated from the mixture and quantified. The amino acids are first automatically derivatized using phenylisothiocyanite (PITC) which reacts with the amino group of amino acids yielding a derivative which absorbs UV light strongly at 254 nm in order to enable detection of the amino acids. The amount of absorbtion is proportional to the concentration of amino acid. The sample is then dissolved in 600 µl 29 mM sodium acetate buffer, pH 5.5 and transferred to an on-line reverse phase HPLC system for separation and quantification of amino acids. The detection limit is usually around 5-10 pmol of any individual amino acid within a sample. The system is calibrated using standard amino acid mixtures and blank runs are included in each batch of samples in order to check for contamination.

3.6 Stable Isotope Analysis

3.6.1. Introduction

The possibility of determining palaeotemperatures from the oxygen isotope signature of carbonates was first suggested by H. C. Urey in 1947. The theory is based on the fact that when calcium carbonate is precipitated from water under equilibrium conditions there is an isotope exchange reaction represented by the following equation

$$^1/_3CaC^{16}O_3 + H_2{}^{18}O \rightleftharpoons {}^1/_3CaC^{18}O_3 + H_2{}^{16}O$$

which results in the calcite becoming enriched in ^{18}O relative to water. Since the fractionation factor is temperature dependent, the isotopic composition of oxygen in calcite in equilibrium within water is also a function of temperature. The temperature dependence of $\delta^{18}O$ of calcite in equilibrium with water was determined experimentally by Epstein et al (1953). Their equation expressing the relationship between the temperature of water and the δ values of calcite and water was later modified by Craig (1965):

$$t°C = 16.9 - 4.2(\delta_c - \delta_w) + 0.13(\delta_c - \delta_w)^2$$

where δ_c is the $\delta^{18}O$ of CO_2 obtained from the carbonate by reaction with phosphoric acid at 25°C and δ_w is the $\delta^{18}O$ of CO_2 equilibrated isotopically at 25°C with the water from which the carbonate was precipitated.

The $\delta^{18}O$ value of oxygen in the seawater has varied with time due to continental glaciations (Hoefs, 1980). Craig (1965) determined that the present ocean has a mean $\delta^{18}O$ value of -0.08‰. Shackleton (1968) estimated that the $\delta^{18}O$ of the oceans changed by 1.0 to 1.4‰ during glacial and interglacial ages of the Pleistocene (Emiliani and Shackleton 1974).

Variations in the temperature and isotopic composition of seawater caused by continental glaciation can be resolved by analysis of benthic foraminifera. The temperature at the bottom of the oceans is assumed to remain constant so that variations in the $\delta^{18}O$ in benthic species record the variations in the overall $\delta^{18}O$ of the seawater.

The effect of the mineral composition of the carbonate on the fractionation of oxygen must also be considered. The calcium carbonate analysed by Epstein et al (1953) included both calcite and aragonite. Horibe and Oba (1972) cultured two species of bivalves of differing mineralogies. The temperature dependence of $\delta^{18}O$ in aragonite, based on *Anadara broughtoni*, is:

$$t°C = 13.85 - 4.54(\delta_c - \delta_w) + 0.04(\delta_c - \delta_w)^2$$

and the temperature dependence of calcite, based on *Patinopecten yessoensis*, is:

$$t°C = 17.04 - 4.34(\delta_c - \delta_w) + 0.16(\delta_c - \delta_w)^2$$

These two equations have similar slopes but different intercepts (fig. 3.6).

3.6.2. $\delta^{13}C$ and $\delta^{18}O$ of shell carbonates

The powdered carbonate samples were prepared for isotopic analysis by dissolution in excess 100% H_3PO_4 at 25°C (McCrea, 1950; Epstein *et al.*, 1953; Wachter and Hayes, 1985). The carbon dioxide gas produced is passed through a 'slush trap' of dry ice and acetone (approx. -78°C) to remove any water vapour. Volatile gaseous contaminants are removed by vacuum pump whilst freezing the carbon dioxide to the temperature of liquid nitrogen (-197°C). The oxygen and carbon isotopic compositions of the CO_2 gas were determined using a Sira 10 mass spectrometer and recorded relative to the Pee Dee Belemnite (PDB) standard carbonate powder (Epstein *et al.*, 1953). The precision of the isotopic determinations inferred from the analysis of standard carbonate powders alongside the shell samples was $\pm$ 0.1‰ (1standard deviation) or better for both $\delta^{18}O$ and $\delta^{13}C$ values.

3.6.3. $\delta^{13}C$ of intracrystalline biomolecules

The samples are placed in evacuated quartz glass tubes and oxidized with excess copper oxide at 850°C for 8 hours to produce carbon dioxide. The carbon dioxide is treated as above by passing it through a 'slush trap' to remove water vapour and freezing it down to remove volatile gaseous contaminants. The isotopic composition of the carbon dioxide is determined by a Sira 10 mass spectrometer. The isotopic ratios are recorded relative to that of the Pee Dee Belemnite (PDB) standard.

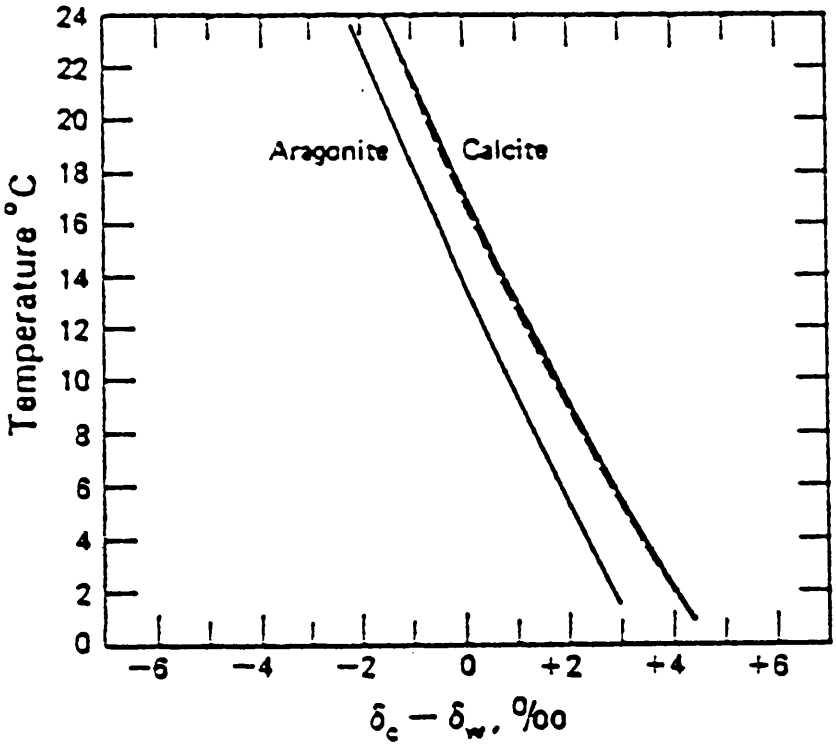

Fig. 3.6 Palaeotemperature scales based on oxygen isotope compositions of calcite and aragonite according to Horibe and Oba (1972). The dashed line is by Epstein and Mayeda (1953) for samples composed primarily of calcite but including some aragonite. From Faure (1986).

CHAPTER 4

STABLE CARBON AND OXYGEN ISOTOPE COMPOSITIONS OF MOLLUSC SHELLS FROM BRITAIN AND NEW ZEALAND

Lynda Mitchell*, Anthony E. Fallick†, Gordon B. Curry*

*Department of Geology and Applied Geology, Glasgow University, Glasgow G12 8QQ^

†Scottish Universities Research and Reactor Centre, East Kilbride G75 0QU

4.1 Abstract.

Stable carbon and oxygen isotope analysis of the carbonate shells of two fossil mollusc species from the Plio-Pleistocene of New Zealand and two Recent species from the west coast of Scotland has revealed an unexpectedly high degree of variability for each species and a strong positive correlation between $\delta^{13}C$ and $\delta^{18}O$ in each case. This phenomenon may be due to kinetic isotope effects which are inherent in fast growing shells or areas of shell. If this is the case then equilibrium isotope partitioning may not have had time to occur before the completion of calcite precipitation. Kinetic effects would tend to favour the lighter isotopes of both carbon and oxygen; it is therefore the highest $\delta^{13}C$ and $\delta^{18}O$ values that are most likely to reflect equilibrium with the environment. Very small carbonate particles often give particularly low $\delta^{13}C$ and $\delta^{18}O$ values. These results have implications for the use of isotopic data in environmental reconstruction based on fast growing shells and may also be applicable to other carbonate precipitating organisms.

4.2 Introduction

Mollusc shells throughout the fossil record have been used as environmental indicators, both by comparing them with closely related or similar recent species (Beu, 1972) and by stable isotope analysis of the shell carbonate or preserved organic molecules (Stevens and Vella, 1981; Krantz *et al.*, 1987; Muhs and Kyser, 1987; Rollins *et al.*, 1987; Abell and Williams, 1989; Romanek and Grossman, 1989; Risk, 1991). However, calcium carbonate may not

always be precipitated in equilibrium with the environment, and in such cases stable isotope analysis of the shell carbonate may be an unreliable technique for environmental reconstruction. Isotopic disequilibrium may be in part due to metabolic effects or kinetic effects that are inherent in fast-growing shells, or areas of shell.

Metabolic effects influence mainly the carbon isotope signature and may reflect changes in the $\delta^{13}C$ of the dissolved inorganic carbon (DIC) from which the carbonate is precipitated. These changes are caused primarily by selective addition or removal of ^{12}C by photosynthesis and, to a lesser extent, by respiration (Swart, 1983). Metabolic effects are likely, therefore, to be most apparent in photosynthesizing organisms. Skeletal $\delta^{13}C$ in corals with symbiotic photosynthesizing algae has, for example, been seen to decrease with greater depth and lesser relative light intensity (Fairbanks and Dodge, 1979). Photosynthetic organisms have been shown to have higher skeletal $\delta^{13}C$ values than non-photosynthetic organisms with comparable $\delta^{18}O$ values (Keith and Weber, 1965; McConnaughey 1989).

Kinetic isotope effects involve discrimination against heavy isotopes of both carbon and oxygen during hydration and hydroxylation of CO_2 in the process of carbonate formation. This process can lead to linear correlations between $\delta^{18}O$ and $\delta^{13}C$ by a) simultaneous fractionation of both carbon and oxygen isotopes during CO_2 exchange across the cell membrane and b) influx of external HCO_3^- by fluid transport which has not been subject to kinetic isotope effects, the addition of which produces an isotopic 'mixing line' (McConnaughey, 1989). Such linear correlations have previously been noted in corals (Emiliani *et al.*,1978; McConnaughey, 1989), cidaroid urchins (Weber and Raup, 1966), various foraminifera (Vinot-Bertouille and Duplessy, 1973; Vergnaud Grazzini, 1976; Gonzalez and Lohmann, 1985) and calcitic algae (Keith and Weber, 1965).

Isotopic disequilibrium effects seem to be particularly strong in cases of rapid skeletal growth. This is probably due to the short time available for isotopic equilibration during carbonate formation. This

has been noted in corals (Land *et al.*, 1975; Erez, 1977 and 1978; Weil *et al.*, 1981; McConnaughey, 1989) and in rapidly growing benthic foraminifera (Vinot-Bertouille and Duplessy, 1973). Strong isotopic disequilibrium effects have also been noted during early, and presumably rapid, growth of *Nautilus* (Eichler and Ristedt, 1966; Cochran *et al.*, 1981; Landman *et al.*, 1983; Taylor and Ward, 1983) and some foraminifera (Vergnaud Grazzini, 1976; Berger *et al.*, 1978; Kahn, 1979; Duplessy *et al.*, 1981; Erez and Honjo, 1981). McConnaughey (1989) noted that $\delta^{18}O$ and $\delta^{13}C$ values tended to approach equilibrium values only at growth rates of below 2 mm per year in a specimen of the coral *Pavona clavus*.

Isotopic disequilibrium effects have also been noted in fast experimental growth of inorganic carbonates. Turner (1982) showed that the extent of fractionation between $CaCO_3$ and HCO_3^- in rate controlled precipitation experiments exhibits an inverse relationship with precipitation rate. At rapid rates, rather than achieving equilibrium, the $\delta^{13}C$ of the carbonate remains the same as that of the dissolved bicarbonate. Only at very slow rates is true equilibrium fractionation approached.

4.3 Methods

Four different bivalve molluscs were investigated: two Recent British species *Pecten maximus* and *Modiolus modiolus* and two fossil New Zealand species *Crassostrea ingens* (mid Pliocene) and *Patro undatus* (late Pliocene or early Pleistocene).

Pecten maximus shells were dredged from the sea bed off Girvan on the west coast of Scotland. *Modiolus modiolus* shells were dredged from nearby coastal waters at Shuna. *Crassostrea ingens* shells were collected from the Middle Waipipi Shellbed, Waipipi Formation, Waitotaran stage, from sea cliffs north of Wanganui, New Zealand. *Patro undatus* shells were collected from the Nukumaru Brown Sand, Nukumaruan stage, from a road cutting 1.6 km south of Maxwell, near Wanganui, New Zealand.

Fragments of each shell were examined by SEM for any signs of alteration or recrystallization and the mineralogy of each species was checked by XRD analysis (table 4.1).

Table 4.1: Results of XRD analysis of shells of *Pecten maximus, Modiolus modiolus, Crassostrea ingens* and *Patro undatus*

Species	Mineralogy
Pecten maximus	>95% calcite
Modiolus modiolus	>95% aragonite
Crassostrea ingens	>95% calcite
Patro undatus	>95% calcite

Shells which had been encrusted by worm tubes or other epibiotic organisms were discarded. The recent specimens had their ligaments removed and the *Modiolus* shells were placed in an oven at 40°C to facilitate the removal of the periostracum. The fossil specimens were cleaned of sediment using a sonic water bath and a dentist's drill. The shells were scrubbed with 2N hydrochloric acid, then with bleach, and finally with distilled water, in order to remove superficial dirt, algae and organic contaminants (section 3.1.2). A number of clean, dried shells of each of the recent species were broken up, mixed together and crushed using an agate TEMA or a metal drum rock crusher (section 3.2.1a).

Following suggestions that the isotopic composition may be affected by particle size (Fritz and Fontes, 1966), the crushed carbonate of each species was divided into ten different particle size fractions between 0 and 150 μm (table 4.2). Size fractions were separated using firstly a series of mesh sieves (Krumbein and Pettijohn, 1961; Folk, 1974; Buller and McManus, 1979). The finest particles below the smallest sieve mesh of 32 μm were then separated by means of sedimentation rates in water (Jackson, 1979).

Table 4.2: Carbonate powder size fractions for isotopic analysis

Fraction	Separation method	Particle size (μm)
1	sieve	125-150
2	sieve	106-125
3	sieve	90-106
4	sieve	75-90
5	sieve	63-75
6	sieve	32-63
7	sedimentation	15-32
8	sedimentation	10-15
9	sedimentation	5-10
10	sedimentation	< 5

Samples were also taken from the outer surface (the fastest growing area of shell) of a large specimen of *Pecten maximus*, starting near the umbo and taken at intervals between the umbo and the outer edge of the shell. These samples were taken using a small dentists drill with a rotating tip, to a depth of about 0.5mm (fig. 4.1).

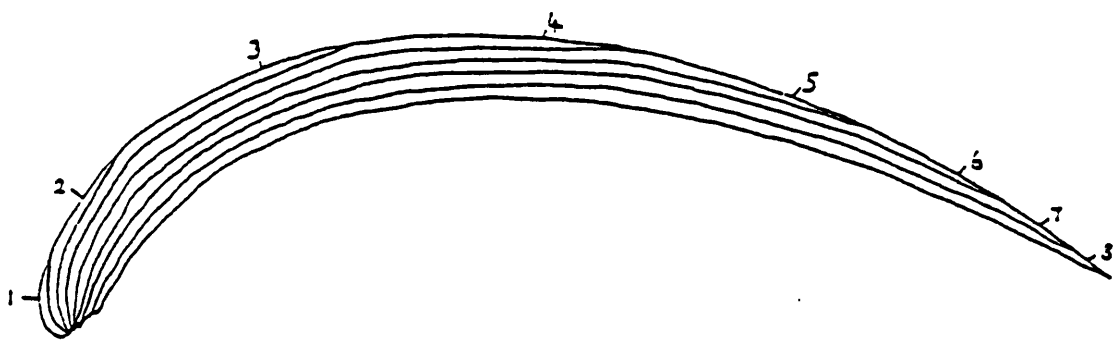

Fig. 4.1. Schematic diagram showing the pattern of yearly growth of *Pecten maximus* and the positions of samples taken from the surface layer of the shell.

The carbonate samples were plasma ashed to remove organic contaminants. The samples were prepared for isotopic analysis by dissolution in excess 100% H_3PO_4 at 25°C (McCrea, 1950; Epstein *et al.*, 1953; Wachter and Hayes, 1985). The oxygen and carbon isotopic compositions of the CO_2 gas were determined using a Sira 10 mass spectrometer and recorded relative to the Pee Dee Belemnite (PDB) standard (Epstein *et al.*, 1953). The precision of the isotopic determinations inferred from the analysis of standard carbonate powders alongside the shell samples was ± 0.1‰ (1s) or better for both $\delta^{18}O$ and $\delta^{13}C$ values.

4.4 Results

Carbon and oxygen isotope analysis of *Pecten maximus* samples showed a strong positive linear correlation between $\delta^{18}O$ and $\delta^{13}C$ values (Fig 4.2). The correlation coefficient r is 0.92 (significant at the 99.9% confidence level).
Modiolus modiolus samples also showed a strong linear correlation between $\delta^{13}C$ and $\delta^{18}O$ values (Fig 4.3). The correlation coefficient is 0.91 (significant at the 99.9% confidence level). The two fossil New Zealand species *Crassostrea ingens* and *Patro undatus* showed a strong positive correlation between $\delta^{18}O$ and $\delta^{13}C$ in both cases (Figs 4.4 and 4.5). For *Crassostrea ingens*, the correlation coefficient is 0.98 (significant at the 99.9% confidence level). For *Patro undatus* the correlation coefficient is 0.95 (significant at the 99.9% confidence level).

When the particle size of the whole shell samples of each species is studied with respect to the $\delta^{18}O$ and $\delta^{13}C$ values, it is noticeable that in all cases the samples with the lowest $\delta^{18}O$ and $\delta^{13}C$ values tend to be the smallest size fractions (Figs 4.6 to 4.9). In all four species, the small grain sizes of less than 32 μm constitute the lowest points on both the $\delta^{18}O$ and the $\delta^{13}C$ scales, and account for about half of the total variation in both the $\delta^{18}O$ and $\delta^{13}C$ values for whole shell samples. However, as the particle size increases above the 32 μm fraction the correlation between grain size and isotope values is lost and the isotope values become independent of particle size.

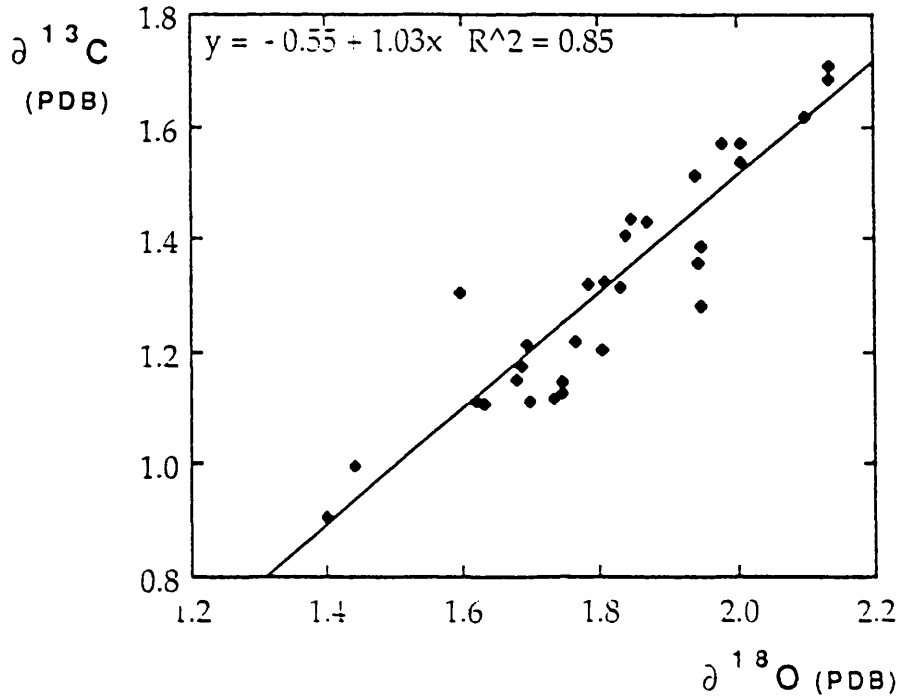

Fig. 4.2. Carbon and oxygen isotope composition of shells of *Pecten maximus*

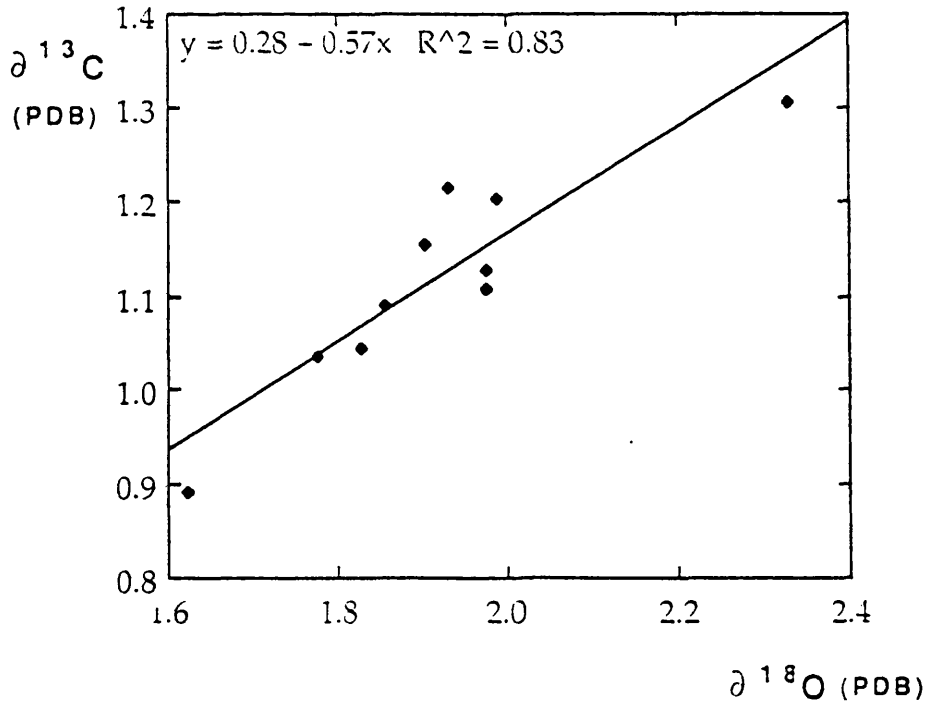

Fig. 4.3. Carbon and oxygen isotope composition of shells of *Modiolus modiolus*

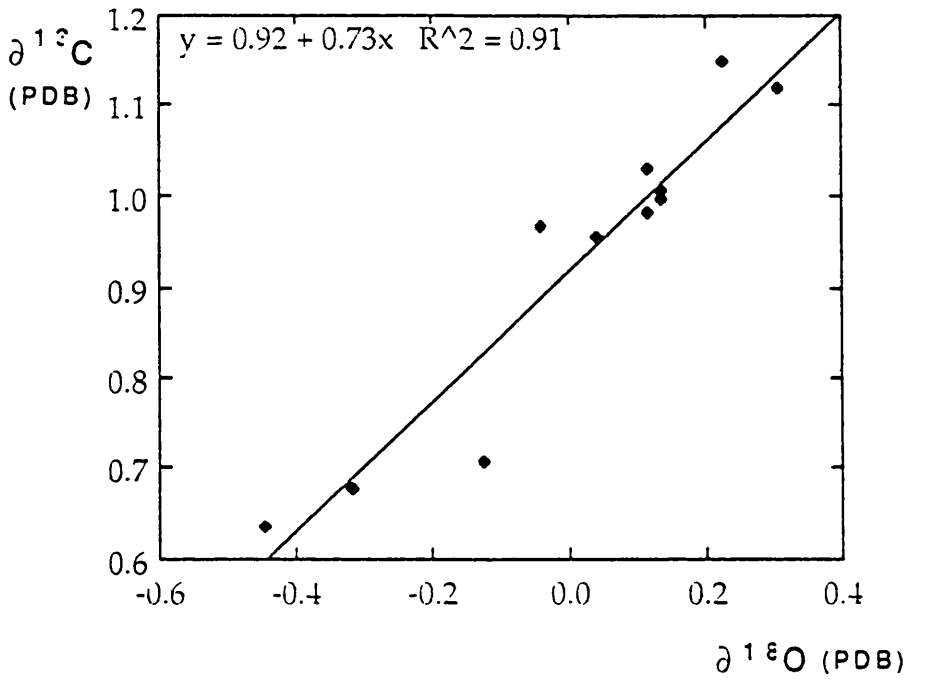

Fig. 4.4. Carbon and oxygen isotope composition of shells of fossil *Patro undatus*

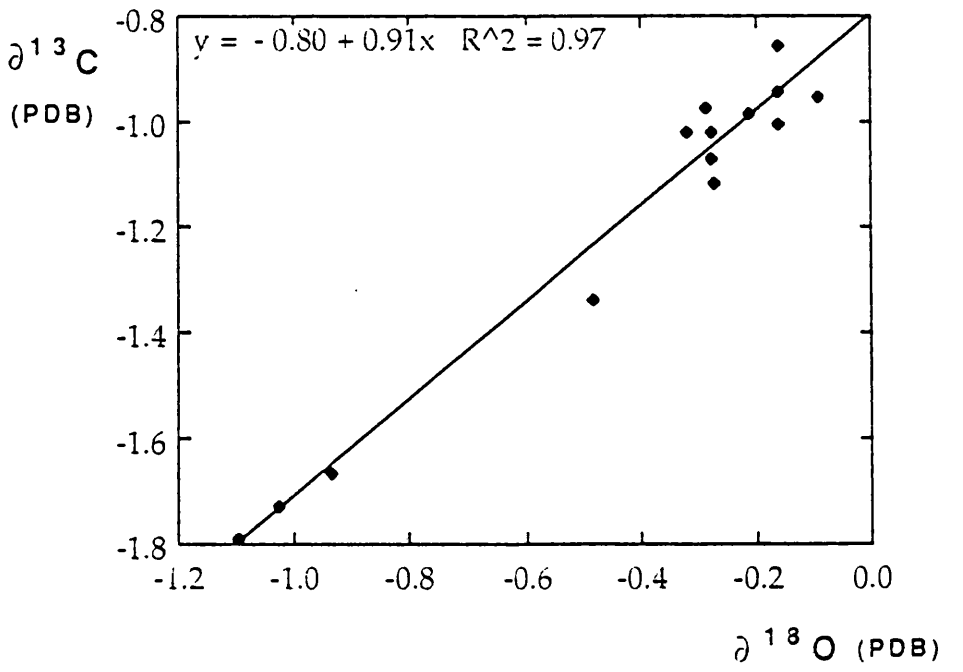

Fig. 4.5. Carbon and oxygen isotopic composition of shells of fossil *Crassostrea ingens*

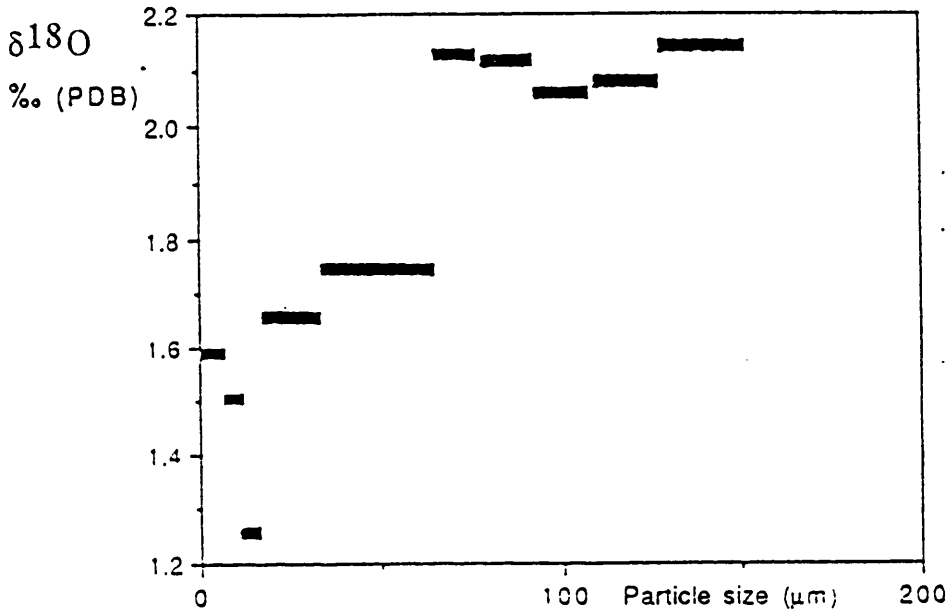

Fig4.6a. $\delta^{18}O$ and particle size for *Pecten maximus*

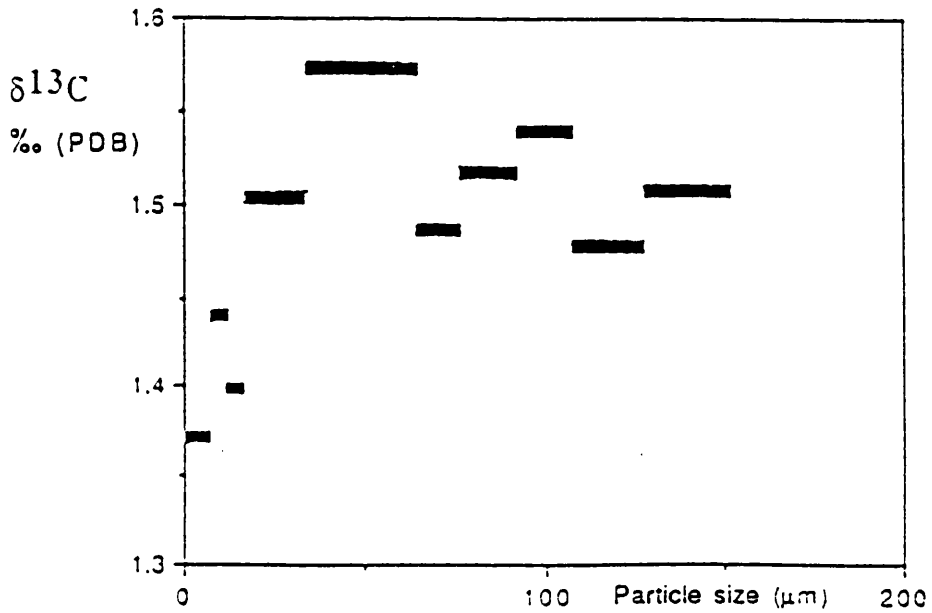

Fig4.6b. $\delta^{13}C$ and particle size for *Pecten maximus*

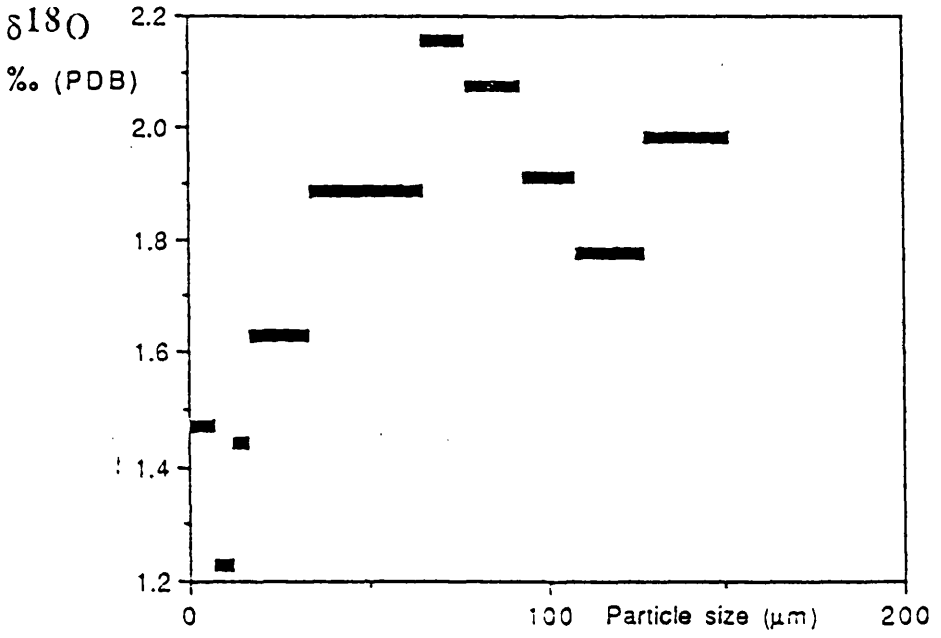

Fig. 4.7a. $\delta^{18}O$ and particle size for *Modiolus modiolus*

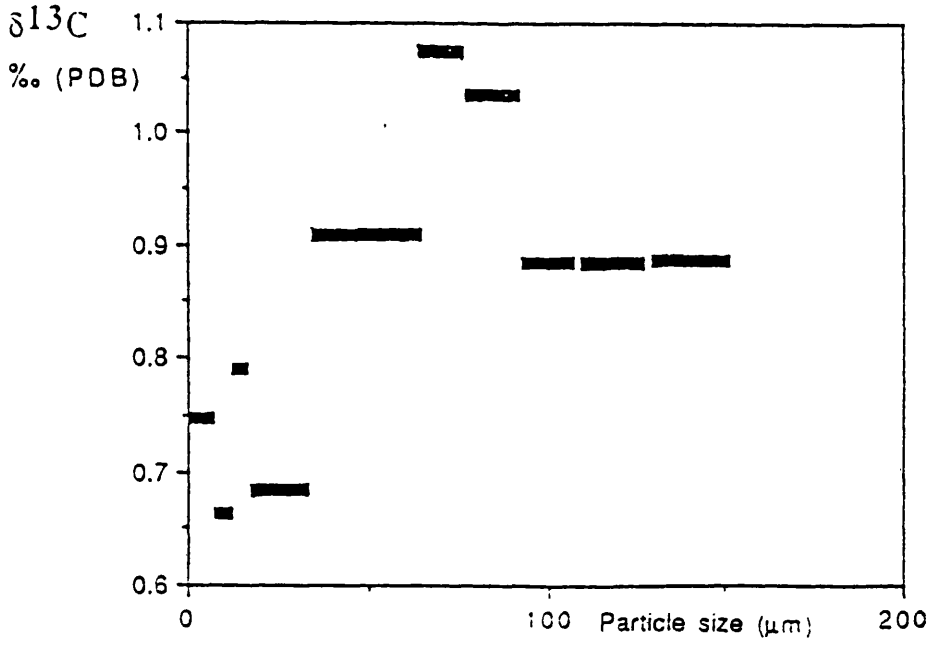

Fig. 4.7b. $\delta^{13}C$ and particle size for *Modiolus modiolus*

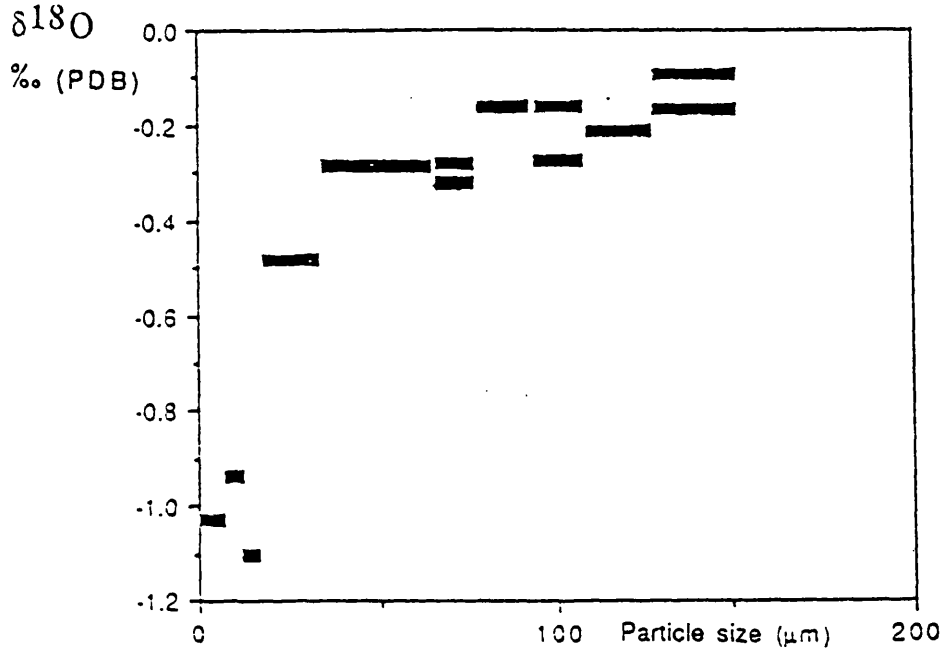

Fig. 4.8 a. $\delta^{18}O$ and particle size for *Crassostrea ingens*

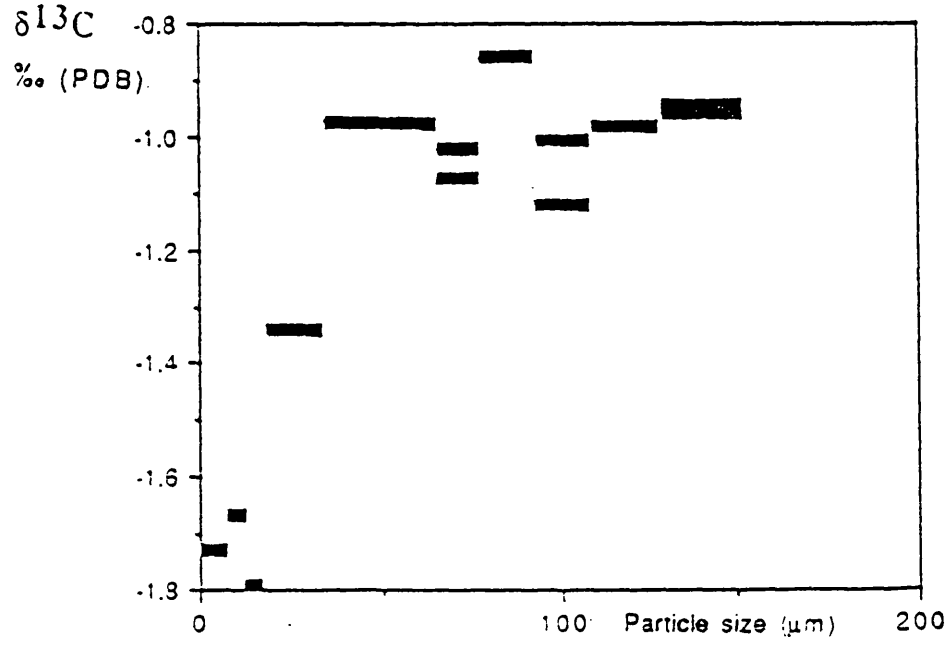

Fig. 4.8 b. $\delta^{13}C$ and particle size for *Crassostrea ingens*

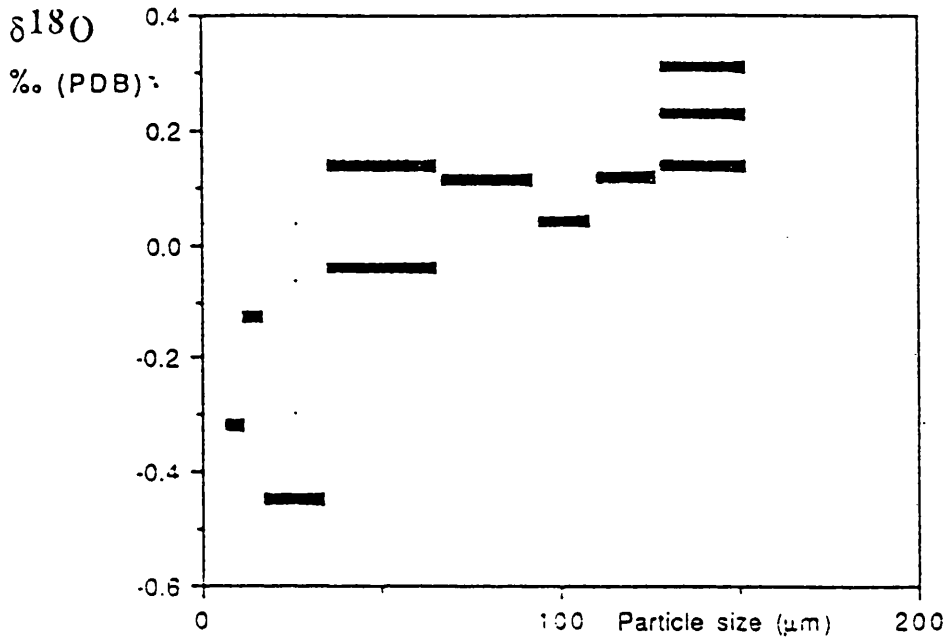

Fig. 4.9 a. $\delta^{18}O$ and particle size for *Patro undatus*

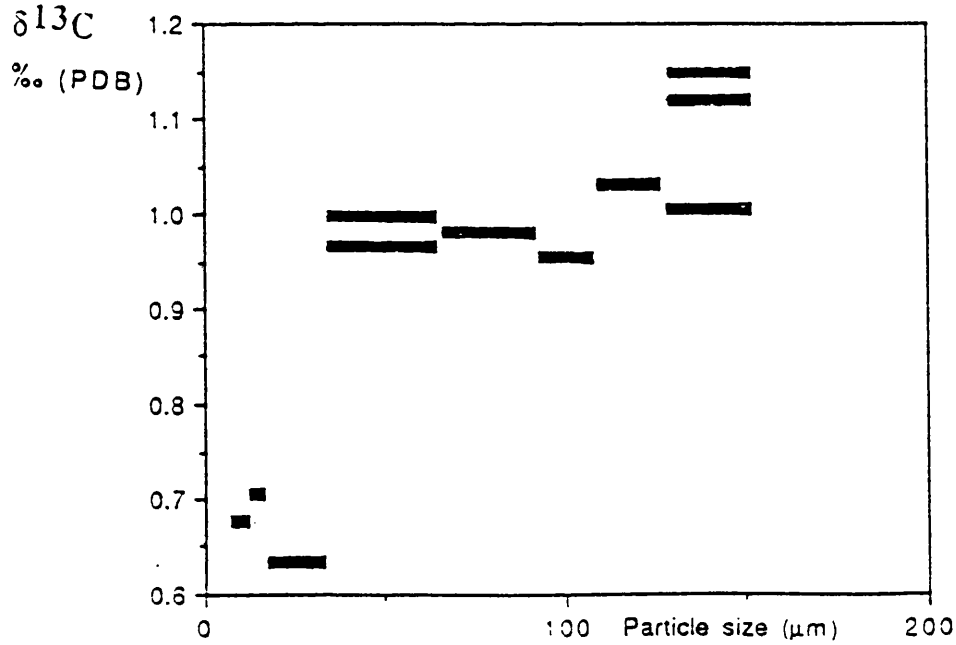

Fig. 4.9 b. $\delta^{13}C$ and particle size for *Patro undatus*

A strong linear correlation is also seen between the $\delta^{13}C$ and $\delta^{18}O$ of the samples taken from the surface layer of *Pecten maximus*. When these results are compared with the whole shell samples from the same species, the surface samples are seen to lie on the same line of correlation as the whole shell samples, but the values of $\delta^{13}C$ and $\delta^{18}O$ are significantly lower (fig 4.10). $\delta^{13}C$ values of the surface samples are up to 4 ‰ lower than those of the whole shell samples. The $\delta^{18}O$ values of the surface samples are up to 5 ‰ lower than the whole shell samples: this difference could be interpreted as a temperature difference of up to 20 degrees centigrade.

4.5 Discussion

The low $\delta^{18}O$ and $\delta^{13}C$ values seen for the very small size fractions could be due to a number of factors. Isotope exchange may have occurred with carbon dioxide or water vapour in the air between the time of crushing and analysis. Small particles would be particularly susceptible to this due to their high ratio of surface area to volume, particularly if their surfaces were damaged by the crushing process (fig 4.11). The smaller size fractions may have contained a high proportion of a particularly isotopically light part of the shell structure: different parts of the shell structure often consist of calcite biocrystals of different sizes and shapes, controlled by a matrix of organic macromolecules secreted by the cells of the organism (Lowenstam and Weiner, 1989). Different biocrystals may grow at different rates and may show different degrees of kinetic isotope fractionation.

The method of size fraction separation (sedimentation rates in water for sizes less than 32 μm; sieves for larger sizes) may also have some influence. The method of using sedimentation rates in water to separate size fractions is imperfect in that each fraction probably contains a proportion of smaller particles. This process also increases the chance of isotope exchange involving water molecules.

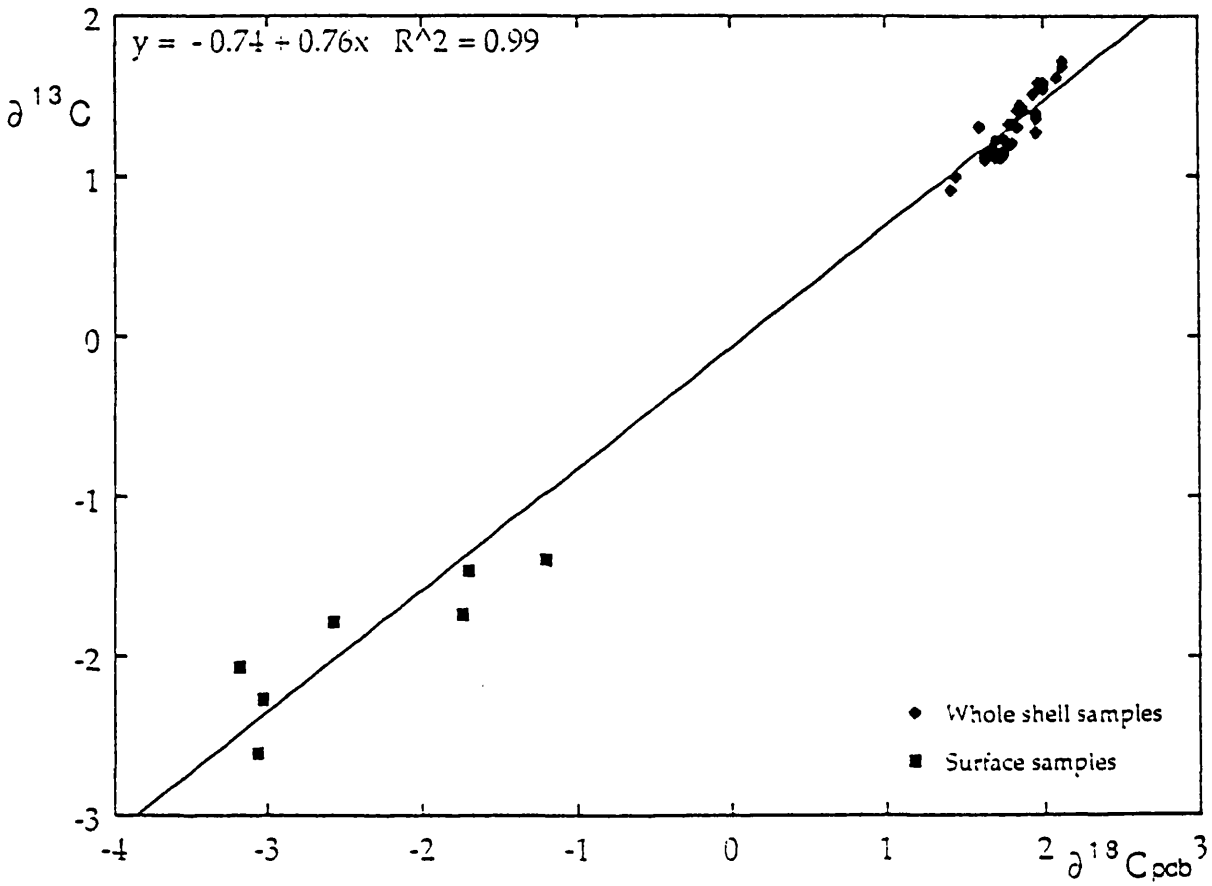

Fig4.10Carbon and oxygen isotope composition of shells of *Pecten maximus* showing data from whole shells and from the shell surface

As the particle size increases above the 32 μm fraction the correlation between grain size and isotope composition is lost. The particle size does not explain the entire spread of the results or the strong positive correlation between $\delta^{13}C$ and $\delta^{18}O$ which has been demonstrated for each of the species investigated. Nor does it explain the fact that samples taken from the surface layer (the fastest growing area of the shell) of *Pecten maximus* should be so strongly depleted in both ^{13}C and ^{18}O whilst still plotting on the same line of correlation between $\delta^{13}C$ and $\delta^{18}O$ as whole shell samples from the same species.

The range of oxygen isotope values for the recent whole shell samples are compatible with the seasonal ocean temperature range on the west coast of Scotland of 8-14 degrees centigrade. However if the range in oxygen isotope values were merely due to temperature effects, a corresponding change in carbon isotope values would not be expected. Any seasonal correlation in $\delta^{13}C$ and $\delta^{18}O$ due to changes in primary productivity or influx of meteoric waters would be likely to be a negative one: greater productivity in the summer would lead to higher $\delta^{13}C$ coinciding with lower $\delta^{18}O$ due to warmer temperatures. A lower $\delta^{13}C$ could arise during or after times of high productivity by the incorporation of bicarbonate from pore waters coming from sediments composed of decomposing organic matter (Romanek and Grossman, 1989), but this phenomenon is more likely in the case of buried, infaunal species than the four epifaunal species considered here. Mixing with meteoric waters would tend to produce a lower $\delta^{13}C$ and is most likely to be significant during winter run-off when colder temperatures will produce a higher $\delta^{18}O$. The isotope values for surface samples of *Pecten maximus* indicate a temperature of up to 32 degrees centigrade which is clearly not compatible with the sea temperature on the west coast of Scotland.

Metabolic effects are unlikely to explain the range and correlation in results as such effects are likely to be very small in non-photosynthetic organisms and would tend to affect the carbon isotope values without influencing $\delta^{18}O$. Kinetic isotope effects however, may affect both the carbon and the oxygen isotope signatures simultaneously, and may particularly affect fast growing biogenic carbonates.

Pecten maximus shells reach a maximum size of up to 15 cm from the umbo to the outer margin of the shell. Annual growth lines show that the life-span is normally up to about eight years (Dare and Deith, 1991). Most growth occurs during the first five years, after which little more carbonate is precipitated each year (Fig 4.12). This may be related to the onset of sexual maturity and may represent a reordering of energy priorities from biomineralization to reproduction (Jones *et al.*, 1986). This gives an average growth rate of at least 2 cm per year. The growth rates of the other three species cannot be determined due to a lack of distinct annual growth lines. However, they are all relatively large species (10-20 cm) so unless their life span is very long their growth rates must be fairly fast, and the growth rates of many other large mollusc species are likely to be comparable.

Normally, when calcium carbonate precipitates slowly from solution, equilibrium isotope partitioning is observed. However, faster precipitation may result in isotopic signatures which are significantly out of equilibrium. Kinetic effects in carbonate precipitating organisms have been described in both fast growing biogenic carbonates (McConnaughey 1989) and in experimental non-biological carbonates (Turner 1982) and appear to involve discrimination against heavy isotopes of both carbon and oxygen during hydration and hydroxylation of CO_2. The lighter isotopes react more easily leading to the formation of isotopically light HCO_3^- in the extracytoplasmic calcifying fluid (ECF) from which the carbonate will precipitate. If the precipitation is fast, therefore, the carbonate will be isotopically light (McConnaughey, 1989).

During the process of carbonate precipitation, however, movement of CO_2 and HCO_3^- across the boundary membrane from the cells to the ECF, and across the boundary from the outside environment to the ECF, may simultaneously equilibrate both carbon and oxygen isotopes of any isotopically light HCO_3^- which remains in solution in the ECF with the environment. Hence the carbonate which precipitates more slowly will be closer to equilibrium.

This process may lead to the range in values and the strong correlation between $\delta^{18}O$ and $\delta^{13}C$ as seen in these shells. The degree of disequilibrium will depend on the rate of growth of the carbonate crystals. Different parts of the shell structure may have different rates of growth. For instance, the outer edge of the shell must grow outward more rapidly than the internal surface will increase in thickness (Fig 4.1). For this reason, carbonate samples from the very outer surface of the shell are likely to be the most isotopically light. Isotope measurements taken of the surface layer of *Pecten maximus* were indeed significantly lighter than the results for the whole shell (Fig 4.10).

4.6 Conclusions

Stable carbon and oxygen isotope analysis of fast growing shells yields a range of values which show a strong positive linear correlation between $\delta^{18}O$ and $\delta^{13}C$. 'Fast' may mean anything over 2 mm per year as in the coral *Pavona clavus* (McConnaughey 1989). Care must be taken, therefore, with mollusc shells commonly used by isotope geochemists for environmental reconstruction. The range in values may be so large that single isotope values from these shells may be extremely unreliable. The highest $\delta^{18}O$ and $\delta^{13}C$ values are most likely to approach equilibrium; departure from equilibrium is likely to reflect kinetic effects which favour the lighter isotopes of both carbon and oxygen in the hydration and hydroxylation of CO_2. Different parts of the shell structure may have different growth rates and yield different isotope results. Very small carbonate particles tended to yield particularly low $\delta^{18}O$ and $\delta^{13}C$ values. These results have implications for environmental analysis using isotope data from fast growing shells and may be applicable to any carbonate precipitating organism.

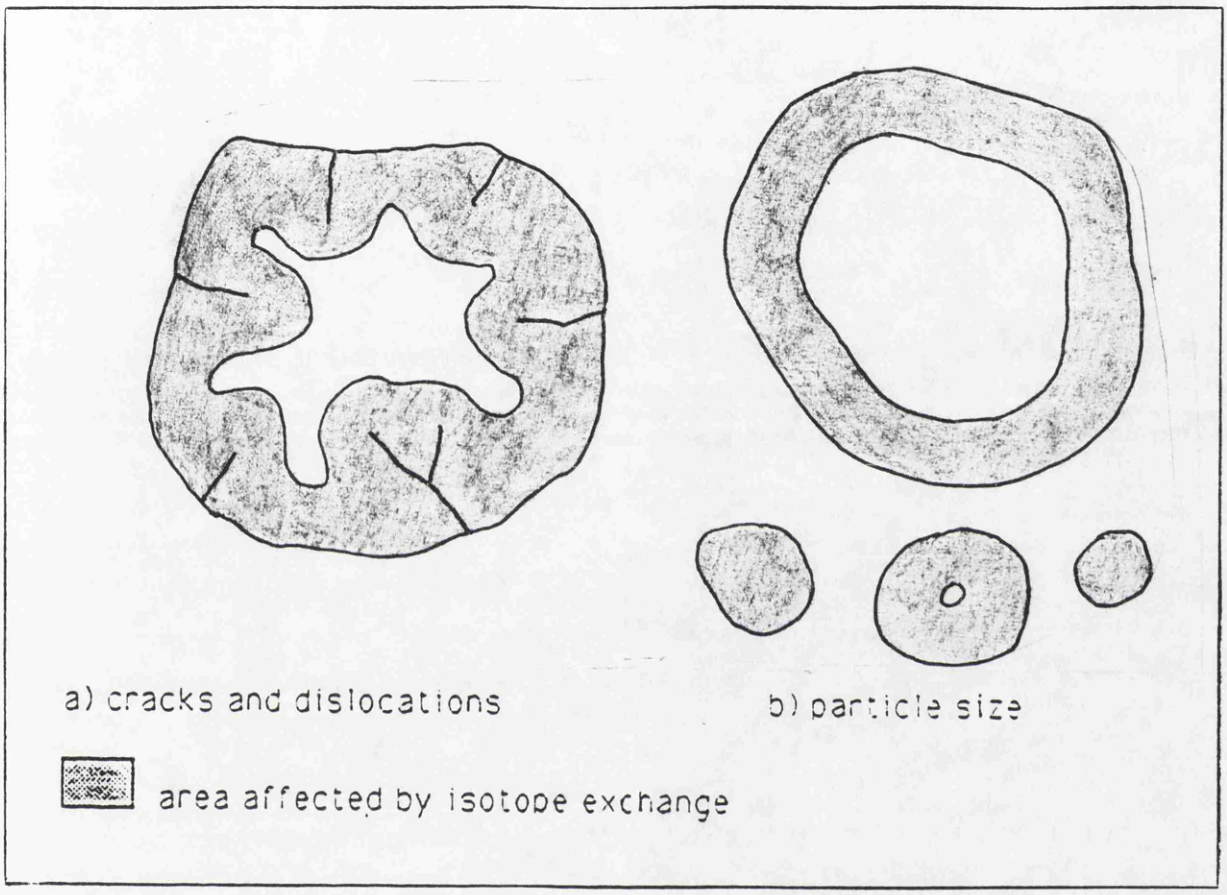

Fig 4.11 Factors affecting isotope exchange between carbonate particles and the surrounding environment

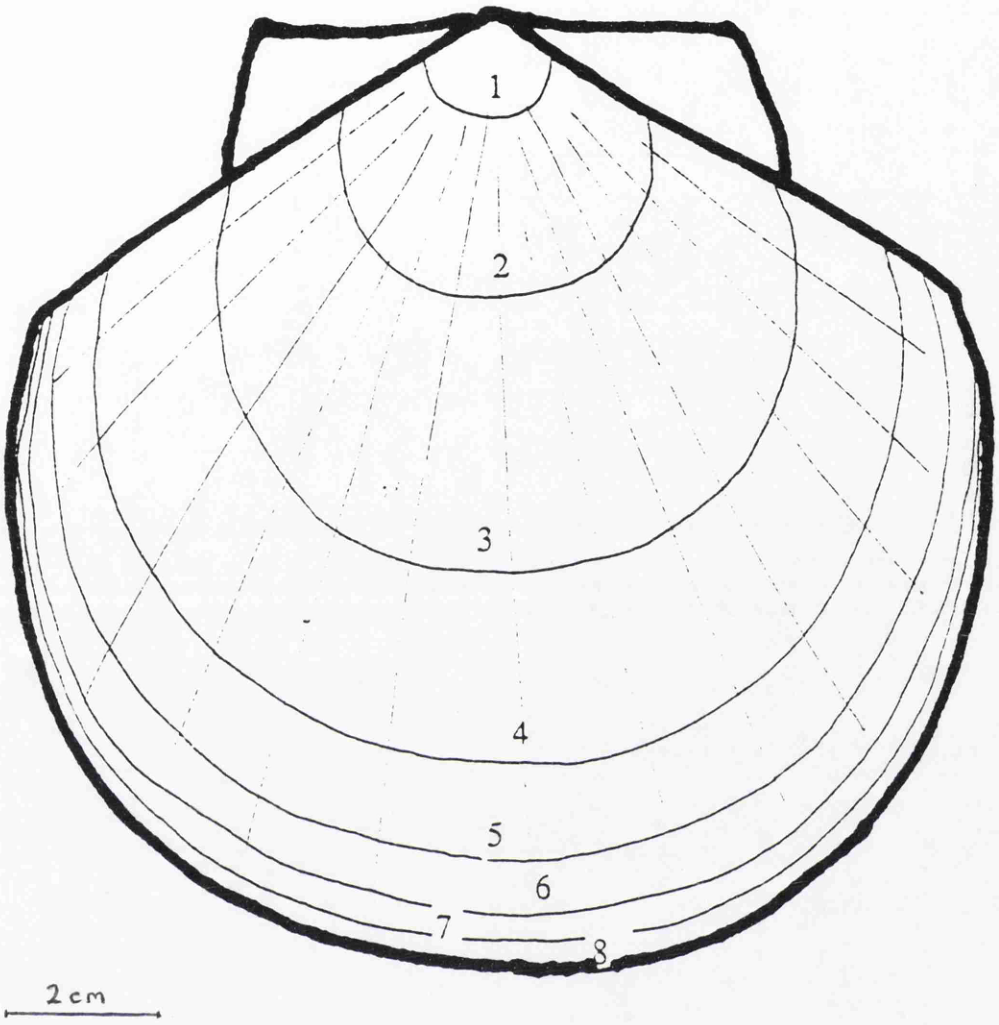

Fig 4.12 Annual growth lines in *Pecten maximus*

Appendix: Data table

Pecten maximus: whole shell samples, mixed particle sizes

$\delta^{18}O$	$\delta^{13}C$	Sample No
1.62	1.11	C8282
1.95	1.39	C8290
2.01	1.54	C8283
1.84	1.41	C8595
1.95	1.36	C8603
1.95	1.28	C8776
1.81	1.21	C8777
1.81	1.33	C8284
1.98	1.57	C8296
1.62	0.89	C8877
1.71	1.11	C8286
2.13	1.71	C8299
2.01	1.57	C8291
2.13	1.68	C8297
1.83	1.31	C8604
1.85	1.44	C8596
2.09	1.62	C8597
1.78	1.32	C8599
1.63	1.11	C8605
1.69	1.21	C8606
1.74	1.11	C8753
1.44	0.99	C8754
1.74	1.13	C8755
1.76	1.22	C8774
1.59	1.31	C8594
1.94	1.51	C8600
1.75	1.15	C8741
1.69	1.17	C8742
1.68	1.15	C8743
1.39	0.91	C8744

Pecten maximus: shell surface samples, mixed particle sizes

$\delta^{18}O$	$\delta^{13}C$	Sample No
-3.19	-2.06	C8879
-3.04	-2.27	C8881
-3.08	-2.61	C8882
-1.69	-1.46	C8884
-1.74	-1.73	C8885
-1.21	-1.39	C8886
-2.58	-1.78	C8887

Modiolus modiolus: whole shell samples, mixed particle sizes

$\delta^{18}O$	$\delta^{13}C$	Sample No
1.99	1.21	C8778
2.33	1.31	C8779
1.78	1.03	C8757
1.98	1.13	C8758
1.83	1.04	C8759
1.91	1.15	C8750
1.98	1.11	C8751
1.93	1.21	C8875
1.86	1.09	C8876
1.87	1.43	C8285

Pecten maximus: whole shell samples, separated particle sizes

$\delta^{18}O$	$\delta^{13}C$	Particle Size (μm)	Sample No
2.14	1.51	125-150	C8768
2.08	1.48	106-125	C8769
2.06	1.54	90-106	C8771
2.12	1.52	75-90	C8772
2.13	1.49	63-75	C8773
1.75	1.57	32-63	C8869
1.66	1.41	15-32	C8870
1.26	1.39	10-15	C8871
1.51	1.44	5-10	C8872
1.59	1.37	0-5	C8874

Modiolus modiolus: whole shell samples, separated particle sizes

$\delta^{18}O$	$\delta^{13}C$	Particle Size (μm)	Sample No
1.98	0.89	125-150	C8761
1.77	0.88	106-125	C8762
1.91	0.88	90-106	C8763
2.07	1.04	75-90	C8764
2.16	1.07	63-75	C8766
1.87	0.91	32-63	C8767
1.63	0.68	15-32	C8889
1.44	0.79	10-15	C8890
1.23	0.66	5-10	C8891
1.47	0.75	0-5	C8892

Crasssostrea ingens: whole shell samples, separated particle sizes

$\delta^{18}O$	$\delta^{13}C$	Particle Size (μm)	Sample No
-0.09	-0.96	125-150	C9295
-0.16	-0.94	125-150	C9300
-0.21	-0.98	106-125	C9312
-0.16	-1.01	90-106	C9297
-0.27	-1.12	90-106	C9313
-0.16	-0.86	75-90	C9298
-0.28	-1.02	63-75	C9299
-0.28	-1.07	63-75	C9299
-0.32	-1.02	63-75	C9325
-0.29	-0.97	32-63	C9373
-0.48	-1.34	15-32	C9374
-1.11	-1.79	10-15	C9375
-0.94	-1.67	5-10	C9376
-1.03	-1.73	0-5	C9377

Patro undatus: whole shell samples, separated particle sizes

$\delta^{18}O$	$\delta^{13}C$	Particle Size (μm)	Sample No
0.13	1.01	125-150	C9302
0.22	1.15	125-150	C9303
0.31	1.12	125-150	C9305
0.11	1.03	106-125	C9306
0.04	0.95	90-106	C9307
0.11	0.98	75-90	C9308
0.13	0.99	32-63	C9311
-0.04	0.97	32-63	C9326
-0.45	0.64	15-32	C9378
-0.13	0.71	10-15	C9379
-0.32	0.68	5-10	C9380

CHAPTER 5

EVIDENCE FOR A PLEISTOCENE INTERGLACIAL COOLING (~1 MY) FROM MOLLUSCAN FAUNAS OF NEW ZEALAND

Lynda Mitchell*, Anthony E. Fallick†, Gordon B. Curry*

*Department of Geology and Applied Geology, Glasgow University, Glasgow G12 8QQ^

†Scottish Universities Research and Reactor Centre, East Kilbride G75 0QU

5.1 Abstract

Stable isotope analysis of a series of fossil and recent mollusc shells from interglacial shell beds near Wanganui, New Zealand, yielded interglacial palaeotemperatures spanning the past 3.6 million years. The results indicate a cooling of about 10°C at about 1 My from earlier warm interglacial temperatures (15-20°C) to cooler interglacial temperatures (5-10°C) which have lasted to the present. This event coincides with a positive excursion in the strontium isotope ratio of seawater indicating greater erosional input to the ocean and with a significant molluscan extinction event in New Zealand. These changes may all be associated with a well documented change in the dominant global climatic cycle from 41 ky periodicity to 100 ky periodicity which occurred at about this time.

5.2 Introduction

The climate during most of the late Pliocene and Pleistocene has been characterized by major ice sheets on both poles. The main Antarctic ice cap formed during the mid Miocene about 14 My ago (Kennett, 1977), and glaciation in the northern hemisphere began at about 3.5 My (Shackleton and Opdyke, 1977; Shackleton et al., 1984). Since this time, Plio-Pleistocene climatic changes have been characterized by large fluctuations in temperature and ice volume (Hays et al., 1976). These fluctuations have been shown to reflect astronomical changes with various periodic components including those of 19, 23, 41 and 100 ky (e.g. Imbrie and Imbrie, 1980). The 19 and 21 ky components are

controlled by changes in the precession of the equinoxes and the 41 ky component by the tilt of the Earth's axis. These periodic climatic variations correspond very closely to their radiative forcing functions (Imbrie et al., 1993) and therefore can be explained by a linear version of the Milankovitch theory. The 100 ky component is associated with variations in the eccentricity of the Earth's orbit; but the large amplitude of the 100 ky climatic cycle seen during the late Pleistocene is not fully explained by the relatively small fluctuations in radiation on this time scale (Imbrie et al., 1989). Analysis of oxygen isotope records from deep sea sediment cores has indicated that the 100 ky cycle has dominated over the past 0.9 or 1.0 My (Pisias and Moore, 1981; Ruddiman et al., 1986), and that this period has also been a time of lower average temperatures and more extreme climatic fluctuations (Prell, 1983). Prior to this the amplitude of the 100 ky cycle is much reduced (Pisias and Moore, 1981). The major change, at 0.9 or 1.0 My, coincides with the isotope stage 22/23 boundary (Prell, 1983) and with an increase in the amount of northern hemisphere ice (Imbrie et al., 1993). The reasons for this change are not fully understood, as variations in the Earth's orbital parameters have not changed appreciably over the past 2 My (Pisias and Moore, 1981). Resonance mechanisms may amplify the relatively small radiative forcing in the 100 ky band (Le Treut and Ghil, 1983). The effect may be due to positive and negative feedback effects associated with physical changes in the Earth's surface, such as the elevation of major mountain ranges (Ruddiman et al., 1986) or the development of larger marine based ice sheets (Pisias and Moore, 1981), which result in a more asymmetrical response to climatic forcing (slower build-up of ice, and more rapid deglaciation). It has been suggested that when large ice sheets exceed a certain size, they cease responding in a linear way to Milankovitch cycles and begin to act as non-linear amplifiers, and that the climate system then exhibits resonance at periods near 100 ky (Imbrie et al., 1993). Hence the climatic response to external forcing may change significantly with time.

5.3 Method

Fossil mollusc shells were collected from shell beds in late Pliocene and Pleistocene shallow marine deposits near Wanganui, New Zealand. This area was chosen for its almost complete sequence of fossiliferous marine sediments spanning 3.6 million years (Fig. 5.1). Shell beds coincide with interglacial stages and are separated by erosional unconformities indicating low sea levels during glacials. Species lists were drawn up for each shell bed in the sequence (appendix) and well preserved specimens of selected species were selected for isotopic analysis (table 5.1). The calcium carbonate composition of each species selected for isotope analysis was determined by XRD in order to determine which equation or combination of equations to use for the conversion of oxygen isotope data to palaeotemperatures (Horibe and Oba, 1972). The shells were cleaned of sediment and soaked in an aqueous solution of bleach to remove contaminating organic matter from the surface. The bleach was removed by washing in MilliQ water and the shells were left to air dry. Powdered carbonate samples were taken from the shells using a dentist's drill with a drill bit of 1 mm diameter. Intercrystalline organic matter was removed from the samples by plasma ashing. Stable isotope analysis was carried out by dissolution in excess 100 % H_3PO_4 at 25°C (McCrea, 1950; Epstein et al., 1953; Wachter and Hayes, 1985). The oxygen and carbon isotopic compositions of the CO_2 gas were determined using a Sira 10 mass spectrometer and recorded relative to the Pee Dee Belemnite (PDB) standard (Epstein et al. 1953). Each sample was analysed in duplicate to ensure that the results were reproducible. This determined that results were likely to reflect temperatures and not kinetic isotope disequilibrium effects (these are characterized by highly variable, non-reproducible results - see previous chapter). The precision of the isotopic determinations inferred from the analysis of standard carbonate powders alongside the shell samples was ±0.1‰ or better for both $\delta^{18}O$ and $\delta^{13}C$ values. Oxygen isotope values were converted to palaeotemperatures using the calcite and aragonite equations of Horibe and Oba (1972). The oxygen isotope value of ocean water was taken as 0‰, which is within margin of error of Craig's (1965) estimate of -0.08‰.

Stage	Substage	Formation	Sample No.
Haweran		Alluvium	
		Rapanui Formation	17,18
		Brunswick Formation	
		Kaiatea Formation	
		Landguard Formation	5,19,20,21
Castlecliffian	Putikian	Putiki Shellbed	
		Mosstown Sand	
		Karaka Siltstone	
		Upper Castlecliff Shellbed	22,23,24
		Shakespeare Cliff Sand	25,26,27,28,29
		Shakespeare Cliff Siltstone	
		Tainui Shellbed	30,31,32
		Pinnacle Sand	
		Lower Castlecliff Shellbed	33,34,35
		Seafield Sand	36,37,38
		Upper Kai Iwi Siltstone	39
		Kupe Formation	8,40,41,42
	Okehuan	Upper Westmere Siltstone	47,48
		Kaikokapu Formation	43,44
		Lower Westmere Siltstone	
		Ophiomorpha Sand	
		Omapu Shellbed	45,46
		Lower Kai Iwi Siltstone	49
		Kaimatira Pumice Sand	50
		Upper Okehu Siltstone	
		Okehu Shell Grit	51,52,53
		Lower Okehu Siltstone	
		Mowhanau Formation	
		Ototoka Siltstone	
		Butler's Shell Conglomerate	54,55
Nukumaruan	Marahauan	Upper Maxwell Formation	
		Mangahou Siltstone	56
		Middle Maxwell Formation	
		Pukekiwi Shell Sand	57
		Lower Maxwell Formation	
		Tewkesbury Formation	
		Waipuru Shellbed	
		Nukumaru Brown Sand	58,59,60
		Mangamako Shellbed	
		Nukumaru Limestone	14
		Ohingaiti Sand	
	Hautawan	Undifferentiated Formations	
		Kuranui Limestone	
		Hautawa Shellbed	61
Waitotaran	Mangapanian	Te Rama Shellbed	
		Parihauhau Shellbed	
		Te Rimu Sand	
		Wilkies Shellbed	62
		Makokako Sand	
		Mangaweka Mudstone	
		Paparangi Sandstone	
	Waipipian	Waverley Formation	
		Upper Waipipi Shellbed	13,65,66
		Middle Waipipi Shellbed	63,67
		Lower Waipipi Shellbed	68
		Snapper Point Shellbed	4
		Rangikura Sandstone	
		Pepper Shell Sand	1,2,3

Fig 5.1 Stratigraphic Column of the Wanganui Series, after Fleming (1953) and Abbott and Carter (1991), showing sample points.

Table 5.1. Shell samples 1-68: Species, locations and ages

1. *Maoricardium spatiosum* - Pepper Shell Sand (c.3.6 My)
2. *Phialopecten marwicki* - Pepper Shell Sand (c.3.6 My)
3. *Maoricardium spatiosum* - Pepper Shell Sand (c.3.6 My)
4. *Maoricardium spatiosum* - Snapper Point Shellbed (c.3.5 My)
5. *Pecten tainui* - Landguard Formation (c.0.35 My)
6. *Anchomasa similis* - Castlecliff Beach (recent)
7. *Paphies (Mesodesma) subtriangulata quoii* - Long Beach (recent)
8. *Tiostrea chilensis* - Kupe Shellbed (c.0.7 My)
9. *Paphies australis* - Te Rauone Beach (recent)
10. *Chione (Austrovenus) stutchburyi* - Warrington Beach (recent)
11. *Paphies (Mesodesma) subtriangulata* - Warrington Beach (recent)
12. *Maoricolpus roseus* - Long Beach (recent)
13. *Maoricardium spatiosum* - Upper Waipipi (c.3.2 My)
14. *Patro undatus* - Nukumaru Limestone (c.1.45 My)
15. *Chione (Austrovenus) stutchburyi* - Te Rauone Beach (recent)
16. *Mactra discors* - Warrington Beach (recent)
17. *Spisula (Crassula) aequilateralis* - Rapanui Formation (c.0.12 My)
18. *Paphies (Mesodesma) subtriangulata* - Rapanui Formation (c.0.12 My)
19. *Tawera spissa* - Landguard Formation (c.0.35 My)
20. *Tiostrea chilensis lutaria* - Landguard Formation (c.0.35 My)
21. *Pecten tainui* - Landguard Formation (c.0.35 My)
22. *Zethalia zelandica* - Upper Castlecliff Shellbed (c.0.43 My)
23. *Paphies (Mesodesma) subtriangulata* - Upper Castlecliff Shellbed (c.0.43 My)
24. *Venericardia purpurata* - Upper Castlecliff Shellbed (c.0.43 My)
25. *Paphies (Mesodesma) subtriangulata* - Shakespeare Cliff Sand (c.0.44 My)
26. *Pecten tainui* - Shakespeare Cliff Sand (c.0.44 My)
27. *Tiostrea chilensis lutaria* - Shakespeare Cliff Sand (c.0.44 My)
28. *Paphies (Mesodesma) subtriangulata* - Shakespeare Cliff Sand (c.0.44 My)
29. *Venericardia purpurata* - Shakespeare Cliff Sand (c.0.44 My)
30. *Tiostrea chilensis lutaria* - Tainui Shellbed (c.0.5 My)
31. *Maoricolpus roseus* - Tainui Shellbed (c.0.5 My)
32. *Venericardia purpurata* - Tainui Shellbed (c.0.5 My)
33. *Pecten tainui* - Lower Castlecliff Shellbed (c.0.6 My)
34. *Maoricolpus roseus* - Lower Castlecliff Shellbed (c.0.6 My)
35. *Venericardia purpurata* - Lower Castlecliff Shellbed (c.0.6 My)
36. *Tiostrea chilensis lutaria* - Tom's Conglomerate (c.0.62 My)
37. *Venericardia purpurata* - Tom's Conglomerate (c.0.62 My)

38. *Paphies (Mesodesma) subtriangulata* - Tom's conglomerate (c.0.62 My)
39. *Tiostrea chilensis lutaria* - base of Upper Kai-Iwi Siltstone (c.0.68 My)
40. *Tiostrea chilensis lutaria* - Kupe Formation (c.0.7 My)
41. *Maoricolpus roseus* - Kupe Formation (c.0.7 My)
42. *Venericardia purpurata* - Kupe Formation (c.0.7 My)
43. *Paphies (Mesodesma) subtriangulata* - Kaikokapu Formation (c.0.78 My)
44. *Venericardia purpurata* - Kaikokapu Formation (c.0.78 My)
45. *Divaricella (Divalucina) huttoniana* - Omapu Shellbed (c.0.85 My)
46. *Amalda (Baryspira) mucronata* - Omapu Shellbed (c.0.85 My)
47. *Amalda (Baryspira) mucronata* - Upper Westmere Shellbed (c.0.8 My)
48. *Maoricolpus roseus* - Upper Westmere Shellbed (c.0.8 My)
49. *Paphies (Mesodesma) subtriangulata* - Lower Kai-Iwi Shellbed (c.0.9 My)
50. *Paphies (Mesodesma) subtriangulata* - Kaimatira Pumice Sand (c.0.95 My)
51. *Maoricrypta (Zeacrypta) monoxyla* - Okehu Shell Grit (c.0.99 My)
52. *Tiostrea chilensis lutaria* - Okehu Shell Grit (c.0.99 My)
53. *Venericardia purpurata* - Okehu Shell Grit (c.0.99 My)
54. *Maoricrypta (Zeacrypta) monoxyla* - Butler's Shell Conglomerate (c.1.07 My)
55. *Chlamys gemmulata* - Butler's Shell Conglomerate (c.1.07 My)
56. *Austrovenus stutchburyi* - Mangahou (c.1.26 My)
57. *Paphies (Mesodesma) subtriangulata* - Pukekiwi (c.1.3 My)
58. *Patro undatus* - Nukumaru Brown Sand (c.1.4 My)
59. *Tiostrea chilensis lutaria* - Nukumaru Brown Sand (c.1.4 My)
60. *Lutraria solida* - Nukumaru Brown Sand (c.1.4 My)
61. *Patro undatus* - Hautawa shellbed (c.2.4 My)
62. *Crassostrea ingens* - Wilkies Bluff (c.2.8 My)
63. *Crassostrea ingens* - Middle Waipipi (c.3.3 My)
64. *Ostrea lutraria* - Te Rauone Beach (recent)
65. *Lima waipipiensis* - Upper Waipipi (c.3.2 My)
66. *Crassostrea ingens* - Upper Waipipi (c.3.2 My)
67. *Maoricardium spatiosum* - Middle Waipipi (c.3.3My)
68. *Crassostrea ingens* - Lower Waipipi (c.3.4 My)

5.4 Results and Discussion

The temperatures obtained from each individual shell bed were plotted against age (Fig. 5.2). The results show a cooling of about 10°C at about 1 My from earlier warm interglacial temperatures (15-20°C) to cooler interglacial temperatures (5-10°C) which have lasted to the present (present New Zealand sea temperatures are around 11°C). Further evidence for a climatic cooling at around 1 My is provided by a significant extinction in molluscan faunas in New Zealand. This can be seen by plotting the percentage of genus groups present in each stratigraphic stage which survive into the next stage (fig. 5.3). The results reveal a sharp decline in the percentage of molluscan groups surviving between the Nukumaruan stage and the Castlecliffian stage, the base of which is marked by the base-Jaramillo magnetic reversal at 1.07 My (Turner and Kamp, 1990). This cooling coincides with the well documented increase in the amplitude of the 100 ky climatic cycle (Pisias and Moore, 1981; Ruddiman et al., 1989; Imbrie et al., 1993) and with a dramatic enrichment of $\delta^{18}O$ values in foraminifera in deep sea cores particularly during glacial phases, indicating larger glacial ice sheets and a colder boreal climate (Imbrie et al., 1993). The results also support those of Stevens and Vella (1981) who noted a significant drop in temperature indicated by isotopic analysis of shells of *Chlamys gemmulata* from the same stratigraphic levels in the Wanganui series. However, Stevens and Vella (1981) did not sample very far to either side of this event and furthermore used inaccurate fission track dating (Seward, 1974) to attribute a spurious age of 0.75 My to this event. Since then, the top-Jaramillo magnetic reversal (0.99 My, Shackleton et al., 1990) has been found at the Okehu Shell Grit, one of the key shellbeds over which the main episode of cooling occurs (fig. 5.1).

Oxygen isotope results from mollusc shells must be treated with some degree of caution: intra- and interspecific variations in rate of growth and seasonality of growth may severely bias an 'average composition' determined from a whole shell sample (Krantz et al., 1987), and the isotope composition may vary significantly even

Fig. 5.2 Palaeotemperatures calculated from stable oxygen isotope ratios plotted against the approximate age of shells

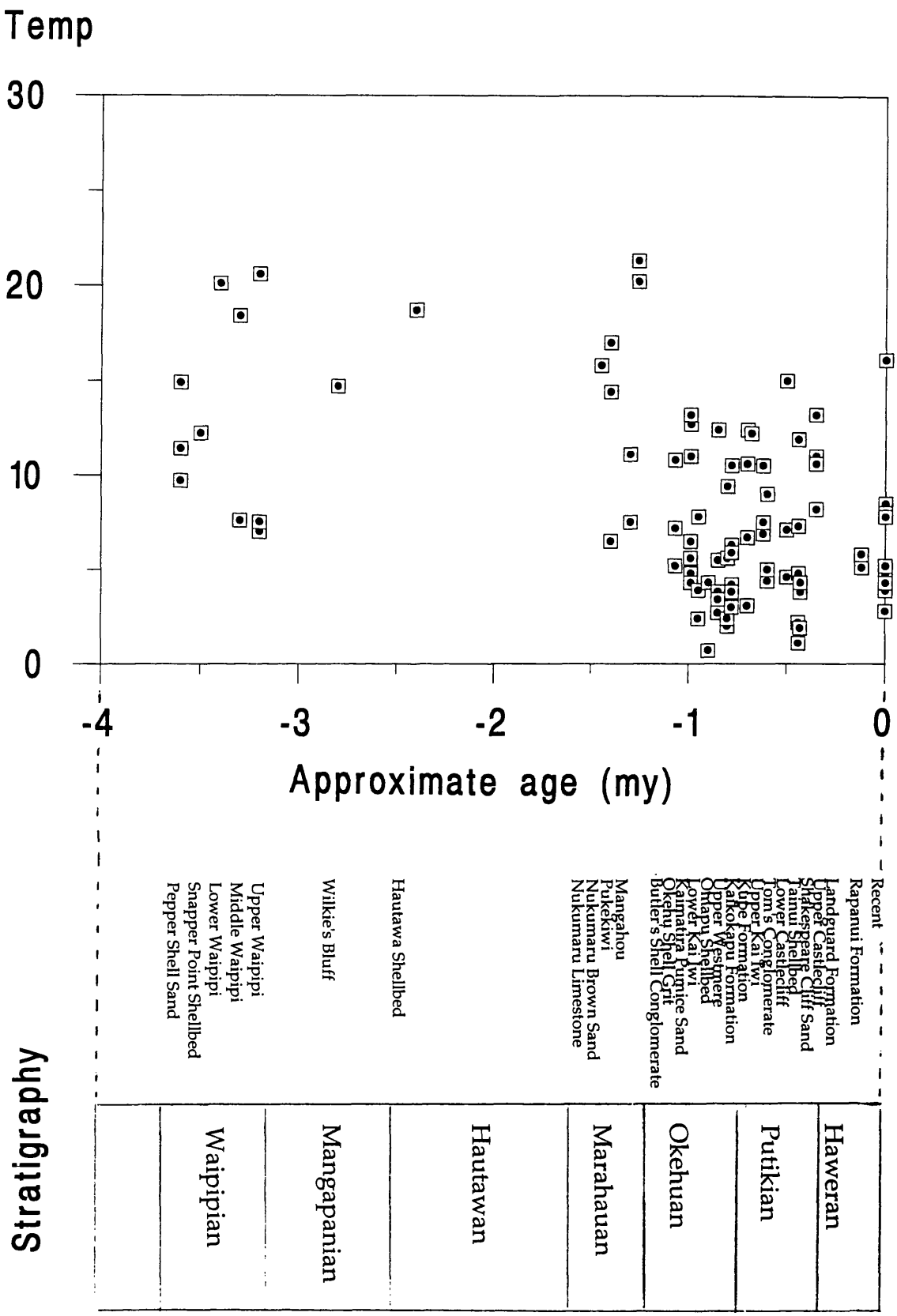

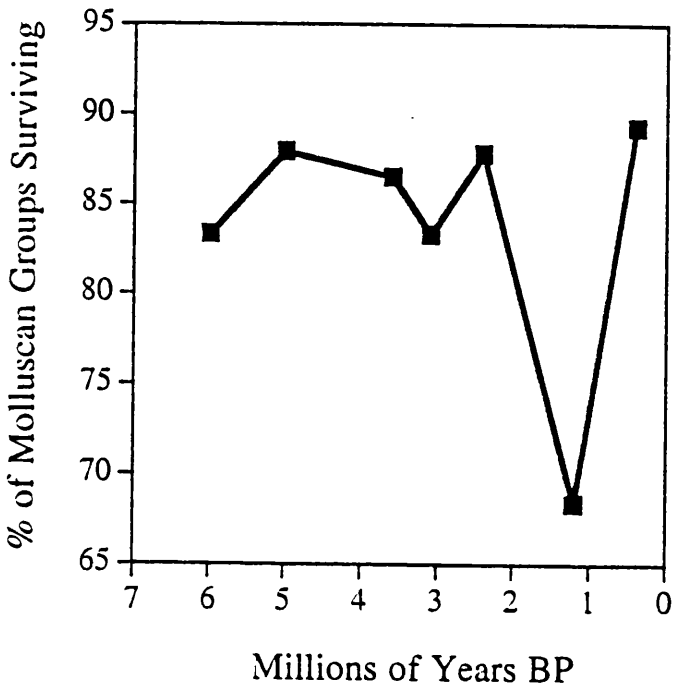

Fig 5.3 - Percentage of New Zealand Molluscan Groups surviving over the last 6 million years. The data have been compiled from stratigraphical range charts presented by Beu and Maxwell (1990), and represent the occurrence records of over 400 taxa of molluscan fossils displayed as 130 genus groups. The points on the graph represent the percentage of molluscan groups that are present in one stage, and survive to the following stage. From left to right on the diagram, the data points represent molluscan groups surviving from 1) the Tongaporutuan Stage (10.5Ma to 6.0Ma) into the Kapitean Stage; 2) from the Kapitean Stage (6.0Ma to 5.0Ma) into the Opoitian Stage; 3) from the Opoitian Stage (5.0Ma to 3.6Ma) into the Waipipian Stage; 4) from the Waipipian Stage (3.6Ma to 3.1Ma) into the Mangapanian Stage; 5) from the Mangapanian Stage (3.1Ma to 2.4Ma) into the Nukumaruan Stage; 6) from the Nukumaruan Stage (2.4Ma to 1.2Ma) into the Castlecliffian Stage; 7) from the Castlecliffian Stage (1.2Ma to 0.4Ma) into the Haweran Stage. The stratigraphic nomenclature and dates are from Beu & Maxwell (1990). Plot reveals a sharp decay in the percentage of molluscan groups suviving from the Nukumaruan into the Castlecliffian Stage around 1.2 Ma, corresponding to the pronounced drop in palaeotemperature determinations shown in Fig 5.2.

within one shell, particularly within shells of large, fast growing molluscs (Mitchell et al., 1994). Therefore, the stable isotope composition of most shell material is likely to reflect summer temperatures rather than yearly averages, and may appear to reflect anomalously warm temperatures due to kinetic effects in fast growing carbonates (McConnaughey, 1989; Mitchell et al., 1994). Shells of different species from within the same shellbed may have different isotopic compositions due to their different modes of life (infaunal or epifaunal), or due to mixing of shells of slightly different ages (and therefore different climate regimes). Many of the shellbeds of the Wanganui series contain current scoured concentrations of shells of burrowing and soft bottom species later colonised by epifaunal and encrusting species. However, the small variations in $\delta^{18}O$ seen within and between shellbeds due to these effects are expected to be consistent throughout the section. The sudden enrichment in $\delta^{18}O$ at about 1 My is so large, and is preceeded by and followed by such long periods of fairly consistent average $\delta^{18}O$ values, that it may not be explained by any of these effects and is considered to be real. The simultaneous extinction of molluscan faunas supports the view that the oxygen isotope record reflects a significant change in climate.

An independent indicater of global climate change is provided by the global strontium isotope ratio of seawater (DePaolo, 1987). The strontium isotope record shows a strong positive excursion at about 1 My (fig 4; Capo and DePaolo, 1990). The largest influence on the strontium isotope ratio of seawater is continental weathering (DePaolo, 1987), mainly of the minerals feldspar and calcite which release strontium from surface rocks into solution and give rivers a high $^{87}Sr/^{86}Sr$ ratio (Capo and DePaolo, 1990). The change in strontium isotope ratio at about 1 My, therefore, indicates a likely increase in the erosional input to the ocean which may be due to either an increase in the rate of precipitation or an increase in the area and height of the continents above sea level (i.e. a drop in sea level or an increase in the height of mountains). This evidence supports the theory that the change in climatic regime may have been associated with either mountain building or an increase in global ice

Fig 5.4 Strontium isotope record for the past 2.5 million years. From Capo and DePaolo (1990).

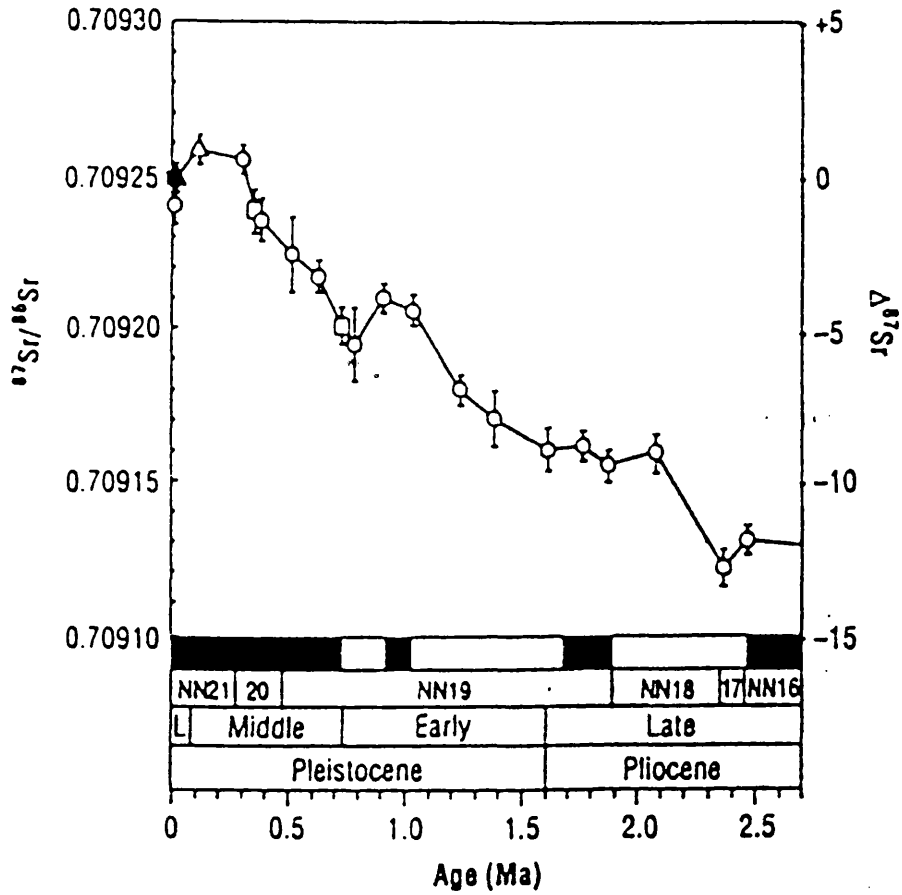

volume. Both of these would be likely to result in the increase in continental weathering indicated by the strontium record.

The well documented shift in the dominant climatic cycle from a 41 ky to a 100 ky cycle has been associated with an increase in global ice volume and glacio-eustatic changes which are of lower frequency but greater amplitude than before (Prell, 1983). Consequently it has been suggested that the average global climate over the past million years has been colder than before but interglacials may have been milder (Prell, 1983). These results show that this may not be the case, and that at least for this region of New Zealand, the past million years have been characterized by significantly cooler interglacials than those of the earlier Pleistocene.

One consequence of the large amplitude fluctuations in temperature and ice volume is that sea level changes are likely to have been much larger than those of the earlier Pleistocene. In general, the early Pleistocene sea level changes would affect only the inner and middle shelf areas, whereas the late Pleistocene sea level changes may have resulted in the alternate flooding and exposure of the entire shelf (Prell, 1983). Indeed, this is reflected in the nature of the glacial unconformities throughout the Wanganui sequence: earlier unconformities (before 1 My) are fully marine whereas some of the later ones show signs of land exposure. Such major marine regressions may have influenced the influx of freshwater into the shelf seas causing changes to the strontium isotope ratio of the ocean but is very unlikely to account for such a large and consistent change in $\delta^{18}O$ as seen here; an influx of freshwater would in any case tend to cause a decrease in $\delta^{18}O$ rather than the increase seen here, which is therefore in our opinion most likely to be a true reflection of interglacial palaeotemperatures linked to the known increase in amplitude of the 100 ky cyclicity in global climate and increase in northern hemisphere glaciation.

This mid Pleistocene cooling, therefore, despite its close link with feedback mechanisms operating mostly in the higher latitudes of the northern hemisphere (mountains and marine based ice sheets), may have resulted in cooler interglacials than before in the southern

hemisphere as well as much cooler glacial periods over the whole globe. These results show that temperatures in the higher latitudes of the Southern hemisphere have undergone a significant change and this is presumably due to the strong feedback effects inherent in this area associated with albedo and the rate of growth and decay of ice. These effects may also be the cause of changing ocean currents resulting in the deflection or channelling of cold Antarctic ocean water in a northerly direction, producing colder sea temperatures around the coasts of the southern land masses.

5.5 Conclusions

There is a significant enrichment in the $\delta^{18}O$ values from mollusc shells from interglacial shellbeds from Wanganui, New Zealand at about 1 My. This is thought to reflect a cooling of about 10°C in interglacial temperatures in this region which coincides with a well documented change in the dominant global climate periodicity from a 41 ky to a 100 ky cycle. Further evidence for climatic change is provided by a significant molluscan extinction event in New Zealand and a positive excursion in the strontium isotope ratio of seawater. The reasons for the increase in amplitude of the 100 ky cycle are not fully understood and are not directly related to insolation, but may be related to feedback effects associated with an increase in the height of major mountain ranges, or with the growth of larger ice sheets in the high latitudes of the northern and southern hemisphere, or with changing ocean currents producing colder sea temperatures around the coasts of the southern land masses.

Appendix 5.1 Data Table

Sample	$\delta^{13}C1$	$\delta^{18}O1$	$\delta^{13}C2$	$\delta^{18}O2$	$\delta^{13}C$ ave	$\delta^{18}O$ ave	C/A	T (°C)	Age (My)
1	0.20	1.25	0.16	1.23	0.18	1.24	40/60	9.7	3.6
2	1.23	0.37	1.56	0.71	1.39	0.54	0/100	11.4	3.6
3	-1.34	0.33	-1.47	0.29	-1.40	0.31	75/25	14.9	3.6
4	-1.55	0.68	-1.55	0.66	-1.55	0.67	40/60	12.2	3.5
5	0.98	1.44	1.66	1.71	1.32	1.57	100/0	10.6	0.35
6	1.65	1.82	1.39	2.24	1.52	2.03	0/100	4.8	0
7	0.93	1.47	0.84	0.92	0.88	1.19	0/100	8.5	0
8	1.74	2.09	0.93	1.06	1.34	1.58	100/0	10.6	0.7
9	1.76	2.23	1.70	2.23	1.73	2.23	0/100	3.9	0
10	1.25	1.30	1.26	1.29	1.26	1.30	0/100	8	0
11	0.01	2.18	1.38	2.11	0.69	2.14	0/100	4.3	0
12	3.07	1.84	3.16	2.03	3.11	2.50	0/100	2.8	0
13	-0.57	1.53	-0.55	1.55	-0.56	1.54	0/100	7	3.2
14	1.56	0.37	1.51	0.21	1.53	0.29	100/0	15.8	1.45
15	0.77	1.31	0.29	1.40	0.53	1.35	0/100	7.8	0
16	0.88	1.95	0.93	1.94	0.91	1.94	0/100	5.2	0
17	1.53	1.43	2.13	2.48	1.83	1.96	0/100	5.1	0.12
18	1.90	1.84	1.48	1.75	1.69	1.80	0/100	5.8	0.12
19	0.48	1.30	0.44	1.22	0.46	1.26	0/100	8.2	0.35
20	2.02	0.93	2.09	0.91	2.05	0.92	100/0	13.2	0.35
21	1.47	1.46	1.49	1.67	1.48	1.47	100/0	11	0.35
22	2.30	2.75	2.30	2.66	2.30	2.71	0/100	1.9	0.43
23	1.22	2.33	0.98	2.16	1.10	2.25	0/100	3.8	0.43
24	1.93	2.20	2.04	2.10	1.98	2.15	0/100	4.3	0.43
25	1.67	2.63	1.71	2.61	1.69	2.62	0/100	2.2	0.44
26	1.69	2.39	1.75	2.54	1.72	2.47	100/0	7.3	0.44
27	1.92	1.19	1.98	1.28	1.95	1.23	100/0	11.9	0.44
28	1.53	2.89	1.54	2.89	1.53	2.89	0/100	1.1	0.44
29	1.59	1.96	1.68	2.10	1.63	2.03	0/100	4.8	0.44
30	0.89	0.49	0.96	0.47	0.92	0.48	100/0	15	0.5
31	2.70	2.15	2.68	1.99	2.69	2.07	0/100	4.6	0.5
32	1.53	1.73	1.34	1.65	1.43	1.68	20/80	7.1	0.5
33	1.07	2.01	1.06	1.99	1.06	2.00	100/0	9	0.6
34	2.32	2.13	2.41	2.14	2.37	2.13	0/100	4.4	0.6
35	1.03	1.98	1.04	1.98	1.03	1.98	0/100	5	0.6

36	2.09	1.56	2.12	1.64	2.11	1.60	100/0	10.5	0.62
37	1.50	1.59	1.55	1.50	1.52	1.54	0/100	6.9	0.62
38	0.92	1.37	0.93	1.46	0.93	1.42	0/100	7.5	0.62
39	1.75	1.20	1.71	1.12	1.72	1.16	100/0	12.2	0.68
40	1.71	1.10	1.68	1.12	1.69	1.11	100/0	12.4	0.7
41	2.60	2.41	2.57	2.44	2.58	2.43	0/100	3.1	0.7
42	1.82	1.90	0.88	1.30	1.35	1.60	0/100	6.7	0.7
43	0.74	2.44	0.76	2.44	0.75	2.44	0/100	3	0.78
44	0.95	1.79	0.92	1.68	0.93	1.74	/95	6.3	0.78
45	0.82	2.29	0.90	2.21	0.86	2.25	0/100	3.8	0.85
46	0.78	2.36	0.78	2.36	0.78	2.36	0/100	3.4	0.85
47	0.17	2.67	0.13	2.67	0.15	2.67	0/100	2	0.8
48	2.46	2.17	2.49	2.19	2.48	2.18	0/100	4.2	0.8
49	1.36	2.94	1.38	3.02	1.37	2.98	0/100	0.7	0.9
50	0.99	2.56	0.97	2.59	0.98	2.57	0/100	2.4	0.95
51	0.76	1.84	0.78	1.87	0.77	1.85	0/100	5.6	0.99
52	2.38	1.03	2.46	1.05	2.42	1.04	100/0	12.7	0.99
53	2.11	1.68	2.11	1.62	2.11	1.65	0/100	6.5	0.99
54	0.29	1.93	0.24	1.94	0.26	1.93	0/100	5.2	1.07
55	1.63	1.49	1.59	1.54	1.61	1.52	100/0	10.8	1.07
56	-0.74	-1.40	-0.69	-1.37	-0.72	-1.38	0/100	20.2	1.26
57	-0.40	0.59	-0.47	0.62	-0.44	0.60	0/100	11.1	1.3
58	1.00	0.00	1.08	0.02	1.04	0.01	100/0	17	1.4
59	0.88	0.63			0.88	0.62	100/0	14.4	1.4
60	-0.48	1.60	-0.46	1.68	-0.47	1.64	0/100	6.5	1.4
61	2.47	-0.39	2.40	-0.39	2.43	-0.39	100/0	18.7	2.4
62	0.56	0.53	0.50	0.77	0.53	0.65	100/0	14.7	2.8
63	-1.02	-0.31			-1.02	-0.31	100/0	18.4	3.3
64	1.14	0.07	1.98	0.86	1.56	0.22	100/0	16.1	0
65	1.73	1.66	1.52	1.87	1.62	1.77	40/60	7.5	3.2
66	-5.04	-2.27	-3.68	0.67	-4.36	-0.80	100/0	20.6	3.2
67	-0.44	1.20	-0.34	1.59	-0.39	1.37	0/100	7.6	3.3
68	-2.23	-0.74	-1.95	-0.63	-2.09	-0.69	100/0	20.1	3.4

Lists of Mollusc Species from each Shellbed

Pepper Shell Sand

Anomia trigonopsis (Hutton)
Atrina pectinata zelandica (Gray)
Chlamys gemmulata (Reeve)
Crassostrea ingens (Zittel)
Crepidula radiata (Hutton)
Eumarcia (Eumarcia) plana (Marwick)
Lima waipipiensis (Marshall and Murdoch)
Maoricardium spatiosum (Hutton)
Miltha neozelanica (Marshall and Murdoch)
Modiolus areolatus (Gould)
Panopea zelandica (Quoy and Gaimard)
Patro undatus (Hutton)
Phialopecten marwicki (Beu)
Polinices waipipiensis (Marwick)
Purpurocardia purpurata (Deshayes)
Thracia magna (Marshall and Murdoch)
Tiostrea chilensis lutaria (Hutton)

Snapper Point Shellbed

Amalda (Baryspira) mucronata (Sowerby)
Anomia trigonopsis (Hutton)
Atrina pectinata zelandica (Gray)
Austrofusus (Austrofusus) pagoda (Finley)
Chlamys gemmulata (Reeve)
Crepidula radiata (Hutton)
Dosinia (Kereia) greyi (Zittel)
Gari lineolata (Gray)
Maoricardium spatiosum (Hutton)
Maoricolpus roseus (Quoy and Gaimard)
Marama (Marama) murdochi (Marwick)
Mesopeplum (Borehamia) crawfordi (Hutton)
Neilo sublaevis (Marwick)
Nemocardium (Pratulum) quinarium (Marwick)
Pelicaria zelandiae (Marshall and Murdoch)
Phialopecten marwicki (Beu)
Polinices waipipiensis (Marwick)
Pteromyrtea dispar (Hutton)
Scalpomactra scalpellum (Reeve)
Stiracolpus huttoni (Cossman)

Lower Waipipi Shellbed

Lutraria solida (Hutton)
Maoricardium spatiosum (Hutton)
Maoricolpus roseus (Quoy and Gaimard)
Panopea zelandica (Quoy and Gaimard)
Pelicaria zelandiae (Marshall and Murdoch)
Phialopecten marwicki (Beu)
Pteromyrta dispar (Hutton)

Scalpomactra scalpellum (Reeve)
Zethalia zelandica (Hombron and Jacquinot)

Middle Waipipi Shellbed

Alcithoe (Leporemax) gatesi (Marwick)
Amalda (Baryspira) mucronata (Sowerby)
Anomia trigonopsis (Hutton)
Austrofusus (Austrofusus) pagoda (Finley)
Cirsotrema zelebori (Dunker)
Crepidula radiata (Hutton)
Divaricella (Divalucina) huttoniana (Vanatta)
Dosinia (Kereia) greyi (Zittel)
Eumarcia (Atamarcia benhami (Marwick)
Eumarcia (Eumarcia) plana (Marwick)
Gari lineolata (Gray)
Glycymerita (Manaia) manaiaensis (Marwick)
Lamprodomina neozelanica (Hutton)
Lima waipipiensis (Marshall and Murdoch)
Maoricardium spatiosum (Hutton)
Maoricolpus roseus (Quoy and Gaimard)
Nemocardium (Pratulum) quinarium (Marwick)
Pelicaria zelandiae (Marshall and Murdoch)
Phialopecten marwicki (Beu)
Polinices waipipiensis (Marwick)
Pteromyrtea dispar (Hutton)
Scalpomactra scalpellum (Reeve)
Taniella planisuturalis (Marwick)

Upper Waipipi Shellbed

Alcithoe (Leporemax) gatesi (Marwick)
Amalda (Baryspira) mucronata (Sowerby)
Anomia trigonopsis (Hutton)
Austrofusus (Austrofusus) pagoda (Finley)
Bassina yatei (Grey)
Chlamys gemmulata (Reeve)
Crassostrea ingens (Zittel)
Crepidula radiata (Hutton)
Divaricella (Divalucina) huttoniana (Vanatta)
Gari lieolata (Gray)
Lamprodomina neozelanica (Hutton)
Leptomya retiaria (Hutton)
Lima waipipiensis (Marshall and Murdoch)
Limaria orientalis (Adams and Reeve)
Lutraria solida (Hutton)
Maoricardium spatiosum (Hutton)
Maoricolpus roseus (Quoy and Gaimard)
Modiolus areolatus (Gould)
Patro undatus (Hutton)
Pelicaria zelandiae (Marshall and Murdoch)
Phialopecten marwicki (Beu)
Polinices waipipiensis (Marwick)
Pteromyrtea dispar (Hutton)
Scalpomactra scalpellum (Reeve)
Stiracolpus huttoni (Cossman)

Struthiolaria (Struthiolaria) papulosa (Martyn)
Thracia magna (Marshall and Murdoch)
Zethalia zelandica (Hombron and Jacquinot)

Wilkies Shellbed

Amalda (Baryspira) mucronata (Sowerby)
Bassina yatei (Gray)
Chlamys gemmulata (Reeve)
Cirsotrema zelebori (Dunker)
Crassostrea ingens (Zittel)
Crepidula radiata (Hutton)
Eumarcia (Eumarcia) plana (Marwick)
Limatula maoria (Finley)
Maoricardium spatiosum (Hutton)
Maoricolpus roseus (Quoy and Gaimard)
Modiolus areolatus (Gould)
Nucula nitidula (Adams)
Patro undatus (Hutton)
Phenatoma rosea (Quoy and Gaimard)
Phialopecten marwicki (Beu)
Pleuromeris marshalli (Marwick)
Purpurocardia purpurata (Deshayes)
Sigapatella novaezelandiae (Lesson)
Talabrica senecta (Powell)
Taniella planisuturalis (Marwick)
Tawera subsulcata (Suter)
Trachycardium (Ovicardium) rossi (Marwick)
Zenatia acinaces (Quoy and Gaimard)

Hautawa Shellbed

Anomia trigonopsis (Hutton)
Atrina pectinata zelandica (Gray)
Austrofusus taitae (Marwick)
Barbatia novaezelandiae (Smith)
Barnea (Anchomasa) similis (Gray)
Chlamys gemmulata (Reeve)
Dosinia (Kereia) greyi (Zittel)
Maoricolpus roseus (Quoy and Gaimard)
Mesopeplum (Mesopeplum) convexum (Quoy and Gaimard)
Modiolus areolatus (Gould)
Myadora striata (Quoy and Gaimard)
Patro undatus (Hutton)
Pleuromeris hectori (Powell)
Purpurocardia purpurata (Deshayes)
Sigapatella novaezelandiae (Lesson)
Stiracolpus symmetricus (Hutton)
Talabrica senecta (Powell)
Tawera subsulcata (Suter)

Nukumaru Limestone

Austrovenus stutchburyi crassitesta (Finlay)
Barytellina crassidens (Marwick)
Chlamys gemmulata (Reeve)
Cirsotrema zelebori (Dunker)
Crepidula radiata (Hutton)
Eumarcia (Eumarcia) plana (Marwick)
Glycymeris shrimptoni (Marwick)
Lutraria solida (Hutton)
Maoricolpus roseus (Quoy and Gaimard)
Paphies crassiformis (Marshall and Murdoch)
Patro undatus (Hutton)
Pleuromeris hectori (Powell)
Purpurocardia purpurata (Deshayes)
Sigapatella novaezelandiae (Lesson)
Spisula (Spisulona) crassitesta (Finlay)
Tawera subsulcata (Suter)
Zethalia zelandica (Hombron and Jacquinot)

Nukumaru Brown Sand

Amalda (Baryspira) australis (Sowerby)
Amalda (Baryspira) mucronata (Sowerby)
Atrina pectinata zelandica (Gray)
Austrovenus stutchburyi crassitesta (Finlay)
Barnea (Anchomasa) similis (Gray)
Barytellina crassidens (Marwick)
Bassina yatei (Gray)
Chlamys gemmulata (Reeve)
Cirsotrema zelebori (Dunker)
Crepidula radiata (Hutton)
Divaricella (Divalucina) huttoniana (Vanatta)
Eumarcia (Eumarcia) plana (Marwick)
Gonimyrtea concinna (Hutton)
Leptomya retiaria (Hutton)
Lutraria solida (Hutton)
Mactra discors (Gray)
Maoricolpus roseus (Quoy and Gaimard)
Myadora striata (Quoy and Gaimard)
Nucula nitidula (Adams)
Panopea zelandica (Quoy and Gaimard)
Paphies australis (Gmelin)
Paphies crassiformis (Marshall and Murdoch)
Paratrophon cheesemani (Hutton)
Patro undatus (Hutton)
Pleuromeris marshalli (Marwick)
Pteromyrtea dispar (Hutton)
Purpurocardia purpurata (Deshayes)
Sigapatella novaezelandiae (Lesson)
Tawera subsulcata (Suter)
Tiostrea chilensis lutaria (Hutton)
Zethalia zelandicum (Hombron and Jacquinot)

Pukekiwi Shell Sand

Amalda (Baryspira) mucronata (Sowerby)
Amphibola crenata (Gmelin)
Austrovenus stutchburyi crassitesta (Finlay)
Barytellina crassidens (Marwick)
Dosinia (Phacosoma) subrosea (Gray)
Eumarcia (Eumarcia) plana (Marwick)
Myadora striata (Quoy and Gaimard)
Paphies australis (Gmelin)
Paphies subtriangulata (Gray)
Patro undatus (Hutton)
Pteromyrtea dispar (Hutton)
Spisula (Crassula) aequilateralilis (Deshayes)
Spisula (Spisulona) crassitesta (Finlay)
Tawera spissa (Hutton)
Zethalia zelandica (Hombron and Jacquinot)

Mangahou Siltstone

Austrovenus stutchburyi crassitesta (Finlay)
Barbatia novaezelandiae (Smith)
Cyclomactra ovata (Gray)
Spisula (Crassula) aequilateralis (Deshayes)

Butler's Shell Conglomerate

Aeneator (Aeneator) marshalli (Murdoch)
Alcithoe (Alcithoe arabica (Gmelin)
Amalda (Baryspira) mucronata (Sowerby)
Amalda (Gracilispira) novaezelandiae (Sowerby)
Amphibola crenata (Gmelin)
Austrovenus stutchburyi (Gray)
Barbatia novaezelandiae (Smith)
Barnea (Anchomasa) similis (Gray)
Barytellina crassidens (Marwick)
Cardita aoteana (Finley)
Chlamys gemmulata (Reeve)
Cirsotrema zelebori (Dunker)
Crepidula radiata (Hutton)
Cyclomactra ovata (Gray)
Dosinia (Austrodosinia) anus (Philippi)
Dosinia (Phacosoma) subrosea (Gray)
Duplicaria (Pervicacia) tristis (Deshayes)
Glycymeris (Glycymerula) modesta (Angas)
Leptomya retiaria (Hutton)
Maoricolpus roseus (Quoy and Gaimard)
Nemocardium pulchellum (Gray)
Notocallista (Striacallista) multistriata (Suter)
Paphies australis (Gmelin)
Paratrophon cheesemani (Hutton)
Phenotoma rosea (Quoy and Gaimard)
Poirieria zelandica (Quoy and Gaimard)
Purpurocardia purpurata (Deshayes)
Ruditapes largillierti (Philippi)
Scalpomactra scalpellum (Reeve)

Sigapatella novaezelandiae (Lesson)
Tanea zelandica (Quoy and Gaimard)
Tawera spissa (Hutton)
Tiostrea chilensis lutaria (Hutton)
Trochus (Coelotrochus) tiaratus (Quoy and Gaimard)
Xymene expansus (Hutton)
Zeacumantus lutulensis (Kiener)
Zethalia zelandica (Hombron and Jacquinot)

Okehu Shell Grit

Aeneator (Aeneator) marshalli (Murdoch)
Alcithoe swainsoni (Marwick)
Amalda (Baryspira) mucronata (Sowerby)
Amalda (Gracilispira) novaezelandiae (Sowerby)
Atrina pectinata zelandica (Gray)
Aulacomya ater maoriana (Iredale)
Austrovenus stutchburyi (Gray)
Barbatia novaezelandica (Smith)
Barnea (Anchomasa) similis (Gray)
Cardita aoteana (Finlay)
Chlamys gemmulata (Reeve)
Cirsotrema zelebori (Dunker)
Crepidula radiata (Hutton)
Cyclomactra ovata (Gray)
Gari stangeri (Gray)
Globisinium drewi (Marwick)
Glycymeris (Glycymerula) modesta (Angas)
Leptomya retiaria (Hutton)
Maoricolpus roseus (Quoy and Gaimard)
Modiolus areolatus (Gould)
Myadora striata (Quoy and Gaimard)
Nemocardium pulchellum (Gray)
Notocallista (Striacallista) multistriata (Suter)
Nucula nitidula (Adams)
Paratrophon cheesemani (Hutton)
Poirieria zelandica (Quoy and Gaimard)
Purpurocardia purpurata (Deshayes)
Sigapatella novaezelandiae (Lesson)
Tanea zelandica (Quoy and Gaimard)
Tawera spissa (Hutton)
Tiostrea chilensis lutaria (Hutton)
Trochus (Coelotrochus) tiaratus (Quoy and Gaimard)
Xymene bonnetti bonnetti (Cossman)
Xymene expansus (Hutton)
Zegalerus tenuis (Gray)
Zenatia acinaces (Quoy and Gaimard)
Zethalia zelandica (Hombron and Jacquinot)

Kaimatira Pumice Sand

Aeneator (Aeneator) delicatulus (Powell)
Amalda (Baryspira) mucronata (Sowerby)
Austrofusus (Austrofusus) glans (Roding)
Barbatia novaezelandiae (Smith)
Barnea (Anchomasa) similis (Gray)

Cardita aoteana (Finlay)
Chlamys gemmulata (Reeve)
Cirsotrema zelebori (Dunker)
Crepidula radiata (Hutton)
Cyclomactra ovata (Gray)
Glaphyrina caudata (Quoy and Gaimard)
Glycymeris (Glycymerula) modesta (Angas)
Leptomya retiaria (Hutton)
Lima colorata (Hutton)
Maoricolpus roseus (Quoy and Gaimard)
Nemocardium pulchellum (Gray)
Notocallista (Striacallista) multistriata (Suter)
Nucula nitidula (Adams)
Paphies subtriangulata (Gray)
Paratrophon cheesemani (Hutton)
Purpurocardia purpurata (Deshayes)
Scalpomactra scalpellum (Reeve)
Sigapatella novaezelandiae (Lesson)
Struthiolaria (Struthiolaria) papulosa (Martyn)
Tanea zelandica (Quoy and Gaimard)
Tawera spissa (Deshayes)
Tiostrea chilensis lutaria (Hutton)
Xymene bonnetti bonnetti (Cossman)
Xymene expansus (Hutton)
Zethalia zelandica (Hombron and Jacquinot)

Lower Kai Iwi Shellbed

Aeneator (Aeneator) delicatulus (Powell)
Alcithoe swainsoni (Marwick)
Amalda (Baryspira) mucronata (Sowerby)
Amalda (Gracilispira) novaezelandica (Sowerby)
Antalis nana (Hutton)
Austrofusus (Austrofusus) glans (Roding)
Buccinulum caudatum (Powell)
Chlamys gemmulata (Quoy and Gaimard)
Dosinia (Kereia) greyi (Zittel)
Dosinia lambata (Gould)
Gari stangeri (Gray)
Globisinum drewi (Murdoch)
Iredalula striata (Hutton)
Maoricolpus roseus (Quoy and Gaimard)
Neilo australis (Quoy and Gaimard)
Nemocardium pulchellum (Gray)
Notocallista (Striacallista) multistriata (Suter)
Paphies australis (Gmelin)
Paphies subtriangulata (Gray)
Paracomitas (Paracomitas) gemmea (Murdoch)
Pelicaria vermis (Martyn)
Poirieria zelandica (Quoy and Gaimard)
Sigapatella novaezelandiae (Lesson)
Tanea zelandica (Quoy and Gaimard)
Varinucula sagittata (Suter)
Xymene bonnetti bonnetti (Cossman)
Zenatia acinaces (Gmelin)

Omapu Shellbed

Aeneator (Aeneator) delicatulus (Powell)
Amalda (Baryspira) mucronata (Sowerby)
Amalda (Gracilispira) novaezelandica (Sowerby)
Antalis nana (Hutton)
Atrina pectinata zelandica (Gray)
Austrofusus (Austrofusus) glans (Roding)
Buccinulum caudatum (Powell)
Chlamys gemmulata (Reeve)
Diplodonta (Zemysina) globus (Finley)
Divaricella (Divalucina) huttoniana (Vanatta)
Dosinia (Kereia) greyi (Zittel)
Dosinia lambata (Gould)
Gari lineolata (Gray)
Globisinium drewi (Murdoch)
Iredalula striata (Hutton)
Maoricolpus roseus (Quoy and Gaimard)
Neilo australis (Quoy and Gaimard)
Nemocardium pulchellum (Gray)
Notocallista (Striacallista) multistriata (Suter)
Nucula nitidula (Adams)
Pelicaria vermis (Martyn)
Phenatoma rosea (Quoy and Gaimard)
Pleuromeris zelandica (Deshayes)
Poirieria zelandica (Quoy and Gaimard)
Scalpomactra scalpellum (Reeve)
Tanea zelandica (Quoy and Gaimard)
Tiostrea chilensis lutaria (Hutton)
Trichosirius inornatus (Hutton)
Xymene bonnetti bonnetti (Cossman)
Zenatia acinaces (Gmelin)

Upper Westmere Shellbed

Amalda (Baryspira) mucronata (Sowerby)
Astraea heliotropium (Martyn)
Austrofusus (Austrofusus) glans (Roding)
Chlamys gemmulata (Reeve)
Diplodonta (Zemysina) globus (Finlay)
Divaricella (Divalucina) huttoniana (Vanatta)
Dosinia (Kereia) greyi (Zittel)
Dosinia lambata (Gould)
Gari lineolata (Gray)
Iredalula striata (Hutton)
Maoricolpus roseus (Quoy and Gaimard)
Neilo australis (Quoy and Gaimard)
Nemocardium pulchellum (Gray)
Notocallista (Striacallista) multistriata (Suter)
Pelicaria vermis (Martyn)
Poirieria zelandica (Quoy and Gaimard)
Sigapatella novaezelandiae (Lesson)
Tanea zelandica (Quoy and Gaimard)
Xymene bonnetti bonnetti (Cossman)
Zenatia acinaces (Gmelin)

Kaikokapu Shell Grit

Amalda (Baryspira) mucronata (Sowerby)
Antalis nana (Hutton)
Austrofusus (Austrofusus) glans (Roding)
Barbatia novaezelandiae (Smith)
Barnea (Anchomasa) similis (Gray)
Cardita aoteana (Finlay)
Cirsotrema zelebori (Dunker)
Chlamys gemmulata (Reeve)
Cyclomactra ovata (Gray)
Glycymeris (Glycymerula) modesta (Angas)
Leptomya retiaria (Hutton)
Nemocardium pulchellum (Gray)
Nucula nitidula (Adams)
Paphies subtriangulata (Gray)
Paratrophon cheesemani (Hutton)
Phenatoma rosea (Quoy and Gaimard)
Poirieria zelandica (Quoy and Gaimard)
Purpurocardia purpurata (Deshayes)
Sigapatella novaezelandiae (Lesson)
Tanea zelandica (Quoy and Gaimard)
Tenuiactaeon ambiguus (Hutton)
Xymene expansus (Hutton)

Kupe Formation

Aeneator denticulus (Powell)
Aeneator marshalli marshalli (Murdoch)
Alcithoe swainsoni (Marwick)
Amalda (Baryspira) mucronata (Sowerby)
Amalda (Gracilispira) novaezelandiae (Sowerby)
Antalis nana (Hutton)
Antimelatoma buchani (Hutton)
Aoteadrillia wanganuiensis (Hutton)
Astraea heliotropium (Martyn)
Atrina pectinata zelandica (Gray)
Aulacomya ater maoriana (Iredale)
Austrofusus (Austrofusus) glans (Roding)
Barnea (Anchomasa) similis (Gray)
Cardita aoteana (Finlay)
Chlamys gemmulata (Reeve)
Cirsotrema zelebori (Dunker)
Crepidula radiata (Hutton)
Cyclomactra ovata (Gray)
Dosinia lambata (Gould)
Dosinia (Phacosoma) subrosea (Gray)
Gari lineolata (Gray)
Gari stangeri (Gray)
Globisinum drewi (Murdoch)
Glycymeris (Glycymerula) modesta (Angas)
Iredalula striata (Hutton)
Leptomya retiaria (Hutton)
Limaria orientalis (Adams and Reeve)
Maoricolpus roseus (Quoy and Gaimard)
Myadora striata (Quoy and Gaimard)
Nemocardium pulchellum (Gray)

Notocallista (Striacallista) multistriata (Sowerby)
Nucula nitidula (Adams)
Paratrophon cheesemani (Hutton)
Pelicaria convexa (Marwick)
Phenatoma rosea (Quoy and Gaimard)
Pleuromeris zelandica (Desheyes)
Poirieria zelandica (Quoy and Gaimard)
Purpurocardia purpurata (Desheyes)
Sigapatella novaezelandiae (Lesson)
Tanea zelandica (Quoy and Gaimard)
Tawera spissa (Deshayes)
Tiostrea chilensis lutaria (Hutton)
Xymene bonnetti bonnetti (Cossman)
Xymene expansus (Hutton)
Zeacolpus (Zeacolpus) vittatus (Hutton)
Zethalia zelandica (Hombron and Jacquinot)

Upper Kai Iwi Shellbed

Alcithoe swainsoni (Marwick)
Amalda (Baryspira) mucronata (Sowerby)
Amalda (Gracilispira) novaezelandiae (Sowerby)
Atrina pectinata zelandica (Gray)
Austrofusus (Austrofusus) glans (Roding)
Chlamys gemmulata (Reeve)
Divaricella (Divalucina) huttoniana (Vanatta)
Dosinia (Kereia) greyi (Zittel)
Globisinum drewi (Murdoch)
Iredalula striata (Hutton)
Leptomya retiaria (Hutton)
Maoricolpus roseus (Quoy and Gaimard)
Myadora boltoni (Smith)
Neilo australis (Quoy and Gaimard)
Notocallista (Striacallista) multistriata (Sowerby)
Pleuromeris zelandica (Deshayes)
Poirieria zelandica (Quoy and Gaimard)
Struthiolaria papulosa (Martyn)
Tanea zelandica (Quoy and Gaimard)
Tawera spissa (Deshayes)
Tiostrea chilensis lutaria (Hutton)
Zenatia acinaces (Quoy and Gaimard)

Tom's Conglomerate

Austrovenus stutchburyi (Gray)
Pleuromeris zelandica (Deshayes)
Purpurocardia purpurata (Deshayes)
Tiostrea chilensis lutaria (Hutton)

Lower Castlecliff Shellbed

Amalda (Baryspira) mucronata (Sowerby)
Austrofusus (Austrofusus) glans (Roding)
Cardita aoteana (Finley)
Crepidula radiata (Hutton)

Chlamys gemmulata (Reeve)
Divaricella (Divalucina) huttoniana (Vanatta)
Gari stangeri (Gray)
Gari lineolata (Gray)
Leptomya retiaria (Hutton)
Limaria orientalis (Adams and Reeve)
Maoricolpus roseus (Quoy and Gaimard)
Maorimactra acuminella (Finlay)
Mesopeplum convexum (Quoy and Gaimard)
Nemocardium pulchellum (Gray)
Notocallista (Striacallista) multistriata (Sowerby)
Notocorbula zelandica (Quoy and Gaimard)
Pecten tainui (Fleming)
Pleuromeris zelandica (Deshayes)
Purpurocardia purpurata (Deshayes)
Scalpomactra scalpellum (Reeve)
Sigapatella novaezelandica (Lesson)
Tanea zelandica (Quoy and Gaimard)
Tawera spissa (Deshayes)
Tiostrea chilensis lutaria (Hutton)
Zeacolpus (Zeacolpus) vittatus (Hutton)

Tainui Shellbed

Aeneator marshalli marshalli (Murduch)
Alcithoe (Leporemax) fusus fusus (Quoy and Gaimard)
Alcithoe swainsoni (Marwick)
Amalda (Baryspira) mucronata (Sowerby)
Amalda (Gracilispira) novaezelandiae (Sowerby)
Antalis nana (Hutton)
Antimelatoma buchani (Hutton)
Aoteadrillia wanganuiensis (Hutton)
Austrofusus (Austrofusus) glans (Roding)
Astraea heliotropium (Martyn)
Atrina pectinata zelandica (Gray)
Barbatia novaezelandiae (Smith)
Cardita aoteana (Finlay)
Chlamys gemmulata (Reeve)
Cirsotrema zelebori (Dunker)
Glycymeris (Glycymerula) modesta (Angas)
Iredalula striata (Hutton)
Maoricolpus roseus (Quoy and Gaimard)
Modiolus areolatus (Gould)
Nemocardium pulchellum (Gray)
Notocorbula zelandica (Quoy and Gaimard)
Pecten tainui (Finlay)
Pelicaria vermis vermis (Martyn)
Pleuromeris zelandica (Deshayes)
Poirieria zelandica (Quoy and Gaimard)
Purpurocardia purpurata (Deshayes)
Scalpomactra scalpellum (Reeve)
Sigapatella novaezelandiae (Lesson)
Struthiolaria papulosa (Martyn)
Tanea zelandica (Quoy and Gaimard)
Tawera spissa (Deshayes)
Tiostrea chilensis lutaria (Hutton)
Zeacolpus vittatus (Hutton)

Shakespeare Cliff Sand

Aeneator marshalli marshalli (Murdoch)
Alcithoe (Leporemax) fusus fusus (Quoy and Gaimard)
Amalda (Baryspira) mucronata (Sowerby)
Antimelatoma buchani (Hutton)
Aoteadrillia wanganuiensis (Hutton)
Astraea heliotropium (Martyn)
Atrina pecinata zelandica (Gray)
Austrofusus (Austrofusus) glans (Roding)
Austrovenus stutchburyi (Gray)
Chlamys gemmulata (Reeve)
Divaricella (Divalucina) huttoniana (Vanatta)
Dosinia (Asa) lambata (Gould)
Dosinia (Phacosoma) subrosea (Gray)
Gari lineolata (Gray)
Maoricolpus roseus (Quoy and Gaimard)
Murexsul octogonus (Quoy and Gaimard)
Notocallista (Striacallista) multistriata (Sowerby)
Paphies subtriangulata (Gray)
Paratrophon cheesemani (Hutton)
Pecten tainui (Fleming)
Purpurocardia purpurata (Deshayes)
Ruditapes largillierti (Philippi)
Scalpomactra scalpellum (Reeve)
Sigapatella novaezelandia (Lesson)
Struthiolaria papulosa (Martyn)
Tanea zelandica (Quoy and Gaimard)
Tawera spissa (Deshayes)
Tiostrea chilensis lutaria (Hutton)
Zeacolpus (Zeacolpus) vittatus (Hutton)
Zethalia zelandica (Hombron and Jacquinot)

Upper Castlecliff Shellbed

Aeneator marsahalli (Murdoch)
Alcithoe (Leporemax) fusus fusus (Quoy and Gaimard)
Alcithoe swainsoni (Marwick)
Amalda (Baryspira) mucronata (Sowerby)
Amalda (Gracilispira) novaezelandiae (Sowerby)
Astraea heliotropium (Martyn)
Atrina pectinata zelandica (Gray)
Austrofusus (Austrofusus) glans (Roding)
Barbatia novaezelandiae (Smith)
Cardita aoteana (Finlay)
Chlamys gemmulata (Reeve)
Crepidula radiata (Hutton)
Divaricella (Divalucina) huttoniana (Vanatta)
Dosinia (Kereia) greyi (Zittel)
Dosinia (Phacosoma) subrosea (Marwick)
Gari lineolata (Gray)
Iredalula striata (Hutton)
Maoricolpus roseus (Quoy and Gaimard)
Modiolus areolatus (Gould)
Murexsul octogonus (Quoy and Gaimard)

Nemocardium pulchellum (Gray)
Notocallista (Striacallista) multistriata (Sowerby)
Nucula nitidula (Adams)
Paphies subtriangulata (Gray)
Poirieria zelandica (Quoy and Gaimard)
Purpurocardia purpurata (Deshayes)
Scalpomactra scalpellum (Reeve)
Sigapatella novaezelandiae (Lesson)
Spisula (Crassula) aequilateralis (Deshayes)
Struthiolaria papulosa (Martyn)
Tanea zelandica (Quoy and Gaimard)
Tawera spissa (Deshayes)
Tiostrea chilensis lutaria (Hutton)
Tugali pliocenica (Finlay)
Zeacolpus vittatus (Hutton)
Zethalia zelandica (Hombron and Jacquinot)

Landguard Formation

Amalda (Baryspira) mucronata (Sowerby)
Amalda (Gracilispira) novaezelandiae (Sowerby)
Austrofusus (Austrofusus) glans (Roding)
Austrovenus stutchburyi (Gray)
Barbatia novaezelandiae (Smith)
Barnea (Anchomasa) similis (Gray)
Chlamys gemmulata (Reeve)
Cirsotrema zelebori (Dunker)
Crepidula radiata (Hutton)
Gari stangeri (Gray)
Mactra discors (Gray)
Maoricolpus roseus (Martyn)
Modiolus areolatus (Gould)
Notocallista (Striacallista) multistriata (Sowerby)
Nucula nitidula (Adams)
Paphies australis (Gmelin)
Pecten tainui aotea (Fleming)
Poirieria zelandica (Quoy and Gaimard)
Purpurocardia purpurata (Deshayes)
Ruditapes largillierti (Philippi)
Scalpomactra scalpellum (Reeve)
Spisula (Crassula) aequilateralis (Deshayes)
Tanea zelandica (Quoy and Gaimard)
Tawera spissa (Deshayes)
Tiostrea chilensis lutaria (Hutton)
Zeacolpus vittatus (Hutton)
Zethalia zelandica (Hombron and Jacquinot)

Rapanui Formation

Alcithoe swainsoni (Marwick)
Amalda (Baryspira) mucronata (Sowerby)
Amalda (Gracilispira) novaezelandiae (Sowerby)
Astraea heliotropium (Martyn)
Aulacomya ater maoriana (Iredale)
Austrofusus (Austrofusus) glans (Roding)
Austrovenus stutchburyi (Gray)

Barbatia novaezelandiae (Smith)
Barnea (Anchomasa) similis (Gray)
Cardita aoteana (Finlay)
Crepidula radiata (Hutton)
Dosinia (Phacosoma) subrosea (Gray)
Gari lineolata (Gray)
Gari stangeri (Gray)
Mactra discors (Gray)
Maoricolpus roseus (Quoy and Gaimard)
Modiolus areolatus (Gould)
Nucula nitidula (Adams)
Paphies australis (Gmelin)
Paphies subtriangulata (Gray)
Purpurocardia purpurata (Deshayes)
Ruditapes largillierti (Philippi)
Scalpomactra scalpellum (Reeve)
Sigapatella novaezelandiae (Lesson)
Spisula (Crassula) aequilateralis (Sowerby)
Struthiolaria papulosa (Martyn)
Tanea zelandica (Quoy and Gaimard)
Tawera spissa (Deshayes)
Tiostrea chilensis lutaria (Hutton)
Zethalia zelandica (Hombron and Jacquinot)

CHAPTER 6

STABLE ISOTOPE AND AMINO ACID PROFILES OF THE NEW ZEALAND GIANT PLIOCENE OYSTER *CRASSOSTREA INGENS*

Lynda Mitchell*, Gordon B. Curry*, Anthony E. Fallick†

*Department of Geology and Applied Geology, Glasgow University, Glasgow G12 8QQ^

†Scottish Universities Research and Reactor Centre, East Kilbride G75 0QU

6.1 Abstract

Stable oxygen and carbon isotope profiles and intracrystalline amino acid profiles (free and total) were determined for the New Zealand giant Pliocene oyster *Crassostrea ingens* by sampling annual growth increments along a sagittal section. These profiles reflect both ontogenetic and environmental change over the life-time of the oyster (approximately 20 years). $\delta^{18}O$ increases gradually from the umbo towards the shell margin, and then levels off about half way along the shell. This pattern probably reflects a decrease in the growth rate of the oyster, rather than a temperature effect. The $\delta^{13}C$ profile shows an initial sharp increase at the umbo, and then gradually decreases towards the shell margin. This may be due to kinetic or metabolic effects associated with the development of a fast growing juvenile into a slower growing, sexually mature adult, or it may be due to the influence of ^{13}C-depleted carbon derived from the oxidation of organic matter in the surrounding sediment. The amino acid profile reveals a gradual decrease in abundance from the umbo to the shell margin, indicative of a progressive increase in the relative amounts of inorganic carbonate to protein over the life of the oyster, that may also be a consequence of decreasing growth rate. Glycine and alanine are the two most common amino acids in both the free and total amino acid profiles: free (i.e. naturally hydrolysed) amino acids account for about three quarters of the total amino acids present.

6.2 Introduction

The majority of studies investigating the isotopic signature and organic content of the skeletons of fossils have concentrated on homogenized, whole-shell samples. Often this is unavoidable because of the small size of the organisms being investigated. However for larger specimens, it is possible to obtain reliable data from precisely located sub-samples. Probably the best examples of this approach are a number of studies that have determined sequential stable oxygen isotope ratios from within individual growth increments of large mollusc shells to provide an overview on annual palaeotemperature cycles (e.g. Krantz et al., 1987; Dare and Deith, 1991; Romanek and Grossman, 1989). In terms of the organic content of fossils, there are large numbers of analyses that have been conducted on homogenised whole shells, in particular of amino acids ((e.g. Miller and Hare, 1980) although Brigham (1983) did collect sub-samples from different parts of a molluscan shell and showed that the amino acid content was greater in the hinge and central part of the shell than in the outer growth edge.

Therefore, for both isotopic and biochemical data, it is clear that there is significant, and potentially very useful, information to be obtained from sub-sampling the shell rather than homogenising it to obtain a single result. In this study, isotopic and biochemical changes on a time scale of approximately twenty years, the life span of the New Zealand giant Pliocene oyster *Crassostrea ingens*, are examined. For comparison, changes in the composition of intracrystalline organic material over the same period are also investigated, using amino acid profiles from the same specimen. This appears to the first time that both isotopic and amino acid profiles have been obtained from a single fossil. Both types of data have the potential to provide valuable information on ontogeny, shell metabolism and palaeo-environment. The advantage of obtaining both isotopic and amino acid data from a single shell is that the conclusions reached from each data set can be compared. It is also of interest to investigate whether isotopic and biochemical aspects of this fossil shell show any signs of being affected by the same environmental and metabolic factors.

6.3 Methods

6.3.1 Collection and Sampling

A well preserved specimen of the giant Pliocene oyster *Crassostrea ingens* (Zittel) were collected from the Upper Waipipi shell bed, which is exposed in coastal cliff section east of Wairoa Stream (NZMS 260 Q22 1:50,000, Patea Series 1, Grid Ref. 482 521), near the town of Waverley, North Island, New Zealand. The Upper Waipipi Shell Bed is late Pliocene in age (approximately 3.2 Ma- Beu and Maxwell, 1990), and is thought to have accumulated in relatively shallow water (less than 25 m - Powell, 1931) on relatively rapidly deposited "soft-bottom sands and silts" (Fleming, 1953). Subsequent scouring of the seabed is thought to have produced a number of richly-fossiliferous shell-beds in an otherwise barren section. The uppermost shellbed, the Upper Waipipi, is dominated by large complete shells of *Crassotrea ingens.*

This specimen was approximately 15cm long and 4cm thick. The shell was sectioned sagittally using a diamond saw, to reveal a series of well-defined growth increments (fig. 6.1). Each growth increment is inclined towards the umbo, is several millimetres thick, and is assumed to represent an annual growth increment. If this assumption is correct, then the specimen would have been at least 20 years old.
As oyster shells are composed of both aragonite and calcite, X-Ray Diffraction (XRD) analyses were first carried out to ensure that samples were taken only from calcitic parts of the shell. These analyses (appendix 6.1) confirmed that the aragonite parts of the shell were essentially restricted to the muscle scars, while the growth increments were composed of calcite.

Samples were taken from each growth increment using a rotating drill tip of 1 mm diameter, which was wide enough to sample most of the thickness of each growth increment. Two adjacent samples were taken from each growth layer in order to determine whether the isotopic composition varied laterally within growth layers (fig. 6.1).

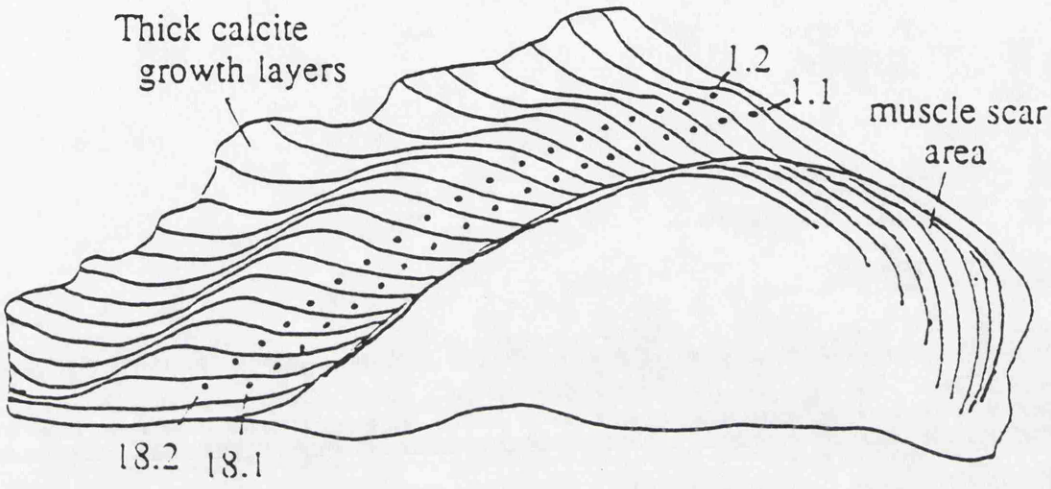

Fig 6.1 Diagram showing longitudinal cross section of shell and positions of sample points

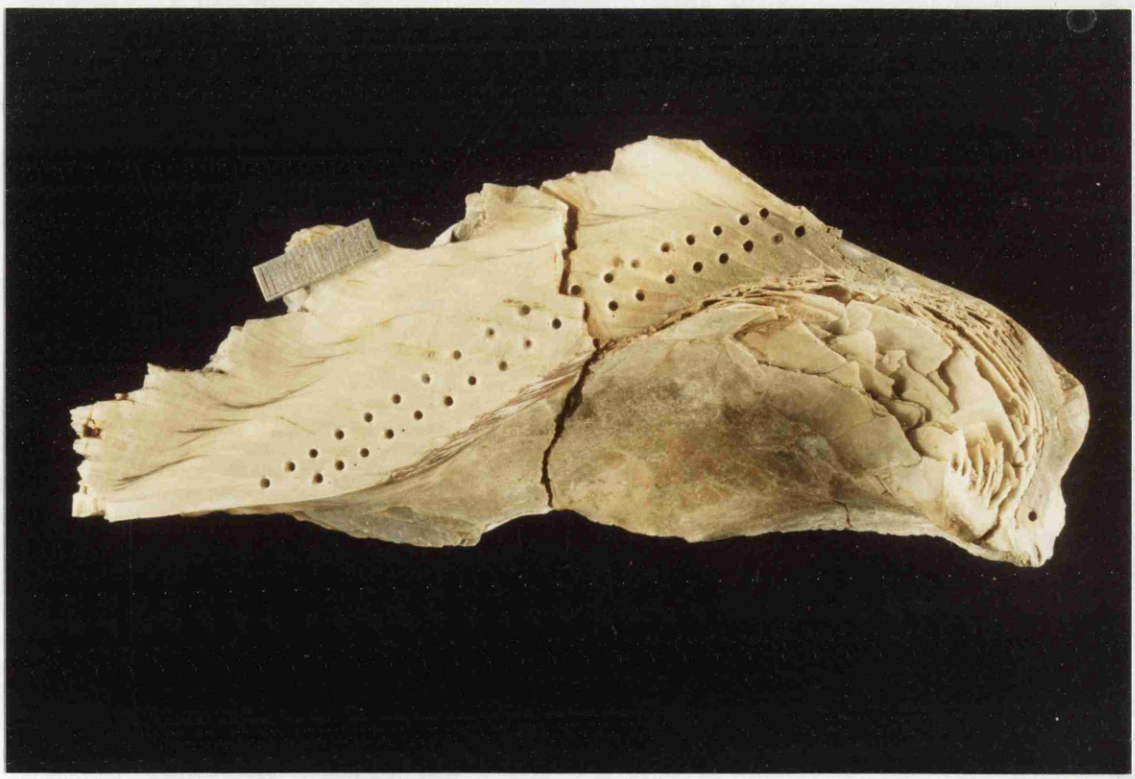

Plate 6.1. Photograph of the longitudinal cross section of *Crassostrea ingens* showing positions of sample points.

The samples were plasma-ashed to remove any contaminating intercrystalline organic matter by oxidation. Amino acid analysis was carried out on the fraction of each sample that remained after isotopic analysis - in many cases there was insufficient material to allow duplicate amino acid analyses from each growth increment, and hence only one amino acid analysis was obtained per increment.

6.3.2 Stable Oxygen and Carbon Isotope Analysis

10-20mg of each sample was prepared for isotopic analysis by dissolution in excess 100% H_3PO_4 at 25°C (McCrea, 1950; Epstein et al., 1953; Wachter and Hayes, 1985). The oxygen and carbon isotopic compositions were determined using a Sira 10 mass spectrometer and recorded relative to the Pee Dee Belemnite (PDB) (Epstein et al., 1953). The precision of the isotopic determinations inferred from the analysis of standard carbonate powders was ±0.1‰ (1s) or better for both $\delta^{18}O$ and $\delta^{13}C$ values.

6.3.3 Amino Acid Analysis

10-20 mg of each sample was dissolved in 2N hydrochloric acid at a ratio of 11µl per mg to release intracrystalline amino acids. The dissolved samples were then centrifuged to remove insoluble residues and analysed using an Applied Biosystems 420H amino acid analyser. Each sample was analysed both with and without hydrolysis in order to determine the total amount of amino acids and the proportion of free amino acids present in each sample (the products of natural hydrolysis of proteins within the shell structure through time.) The free amino acids were subtracted from the total amino acids to give the proportions of amino acids that were protein- or peptide-bound.

6.4 Results

6.4.1 Stable Isotope Profiles

The stable oxygen isotope profile shows a gradual increase from about -0.2‰ to about +0.7‰, levelling off approximately half way from the umbo to the shell margin (fig. 6.2). The average difference between sample pairs is about 0.3‰.

The stable carbon isotope profile shows a rapid increase from about -8.5‰ to -3.5‰ followed by a gradual decrease towards a constant value of about -6.5‰ (fig. 6.3). The average difference between sample pairs is about 0.7‰, but this is largely attributable to large differences in the first few sample pairs; the difference in carbon isotope values between sample pairs decreases significantly from the umbo to the shell margin (fig. 6.3).

6.4.2 Amino Acid Profiles

Total Amino Acids

The total amino acid profile reveals a general gradual decrease in amino acid content from about 400 pmol/mg to about 200 pmol/mg from the umbo to the margin of the shell. Samples 1 and 16 are clearly anomalous (figs 6.4a and b).

Total Individual Amino Acids

Glycine and alanine are the most abundant amino acids, together accounting for about three quarters of the total. Both show a gradual decrease in abundance from the umbo to the margin of the shell (figs 6.5a and b). Other, less abundant amino acids (aspartic acid, glutamic acid, serine, proline, valine, lysine and leucine) also show a gradual decrease in abundance from the umbo to the shell margin (figs 6.5c-i). The remaining amino acids are present in very small quantities in some samples (see data table, appendix 6.3). The individual amino acid content of samples 1 and 16 are again clearly anomalous for almost all of the individual amino acids.

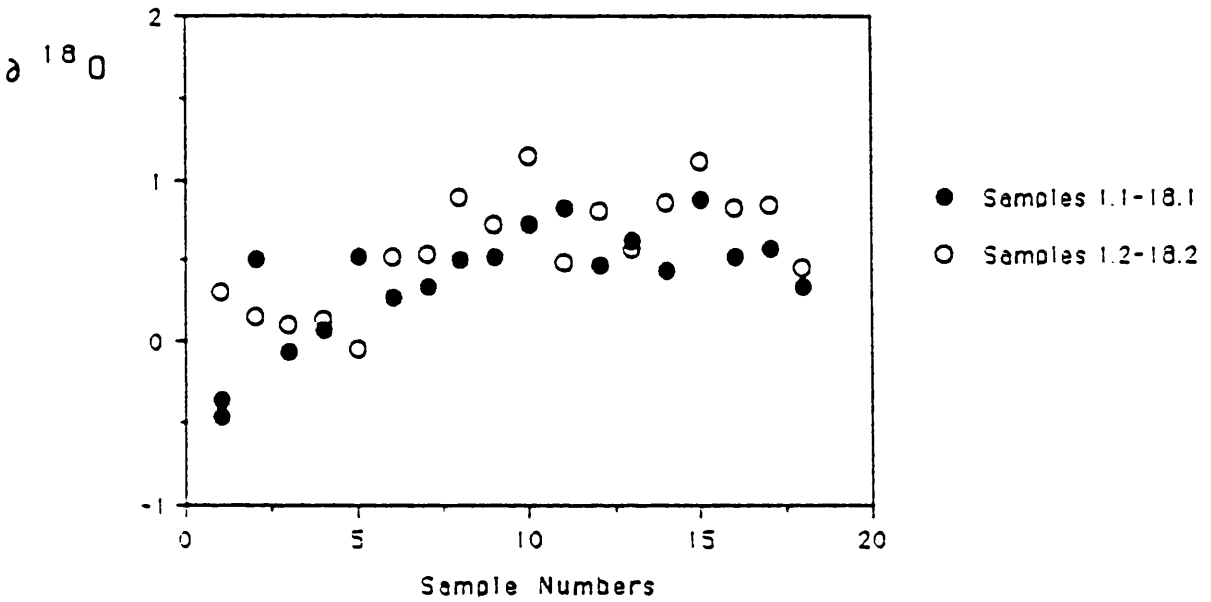

Fig 6.2 The oxygen isotope profile from the umbo to the shell margin of *Crassostrea ingens*

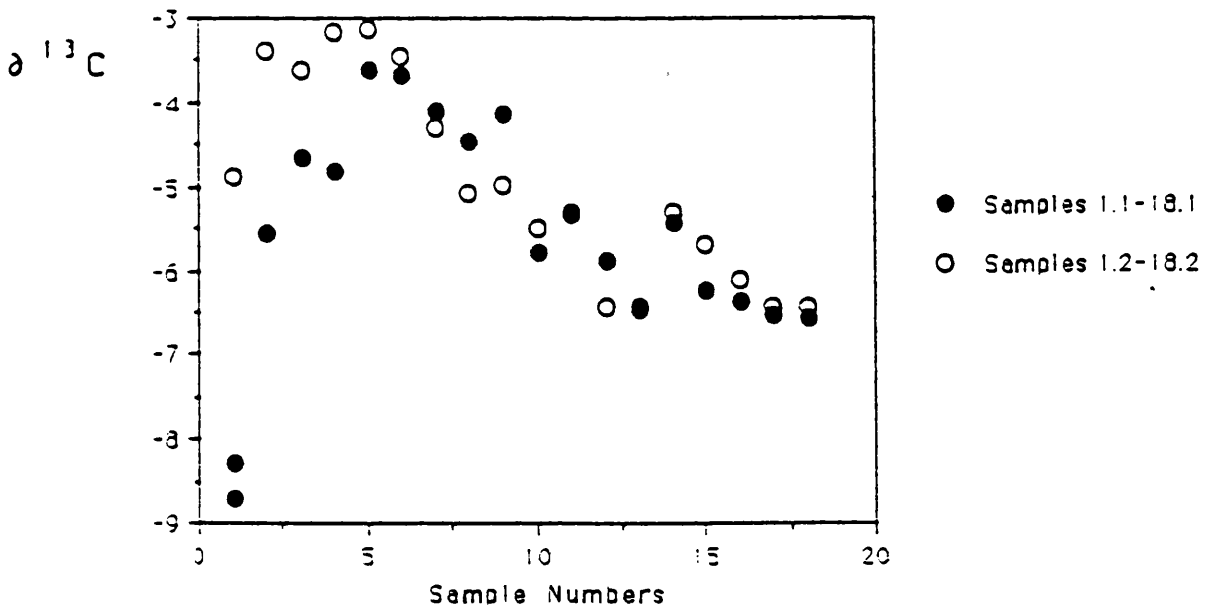

Fig 6.3 The carbon isotope profile from the umbo to the shell margin of *Crassostrea ingens*

Fig 6.4a Total amino acids present in samples 1-18.
Sample nos 1 and 16 are outliers and are probably contaminated.

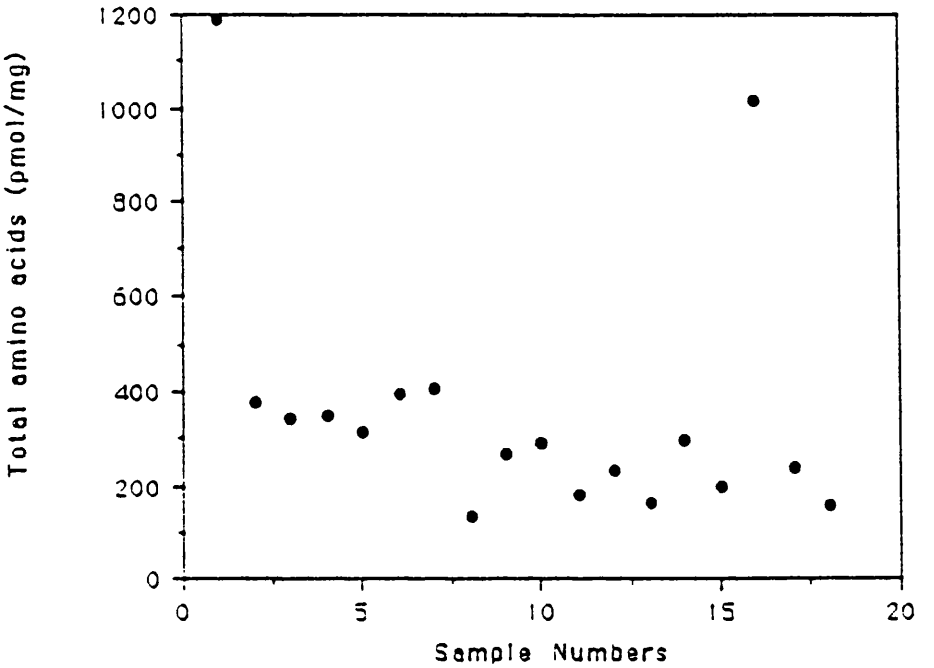

Fig 6.4b Total amino acids in samples 1-18,
with samples 1 and 16 omitted

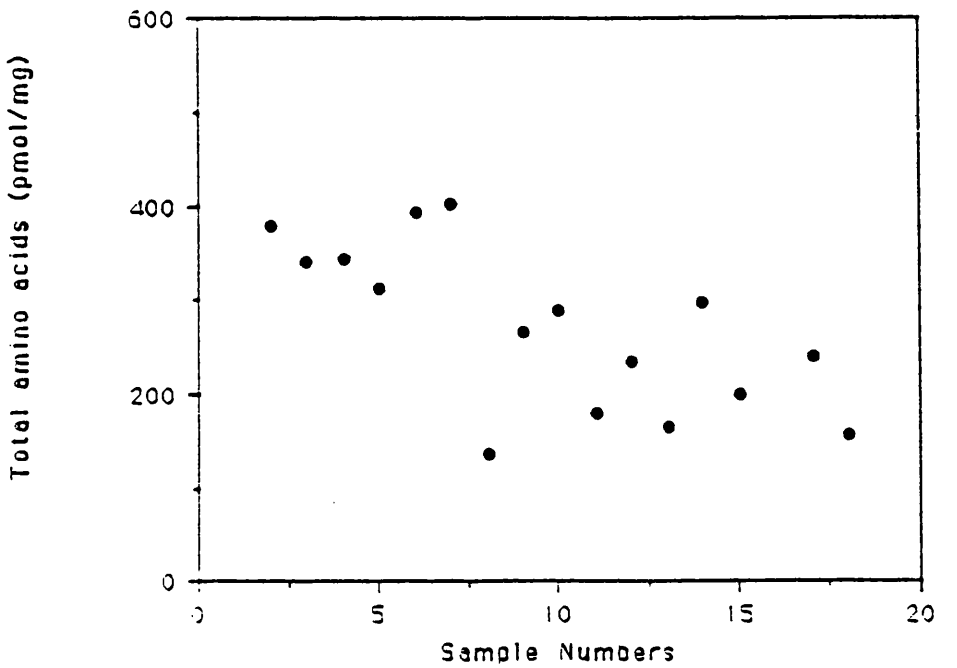

Fig 6.5a Total glycine in samples 1-18
Samples 1 and 16 omitted

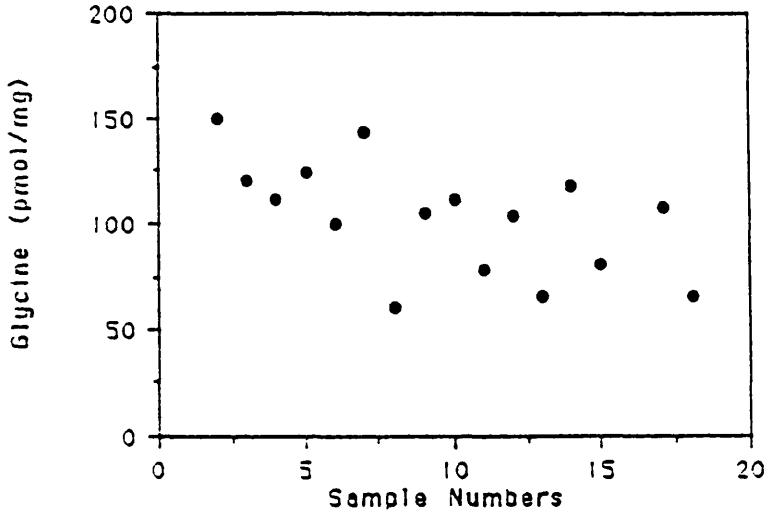

Fig 6.5b Total alanine in samples 1-18
Samples 1 and 16 omitted

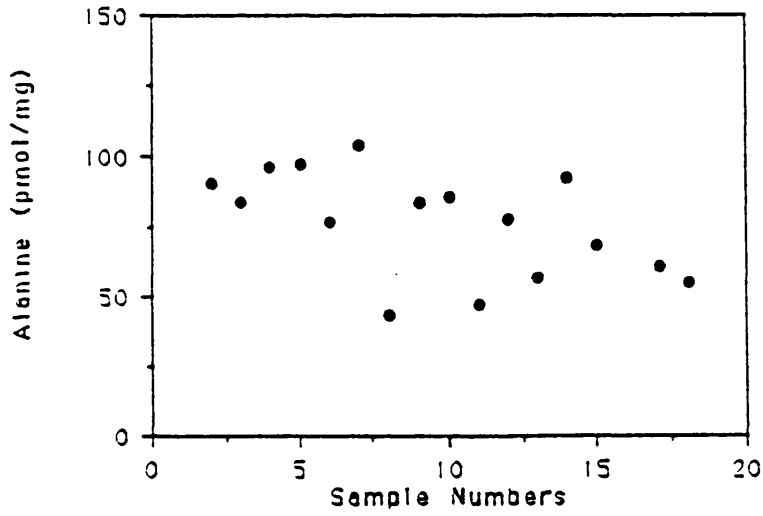

Fig 6.5c Total aspartic acid in samples 1-18
Samples 1 and 16 omitted

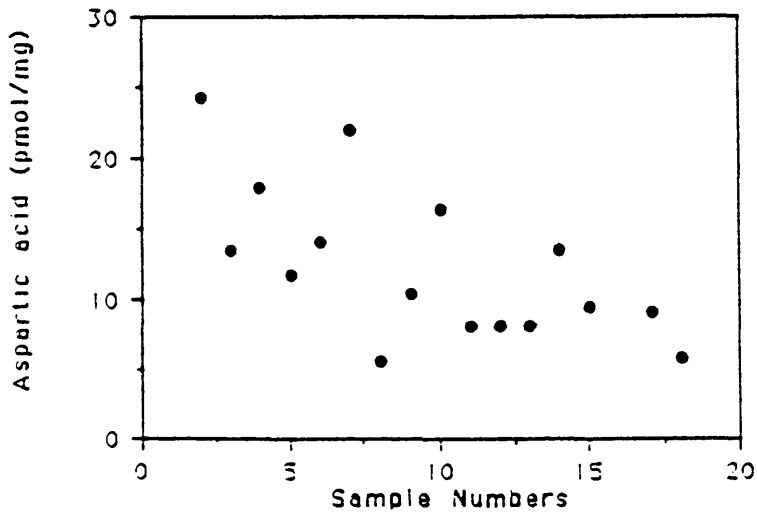

Fig 6.5d Total proline in samples 1-18
Samples 1 and 16 omitted

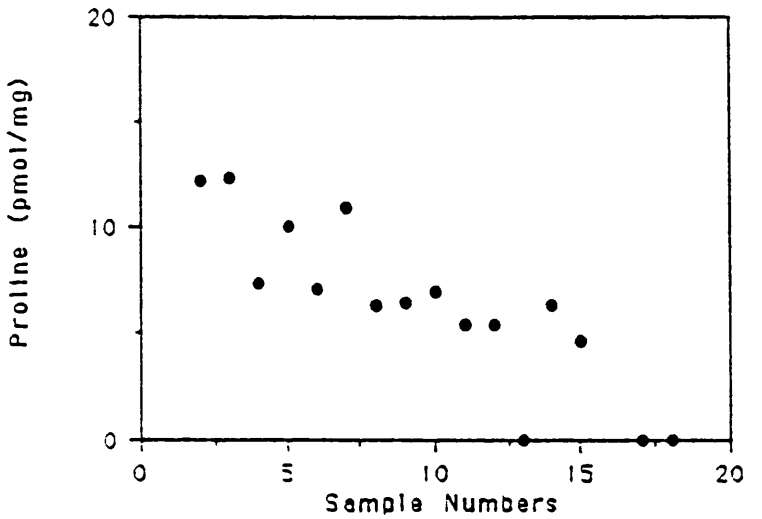

Fig 6.5e Total serine in samples 1-18
Samples 1 and 16 omitted

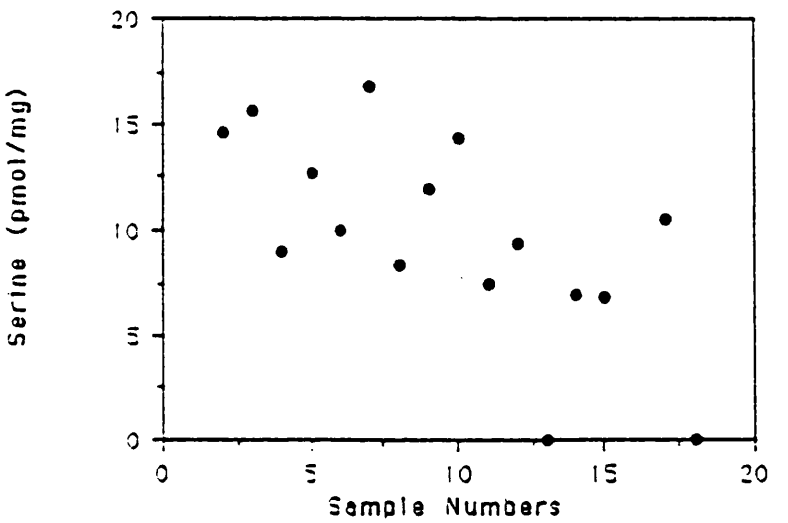

Fig 6.5f Total glutamic acid in samples 1-18
Samples 1 and 16 omitted

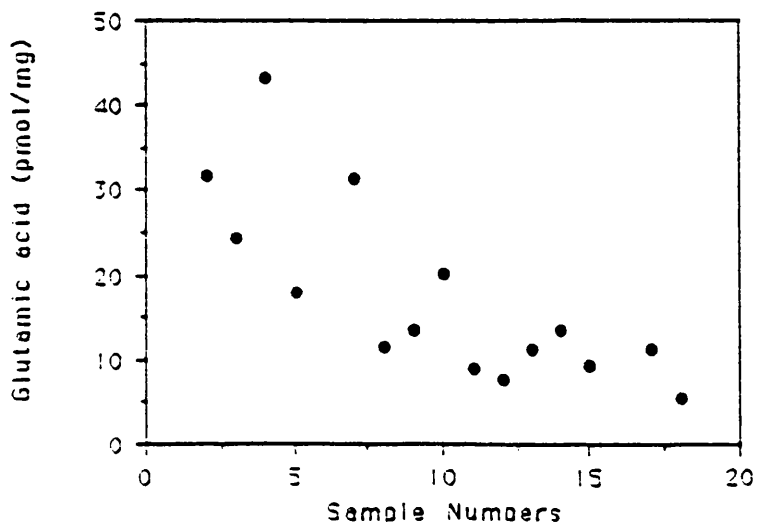

Fig 6.5g Total valine in samples 1-18
Samples 1 and 16 omitted

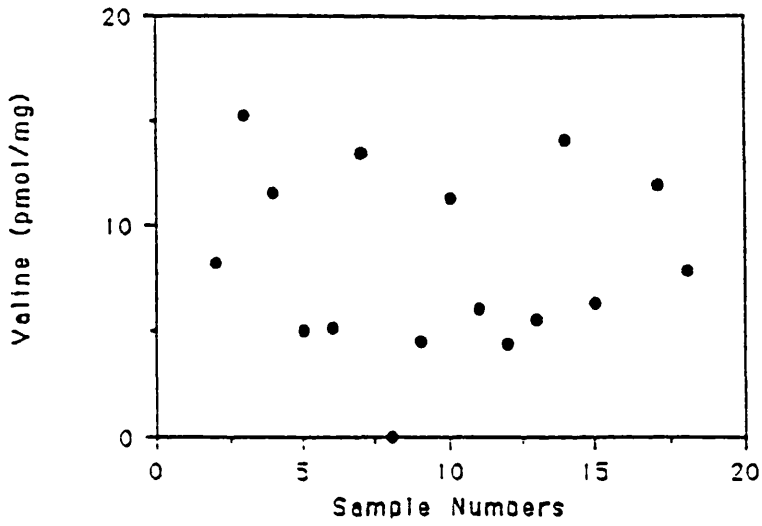

Fig 6.5h Total lysine in samples 1-18
Samples 1 and 16 omitted

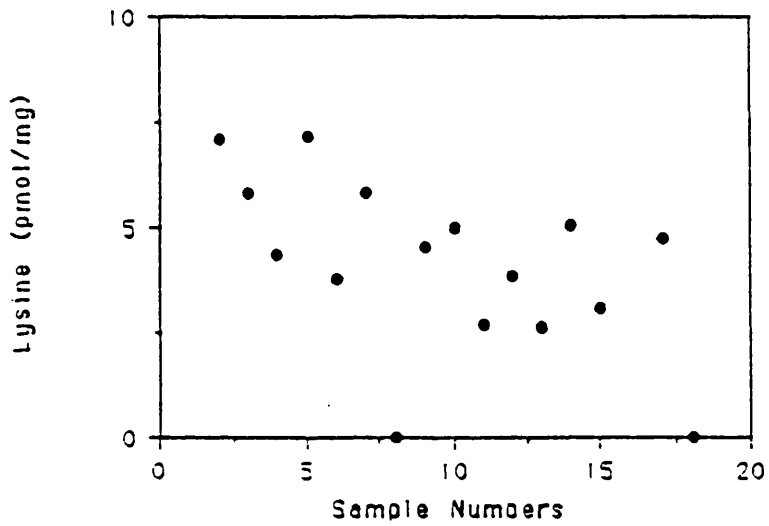

Fig 6.5i Total leucine in samples 1-18
Samples 1 and 16 omitted

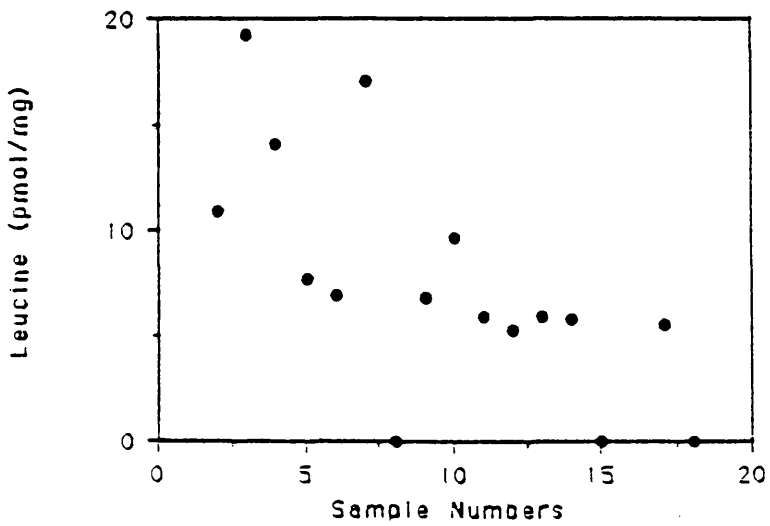

Free Amino Acids

The free amino acid profile shows a gradual decrease in abundance from about 300 pmol/mg to about 150 pmol/mg from the umbo to the shell margin (fig. 6.6). There are no outliers. The free amino acids therefore account for approximately three quarters of the total amino acids; and hence about one quarter of the total amino acids in the shell remain non-hydrolysed. However, the actual percentage of free amino acids is quite variable between sample points (fig. 6.7). Samples 1 and 16 have comparable abundances of free amino acids to the other samples, but are characterised by signifinantly lower percentages of free amino acids.

Free Individual Amino Acids

Glycine and alanine are the most abundant free amino acids, together accounting for most of the free amino acid total. Both show a gradual decrease in abundance from the umbo to the shell margin (figs 6.8a and b). A decrease in abundance can also be seen in free aspartic acid (fig. 6.8c), though it is present in smaller quantities. Other amino acids are present in small amounts in some samples (see data table, appendix 6.4).

Total Peptide Bound Amino Acids (calculated by subtracting the free amino acids from the total amino acids)

There is a decrease in peptide bound amino acids from about 150 pmol/mg to about 50 pmol/mg from the umbo to the shell margin. The decrease is rapid at first and gradually levels off about half way towards the shell margin. Samples 1 and 16 are once again outliers among the data (figs 6.9a and b).

Individual Peptide-Bound Amino Acids

Glycine is the most common peptide-bound amino acid, accounting for approximately two thirds of the peptide-bound total and decreasing from about 100 pmol/mg to about 20 pmol/mg from the umbo to the shell margin (fig. 6.10a). Glutamic acid is the second most abundant peptide-bound amino acid and also shows a gradual slight decline from the umbo to the shell margin (fig. 6.10b). Other

Fig 6.6 Free amino acids in samples 1-18

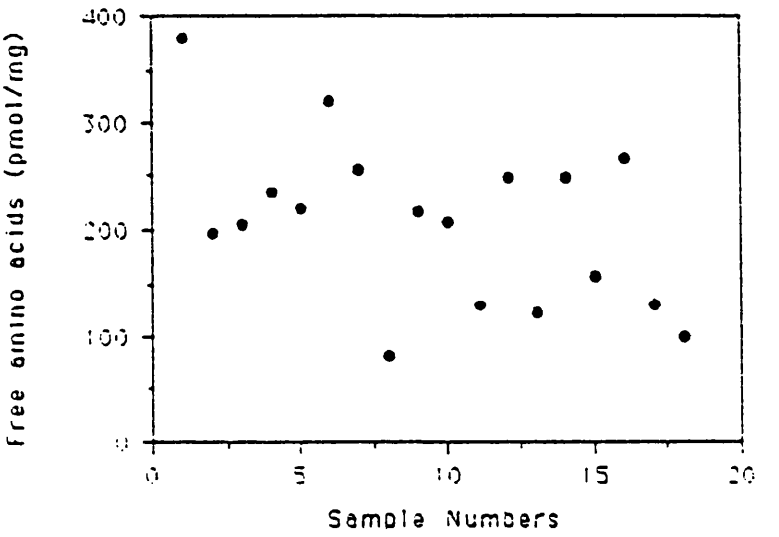

Fig 6.7 % free amino acids in samples 1-18

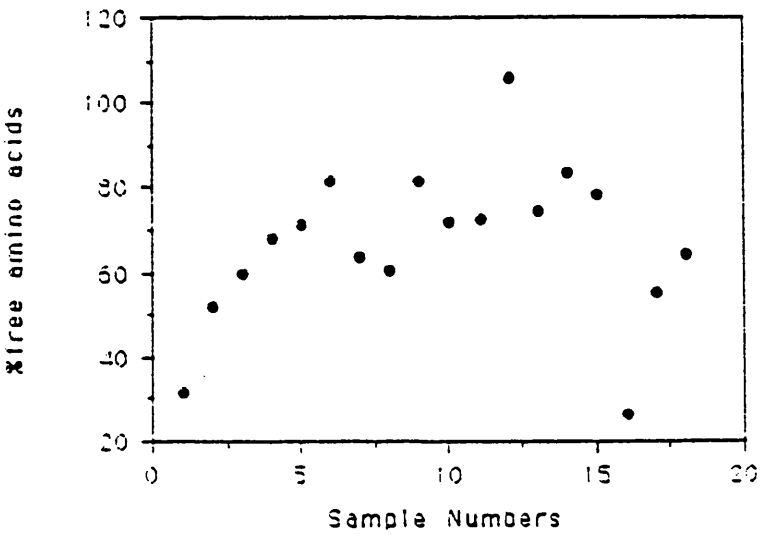

Fig 6.8a Free glycine in samples 1-18

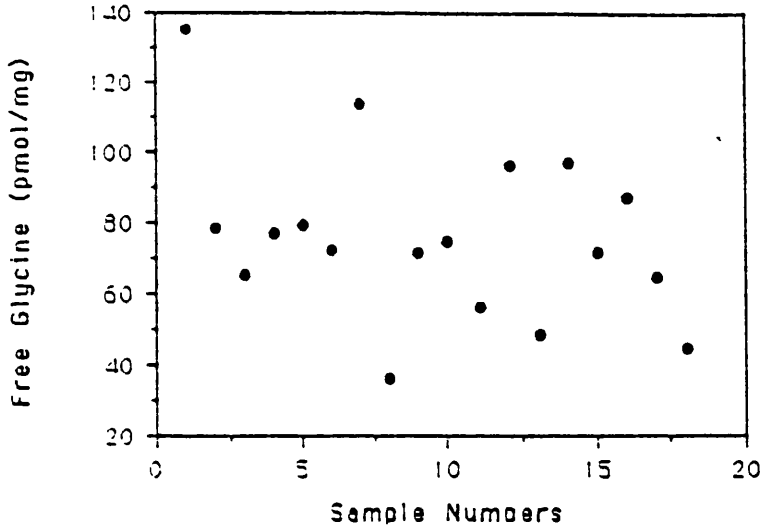

Fig 6.8b Free alanine in samples 1-18

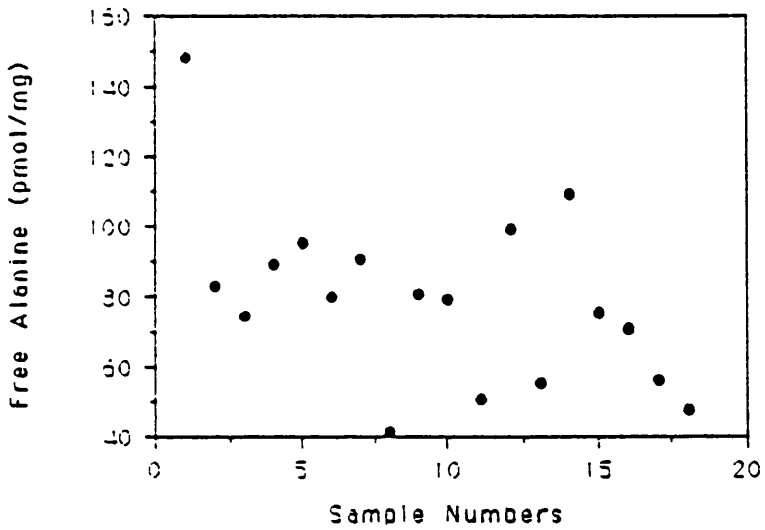

Fig 6.8c Free aspartic acid in samples 1-18

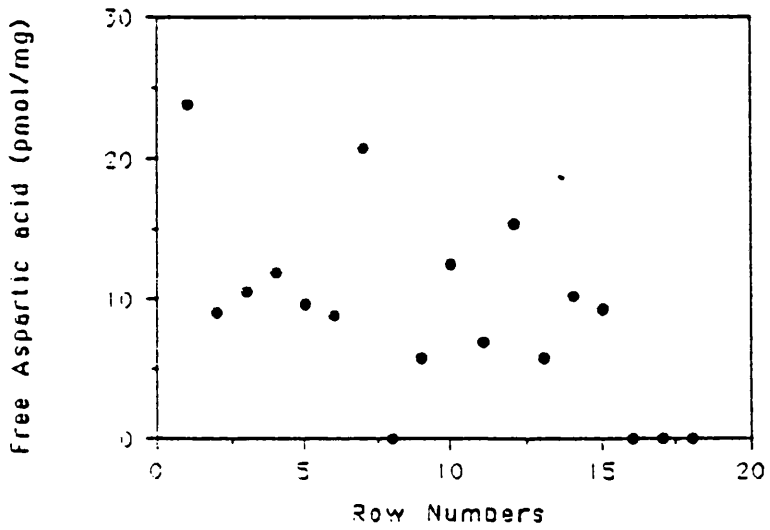

Fig 6.9a Peptide bound amino acids in samples 1-18

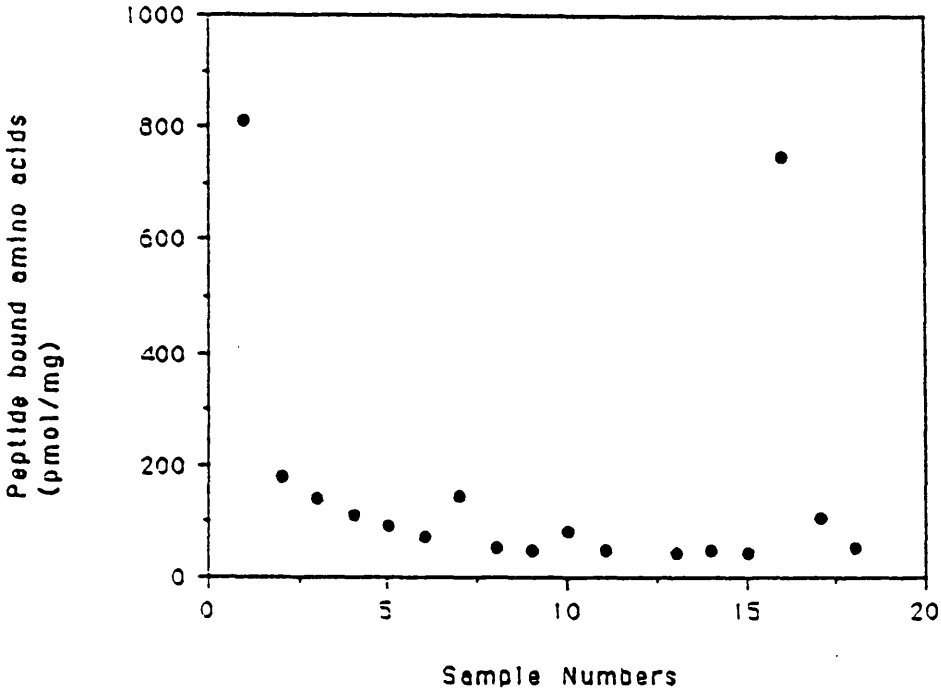

Fig 6.9b Peptide bound amino acids in samples 1-18
Samples 1 and 16 omitted

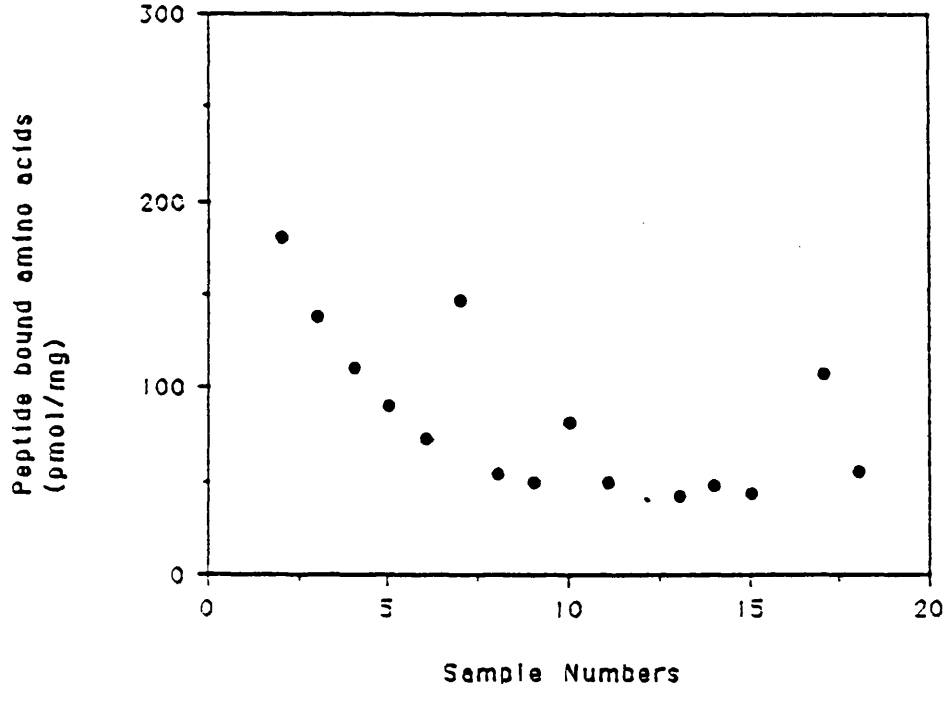

Fig 6.10a Peptide bound glycine in samples 1-18
Samples 1 and 16 omitted

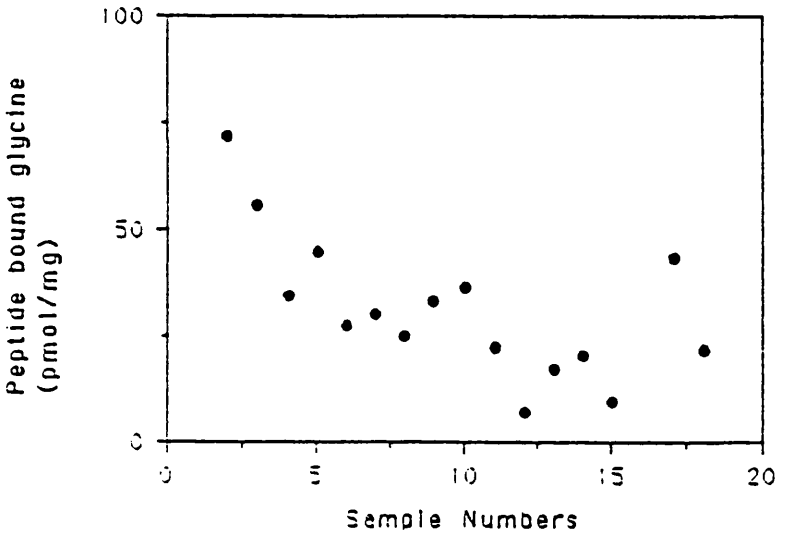

Fig 6.10b Peptide bound glutamic acid in samples 1-18
Samples 1 and 16 omitted

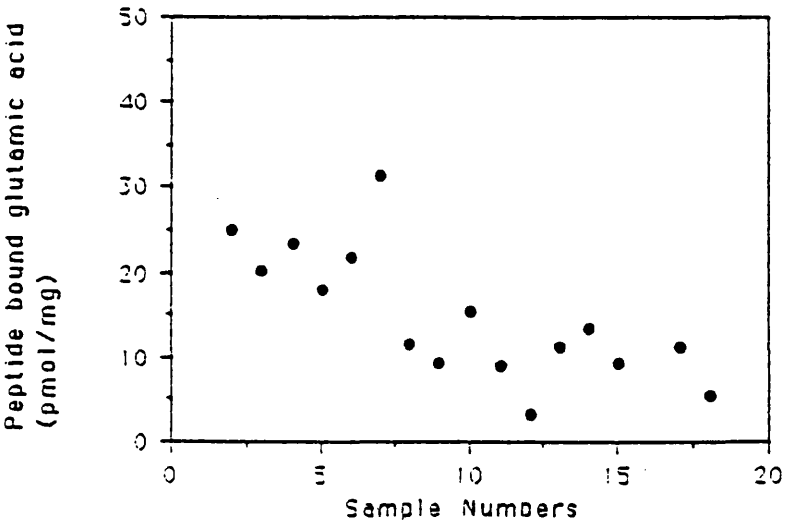

bound amino acids are are present in small quantities in some samples. Sample points 1 and 16 are outliers in virtually every case.

Anomalous Samples 1 and 16

Samples 1 and 16 yield anomally high abundances of total amino acids compared to the other samples (fig. 6.4a). However, these samples do not contain unduly large amounts of free amino acids (fig. 6.6), as the percentage of free amino acids is low in both cases (fig. 6.7). This suggests that these anomalous results are not an indigeneous phenomenon, but are caused by contamination, and that the contamination is in the form of peptide bound amino acids, presumably in the form of intact proteins or peptides. Contamination of samples is a major problem of all investigations of amino acids in fossils, because amino acids are virtually ubiquitous on the surface of the earth and in sediments of the upper lithosphere (Bada 1991; Walton & Curry 1991; Curry 1993, Curry *et al.* in press).

To further investigate the nature of this contamination, the peptide-bound amino acid compositions of samples 1 and 16 are compared with each other and with the compositions of the other samples in figs 6.11a and b. The anomalous nature of both samples is readily apparent; sample 1 contains abundant glutamic acid, glycine, alanine, valine and leucine whereas sample 16 is particularly rich in glycine. The amino acid composition of sample 16 is very similar to that demonstrated from contamination due to contact with human fingertips (Walton & Curry 1991), suggesting that injudicious handling of the sample was the source of this particular contamination. The fact that such contamination could occur despite the rigorous procedures adopted during this study, and designed to avoid this possibility, is a clear warning of the need not only for great care in sample preparation but also for careful analysis of the results.

An important method of analysing the results of such studies is multivariate analysis (e.g. Walton & Curry 1991). Thus principal component analysis was applied to the dataset generated during the present study, allowing the data to be summarized in a form in

Fig 6.11a Amino acid composition of samples 1-18 showing anomalous composition of sample 1 Sample 16 omitted

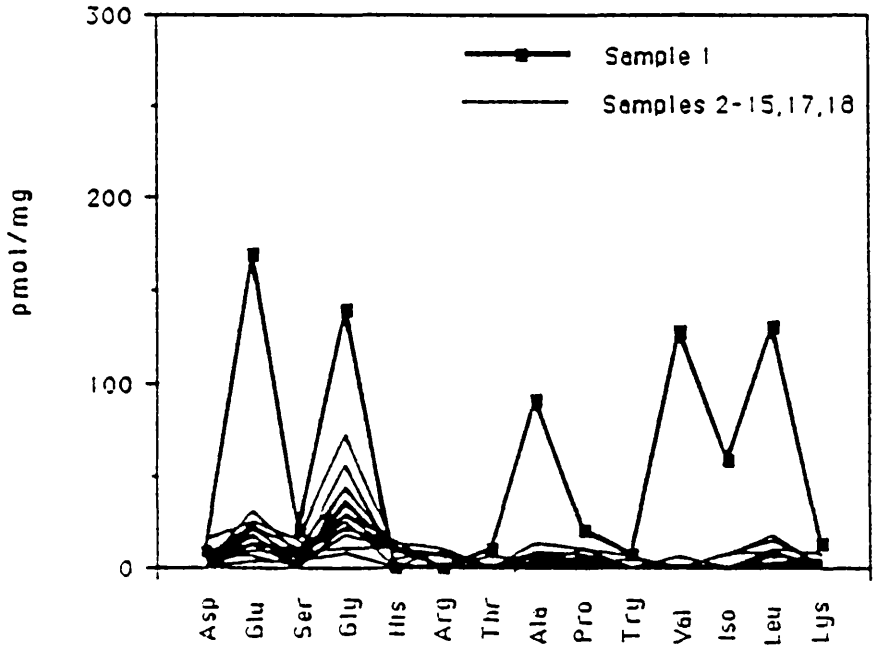

Fig 6.11b Amino acid composition of samples 1-18 showing anomalous composition of sample 16 Sample 1 omitted

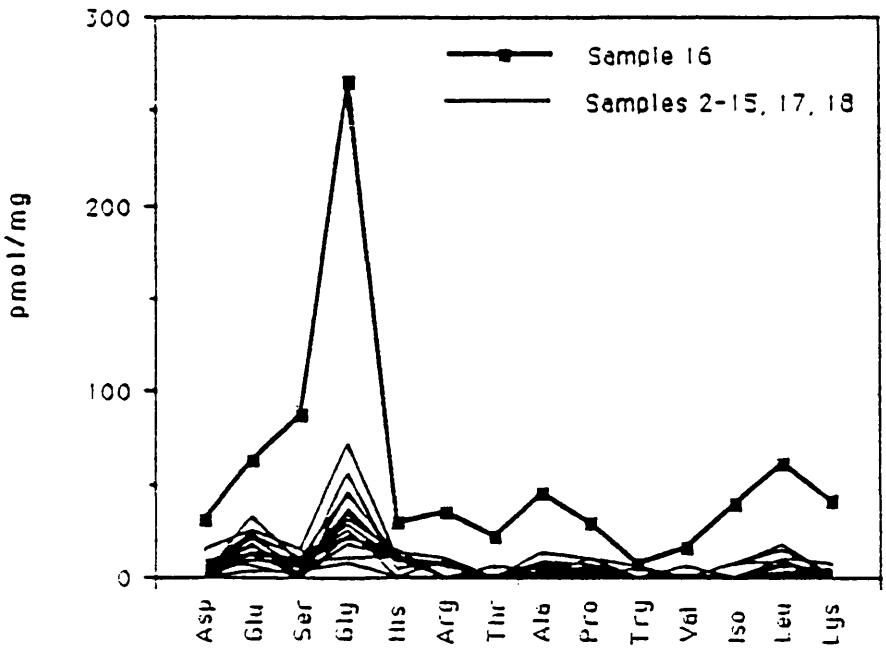

which most of the variation is contained within fewer, derived variables, that can be plotted into a two dimensional scatter plot (fig. 6.12), in which samples that are closely related plot closely together. The first principal component (vertical axis in fig. 6.12) contains 65.5% (table 6.1) of the total variability present in the dataset, and clearly separates samples 1 and 16 from the rest of the samples (fig. 6.12). Analysis of the eigenvector values, indicates that this separation is primarily due to differences in the amount of glycine (-0.315), proline (-0.307) and phenylalanine (-0.306). The second principal component, containing 16.6% of the total variability in the dataset, clearly separates samples 1 and 16 from each other (fig. 6.12). This is mainly due to differences in the amounts of histidine (0.482), valine (-0.392), glutamic acid (-0.355) and alanine (-0.355). The signs of the eigenvalues indicate the direction of the sample along the eigenvector. The first two principal components together contain a high percentage (82.1%) of the total variability, confirming the results of this analysis are valid (Sneath and Sokal 1973).

6.5 Discussion

6.5.1 The Oxygen Isotope Profile

The oxygen isotope profile shows a gradual increase in $\delta^{18}O$ to about half way from the umbo to the shell margin followed by a levelling off. This may could be due to either environmental or ontogenetic factors, or both. If entirely due to environmental effects, then this $\delta^{18}O$ profile would indicate a general cooling of about four or five degrees centigrade during the first half of the life of this specimen. This is considered unlikely, in an estimated time span of about ten years. On the other hand, if due to an ontogenetic effect, the data would reflect a growth rate that was initially fast, causing the $\delta^{18}O$ values to be isotopically lighter than the equilibrium value due to kinetic effects (McConnaughey, 1989). Growth would then have slowed down as sexual maturity was reached and energy became redirected towards reproduction. Upon reaching sexual maturity some species (e.g. *Tridacna maxima*) show a period of slower growth during the middle of the summer as their

Fig 6.12 Scatterplot of the first two principal components of the relative proportions of amino acids in samples 1-18

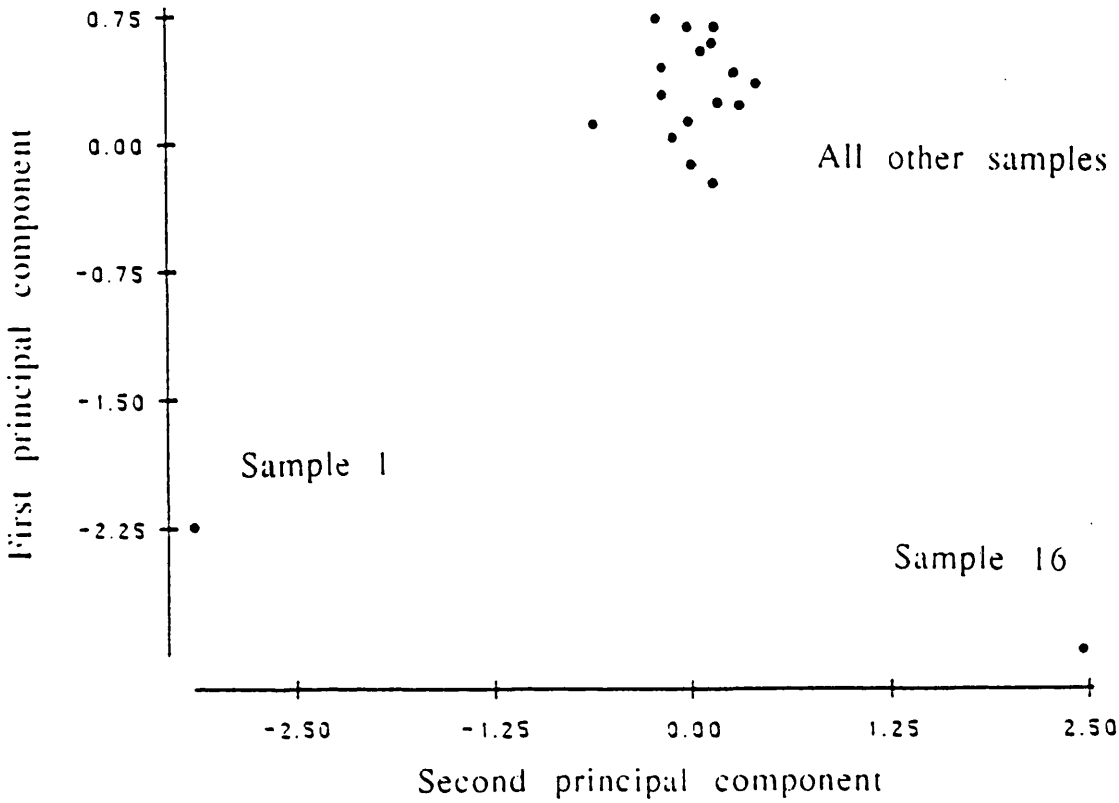

Principal Component Analysis

EigenValues

	Values	Variance Proportion
e1	9.828	65.5
e2	2.490	16.6
e3	1.047	7.0
e4	0.502	3.3
e5	0.465	3.1
e6	0.289	1.9
e7	0.159	1.1
e8	0.092	0.6
e9	0.064	0.4
e10	0.043	0.3
e11	0.010	0.1
e12	0.005	0.0
e13	0.003	0.0
e14	0.003	0.0
e15	0.000	0.0

EigenVectors

	V1	V2
Asp	-0.284	-0.100
Glu	-0.201	-0.355
Ser	-0.284	0.263
Gly	-0.315	0.044
His	-0.113	0.482
Arg	-0.258	0.266
Thr	-0.278	0.135
Ala	-0.244	-0.355
Pro	-0.307	-0.070
Try	-0.287	0.121
Val	-0.237	-0.392
Met	0.011	0.003
Leu	-0.275	-0.298
Phe	-0.306	0.059
Lys	-0.282	0.284

Table 6.1 Principal component analysis of the relative proportion data, showing the first two eigenvectors

energy is redirected towards reproduction (Jones *et al.*, 1986). This effect may result in a general slowing of the growth rate as the shell gets older (Donner and Nord, 1985; Deith, 1983).
The differences in the results for sample pairs from each particular growth increment is probably the result of seasonal or intra-incremental temperature differences. Mollusc shells have shown annual cycles in oxygen isotope values which correspond to seasonal temperature changes (e.g. Williams et al., 1981; Jones et al., 1983). There is an average difference of about 0.3‰ in the oxygen isotope values of sample pairs (fig 6.2), corresponding to a temperature difference of one or two degrees centigrade within each growth increment. The maximum difference, of about 0.7‰, would indicate a temperature difference of about 3°C. Such temperature differences are well within the normal seasonal temperature range for a mid-latitude geographical position, and indeed are significantly smaller than the expected annual temperature range. However, samples were all taken from the mid points of growth increments, so would not reflect the coldest temperatures. Also, shells may not record the coldest or warmest temperatures of the year if growth ceases or slows down during extremes of temperature (Jones, 1980; Schifano and Censi, 1983). The seasonal temperature range would probably therefore be significantly greater than 3°C, and the temperatures indicated by the oxygen isotope values will be warmer than the yearly average.

6.5.2 The Carbon Isotope Profile

The carbon isotope profile shows a rapid initial increase followed by a more gradual decrease towards a steady value. Trends towards lower $\delta^{13}C$ values through ontogeny have been noted previously (e.g. Jones et al., 1983; Wefer, 1985; Grossman et al., 1986; Romanek and Grossman, 1989) and have been attributed to the effects of metabolic changes from a fast growing juvenile to a slower growing, sexually mature adult (Krantz et al.,1987). However, the decrease in $\delta^{13}C$ may also reflect the influence of ^{13}C-depleted carbon from the oxidation of organic sediments as the oyster grew larger and older and became partly buried within the sediment. The initial sharp increase is more difficult to explain, but could be due to kinetic

effects associated with an initially fast growth rate slowing down to a more moderate growth rate. Turner (1982) observed that carbon isotope fractionation in inorganic carbonate precipitates decreased with increasing precipitation rate. McConnaughey (1989) noted that fractionation of both oxygen and carbon isotopes is suppressed in fast growing biogenic carbonates.
The difference in carbon isotope values between sample pairs decreases significantly from the umbo to the shell margin (fig. 6.3). This indicates that the variation in carbon isotope values within growth increments is large during the early stages of growth, and later becomes much more uniform. This may be due to growth being initially spasmodic, with short fast bursts of growth indispersed with slower periods, later becoming more uniformly slow. Rapid early growth may correspond with times of plentiful food supply, and the isotopically light carbon from organic food molecules is likely to be directed primarily towards biomineralization at these early stages. The overall shape of the carbon isotope profile is probably due to a complex interplay between metabolic and kinetic effects associated with both ontogeny and environment.

6.5.3 Amino Acid Profiles

Total Amino Acids
The results show a gradual decrease in abundance of amino acids from the umbo to the outer margin of the shell. These data support the results of Brigham (1983) who reported a significantly higher concentration of amino acids in the hinge area and central part of the shell than in the outer growth edge. Brigham (1983) suggests that this pattern may be due to leaching of the thin shell growth edge, or the presence of a protein-rich inner layer lining the valve out to the pallial line, or differences in the proportion of inorganic carbonate to protein produced in different areas during shell growth. The possibility of leaching in *Crassostrea ingens* is unlikely as the shell is uniformly thick and robust and has no thin growth edge. The profile is not explained by the presence of a protein-rich layer out to the pallial line because the decrease in amino acids is

very gradual from the umbo to the shell margin and does not decrease suddenly at any point.
However, differences in the proportion of inorganic carbonate to protein could result from a change in the growth rate of the shell. One of the functions of intracrystalline proteins in biogenic carbonates is to provide a substrate for crystal nucleation (Lowenstam and Weiner, 1989). In a crude sense, therefore, it may be that there is a correlation between the quantity of protein present and the rate of shell growth. As the shell gets older and the production of protein substrates declines, shell growth rate will decrease and the amount of intracrystalline amino acids found within the shell will decrease accordingly.

Individual Amino Acids

Glycine and alanine are the most common free amino acids. This may be partly due to the fact that they are common products of other amino acid reactions. For instance, decomposition reactions of valine, serine, threonine, methionine and tyrosine can all produce glycine (Vallentyne, 1964). Similarily, decomposition reactions of serine, aspartic acid, phenylanaline and tyrosine could all produce alanine (Vallentyne 1964). The rates of these amino acid reactions may be significantly increased by the presence of carbohydrates which occur in the intracrystalline organic matter in small quantities and by the geothermal gradient during burial (Vallentyne, 1964, 1968). Glycine and alanine are also two of the most thermally stable free amino acids (Abelson 1954), and are therefore unlikely to break down any further.
The percentage of free amino acids compared with total amino acids present is about 75% but is quite variable between sample points (fig. 6.7). This shows that the rate of natural hydrolysis of amino acids varies quite significantly even within the confines of one shell. In one sample the amount of free amino acids is even greater than the amount of total amino acids, leading to an apparent free amino acid content of greater than 100% (fig. 6.7); this is probably due to the degradation of small amounts of insoluble proteins which produces free amino acids from a source not taken account of in the analysis of total (soluble) amino acids (Walton, 1992).

There is also variability in the free percentages of different individual amino acids. This may be partly due to different rates of hydrolysis for different amino acids, but will also reflect the appearance of certain free amino acids as reaction products of other amino acids, as described above. For example, the large amount of free alanine present is probably partly due to the hydrolysis of peptide bound alanine and partly due to its appearance as a reaction product of other amino acid reactions. Differences in the relative abundance of individual amino acids are related to both the strength of the peptide bond and the stability of the amino acid in the free state (Miller and Hare, 1980).

6.6 Conclusions

Oxygen and carbon stable isotope profiles can be related to both environment and ontogeny. Intracrystalline amino acid profiles reflect both ontogeny and complex processes of amino acid diagenesis. Both isotope profiles and bulk intracrystalline amino acid profiles can be linked to the changing growth rate of the shell. The changing growth rate indicated by the bulk amino acid profiles supports that indicated by the stable isotope data. The isotope data do not reflect environmental factors alone: care must be taken in environmental reconstruction using isotopic data from shell carbonates.

Appendix6.1XRD traces showing calcium carbonate composition of the growth layers and muscle scar area of *Crassostrea ingens*

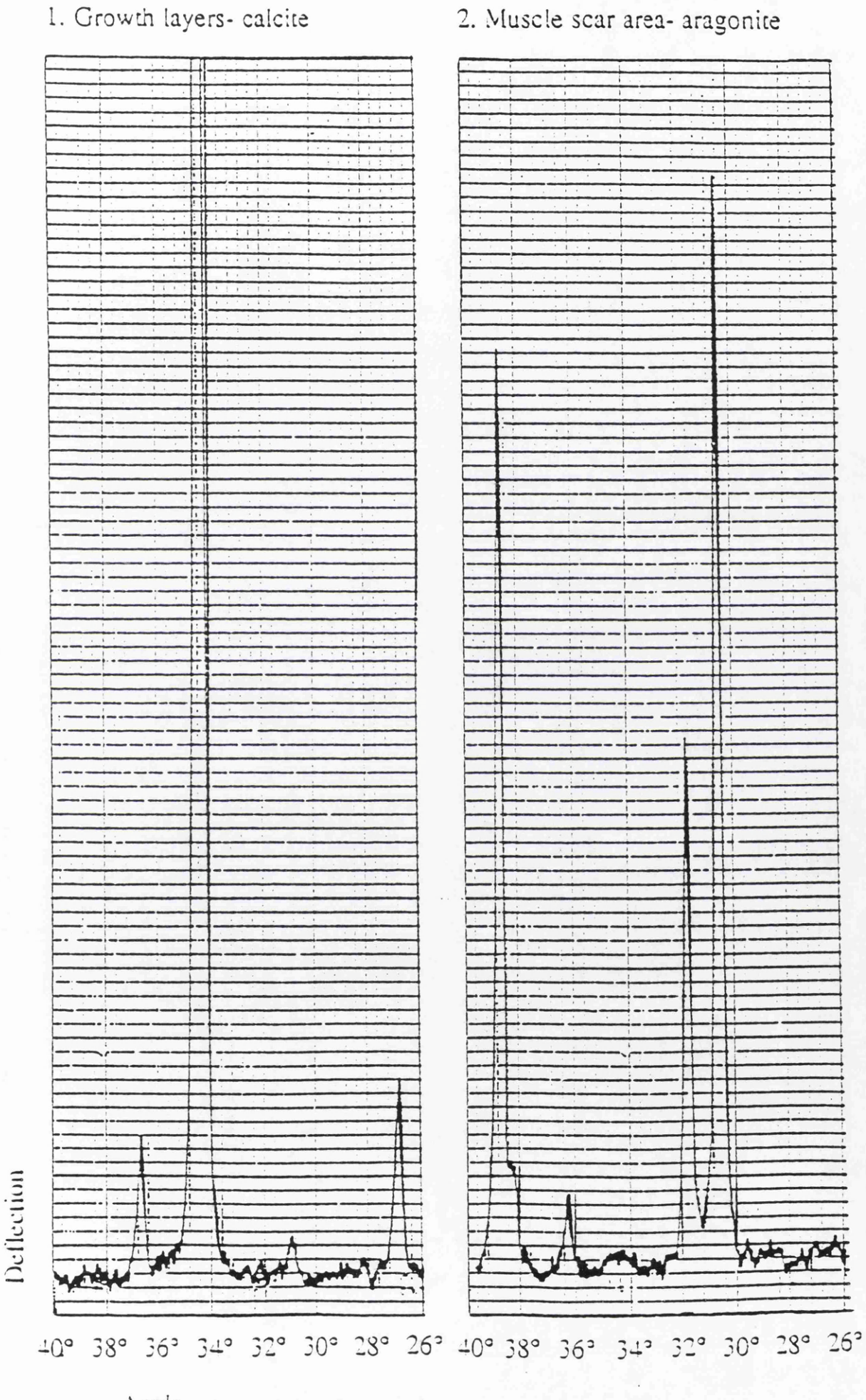

Appendix 6.2 Stable Isotope Data

Sample	$\delta^{13}C$	$\delta^{18}O$
1.1	-8.71	-0.46
2.1	-5.58	0.51
3.1	-4.64	-0.06
4.1	-4.80	0.08
5.1	-3.61	0.53
6.1	-3.63	0.27
7.1	-4.10	0.35
8.1	-4.45	0.51
9.1	-4.63	0.53
10.1	-5.80	0.72
11.1	-5.32	0.83
12.1	-5.87	0.47
13.1	-6.47	0.62
14.1	-5.48	0.44
15.1	-6.24	0.87
16.1	-6.36	0.52
17.1	-6.52	0.58
18.1	-6.57	0.34

Sample	$\delta^{13}C$	$\delta^{18}O$
1.2	-8.28	-0.37
2.2	-3.39	0.15
3.2	-3.60	0.10
4.2	-3.17	0.15
5.2	-3.14	-0.04
6.2	-3.44	0.53
7.2	-4.31	0.53
8.2	-5.07	0.89
9.2	-4.97	0.72
10.2	-5.49	1.14
11.2	-5.33	0.48
12.2	-6.42	0.82
13.2	-6.42	0.57
14.2	-5.29	0.86
15.2	-5.70	1.12
16.2	-6.11	0.83
17.2	-6.43	0.84
18.2	-6.42	0.45

Appendix 6.3 Total Amino Acids

(Amino acids in pmol per mg of shell).

Sample	Aspartic acid	Glutamic acid	Serine	Glycine
1	32.73	179.32	30.84	275.55
2	24.15	31.62	14.66	150.52
3	13.46	24.43	15.66	120.90
4	17.94	43.40	9.03	111.44
5	11.66	17.90	12.64	123.87
6	14.11	154.50	10.01	99.51
7	21.86	31.36	16.75	144.08
8	5.59	11.40	8.40	60.68
9	10.48	13.42	11.97	104.68
10	16.29	20.06	14.41	111.11
11	8.03	9.04	7.45	78.64
12	8.06	7.57	9.33	103.60
13	8.07	11.31	0.00	65.93
14	13.51	13.55	6.94	117.33
15	9.40	9.18	6.86	81.15
16	30.49	66.75	98.71	351.54
17	9.09	11.11	10.53	108.12
18	5.86	5.40	0.00	66.00

Sample	Histidine	Arginine	Threonine	Alanine
1	0.00	9.04	9.91	239.73
2	10.88	7.64	0.00	90.55
3	11.03	7.29	0.00	83.61
4	10.63	7.80	0.00	96.04
5	19.02	0.00	0.00	96.74
6	8.87	0.00	7.08	76.64
7	13.82	9.88	0.00	104.07
8	0.00	0.00	0.00	43.33
9	19.66	0.00	0.00	83.78
10	9.05	0.00	0.00	85.60
11	9.74	0.00	0.00	46.70
12	0.00	9.42	0.00	77.97
13	8.55	0.00	0.00	56.62
14	13.99	8.27	0.00	92.70
15	10.32	0.00	0.00	68.68
16	29.71	34.86	21.96	116.20
17	11.86	0.00	6.08	61.01
18	9.15	6.29	0.00	54.64

Sample	Proline	Tryptophan	Valine	Methionine
1	33.70	7.04	138.88	0.00
2	12.19	0.00	8.15	0.00
3	12.28	0.00	15.30	6.41
4	7.33	4.70	11.55	0.00
5	10.02	0.00	4.96	0.00
6	7.11	0.00	5.10	0.00
7	10.88	6.47	13.45	0.00
8	6.23	0.00	0.00	0.00
9	6.38	0.00	4.52	0.00
10	6.88	0.00	11.29	0.00
11	5.41	0.00	6.06	0.00
12	5.38	0.00	4.42	0.00
13	0.00	0.00	5.47	0.00
14	6.29	0.00	14.09	0.00
15	4.66	0.00	6.25	0.00
16	34.53	13.7	39.50	0.00
17	0.00	0.00	11.95	0.00
18	0.00	0.00	7.80	0.00

Sample	Leucine	Phenylalanine	Lysine	Total
1	137.76	10.72	12.51	1186.00
2	10.84	3.92	7.12	378.40
3	19.18	0.00	5.84	343.20
4	14.09	0.00	4.38	346.13
5	7.69	0.00	7.18	311.67
6	6.94	0.00	3.77	393.80
7	17.09	0.00	5.84	403.33
8	0.00	0.00	0.00	135.67
9	6.84	0.00	4.58	266.20
10	9.66	0.00	4.98	289.67
11	5.92	0.00	2.68	179.67
12	5.31	0.00	3.82	234.67
13	5.87	0.00	2.62	164.27
14	5.73	0.00	5.08	297.73
15	0.00	0.00	3.10	199.47
16	65.98	26.50	43.98	1013.47
17	5.51	0.00	4.72	239.80
18	0.00	0.00	0.00	155.47

Appendix 6.4 Free Amino Acids

(Amino Acids in pmol per mg of shell).

Sample	Aspartic acid	Glutamic acid	Serine	Glycine
1	23.88	10.24	9.53	135.43
2	8.96	6.73	0.00	78.45
3	10.58	4.23	11.65	65.38
4	11.95	19.92	10.91	76.57
5	9.69	0.00	13.05	79.12
6	8.86	133.16	0.00	72.24
7	20.72	0.00	9.52	114.06
8	0.00	0.00	0.00	35.92
9	5.73	4.16	6.27	71.25
10	12.47	4.60	10.46	74.62
11	6.91	0.00	0.00	56.14
12	15.34	4.46	7.04	96.28
13	5.84	0.00	0.00	48.45
14	10.18	0.00	0.00	96.56
15	9.32	0.00	0.00	71.45
16	0.00	4.14	11.89	86.61
17	0.00	0.00	0.00	64.85
18	0.00	0.00	0.00	44.36

Sample	Threonine	Arginine	Histidine	Alanine
1	0.00	9.73	0.00	148.21
2	0.00	0.00	0.00	82.70
3	0.00	0.00	7.28	74.85
4	0.00	0.00	0.00	89.04
5	0.00	0.00	10.00	95.09
6	5.36	0.00	0.00	79.76
7	0.00	0.00	0.00	90.62
8	0.00	0.00	0.00	41.65
9	0.00	0.00	9.97	80.94
10	0.00	0.00	0.00	79.40
11	0.00	0.00	0.00	50.42
12	0.00	0.00	0.00	98.91
13	0.00	0.00	0.00	55.13
14	0.00	8.21	0.00	109.21
15	0.00	0.00	0.00	75.17
16	0.00	0.00	0.00	70.91
17	0.00	0.00	0.00	56.29
18	0.00	0.00	0.00	47.58

Sample	Proline	Tryptophan	Valine	Isoleucine
1	13.11	0.00	10.56	11.31
2	5.52	0.00	7.15	8.30
3	5.18	0.00	17.58	0.00
4	4.84	0.00	14.37	0.00
5	0.00	0.00	7.04	0.00
6	4.68	0.00	14.61	0.00
7	0.00	0.00	17.40	0.00
8	0.00	4.30	0.00	0.00
9	0.00	0.00	30.65	0.00
10	5.48	4.83	5.47	0.00
11	0.00	4.62	6.31	0.00
12	4.68	4.71	7.14	0.00
13	0.00	0.00	6.50	0.00
14	0.00	4.63	12.83	0.00
15	0.00	0.00	0.00	0.00
16	5.05	6.28	22.79	0.00
17	0.00	0.00	11.11	0.00
18	0.00	0.00	7.49	0.00

Sample	Leucine	Lysine	Total
1	6.53	0.00	378.40
2	0.00	0.00	198.00
3	4.27	3.75	204.60
4	4.80	3.46	236.13
5	4.63	2.81	221.47
6	0.00	2.87	321.20
7	0.00	4.07	256.67
8	0.00	0.00	82.13
9	5.65	2.78	217.07
10	7.40	3.67	208.27
11	5.73	0.00	129.80
12	6.14	3.04	247.87
13	6.71	0.00	122.47
14	4.82	3.01	249.33
15	0.00	0.00	156.20
16	4.34	3.16	265.47
17	0.00	0.00	132.00
18	0.00	0.00	99.73

CHAPTER 7

DIAGENESIS AND SURVIVAL OF INTRACRYSTALLINE AMINO ACIDS IN FOSSIL AND RECENT MOLLUSC SHELLS FROM BRITAIN AND NEW ZEALAND

Lynda Mitchell and Gordon B. Curry

Department of Geology and Applied Geology, Glasgow University, Glasgow G12 8QQ^

7.1 Abstract

Amino acid analysis was carried out on intracrystalline organic material from fossil and recent mollusc shells from South Wanganui Basin, New Zealand, ranging in age from 3.6 My to Recent. The absolute abundance of amino acids is highly variable but shows a gradual decline through time due to diagenetic effects. The proportion of peptide-bound amino acids decreases with time, and there is a corresponding increase in free amino acids as proteins are broken down by natural hydrolysis. In shells older than 0.5 My, most amino acids are free, and the rate of decay of peptide bonds appears to slow appreciably, with small proportions of peptide-bound amino acids occurring in shells throughout the time span investigated. The quantities of free amino acids reach a peak between 0.5 and 1 My, after which there is a general decrease in most individual amino acids, presumably because they decay or become incorporated into predominantly insoluble geopolymers. Alanine is a notable exception, increasing in older samples because it is a common by-product of the breakdown of other amino acids.

Amino acid data from different species and from shell beds of different ages were compared using multivariate statistical techniques. The results indicate that, despite the effects of diagenesis, the original biochemical distinction between different groups of molluscs (i.e. different proteins within the shell) survives for at least 3.6 My, and may be detectable in older specimens provided sufficient original amino acids remain.

7.2 Introduction

In order to gain meaningful information from organic molecules in fossil shells, it is necessary to isolate original organic matter which has not been contaminated or replaced by more recent biomolecules. For this purpose, intracrystalline biomolecules are used. These molecules are trapped within the crystals of the shell during biomineralization and are therefore protected from contamination by outside sources until released by decalcification. Many of these molecules may have been actively involved in the process of shell formation by acting as a nucleation site for crystal growth (Lowenstam and Weiner, 1989). The molecules which are involved in the biomineralization process are usually proteins and protein-like macromolecules secreted by the cells of the mantle, which form a matrix within and around which calcium carbonate crystals are precipitated (Lowenstam and Weiner, 1989). Each protein molecule consists of a chain of amino acids, the order of which is determined by the sequence of nucleotides in the DNA which controls its production. These amino acids are therefore directly related to genotype and may represent useful taxonomic indicators after the protein sequence has been destroyed (Walton, 1992). The interpretation of amino acid data from fossil shells, however, is complicated by the fact that individual amino acids vary in stability, and can decompose at varying rates into other compounds or into other amino acids (Vallentyne, 1964; 1968). Hence the amino acid compositions of fossil shells are likely to be less easy to interpret and will reflect complicated amino acid diagenesis reactions as well as original taxonomic variability. The purpose of this paper is to analyse both the peptide bound and the free (i.e. naturally hydrolysed) amino acids from within shells of different ages, in order to investigate the state of preservation of intracrystalline proteins and the extent to which original biochemical discrimination between different taxonomic groups survives the fossilization process.

7.3 Method

Fossil mollusc shells were collected from sea cliffs and inland exposures in the South Wanganui Basin, New Zealand (fig. 2.1). This area was chosen for its almost continuous sequence of late Pliocene and Pleistocene fossiliferous shallow marine deposits containing abundant mollusc shells. The sequence consists of poorly consolidated layers of sand and mud deposited mainly during interglacials and separated by unconformities associated with glacial marine regressions. Recent mollusc shells were collected from near shore locations and from beaches around the coasts of the North and South Islands of New Zealand (fig. 2.3).

Well preserved shells of various species were selected from shell beds at different levels in the Wanganui sequence (fig 7.1) along with related Recent species. Specimens were taken from each of 28 shellbeds, making 60 specimens in all (table 7.1). Each specimen was examined by SEM to check for signs of recrystallization, and XRD analysis was used to check that aragonite shells had not reverted to calcite, as such recrystallization would have allowed contamination of intracrystalline biomolecules. The shells were cleaned of sediment and algae and the ligaments removed. Where necessary the shells were placed in a cool oven at 40°C to dry out the periostracum which was then removed. Each shell was washed in water then soaked in an aqueous solution of bleach to remove any remaining organic molecules from the surface by oxidation. The shells were then rinsed in clean Milli Ro^{TM} water and left to air dry.

Small carbonate samples were taken from each shell using a small drill with a rotating tip with a diameter of 1 mm. Intercrystalline organic matter was removed from the carbonate powder by plasma ashing. The samples were dissolved in 2N hydrochloric acid at a ratio of 11µl per mg of shell and centrifuged to remove insoluble compounds. Analysis was carried out using an Applied Biosystems 420H amino acid analyser (section 3.5). Each sample was analysed both with and without hydrolysis in order to determine the proportion of amino acids present in the free state, i.e. the extent to

Table 7.1 Shell samples 1-60: species, superfamilies, locations and ages

1. *Maoricardium spatiosum* (Cardiacea)- Pepper Shell Sand (c.3.6 my)
2. *Phialopecten marwicki* (Pectinacea)- Pepper Shell Sand (c.3.6 my)
3. *Maoricardium spatiosum* (Cardiacea)- Pepper Shell Sand (c.3.6 my)
4. *Maoricardium spatiosum* (Cardiacea)- Snapper Point Shellbed (c.3.5 my)
5. *Pecten tainui* (Pectinacea)- Landguard Formation (c.0.35 my)
6. *Anchomasa similis* (Pholadacea)- Castlecliff Beach (recent)
7. *Paphies (Mesodesma) subtriangulata* (Mesodesmatacea)- Long Beach (recent)
8. *Tiostrea chilensis* (Ostreacea)- Kupe Shellbed (c.0.7 my)
9. *Paphies australis* (Mesodesmatacea)- Te Rauone Beach (recent)
10. *Chione (Austrovenus) stutchburyi* (Veneracea)- Warrington Beach (recent)
11. *Maoricolpus roseus* (Cerithiacea)- Long Beach (recent)
12. *Maoricardium spatiosum* (Cardiacea)- Upper Waipipi (c.3.2 my)
13. *Patro undatus* (Anomiacea)- Nukumaru Limestone (c.1.45 my)
14. *Chione (Austrovenus) stutchburyi* (Veneracea)- Te Rauone Beach (recent)
15. *Mactra discors* (Mactracea)- Warrington Beach (recent)
16. *Spisula (Crassula) aequilateralis* (Mactracea)- Rapanui Formation (c.0.12 my)
17. *Paphies (Mesodesma) subtriangula* (Mesodesmatacea)- Rapanui Formation (c.0.12 my)
18. *Tawera spissa* (Veneracea)- Landguard Formation (c.0.35 my)
19. *Tiostrea chilensis lutaria* (Otreacea)- Landguard Formation (c.0.35 my)
20. *Pecten tainui* (Pectinacea)- Landguard Formation (c.0.35 my)
21. *Zethalia zelandica* (Trochacea)- Upper Castlecliff Shellbed (c.0.43 my)
22. *Paphies (Mesodesma) subtriangulata* (Mesodesmatacea)- U. Castlecliff Shellbed (c.0.43 my)
23. *Venericardia purpurata* (Carditacea)- Upper Castlecliff Shellbed (c.0.43 my)
24. *Paphies (Mesodesma) subtriangulata* (Mesodesmatacea)- Shakespeare Cliff Sand(c.0.44 my)
25. *Pecten tainui* (Pectinacea)- Shakespeare Cliff Sand (c.0.44 my)
26. *Tiostrea chilensis lutaria* (Ostreacea)- Shakespeare Cliff Sand (c.0.44 my)
27. *Paphies (Mesodesma) subtriangulata* (Mesodesmatacea)- Shakespeare Cliff Sand(c.0.44 my)
28. *Venericardia purpurata* (Carditacea)- Shakespeare Cliff Sand (c.0.44 my)
29. *Tiostrea chilensis lutaria* (Ostreacea)- Tainui Shellbed (c.0.5 my)
30. *Maoricolpus roseus* (Cerithiacea)- Tainui Shellbed (c.0.5 my)
31. *Venericardia purpurata* (Carditacea)- Tainui Shellbed (c.0.5 my)
32. *Pecten tainui* (Pectinacea)- Lower Castlecliff Shellbed (c.0.6 my)
33. *Maoricolpus roseus* (Cerithiacea)- Lower Castlecliff Shellbed (c.0.6 my)
34. *Venericardia purpurata* (Carditacea)- Lower Castlecliff Shellbed (c.0.6 my)
35. *Venericardia purpurata* (Carditacea)- Tom's Conglomerate (c.0.62 my)
36. *Tiostrea chilensis lutaria* (Ostreacea)- base of Upper Kai-Iwi Siltstone (c.0.68 my)
37. *Maoricolpus roseus* (Cerithiacea)- Kupe Formation (c.0.7 my)
38. *Venericardia purpurata* (Carditacea)- Kupe Formation (c.0.7 my)
39. *Paphies (Mesodesma) subtriangulata* (Mesodematacea)- Kaikokapu Formation (c.0.78 my)
40. *Venericardia purpurata* (Carditacea)- Kaikokapu Formation (c.0.78 my)
41. *Divaricella (Divalucina) huttoniana* (Lucinacea)- Omapu Shellbed (c.0.85 my)
42. *Amalda (Baryspira) mucronata* (Muricacea)- Omapu Shellbed (c.0.85 my)
43. *Amalda (Baryspira) mucronata* (Muricacea)- Upper Westmere Shellbed (c.0.8 my)
44. *Maoricolpus roseus* (Cerithiacea)- Upper Westmere Shellbed (c.0.8 my)
45. *Paphies (Mesodesma) subtriangulata* (Mesodesmatacea)- Lower Kai-Iwi Shellbed (c.0.9 my)
46. *Paphies (Mesodesma) subtriangulata* (Mesodesmatacea)- Kaimatira Pumice Sand(c.0.95 my)
47. *Maoricrypta (Zeacrypta) monoxyla* (Calyptraeacea)- Okehu Shell Grit (c.0.99 my)
48. *Tiostrea chilensis lutaria* (Ostreacea)- Okehu Shell Grit (c.0.99 my)
49. *Venericardia purpurata* (Carditacea)- Okehu Shell Grit (c.0.99 my)
50. *Maoricrypta (Zeacrypta) monoxyla* (Calyptraeacea)- Butler's Shell Conglom. (c.1.07 my)
51. *Chlamys gemmulata* (Pectinacea)- Butler's Shell Conglomerate (c.1.07 my)
52. *Austrovenus stutchburyi* (Veneracea)- Mangahou (c.1.26 my)
53. *Patro undatus* (Anomiacea)- top of Nukumaru Brown Sand (c.1.4 my)
54. *Lutraria solida* (Mactracea)- Nukumaru Brown Sand (c.1.4 my)
55. *Patro undatus* (Anomiacea)- Hautawa shellbed (c.2.4 my)
56. *Crassostrea ingens* (Ostreacea)- Middle Waipipi (c.3.3 my)
57. *Lima waipipiensis* (Limacea)- Upper Waipipi (c.3.2 my)
58. *Crassostrea ingens* (Ostreacea)- Upper Waipipi (c.3.2 my)
59. *Maoricardium spatiosum* (Cardiacea)- Middle Waipipi (c.3.3 my)
60. *Crassostrea ingens* (Ostreacea)- Lower Waipipi (c.3.4 my)

Stage	Substage	Formation	Sample No.
Haweran		Alluvium	
		Rapanui Formation	16,17
		Brunswick Formation	
		Kaiatea Formation	
		Landguard Formation	5,18,19,20
Castlecliffian	Putikian	Putiki Shellbed	
		Mosstown Sand	
		Karaka Siltstone	
		Upper Castlecliff Shellbed	21,22,23
		Shakespeare Cliff Sand	24,25,26,27,28
		Shakespeare Cliff Siltstone	
		Tainui Shellbed	29,30,31
		Pinnacle Sand	
		Lower Castlecliff Shellbed	32,33,34
		Seafield Sand	35
		Upper Kai Iwi Siltstone	36
		Kupe Formation	8,37,38
	Okehuan	Upper Westmere Siltstone	43,44
		Kaikokapu Formation	39,40
		Lower Westmere Siltstone	
		Ophiomorpha Sand	
		Omapu Shellbed	41,42
		Lower Kai Iwi Siltstone	45
		Kaimatira Pumice Sand	46
		Upper Okehu Siltstone	
		Okehu Shell Grit	47,48,49
		Lower Okehu Siltstone	
		Mowhanau Formation	
		Ototoka Siltstone	
		Butler's Shell Conglomerate	50,51
Nukumaruan	Marahauan	Upper Maxwell Formation	
		Mangahou Siltstone	52
		Middle Maxwell Formation	
		Pukekiwi Shell Sand	
		Lower Maxwell Formation	
		Tewkesbury Formation	
		Waipuru Shellbed	
		Nukumaru Brown Sand	53,54
		Mangamako Shellbed	
		Nukumaru Limestone	13
		Ohingaiti Sand	
	Hautawan	Undifferentiated Formations	
		Kuranui Limestone	
		Hautawa Shellbed	55
Waitotaran	Mangapanian	Te Rama Shellbed	
		Parihauhau Shellbed	
		Te Rimu Sand	
		Wilkies Shellbed	
		Makokako Sand	
		Mangaweka Mudstone	
		Paparangi Sandstone	
	Waipipian	Waverley Formation	
		Upper Waipipi Shellbed	12,57,58
		Middle Waipipi Shellbed	56,59
		Lower Waipipi Shellbed	60
		Snapper Point Shellbed	4
		Rangikura Sandstone	
		Pepper Shell Sand	1,2,3

Fig 7.1 Stratigraphic Column of the Wanganui Series, after Fleming (1953) and Abbott and Carter (1991), showing sample points.

which the intracrystalline proteins in each shell had been naturally hydrolysed.

Some common proteinogenic amino acids are easily destroyed by hydrolysis. These include asparagine and glutamine (these get hydrolysed to aspartic acid and glutamic acid), methionine and cysteine (these are break down due to the oxidation of side-chain sulphur atoms) and tryptophan (this is lost due to the breaking of the carbon double bond present within its ring structure). These reactions are likely to have occurred by natural hydrolysis long before analysis. Therefore, in this study, amounts of original asparagine and glutamine are included in the figures for aspartic acid and glutamic acid respectively, and methionine, cysteine and tryptophan are not quantified. The resulting changes in bulk amino acid composition apply consistently to all samples and therefore do not affect sample relationships. Data are presented as picomoles per milligram of shell (pmol/mg), which is the form in which the raw data are obtained from the amino acid analyser. This is equivalent to nanomoles per gram of shell.

Peptide bound amino acids are calculated by subtracting the free amino acids from the total amino acids. Sometimes this results in a negative value, apparently indicating that there are more free amino acids than total amino acids, an impossible conclusion. This problem is due to the fact that for total amino acid analysis, peptide bonds must be first hydrolysed using hydrochloric acid. This can result in the total destruction of some amino acids as outlined above. In addition, certain other amino acids may suffer some small losses as a result of this hydrolysis. For example, losses of the amino acids serine, threonine and tyrosine may be in the order of 10-20%. When this problem occurs, and the calculated value for the peptide bound amino acids is negative, the value is taken to be zero.

The amino acid data were analysed statistically by means of principal component analysis techniques using the programme 'Datadesk™' on an Apple Macintosh™ microcomputer. The aim was to investigate the relationships between the amino acid compositions of different samples using a suitable multivariate

procedure. In this way a high percentage of the total variance between samples can be expressed on a three dimensional, rotating plot. Groups of samples were chosen that were known to be taxonomically related (e.g. the mollusc superfamilies Cardiacea, Carditacea, Pectinacea, Mactracea, Ostreacea, Anomiacea, Mesodesmatacea, Veneracea and Cerithiacea). Groups of samples from three, four or five superfamilies were plotted together according to their amino acid compositions.

7.4 Changes in Amino Acid Compositions through Time

The total intracrystalline amino acid compositions of all 60 samples is shown in fig 7.2. The data reveal a high degree of variability, even in recent samples in which the absolute yield of amino acids ranges from about 400 to 1200 pmol/mg. This level of variability is maintained in fossil samples. Statistically there is an overall decline in abundance through time, but the very low coefficient of correlation (0.38) is testimony to the highly variable nature of the amino acid data. Clearly different taxa of molluscs have very different quantities of proteins present in their shells and this is reflected in the variable yields from related fossil taxa. A gradual decline through time is also seen in most individual amino acids with the notable exception of alanine which increases quite significantly (fig 7.3). A few amino acids, such as histidine and tyrosine, are present in such small quantities that the pattern is distorted due to the effect of the detection limit of the amino acid analyser (about 5 pmol/mg), which results in a 'gap' in the results below this value.

Free amino acids are rare in Recent samples, but rapidly become an increasingly important component of the total amino acid yield (fig 7.4). Many of the individual amino acids show a pattern of rapid initial increase during the first 0.5 My followed by a gradual decline in older specimens, probably due to the decay of amino acids to form compounds that are not detected by the amino acid analyser (fig 7.5). Alanine shows a marked increase over the whole period. The total free amino acids show an initial increase followed by a

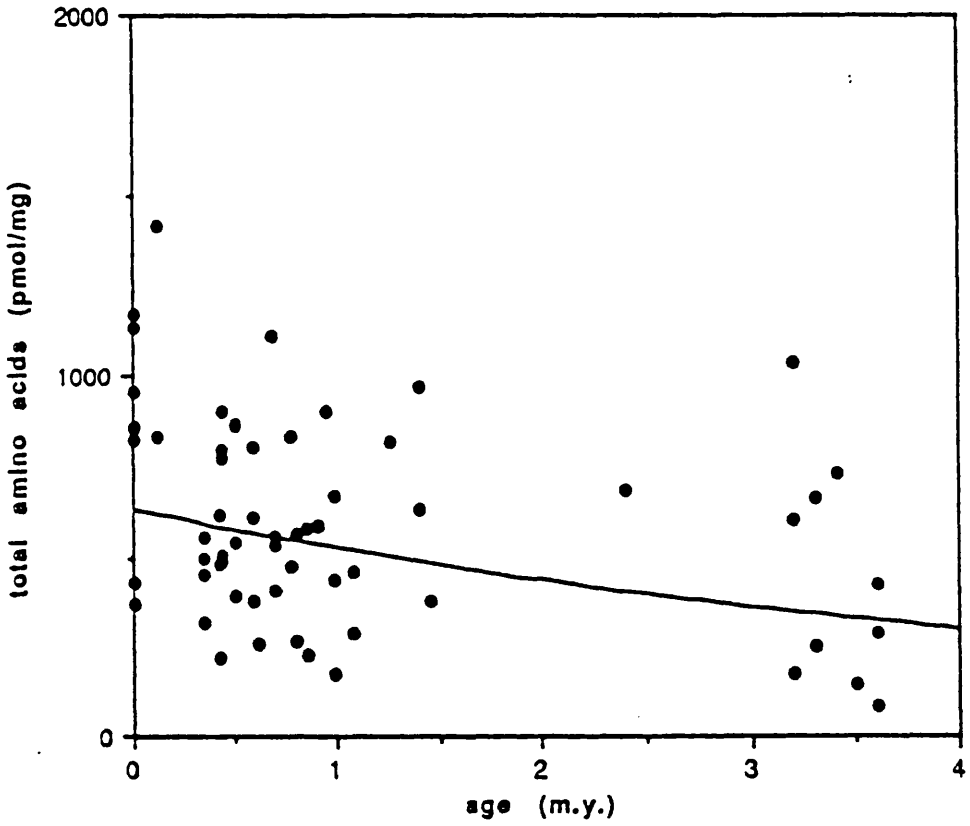

Fig 7.2 Total intracrystalline amino acids in all samples plotted against sample age

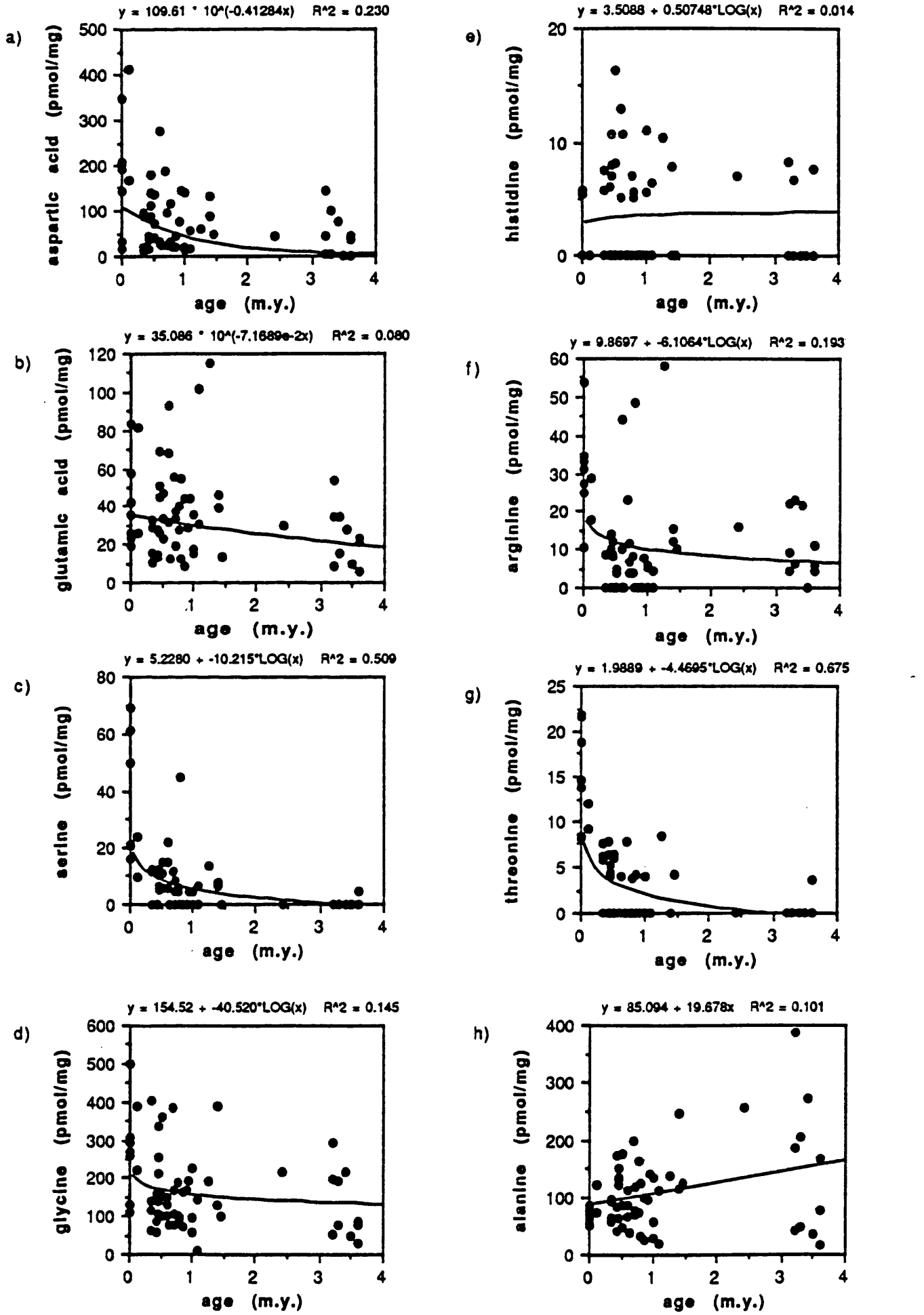

Fig. 7.3 Amount of total intracrystalline amino acids plotted against sample age

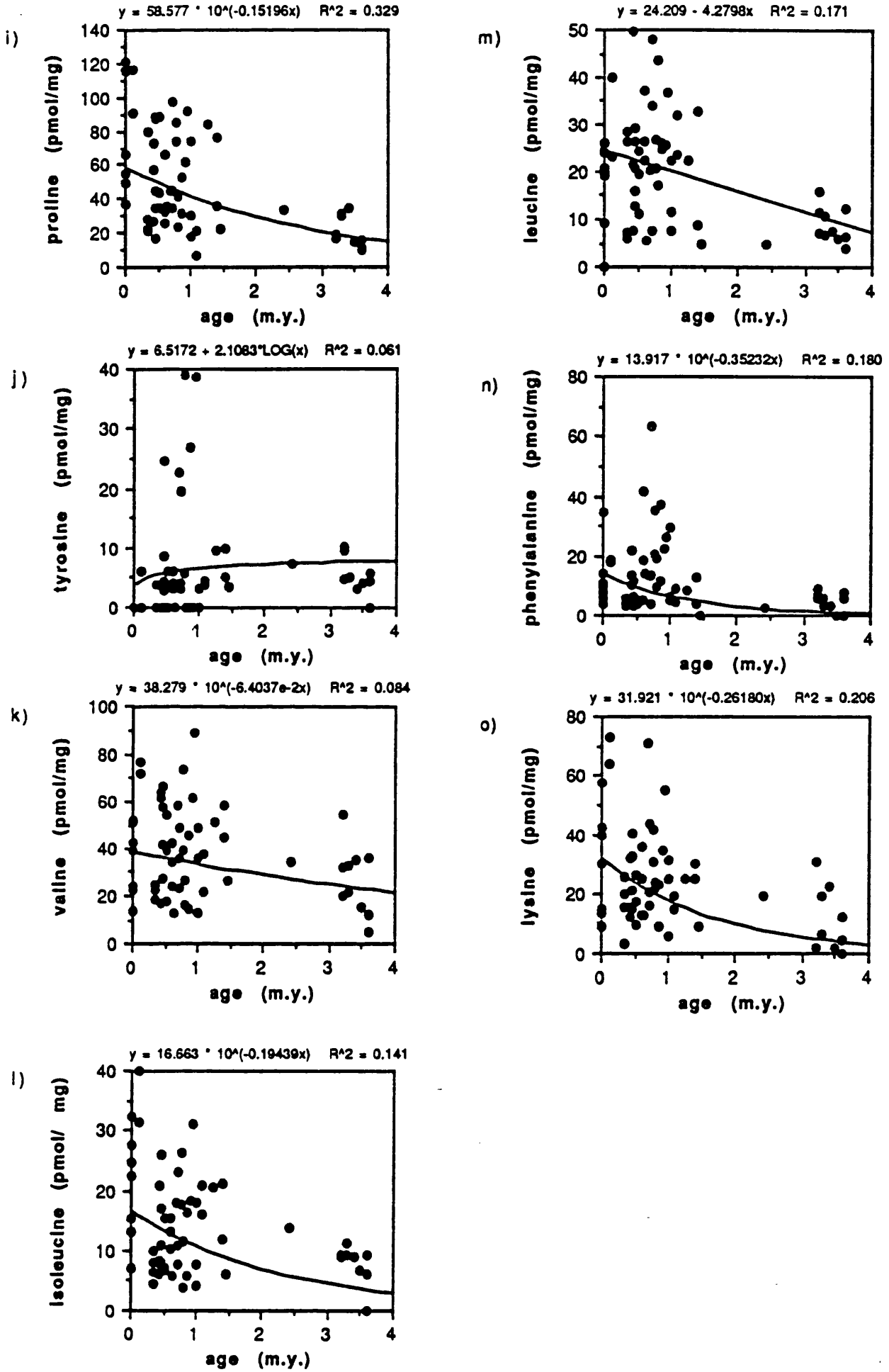

Fig. 7.3 Amount of total intracrystalline amino acids plotted against sample age

levelling off as the decline in most individual free amino acids is offset by the increase in alanine, this being the most abundant individual free amino acid. The absolute yield of free amino acids from different specimens is, like the total yield, highly variable. As expected, the rapid initial increase in free amino acids is matched by a rapid initial decrease in peptide bound amino acids (fig 7.6). This pattern is seen in most individual peptide bound amino acids except histidine and tyrosine, which are present in such small quantities as to show no pattern (fig 7.7).

These results are largely as might be expected. The gradual decrease in total amino acids through time is likely to be a function of biochemical reactions which gradually break down some of the amino acids into other compounds which are not detected by the amino acid analyser. In recent shells, the large amounts of peptide bound amino acids and small numbers of free amino acids show that protein preservation is good. The rapid initial increase in free amino acids and corresponding decrease in peptide bound amino acids, however, show that the proteins in fossil shells are poorly preserved as they quickly break down due to natural hydrolysis through time, producing a mixture of free amino acids and other compounds. Most of the peptide bonds are broken within the first 0.5 million years. However, some peptide bound amino acids do remain in the oldest samples, indicating that hydrolysis has not been complete and that some peptides may persist for a long time.

These results are consistent with the results of Walton (1992) who found that the proportion of amino acids present in the free state in brachiopod shells rises from negligible amounts in recent specimens to greater than 58% by 0.2 million years of age, and generally greater than 80% by 0.5 million years, showing that brachiopod shell proteins also tend to undergo very rapid initial hydrolysis. Excellent physical preservation therefore, does not necessarily indicate good biochemical preservation (Weiner and Lowenstam, 1980; Towe, 1980). Previous studies have shown that the rate of this natural hydrolysis is dependent upon many factors: water availability and temperature (and therefore burial history) being amongst the most important (Vallentyne, 1964; 1968; Ho,

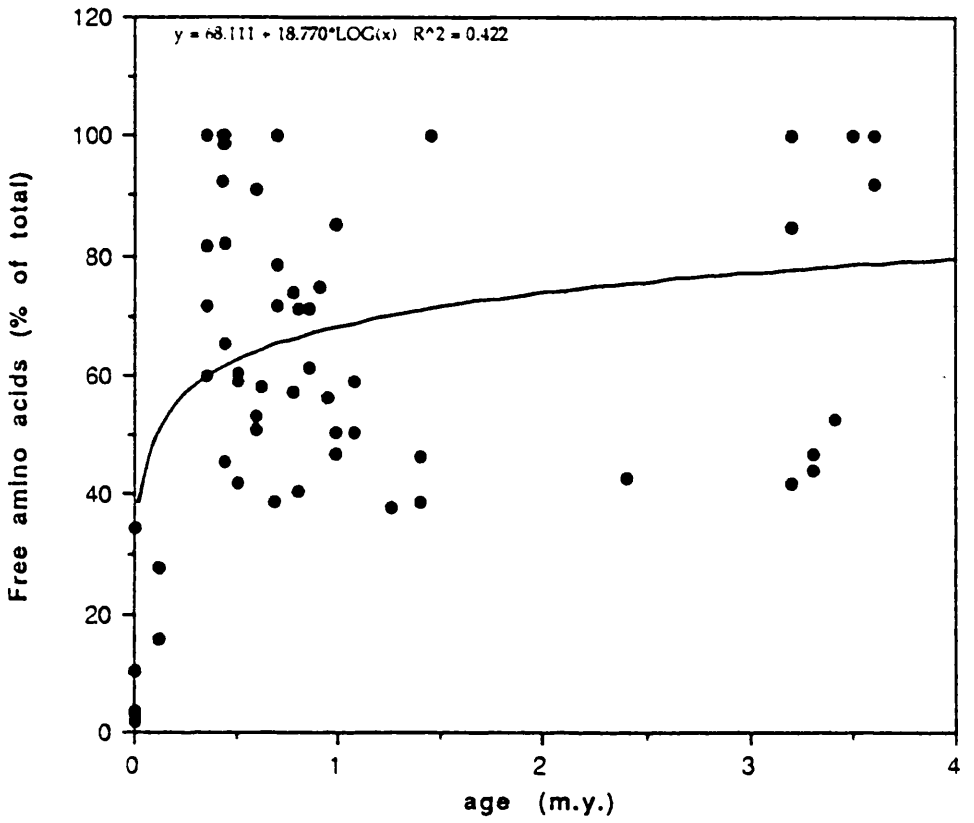

Fig 7.4 Free intracrystalline amino acids as a percentage of the total intracrystalline amino acids in all samples plotted against sample age

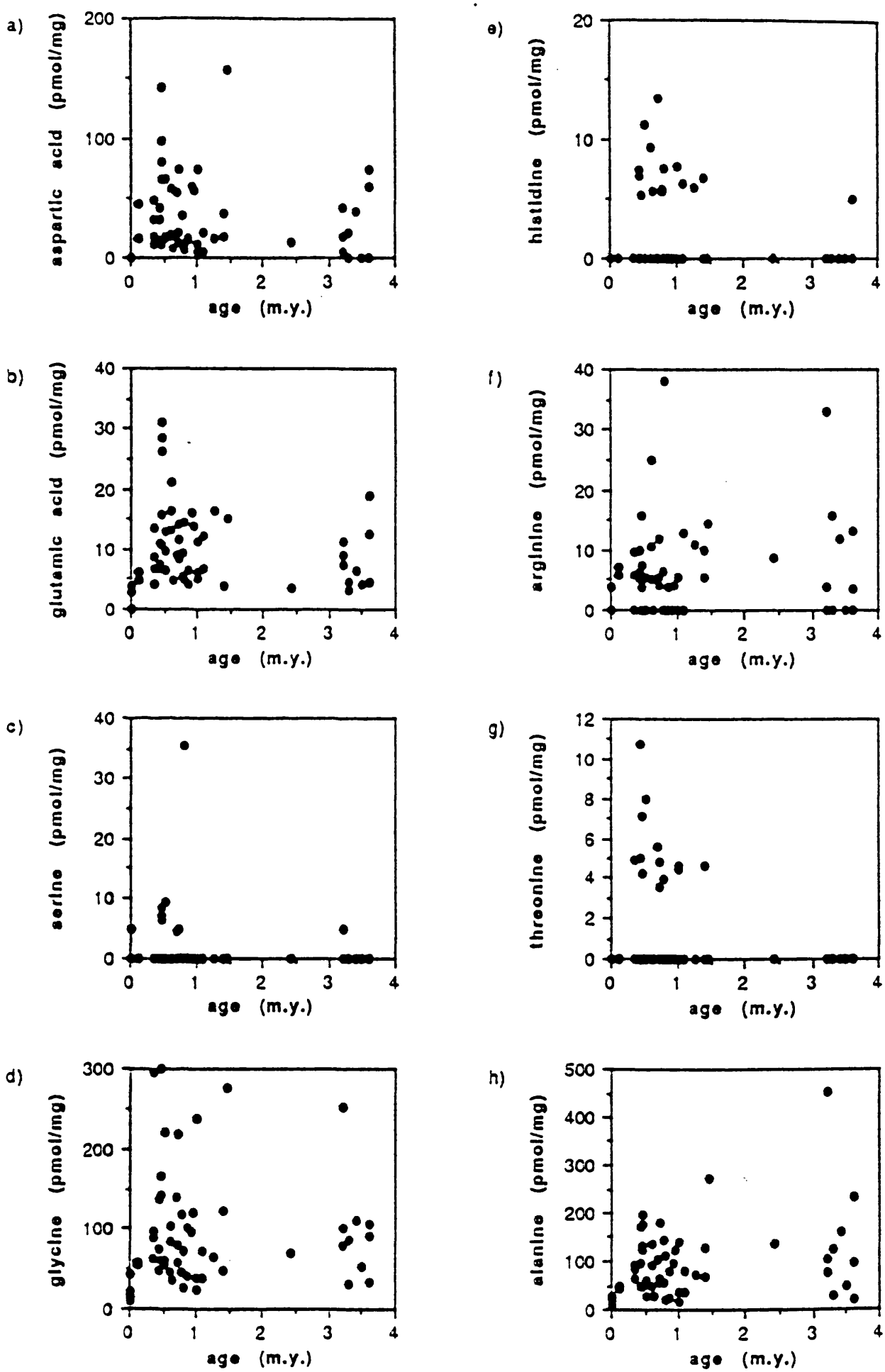

Fig. 7.5 Amount of free intracrystalline amino acids plotted against sample age

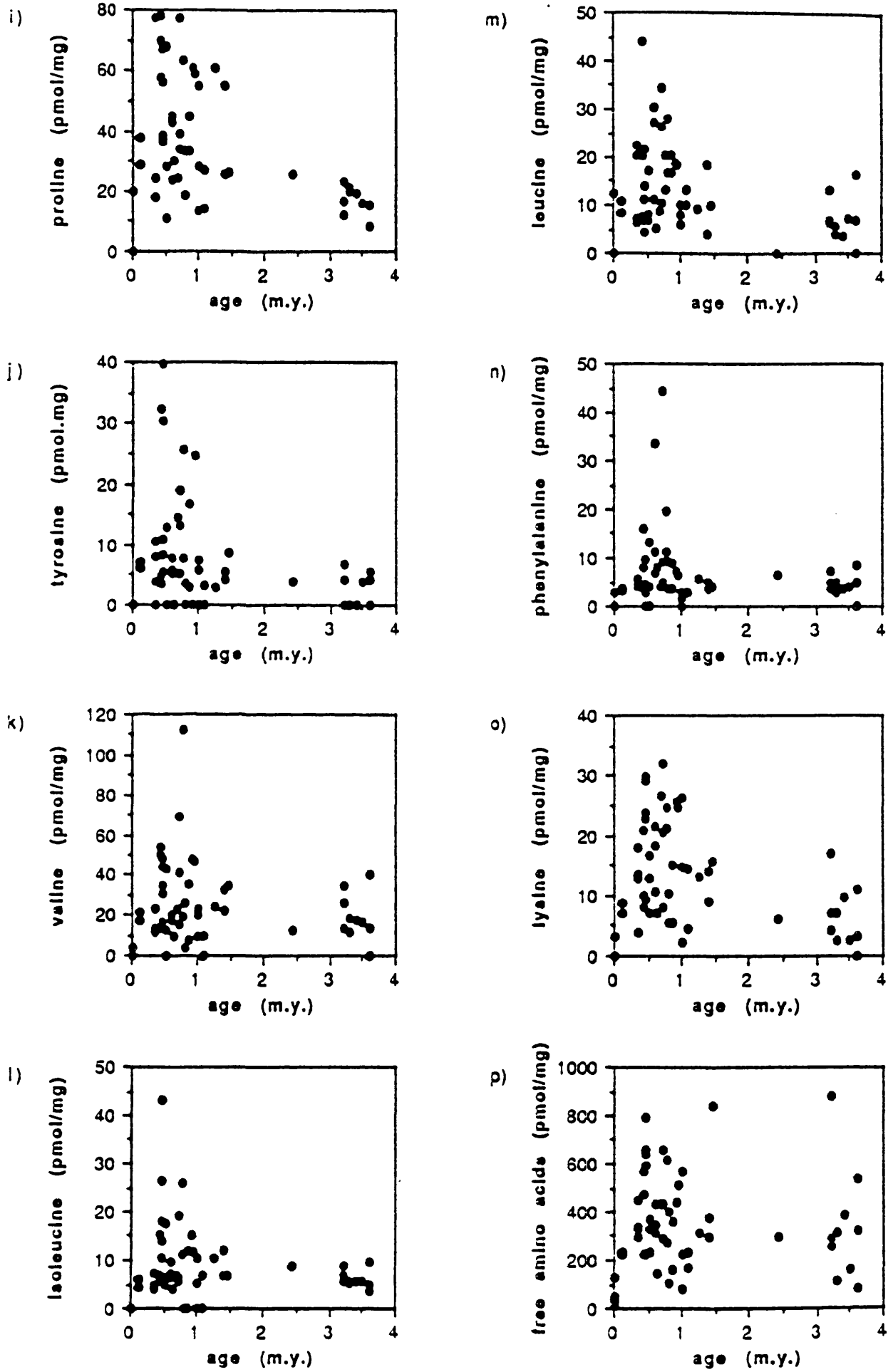

Fig. 7.5 Amount of free intracrystalline amino acids plotted against sample age

1966). The strength of the peptide bonds, and therefore the rate at which they can be broken, is dependent upon the nature of the residues on either side of the bond (van Kleef et al., 1975; Kahne and Still, 1988; Eglington and Logan, 1991). The rate of hydrolysis is also affected by the presence of other biomolecules such as carbohydrates which are present within shells (Vallentyne, 1964), and metal ions (Ikawa and Snell, 1954), both of which tend to speed up the reactions. The speed of amino acid decomposition reactions, therefore, is very difficult to predict and may not directly relate to the thermal stability of individual pure amino acids as determined by Vallentyne (1964).

The changes in individual amino acids show that most amino acids gradually decrease through time as they break down into other compounds. Those which increase through time, i.e. alanine, must be a reaction product, as long as the shell is functioning as a closed system. Alanine is known to be a common product of other amino acid reactions, for instance the decomposition of the relatively unstable amino acids serine, threonine and aspartic acid (Bada et al., 1978; Bada and Miller, 1970). Alanine is also one of the most stable amino acids (Vallentyne, 1964). The production of proteinogenic amino acids such as alanine from the decomposition of other amino acids, along with its high stability, explains its anomalously high concentration in these fossils and in others (e.g. Bada and Man, 1980).

7.5 Taxonomic Implications

The results of principal component analysis show that samples can be grouped according to their amino acid compositions in ways which reflect their taxonomic groupings (fig 7.8). These relationships seem robust despite amino acid diagenesis as the fossils get older, at least within the period of this study. This may be because the diagenesis reactions in all samples are very similar, involving the gradual decomposition of most amino acids and the production of diagenetic alanine and various other compounds. Individual standard amino acids break down at different rates

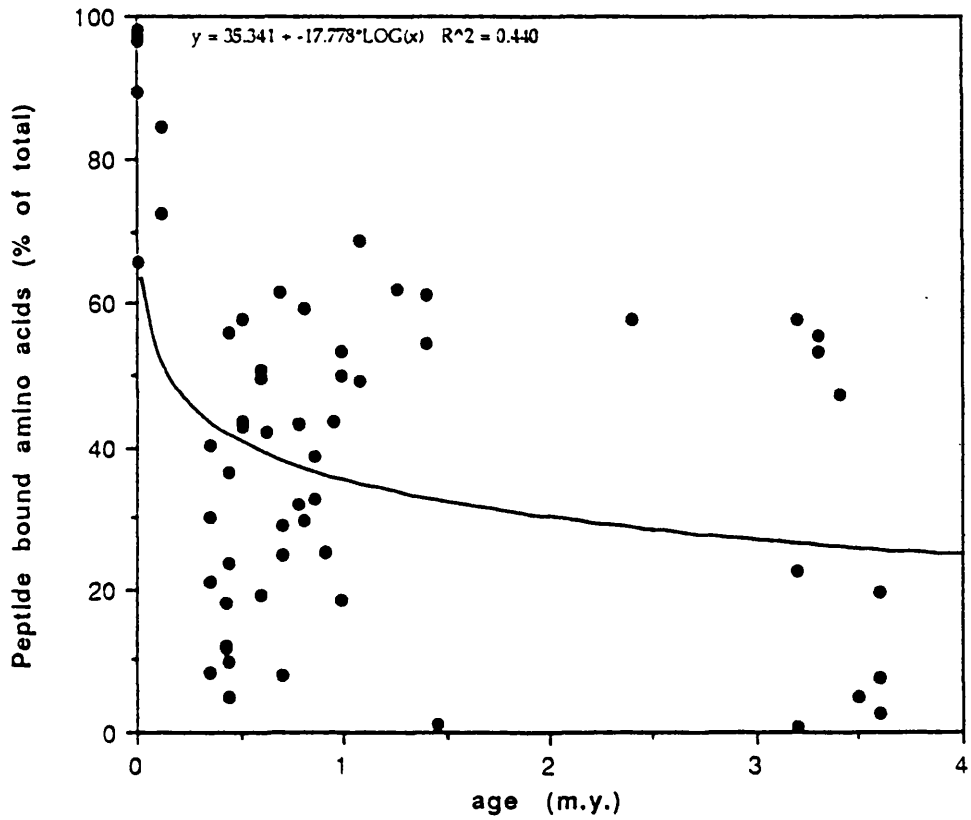

Fig 7.6 Peptide bound intracrystalline amino acids as a percentage of the total intracrystalline amino acids in all samples plotted against sample age

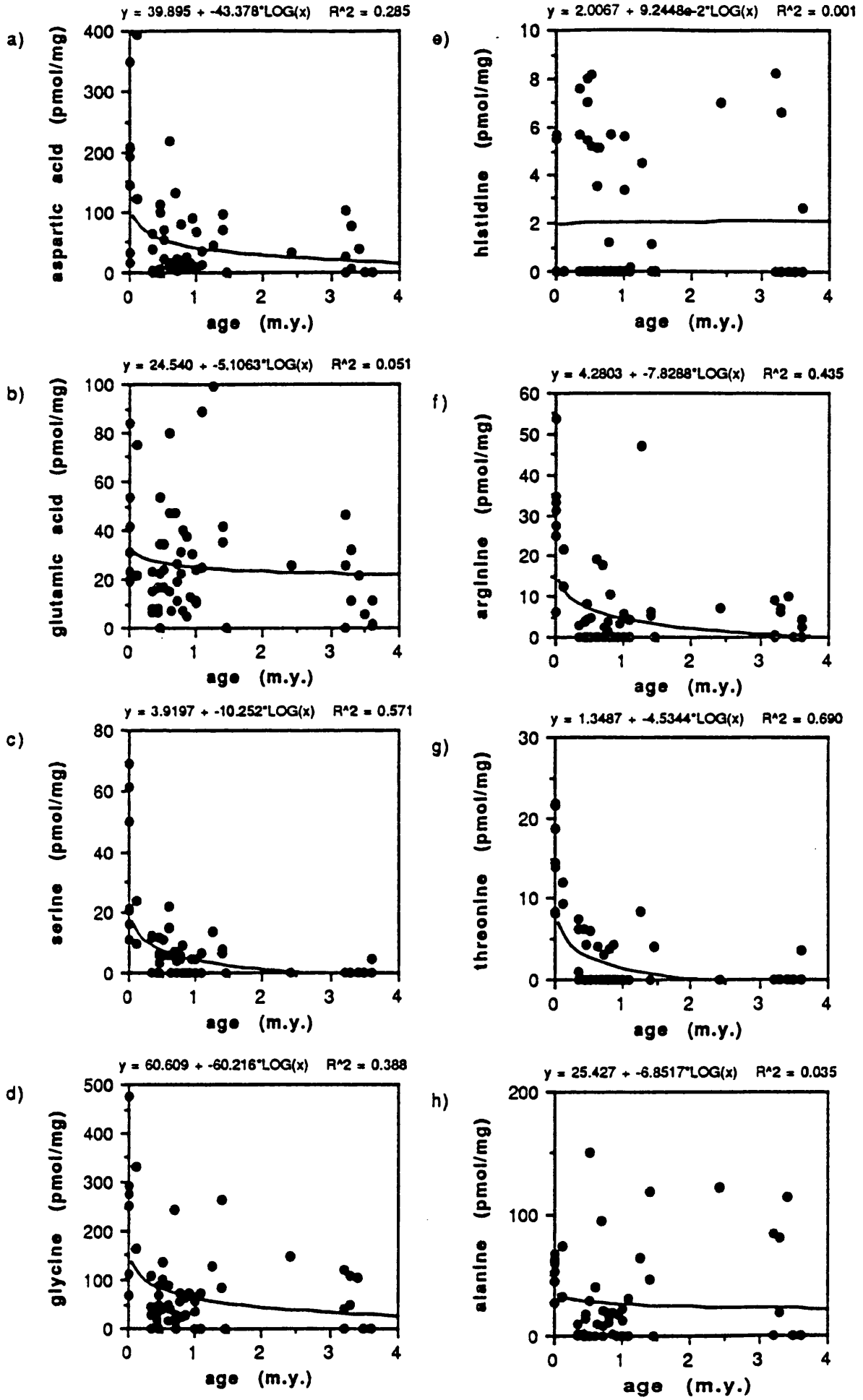

Fig. 7.7 Amount of peptide bound intracrystalline amino acids plotted against sample age

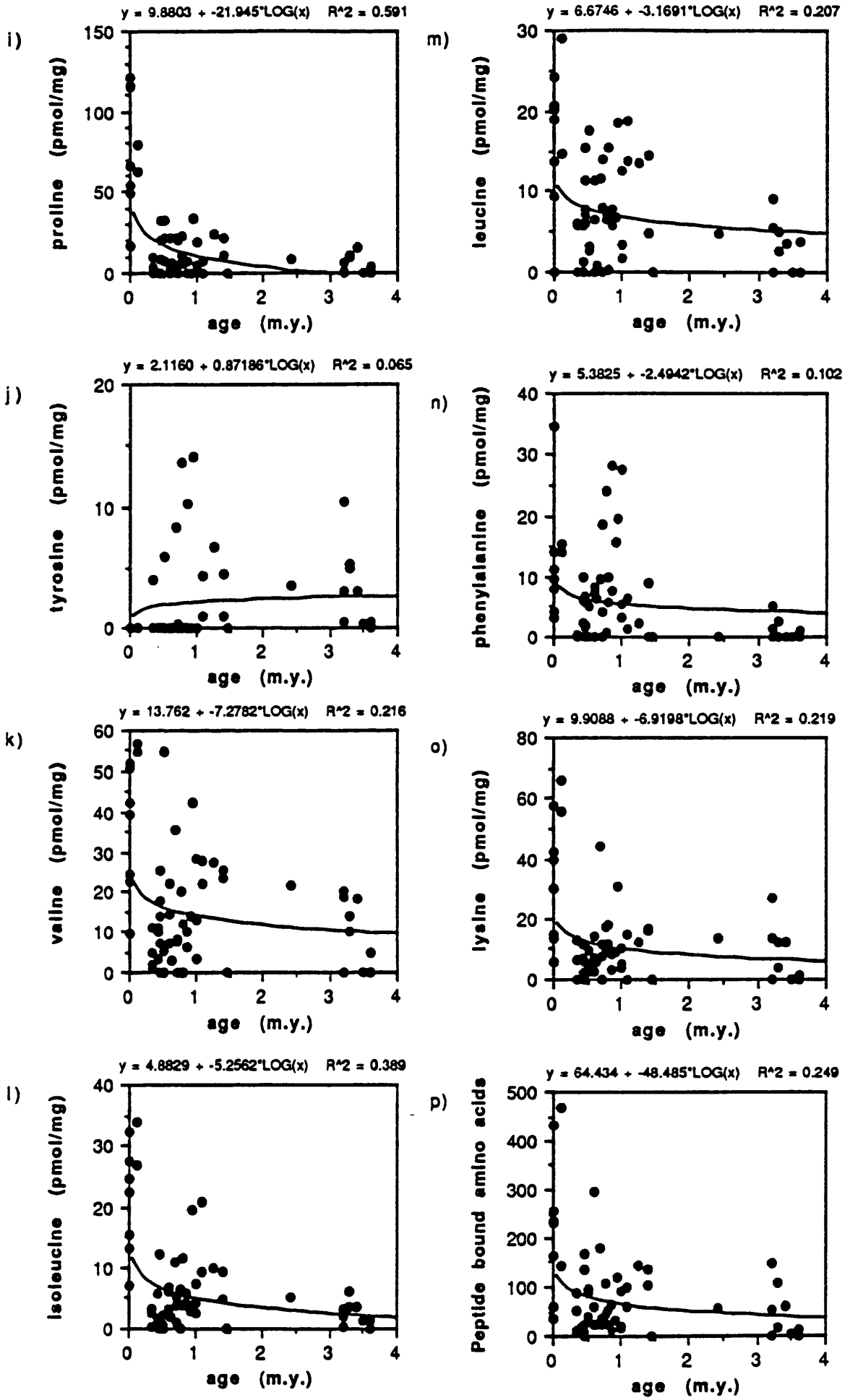

Fig. 7.7 Amount of peptide bound intracrystalline amino acids plotted against sample age

experimentally, but in mixtures all the reactions are speeded up and the situation is more complicated because decomposition can occur through many more pathways. Rate depends on temperature, water, the nature of the residues on either side of the bond, and presence of other compounds (Ikawa and Snell, 1954; Vallentyne, 1964; 1968; Ho, 1966; van Kleef et al., 1975; Kahne and Still, 1988; Eglington and Logan, 1991). Some of the amino acids most stable to pyrolysis have been shown to be some of the least stable when fossilised (Jones and Vallentyne, 1960). In this study, most amino acids appear to decompose at fairly similar rates despite their differing thermal stabilities. This means that the proportions of most individual amino acids present within shells of different species are relatively unaffected by diagenesis. The process is ubiquitous in all samples so does not affect relationships, as long as there is enough of the original amino acid left to give a taxonomic signature. When this is finally lost, the taxonomic relationships will quickly be destroyed.

Some morphologically similar groups plot together (fig. 7.8). For example, samples from superfamily Ostreacea (*Tiostrea chilensis lutaria* and *Crassostrea ingens*) and Anomiacea (*Patro undatus*) all have an oyster like appearance. Although the order of amino acids in the shell matrix proteins is derived directly from the DNA and therefore reflects genotype rather than phenotype, the shell morphology is in turn controlled by the shell matrix proteins (Lowenstam and Weiner, 1989), so would be expected to follow the same relationships. Therefore, it is interesting to speculate that whilst the overall genotypes of unrelated species may be very different from each other, in cases of similar shell morphology in unrelated species the sections of DNA which control the production of shell matrix proteins may be very similar. This may be a case of reconvergent evolution, resulting in the reconvergence of the morphologies of species that had previously diverged. Therefore, the use of amino acids from shell matrix proteins, though it reflects genotype, may only reflect the part of the genotype which controls shell morphology. The taxonomic relationships inferred from intracrystalline amino acids, therefore, may only reinforce relationships already inferred using the physical measurements of

Fig. 7.8 Three dimensional rotating plots of the first three principal components of amino acid data for various mollusc superfamilies.

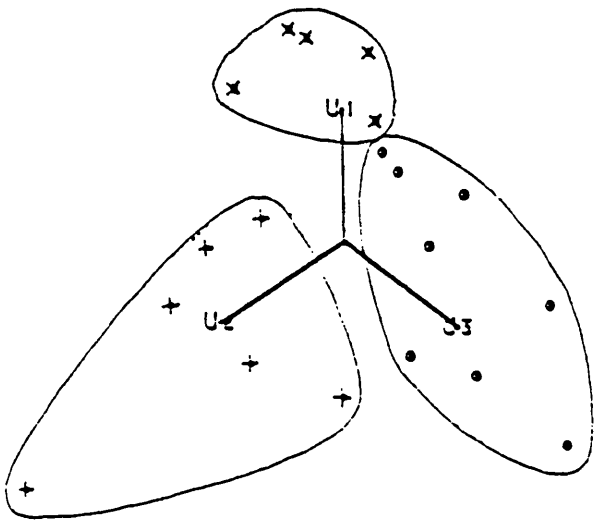

× Cardiacea
• Carditacea
+ Pectinacea

a) Superfamilies Cardiacea, Carditacea and Pectinacea.

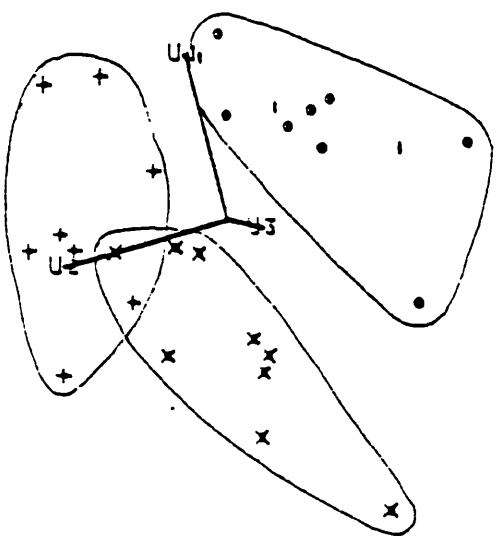

+ Carditacea
× Mesodesmatacea
• Ostreacea
ı Anomiacea

b) Superfamilies Carditacea, Mesodesmatacea, Ostreacea and Anomiacea.

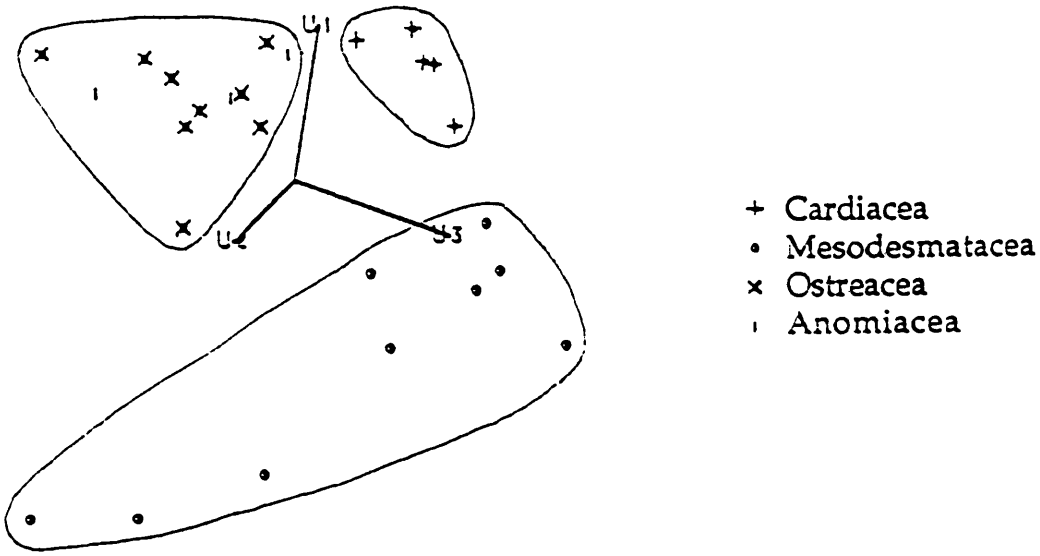

c) Superfamilies Cardiacea, Mesodesmatacea, Ostreacea and Anomiacea.

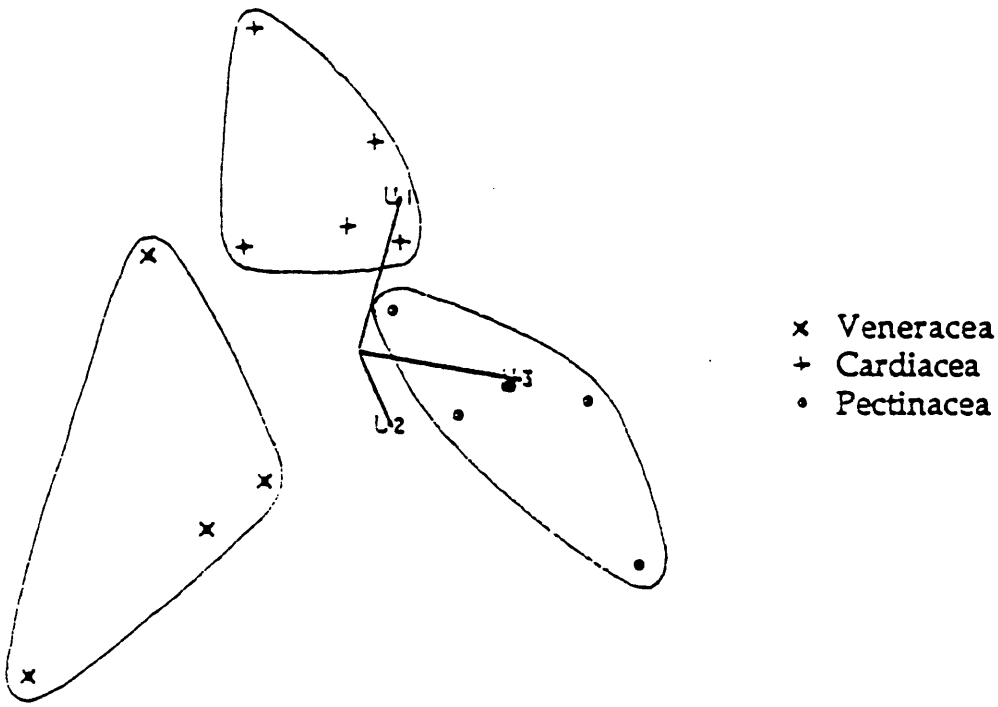

d) Superfamilies Veneracea, Cardiacea and Pectinacea.

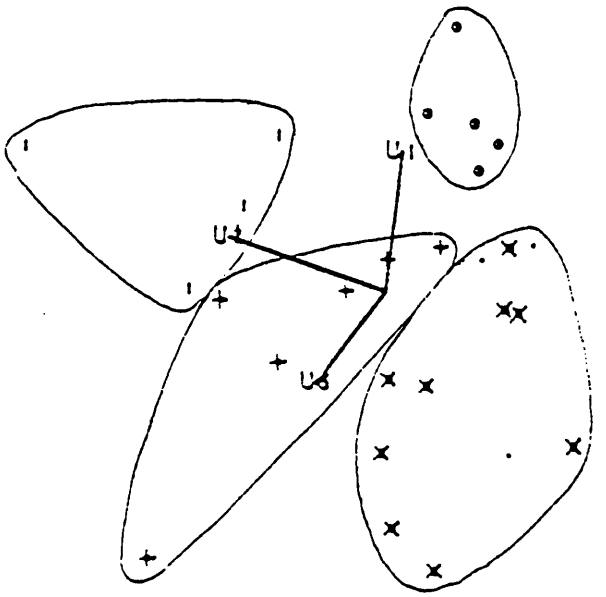

+ Pectinacea
• Cardiacea
' Cerithiacea
× Ostreacea
· Anomiacea

e) Superfamilies Pectinacea, Cardiacea, Cerithiacea, Ostreacea and Anomiacea.

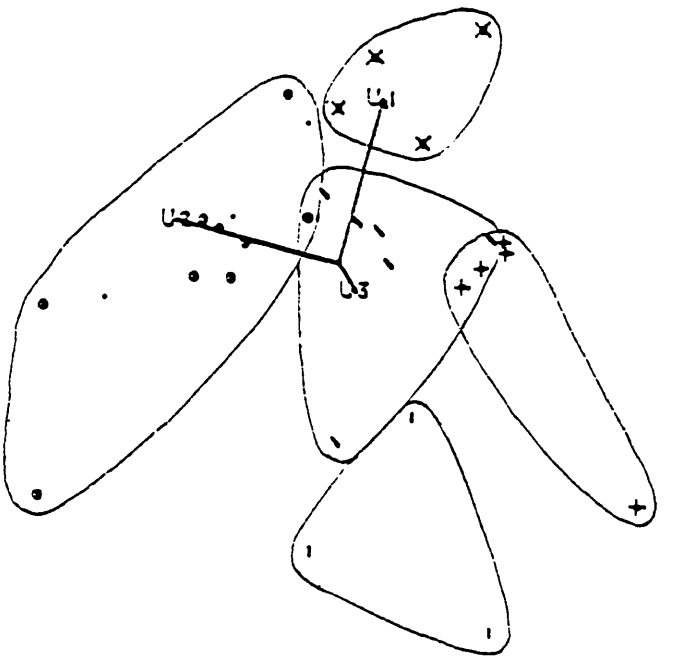

' Mactracea
\ Pectinacea
+ Cerithiacea
× Cardiacea
• Ostreacea
· Anomiacea

f) Superfamilies Mactracea, Pectinacea, Cerithiacea, Cardiacea, Ostreacea and Anomiacea.

shell morphology. Walton (1992) showed that the intracrystalline amino acid assemblages of recent brachiopods reinforced existing (morphological) taxonomy. However, considering the lack of soft parts available from fossils, and the general lack of preserved DNA, the intracrystalline amino acid compositions of hard parts may nontheless be one of the best indications of genotype available in the fossil record.

7.6 Conclusions

There is a gradual decline in most intracrystalline amino acids through time as they decompose to other compounds. Alanine shows an increase (at least over the time scale of this study) because it is a common product of other amino acid decomposition reactions. In recent shells, most amino acids are still peptide bound and the number of free amino acids is small. However, most of the peptide bonds are broken within the first 0.5 My. Free amino acids are therefore at a maximum at about 0.5-1 My after which there is a decline, except in alanine which continues to increase as other amino acids are broken down. Taxonomic relationships can still be inferred from intracrystalline amino acid compositions even after amino acid diagenesis reactions, as long as there is enough original amino acid left to give a taxonomic signal. This is because amino acid diagenesis reactions are fairly ubiquitous in all samples and most intracrystalline amino acids decompose at quite similar rates. The results of multivariate analysis of the amino acid compositions of different species tend to reinforce morphological taxonomy.

Appendix 7.1 Total intracrystalline amino acids (pmol/mg)

Sample	Age	Asp	Glu	Ser	Gly	His	Arg	Thr	Ala	Pro	Tyr	Val	Iso	Leu	Phe	Lys	Total
1	3.6	0	5.58	0	30.47	7.66	5.97	0	15.98	9.96	0	4.99	0	3.88	0	0	84.49
2	3.6	36.33	21.01	4.44	78.39	0	11.19	3.56	165.9	15.45	4.35	35.83	9.32	12.58	7.52	12.2	418
3	3.6	42.11	23.26	0	87.23	0	4.13	0	75.39	11.58	5.85	12.33	5.94	6.49	5.53	4.17	284
4	3.5	0	9.6	0	46.23	0	0	0	36.61	14.01	4.19	15.3	6.77	6.14	0	2	140.9
5	0.35	94.43	32.2	12.05	137.1	0	8.42	6.2	95.63	21.75	3.98	22.25	7.94	28.36	3.65	25.52	499.5
6	0	15.52	22.67	15.89	130	0	27.16	8.38	78.36	54.54	0	22.66	13.01	20.61	8	13.23	430.1
7	0	144.6	19.47	21.39	260.3	5.51	31.17	21.57	70.05	116.9	0	51.01	27.52	19.03	11.05	57.84	857.4
8	0.7	94.79	19.18	4.34	166.2	0	11.32	7.88	119.7	34.24	3.06	36.17	7.52	7.53	3.86	20.48	536.3
9	0	193	41.84	61.71	498.3	5.68	34.8	21.75	86.23	115.4	0	42.12	22.41	20.14	14.13	14.43	1172
10	0	349.7	83.72	69.14	308.2	0	53.8	18.71	81.7	66.14	0	39.26	15.21	0	4.09	42.08	1132
11	0	30.44	35.13	16.1	111.1	0	10.43	8.14	54.99	36.79	0	13.6	7.05	26.06	6.05	8.85	364.7
12	3.2	3.19	8.91	0	52.47	0	4.17	0	40.24	17.12	4.78	19.76	9.16	7.24	7.13	2.18	176.4
13	1.45	47.9	13.47	0	99	0	10.02	4.19	126	22.82	3.58	26.13	6.17	4.78	0	8.99	373
14	0	204.3	57.31	50.15	268.1	0	32.94	13.85	50.5	48.83	0	24.35	24.54	9.34	9.75	30.13	824.1
15	0	206.9	26.01	20.46	292.5	0	24.73	14.51	65.39	120.9	0	52.06	32.2	24.16	34.44	39.65	953.8
16	0.12	167	26.07	9.4	221	0	17.9	9.29	73.97	90.77	5.93	71.84	31.42	23.08	17.64	73.04	838.3
17	0.12	410.5	81.58	23.46	386.6	0	28.67	11.91	120.7	116.6	0	77.19	39.99	39.8	18.51	64.27	1420
18	0.35	20.38	15.09	0	60.67	5.71	8.61	5.88	56.91	79.91	0	24.81	9.77	7.16	5.91	15.51	316.3
19	0.35	11.16	10.34	0	404.6	0	0	0	63.93	22.54	0	24.27	4.48	6.09	3.18	3.45	554.1
20	0.35	86.24	28.66	11.37	115.2	7.58	0	7.51	92.47	27.98	0	18.71	6.47	26.41	3.81	19.94	452.3
21	0.43	34.04	27.38	0	157.2	0	10.08	0	171.8	57.49	0	64.07	8.22	49.57	22.08	15.33	617.2
22	0.43	44.09	14.57	0	85.64	6.05	13.78	7.83	83.33	73.12	3.56	61.47	20.76	21.63	10.04	32.08	478
23	0.43	14.48	13.45	0	59.65	0	0	6.32	41.96	26.85	0	16.48	5.96	7.42	13.45	12.05	218.1
24	0.44	87.79	25.69	5.07	253.5	8.04	8.55	5.11	149.7	88.55	8.53	57.74	16.85	20.93	6.64	32.72	775.4
25	0.44	86.26	25.77	10.54	140.8	0	0	0	132.1	16.41	0	27.02	10.9	26.54	5.8	20.99	503.2
26	0.44	140.7	50.48	12.29	334.7	0	0	0	134.4	35.1	4.64	41.45	7.99	12.97	4.41	20.91	799.9
27	0.44	178.9	69.58	11.75	210.7	7.05	11.95	3.94	120.9	87.22	24.62	66.06	25.89	29.23	11.46	40.55	899.8
28	0.44	111.1	44.68	6.61	107.2	10.74	7.94	4.41	63.43	45.13	2.84	41.7	7.84	15.92	3.25	14.59	487.3
29	0.5	135.7	33.56	10.62	359.3	0	0	6.08	177.4	43.67	5.97	54.7	6.93	11.13	3.77	17.39	866.2
30	0.5	71.28	47.12	14.9	102.5	8.12	4.77	0	48.74	35.2	0	17.71	6.82	19.76	4.28	9.88	391.1
31	0.5	39.41	23.51	5.8	154.8	16.36	3.82	6.33	87.64	89	3.59	39.09	15.2	24.21	5.02	26.37	540.1

Appendix 7.1 Total intracrystalline amino acids (pmol/mg)

32	0.6	275.4	93.56	21.87	149.7	0	0	0	111.2	25.35	4.02	34.53	13.08	37.1	5.44	35.54	806.7
33	0.6	28.98	31.53	6.05	100.6	5.09	9.93	0	68.41	32.37	3.29	24.17	10.21	26.31	18.32	13.07	378.4
34	0.6	31.58	67.97	14.6	131.8	12.91	44.17	0	86.67	66.45	6.09	42.4	15.45	22.48	41.76	25.06	609.4
35	0.62	24.32	12.41	0	77.5	10.65	0	4.09	37.9	35.39	0	13.12	5.66	5.67	14.34	12.64	253.7
36	0.68	186.9	56.06	11.58	385.5	0	22.95	0	199.8	45.09	22.85	58.75	17.84	20.42	13.63	70.78	1112
37	0.7	23.43	37.75	0	107	0	3.89	0	71.99	44.44	4.2	23.1	10.85	48.14	13.33	15.75	403.9
38	0.7	24.9	33.3	8.31	76.53	0	6.63	0	75.5	97.82	19.42	49.17	23.18	34.1	63.06	43.44	555.4
39	0.78	114.1	40.41	4.61	188.5	0	8	0	163	85.5	39.1	74	26.11	26.84	20.42	41.78	832.3
40	0.78	31.34	27.93	5.74	101.6	7.01	3.9	0	75.11	74.08	5.72	39.19	17.58	20.6	35.21	31.04	476
41	0.85	42.71	44.21	0	163.3	0	0	4.29	98.32	52.49	26.78	45.55	16.24	26.13	37.16	23.22	580.4
42	0.85	20.96	8.79	0	69.94	0	0	0	26.66	31.09	0	14.44	5.91	24.66	11.44	8.97	222.9
43	0.8	23.64	12.23	0	92.57	5.66	0	3.87	31.74	23.88	0	15.73	3.7	17.24	9.33	23.73	263.3
44	0.8	20.61	54.74	44.71	98.4	5.2	48.55	0	125.8	40.94	0	26.11	11.4	43.52	19.28	21.54	560.8
45	0.9	75.73	28.74	0	165.7	0	0	0	94.51	61.14	0	61.61	18.25	25.67	22.69	34.28	588.3
46	0.95	146	43.94	4.36	190.1	0	7.52	0	140.4	92.24	38.78	89.1	31.18	37	26.27	55.19	902.1
47	0.99	10.18	15.12	0	59.83	5.6	0	0	28.49	18.02	0	12.53	4.21	11.49	5.37	5.77	176.6
48	0.99	141.6	35.46	4.44	227.1	0	5.17	0	135	30.23	3.06	36.22	7.84	7.71	6.13	31.05	671
49	0.99	18.6	17.64	4.67	94.75	11.1	5.72	3.91	57.64	73.76	3.1	48.76	17.93	22.43	29.3	24.95	434.3
50	1.07	17.06	101.3	0	7.96	6.35	0	0	20.26	6.88	4.37	37.59	20.84	31.99	9.13	19.31	283
51	1.07	54.79	31.19	6.3	143.8	0	4.23	0	111.6	20.93	3.93	21.91	16	23.56	4.16	14.52	456.8
52	1.26	60.59	115.5	13.26	192.7	10.41	58.26	8.39	136.4	84.51	9.7	51.03	20.46	22.55	8.02	24.99	816.7
53	1.4	132.6	45.66	6.39	387.5	0	15.39	0	245.7	36.09	10.04	45.04	11.73	8.68	3.56	25.25	973.6
54	1.4	86.81	39.17	7.48	130.2	7.77	11.85	0	114.1	76.49	5.27	58.05	21.04	32.66	12.59	30.1	633.6
55	2.4	44.18	29.32	0	216	7.03	15.75	0	257.5	33.6	7.32	34.14	13.87	4.86	2.68	19.23	685.4
56	3.3	98.32	34.88	0	194.3	0	23.08	0	203.6	30.3	5.21	32.71	11.18	6.61	3.17	19.13	662.5
57	3.2	43.03	34.87	0	197.3	8.24	9.25	0	185.7	18.8	10.37	32.3	8.86	15.83	8.93	31.04	604.5
58	3.2	142	53.4	0	291.9	0	22.32	0	388.3	17.04	9.64	54.54	8.9	11.75	5.79	30.56	1036
59	3.3	5.96	15.47	0	78.57	6.64	6.09	0	47.25	30.97	5	21.6	9.29	10.69	5.58	6.35	249.5
60	3.4	75.49	28.25	0	215.5	0	21.57	0	273.3	34.96	3.05	35.06	9.09	7.45	3.15	22.18	729

Appendix 7.2 Free intracrystalline amino acids (pmol/mg)

Sample	Age	Asp	Glu	Ser	Gly	His	Arg	Thr	Ala	Pro	Tyr	Val	Iso	Leu	Phe	Lys	Total
1	3.6	0	4.4	0	32.81	5	3.57	0	19.76	8.43	0	0	3.7	0	0	0	77.67
2	3.6	59.84	19.04	0	104.5	0	13.26	0	232.6	15.48	4.25	40.11	9.42	16.31	8.47	11.03	534.3
3	3.6	74.3	12.35	0	90.35	0	0	0	96.67	8.52	5.38	13.24	4.65	6.88	4.69	3.22	320.3
4	3.5	0	4.12	0	52.7	0	0	0	47.48	15.96	3.89	16.04	5.65	7.37	3.99	2.46	159.7
5	0.35	31.31	8.69	0	94.96	0	5.62	0	86.02	17.66	0	11.14	4.7	22.54	4.47	12.81	299.9
6	0	0	2.74	0	17.45	0	0	0	24.96	0	0	0	0	0	0	0	45.15
7	0	0	0	0	9.24	0	0	0	7.94	0	0	0	0	0	0	0	17.18
8	0.7	72.9	8.26	0	217.3	0	11.7	4.82	180	33.77	13.03	68.94	6.51	10.54	4.67	20.62	653.1
9	0	0	0	0	21.21	0	0	0	18.88	0	0	0	0	0	0	0	40.09
10	0	0	0	0	16.18	0	0	0	20.5	0	0	0	0	0	0	0	36.68
11	0	0	3.77	4.93	42.13	0	3.97	0	27.66	19.78	0	3.78	0	12.4	2.91	3.14	124.5
12	3.2	4.7	11.13	4.77	100.5	0	3.7	0	74.28	22.81	4.26	26.24	8.99	13.07	7.08	7.05	288.6
13	1.45	156.4	15.05	0	276.3	0	14.4	0	271.1	25.97	8.57	34.68	6.82	9.87	3.87	15.71	838.7
14	0	0	3.91	0	16.15	0	0	0	6.24	0	0	0	0	0	0	0	26.3
15	0	0	2.73	0	14.56	0	0	0	6.63	0	0	0	0	0	0	0	23.92
16	0.12	45.25	4.82	0	57.84	0	5.6	0	42.18	28.69	7	17.21	4.42	8.44	3.55	7	232
17	0.12	16.16	6.08	0	55.66	0	6.95	0	47.18	37.79	6.04	20.77	6.01	10.81	3.13	8.68	225.3
18	0.35	16.91	6.8	0	62.99	0	9.55	4.9	82.8	77.16	10.51	23.08	7.07	7.31	5.6	17.88	332.6
19	0.35	11.3	4.2	0	296.4	0	0	0	65.85	24	8	23.21	4.2	6.5	3.91	3.8	451.4
20	0.35	48.75	13.5	0	88.62	0	5.62	0	91.24	18.23	3.72	13.69	3.99	20.4	4.15	13.31	325.2
21	0.43	32.42	10.97	0	135.8	7.31	6.44	4.97	170.7	69.58	3.38	53.78	6.7	43.92	15.86	8.01	569.8
22	0.43	42.28	6.76	0	74.78	6.83	9.79	10.71	96.06	78.16	32.17	50.22	15.16	20.32	7.92	20.73	471.9
23	0.43	13.77	7.28	0	49.2	0	5.12	0	47.92	57.81	4.9	12.98	5.53	7.69	3.68	9.86	225.7
24	0.44	80.38	26.4	8.29	166.6	0	15.56	7.15	131.8	56.22	30.52	43.76	26.3	13.99	0	29.86	636.9
25	0.44	97.67	31.09	7.17	166.2	0	4.9	0	197	36.27	8.32	31.11	43.04	11.09	0	23.79	657.7
26	0.44	141.7	28.44	6.38	299.7	0	3.97	0	175.5	38.2	10.88	34.34	18.08	6.86	2.92	22.86	789.8
27	0.44	65.66	15.66	0	142.7	0	7.41	4.2	125.6	67.25	39.6	48.25	13.81	21.5	9.65	29.02	590.3
28	0.44	10.61	10.52	0	59.2	5.34	0	0	48.26	36.9	5.36	16.22	10.58	4.55	4.28	9.14	221
29	0.5	65.33	9.55	0	221.7	0	0	0	26.4	10.87	0	0	6.43	8.03	4.1	12.74	365.2
30	0.5	15.76	12.65	9.19	60.51	0	0	0	50.52	28.42	0	12.64	4.71	17.01	13.3	7.16	231.9
31	0.5	17.84	6.48	0	55.52	11.2	5.42	7.97	58.41	67.96	12.71	42.9	17.47	6.61	0	16.71	327.2

Appendix 7.2 Free intracrystalline amino acids (pmol/mg)

32	0.6	57.98	13.17	0	103.5	0	5.14	0	136.2	23.55	5.7	19.92	6.51	30.5	6.82	21.59	430.6
33	0.6	19.79	16.37	0	84.31	0	10.5	0	93.08	42.82	5.02	16.89	7.14	27.2	11.05	10.46	344.6
34	0.6	16.88	21	0	44.89	9.36	25.09	0	47.36	44.52	7.6	20.28	9.5	11.22	33.53	18.31	309.5
35	0.62	7.67	4.89	0	36.05	5.57	0	0	28.98	29.81	0	10.04	3.88	5.06	8.03	7.14	147.1
36	0.68	55.18	8.93	4.47	139.6	0	5.12	5.57	105.9	24.03	14.51	23.35	6.99	8.87	3.92	26.55	433
37	0.7	12.01	11.5	0	79.67	0	5.46	0	63.69	39.36	5.18	15.1	5.67	34.28	9.26	8.12	289.3
38	0.7	21.25	14.13	4.71	58.77	13.37	4.04	3.53	55.04	77.57	19.04	41.49	19.28	26.28	44.45	31.99	434.9
39	0.78	35.34	9.38	0	117.9	5.54	6.39	3.98	143.3	63.25	25.46	112.4	26.14	20.34	19.78	24.74	614
40	0.78	10.56	5.33	0	46.54	5.79	0	0	56.62	63.55	7.62	18.93	11.03	13.36	11.21	21.26	271.8
41	0.85	16.46	6.42	0	101.2	0	0	0	78.79	44.77	16.48	35.61	12.19	20.35	8.92	14.99	356.2
42	0.85	13.77	4.2	0	41.94	0	3.92	0	24.62	33.28	2.84	8.13	0	16.88	3.65	5.56	158.8
43	0.8	7.14	4.67	0	26.26	0	0	0	20.19	18.42	0	3.91	0	16.89	3.65	5.56	106.7
44	0.8	9.51	14.43	35.66	73.15	7.47	38.22	0	111.2	33.42	3.53	26	0	28.05	9.32	10.17	400.1
45	0.9	58.57	15.89	0	94.83	0	0	0	94.96	61.11	0	47.54	15.27	18.92	7.11	25.57	439.8
46	0.95	56.14	13.9	0	120.2	0	4.31	0	122.2	58.86	24.69	46.95	11.58	18.58	6.6	24.49	508.5
47	0.99	5.15	4.97	0	23.08	0	0	0	16.18	13.51	0	9.3	0	8.18	0	2.16	82.53
48	0.99	74.18	11.25	0	238.7	0	5.29	4.42	138.2	27.95	7.3	23.09	5.22	6.12	2.95	26.24	570.9
49	0.99	10.58	6.11	0	37.91	7.71	0	4.6	35.1	54.9	5.92	20.34	10.5	10.01	1.79	14.83	220.3
50	1.07	4.91	12.16	0	38.16	6.23	12.83	0	36.67	26.72	0	9.6	0	13.17	2.85	4.46	167.8
51	1.07	20.3	6.69	0	72.07	0	0	0	81.66	13.8	3.04	0	6.79	9.92	2.97	14.36	231.6
52	1.26	15.55	16.46	0	64.13	5.91	11.03	0	72.51	60.56	2.98	23.66	10.53	9.1	5.8	13.1	311.3
53	1.4	36.6	3.97	0	122	0	9.89	0	127.5	25.57	5.56	21.67	6.9	3.96	4.79	8.89	377.3
54	1.4	17.99	3.98	0	47.03	6.68	5.45	4.63	67.51	55.06	4.31	32.47	11.89	18.22	3.74	14.23	293.2
55	2.4	12.83	3.63	0	68.89	0	8.69	0	135.9	25.38	3.79	12.59	8.68	0	6.49	6.09	292.9
56	3.3	20.96	3.08	0	85.71	0	15.73	0	123.5	20.88	0	18.64	5.16	3.98	4.71	7.19	309.6
57	3.2	17.6	9.02	0	79.3	0	0	0	102.5	12.39	0	13.36	5.5	6.76	3.69	4.2	254.3
58	3.2	40.83	7.26	0	252.5	0	32.93	0	452.8	16.42	6.57	34.24	6.93	6.22	4.66	17.11	878.5
59	3.3	0	4.51	0	30.54	0	0	0	27.31	19.98	0	11.4	5.75	5.67	2.91	2.62	110.7
60	3.4	37.64	6.31	0	111.5	0	11.69	0	159.2	19.29	0	16.84	5.65	3.76	3.57	9.71	385.1

Appendix 7.3 Peptide bound inracrystalline amino acids (pmol/mg)

Sample	Age	Asp	Glu	Ser	Gly	His	Arg	Thr	Ala	Pro	Tyr	Val	Iso	Leu	Phe	Lys	Free
1	3.6	0	1.18	0	-2.34	2.66	2.4	0	-3.78	1.53	0	4.99	-3.7	3.88	0	0	6.82
2	3.6	-23.5	1.97	4.44	-26.1	0	-2.07	3.56	-66.7	-0.03	0.1	-4.28	-0.1	-3.73	-0.95	1.17	-116
3	3.6	-32.2	10.91	0	-3.12	0	4.13	0	-21.3	3.06	0.47	-0.91	1.29	-0.39	0.84	0.95	-36.2
4	3.5	0	5.48	0	-6.47	0	0	0	-10.9	-1.95	0.3	-0.74	1.12	-1.23	-3.99	-0.46	-18.8
5	0.35	63.12	23.51	12.05	42.13	0	2.8	6.2	9.61	4.09	3.98	11.11	3.24	5.82	-0.82	12.71	199.5
6	0	15.52	19.93	15.89	112.6	0	27.16	8.38	53.4	54.54	0	22.66	13.01	20.61	8	13.23	384.9
7	0	144.6	19.47	21.39	251.1	5.51	31.17	21.57	62.11	116.9	0	51.01	27.52	19.03	11.05	57.84	840.2
8	0.7	21.89	10.92	4.34	-51.1	0	-0.38	3.06	-60.3	0.47	-9.97	-32.8	1.01	-3.01	-0.81	-0.14	-117
9	0	193	41.84	61.71	477.1	5.68	34.8	21.75	67.35	115.4	0	42.12	22.41	20.14	14.13	14.43	1132
10	0	349.7	83.72	69.14	292.1	0	53.8	18.71	61.2	66.14	0	39.26	15.21	0	4.09	42.08	1095
11	0	30.44	31.36	11.17	68.97	0	6.46	8.14	27.33	17.01	0	9.82	7.05	13.66	3.14	5.71	240.3
12	3.2	-1.51	-2.22	-4.77	-48.1	0	0.47	0	-34	-5.69	0.52	-6.48	0.17	-5.83	0.05	-4.87	-112
13	1.45	-108	-1.58	0	-177	0	-4.38	4.19	-145	-3.15	-4.99	-8.55	-0.65	-5.09	-3.87	-6.72	-466
14	0	204.3	53.4	50.15	251.9	0	32.94	13.85	44.26	48.83	0	24.35	24.54	9.34	9.75	30.13	797.8
15	0	206.9	23.28	20.46	277.9	0	24.73	14.51	58.76	120.9	0	52.06	32.2	24.16	34.44	39.65	929.9
16	0.12	121.7	21.25	9.4	163.1	0	12.3	9.29	31.79	62.08	-1.07	54.63	27	14.64	14.09	66.04	606.3
17	0.12	394.4	75.5	23.46	330.9	0	21.72	11.91	73.54	78.83	-6.04	56.42	33.98	28.99	15.38	55.59	1195
18	0.35	3.47	8.29	0	-2.32	5.71	-0.94	0.98	-25.9	2.75	-10.5	1.73	2.7	-0.15	0.31	-2.37	-16.2
19	0.35	-0.14	6.14	0	108.2	0	0	0	-1.92	-1.46	-8	1.06	0.28	-0.41	-0.73	-0.35	102.7
20	0.35	37.49	15.16	11.37	26.57	7.58	-5.62	7.51	1.23	9.75	-3.72	5.02	2.48	6.01	-0.34	6.63	127.1
21	0.43	1.62	16.41	0	21.4	-7.31	3.64	-4.97	1.13	-12.1	-3.38	10.29	1.52	5.65	6.22	7.32	47.45
22	0.43	1.81	7.81	0	10.86	-0.78	3.99	-2.88	-12.7	-5.04	-28.6	11.25	5.6	1.31	2.12	11.35	6.06
23	0.43	0.71	6.17	0	10.45	0	-5.12	6.32	-5.96	-31	-4.9	3.5	0.43	-0.27	9.77	2.19	-7.67
24	0.44	7.41	-0.71	-3.22	86.93	8.04	-7.01	-2.04	17.84	32.33	-22	13.98	-9.45	6.94	6.64	2.86	138.5
25	0.44	-11.4	-5.32	3.37	-25.4	0	-4.9	0	-64.9	-19.9	-8.32	-4.09	-32.1	15.45	5.8	-2.8	-155
26	0.44	-1.06	22.04	5.91	35	0	-3.97	0	-41.1	-3.1	-6.24	7.11	-10.1	6.11	1.49	-1.95	10.19
27	0.44	113.2	53.92	11.75	67.97	7.05	4.54	-0.26	-4.69	19.97	-15	17.81	12.08	7.73	1.81	11.53	309.5
28	0.44	100.5	34.16	6.61	47.95	5.4	7.94	4.41	15.17	8.23	-2.52	25.48	-2.74	11.37	-1.03	5.45	266.3
29	0.5	70.36	24.01	10.62	137.6	0	0	6.08	151	32.8	5.97	54.7	0.5	3.1	-0.33	4.65	501
30	0.5	55.52	34.47	5.71	42	8.12	4.77	0	-1.78	6.78	0	5.07	2.11	2.75	-9.02	2.72	159.2
31	0.5	21.57	17.03	5.8	99.25	5.16	-1.6	-1.64	29.23	21.04	-9.12	-3.81	-2.27	17.6	5.02	9.66	212.9

Appendix 7.3 Peptide bound intracrystalline amino acids (pmol/mg)

32	0.6	217.4	80.39	21.87	46.13	0	-5.14	0	-25	1.8	-1.68	14.61	6.57	6.6	-1.38	13.95	376.1
33	0.6	9.19	15.16	6.05	16.33	5.09	-0.57	0	-24.7	-10.5	-1.73	7.28	3.07	-0.89	7.27	2.61	33.74
34	0.6	14.7	46.97	14.6	86.95	3.55	19.08	0	39.31	21.93	-1.51	22.12	5.95	11.26	8.23	6.75	299.9
35	0.62	16.65	7.52	0	41.45	5.08	0	4.09	8.92	5.58	0	3.08	1.78	0.61	6.31	5.5	106.6
36	0.68	131.8	47.13	7.11	245.9	0	17.83	-5.57	93.93	21.06	8.34	35.4	10.85	11.55	9.71	44.23	679.3
37	0.7	11.42	26.25	0	27.32	0	-1.57	0	8.3	5.08	-0.98	8	5.18	13.86	4.07	7.63	114.6
38	0.7	3.65	19.17	3.6	17.76	-13.4	2.59	-3.53	20.46	20.25	0.38	7.68	3.9	7.82	18.61	11.45	120.4
39	0.78	78.74	31.03	4.61	70.58	-5.54	1.61	-3.98	19.64	22.25	13.64	-38.4	-0.03	6.5	0.64	17.04	218.3
40	0.78	20.78	22.6	5.74	55.02	1.22	3.9	0	18.49	10.53	-1.9	20.26	6.55	7.24	24	9.78	204.2
41	0.85	26.25	37.79	0	62.13	0	0	4.29	19.53	7.72	10.3	9.94	4.05	5.78	28.24	8.23	224.3
42	0.85	7.19	4.59	0	28	0	-3.92	0	2.04	-2.19	-2.84	6.31	5.91	7.78	7.79	3.41	64.07
43	0.8	16.5	7.56	0	66.31	5.66	0	3.87	11.55	5.46	0	11.82	3.7	0.35	5.68	18.17	156.6
44	0.8	11.1	40.31	9.05	25.25	-2.27	10.33	0	14.54	7.52	-3.53	0.11	11.4	15.47	9.96	11.37	160.6
45	0.9	17.16	12.85	0	70.89	0	0	0	-0.45	0.03	0	14.07	2.98	6.75	15.58	8.71	148.6
46	0.95	89.83	30.04	4.36	69.97	0	3.21	0	18.18	33.38	14.09	42.15	19.6	18.42	19.67	30.7	393.6
47	0.99	5.03	10.15	0	36.75	5.6	0	0	12.31	4.51	0	3.23	4.21	3.31	5.37	3.61	94.08
48	0.99	67.4	24.21	4.44	-11.6	0	-0.12	-4.42	-3.21	2.28	-4.24	13.13	2.62	1.59	3.18	4.81	100.1
49	0.99	8.02	11.53	4.67	56.84	3.39	5.72	-0.69	22.54	18.86	-2.82	28.42	7.43	12.42	27.51	10.12	214
50	1.07	12.15	89.12	0	-30.2	0.12	-12.8	0	-16.4	-19.8	4.37	27.99	20.84	18.82	6.28	14.85	115.3
51	1.07	34.49	24.5	6.3	71.69	0	4.23	0	29.9	7.13	0.89	21.91	9.21	13.64	1.19	0.16	225.2
52	1.26	45.04	99	13.26	128.5	4.5	47.23	8.39	63.91	23.95	6.72	27.37	9.93	13.45	2.22	11.89	505.4
53	1.4	96	41.69	6.39	265.6	0	5.5	0	118.1	10.52	4.48	23.37	4.83	4.72	-1.23	16.36	596.4
54	1.4	68.82	35.19	7.48	83.21	1.09	6.4	-4.63	46.54	21.43	0.96	25.58	9.15	14.44	8.85	15.87	340.4
55	2.4	31.35	25.69	0	147.1	7.03	7.06	0	121.6	8.22	3.53	21.55	5.19	4.86	-3.81	13.14	392.5
56	3.3	77.36	31.8	0	108.6	0	7.35	0	80.09	9.42	5.21	14.07	6.02	2.63	-1.54	11.94	352.9
57	3.2	25.43	25.85	0	118	8.24	9.25	0	83.22	6.41	10.37	18.94	3.36	9.07	5.24	26.84	350.2
58	3.2	101.2	46.14	0	39.36	0	-10.6	0	-64.5	0.62	3.07	20.3	1.97	5.53	1.13	13.45	157.6
59	3.3	5.96	10.96	0	48.03	6.64	6.09	0	19.94	10.99	5	10.2	3.54	5.02	2.67	3.73	138.8
60	3.4	37.85	21.94	0	104	0	9.88	0	114.1	15.67	3.05	18.22	3.44	3.69	-0.42	12.47	343.9

CHAPTER 8

SEPARATION OF INDIVIDUAL AMINO ACIDS FOR STABLE CARBON ISOTOPE ANALYSIS

8.1 Abstract

An attempt was made to separate amino acids for stable carbon isotope analysis. The aim was to recover individual amino acids that had not been derivatized. The technique used was hplc. However, the results do not show good separation at high sensitivity. Glycine in particular is spread across the whole range of retention times and is mixed with many of the other amino acids. Many of the peaks overlap. Some amino acids show two or more peaks. Separation of underivatized amino acids can therefore be problematical and there may at present be no alternative but to derivatize and attempt to correct for the resulting change in carbon isotope values.
Carbon isotope analysis of bacterially produced standard amino acid samples shows significant variation in $\delta^{13}C$ between different individual amino acids. This may reflect different environments of production or may reflect biological fractionation effects.

8.2 Introduction

The great majority of stable carbon isotope analyses of organic matter have concentrated on whole organisms or parts of organisms containing complex mixtures of molecules (Deines, 1980). This is not ideal because such an approach yields average values and a great deal of detailed information is lost. Recently techniques for separating individual biomolecules have improved such that carbon isotope analysis of individual amino acids has become possible. For example, Engel et al. (1990) separated amino acids from the Murchison meteorite for carbon isotope analysis using gas chromatography and isotope ratio mass spectrometry (GC-IRMS). Ostrom et al. (1993) also used GC-MS to separate and analyse amino acids from bones and teeth. However the techniques used are complicated and specialist equipment is needed.

Many methods of separation of organic molecules (such as GC-MS) use derivatization (the addition of an extra molecule, or derivative, to each organic molecule) in order to facilitate separation and detection of individual types of biomolecule. This is needed because many biomolecules, particularly small biomolecules, absorb UV light at similar wavelengths to the buffer solutions which they are in. This causes considerable problems, as many techniques depend on differential UV absorption between solute and solvent for detection of biomolecules. However, such treatment of amino acids is complicated by the addition of carbon in the required derivatization. This can change the carbon isotope signature of the amino acid and must then be corrected for. There may also be isotopic fractionation during derivatization. It is therefore preferable to keep the amino acids in their natural state, as derivatization may alter the carbon isotope value. Hence in this study we attempted to separate the underivatized amino acids from mollusc shells by hplc, and the eluate, which could not be detected by means of UV absorbtion, was analysed by an Applied Biosystems 420H amino acid analyser.

It has been suggested that the carbon isotope signatures of biologically produced organic compounds may be thermodynamically controlled by mechanisms of biological fractionation involving enzymes (Galimov, 1985). This is because if any atom in any compound is replaced by its isotope, the free energy of the compound is changed. This free energy change is called the thermodynamic isotopic factor or ß factor, and has a different value for different compounds. At equilibrium the total free energy of the system will be minimal. This condition is satisfied if the isotopic ratios characterizing the compounds are distributed proportionally to their ß factors. The higher the ß factor the higher the content of the heavy isotope in the corresponding compound. Galimov has shown furthermore that the ß factor can be calculated for any given carbon compound. It is therefore theoretically possible to predict the relative isotopic compositions from the chemical structure of biomolecules.

8.3 Method

The organic molecules found within mollusc shells can be divided into two main categories: intercrystalline and intracrystalline. Intercrystalline biomolecules are those which lie between the calcium carbonate crystals and are therefore easily leached and contaminated with molecules from the surrounding environment. Intracrystalline biomolecules, however, are completely enclosed within the crystals and protected from interactions with the environment from the time of crystallization. It is these therefore that are of interest and must be isolated by removing first the intercrystalline molecules and then the carbonate matrix. Once isolated, the intracrystalline organic matter must be hydrolysed to break the peptide bonds and release individual amino acids ready for separation. Standard bacterially produced amino acid samples were also prepared for carbon isotope analysis in order to compare the carbon isotope values with those of the shell amino acid samples and with each other.

Shells of *Pecten maximus* were dredged from the sea floor off Girvan on the west coast of Scotland. The ligaments were removed and the shells were scrubbed clean then soaked in an aqueous solution of bleach for at least 2 hours to remove any remaining organic molecules from the surface by oxidation. Each shell was washed thoroughly in Milli Ro water and left to air dry. The shells were then smashed into fragments with a hammer and powdered using a metal drum rock crushing machine. The powdered carbonate was then soaked in 10 % bleach for at least 12 hours to remove all intercrystalline molecules by oxidation. Bleach was then removed by repeated washing of the powdered samples in clean Milli Q water and centrifugation. The wet powder was frozen and lyopholized to a dry powder.

A 600 gram sample of powder was dissolved in an aqueous solution of 20 % EDTA (ethylene diamino tetra acetic acid) at pH 8. The resulting solution was centrifuged to remove insoluble residues. A Millipore Minitan tangential flow filtration system with 10 kDa cutoff filters was used to remove the EDTA solution and concentrate up the solution of soluble organic molecules. Using this system it was possible to reduce the solution to approximately 30 ml of organic molecules in water. Further

concentration to approximately 1 ml was achieved using an Amicon minicon B15 concentrator. The concentrated sample was freeze dried and then hydrolysed using 6N hydrochloric acid vapour at 165 degrees centigrade for one hour. The sample was again freeze dried to remove traces of HCl and then redissolved in clean Milli Q water ready to be injected into the hplc system.

An attempt was made to separate the amino acids using a Jones Chromatography Spherisorb amino 5μ column (25cm length, 4.6 mm inside diameter) with mobile phases A: 10 mM potassium phosphate, pH 4.3; B: acetonitrile/water in a ratio of 100:14. This column was designed to separate amino acids. ABI hplc grade acetonitrile and milli-Q water were used in all solutions. The solutions were degassed by ultrasonication prior to use. The following elution program was used: 5% solvent A and 95% solvent B for 20 min; 30% solvent A and 70% solvent B for 7 min; 50% solvent A and 50 % solvent B for 3 min. The flow rate was 1 ml/min. The eluate was monitored by UV absorbtion at a frequency of 254nm but was not well detected by the hplc system due to absorbing UV at the same wavelength as the buffers. The fractionated eluate was therefore collected in eppendorf tubes at intervals of 30 seconds (giving 60 samples per 30 minute run; each sample consisting of 0.5 ml of solution). The collected samples were analysed using an Applied Biosystems 420H amino acid analyser system (Dupont et al., 1989) in order to determine the precise sequence and quantities of the amino acids released from the column.

Standard Sigma L-amino acids (Kit No. LAA-21) were prepared for carbon isotope analysis for comparison with the amino acids separated from the shells. The standard amino acid samples were placed in evacuated quartz glass tubes and oxidized with copper oxide at 850 degrees centigrade for 8 hours to produce carbon dioxide. The carbon dioxide gas was passed through a 'slush trap' of dry ice and acetone at -78 degrees centigrade to remove water vapour. Volatile gaseous contaminants were removed by vaccuum pump whilst freezing the carbon dioxide to the temperature of liquid nitrogen (-197 degrees C). The isotopic composition of the carbon dioxide was determined using a Sira 10 mass spectrometer and recorded relative to the Pee Dee Belemnite (PDB) standard (Epstein et al., 1953).

8.4 Results

Separation of underivatized amino acids by hplc proved to be poor (figs 8.1 a-p). Glycine in particular is present in most of the eluate and contaminates many of the other amino acids. Many of the peaks overlap, and some amino acids (glycine, alanine, proline, tyrosine, glutamic acid, serine, histidine, arginine, aspartic acid, lysine) show two or more peaks. Some amino acids do not show up at all: for example, asparagine and glutamine are completely converted to aspartic acid and glutamic acid during the hydrolysis stage. Cysteine is lost due to the oxidation of the sulphur atom on its side chain. None of the amino acid peaks were considered pure enough for carbon isotope analysis.

The results of carbon isotope analyses of the bacterially produced standard amino acid samples show a significant variation between individual amino acids. The carbon isotope signatures vary between -33.18 per mil for glycine and -13.93 per mil for lysine (table 8.1). The carbon isotope signature of a pure graphite standard was -25.38. The results are plotted against the corresponding ß factors for each compound (taken from Galimov, 1985) in fig. 8.2.

Table 8.1 ß factors for the amino acids glycine, alanine, glutamic acid, aspartic acid, serine and lysine (taken from Galimov, 1985) and experimental carbon isotope values for standard amino acid samples.

Amino Acid	ß factor	$\delta^{13}C$
Glycine	1.1783	-33.18
Alanine	1.1702	-23.57
Glutamic Acid	1.1769	-26.04
Aspartic Acid	1.1832	-23.97
Serine	1.1797	-16.55
Lysine	1.1651	-13.93

Fig 8.1 Individual amino acids coming off the hplc after separation. The y axes show UV absorbtion (measuring amount of amino acids present) and the x axes show retention time (minutes).

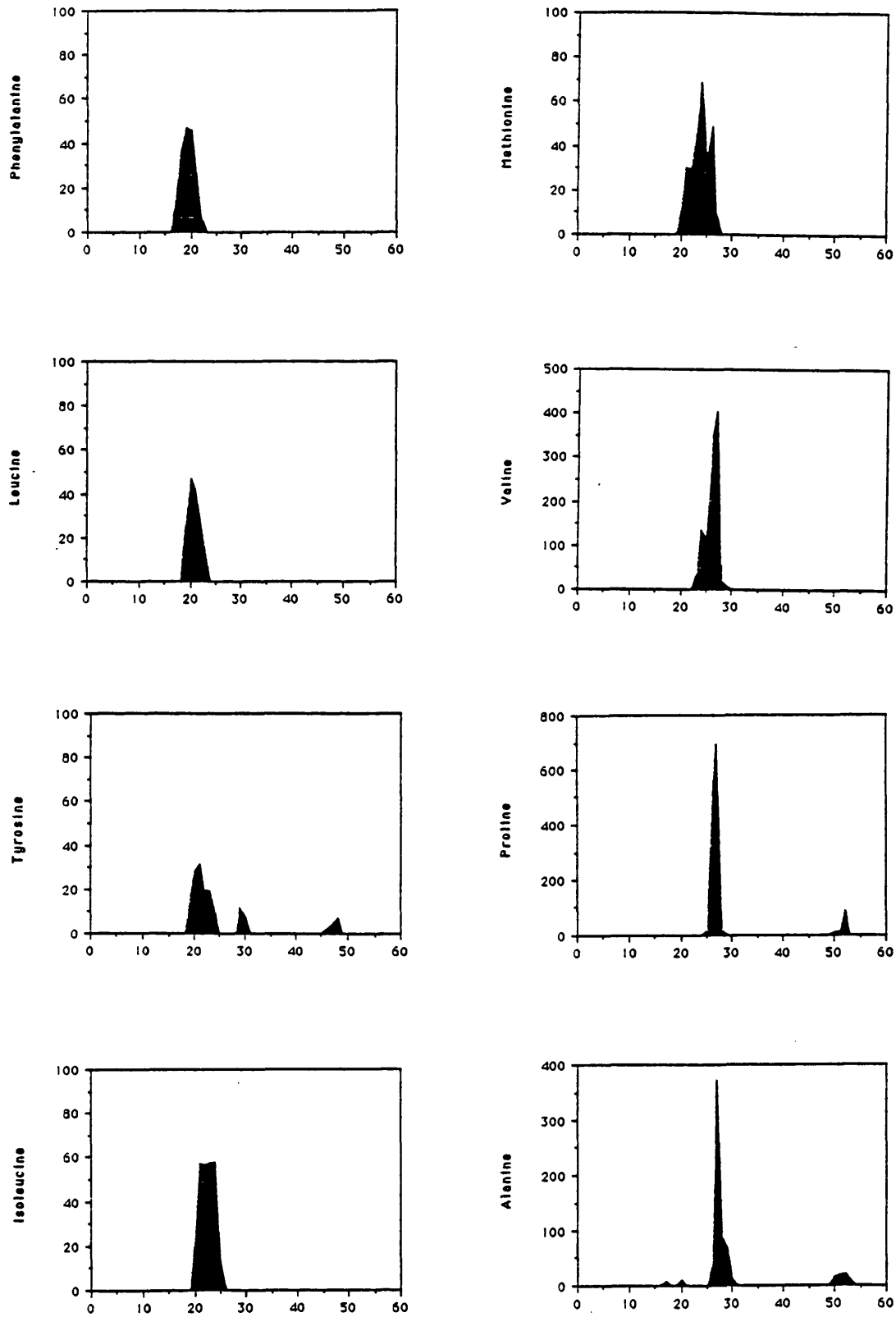

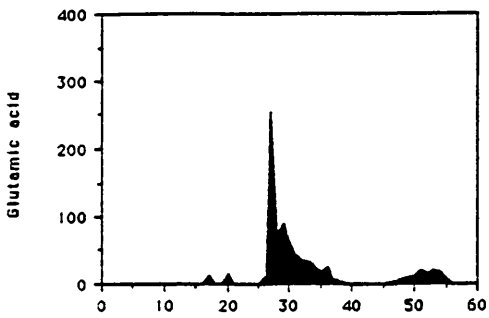
Glutamic acid
400
300
200
100
0
0 10 20 30 40 50 60

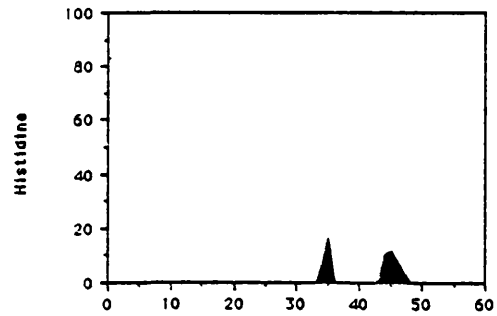
Histidine
100
80
60
40
20
0
0 10 20 30 40 50 60

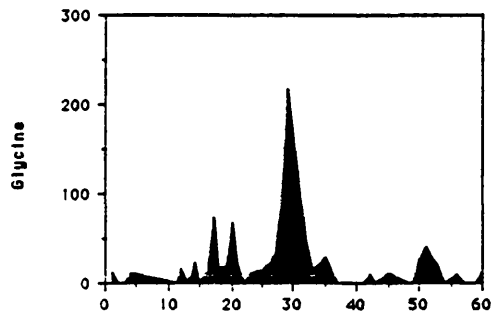
Glycine
300
200
100
0
0 10 20 30 40 50 60

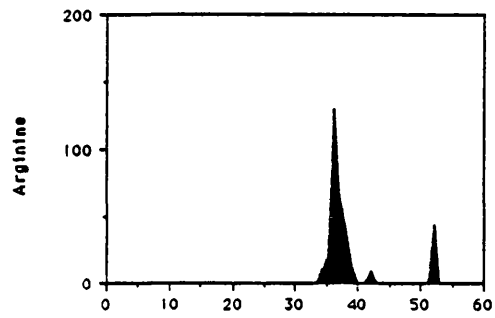
Arginine
200
100
0
0 10 20 30 40 50 60

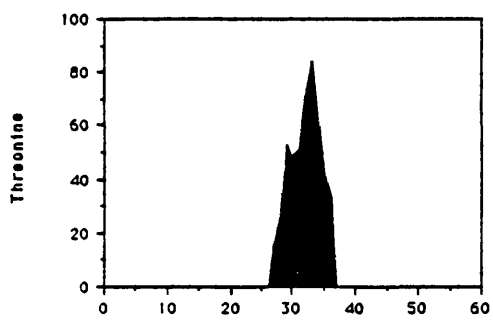
Threonine
100
80
60
40
20
0
0 10 20 30 40 50 60

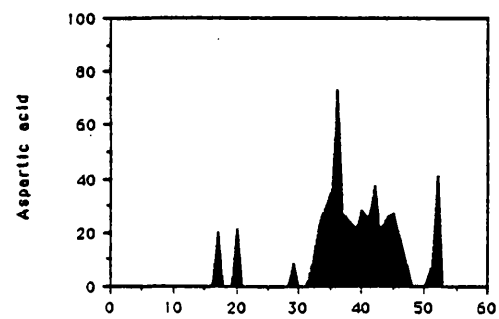
Aspartic acid
100
80
60
40
20
0
0 10 20 30 40 50 60

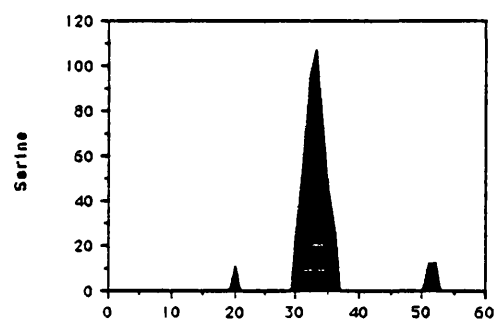
Serine
120
100
80
60
40
20
0
0 10 20 30 40 50 60

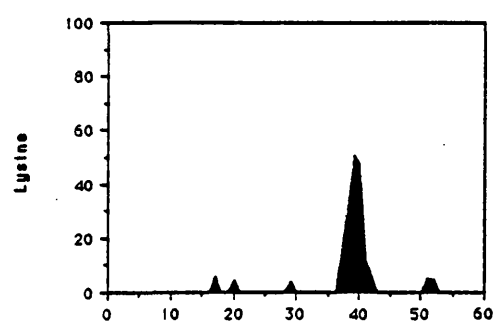
Lysine
100
80
60
40
20
0
0 10 20 30 40 50 60

Fig. 8.2 Graph showing the relationship between experimental $\delta^{13}C$ values for standard bacterially produced amino acids and ß factors calculated for each amino acid (Galimov, 1985).

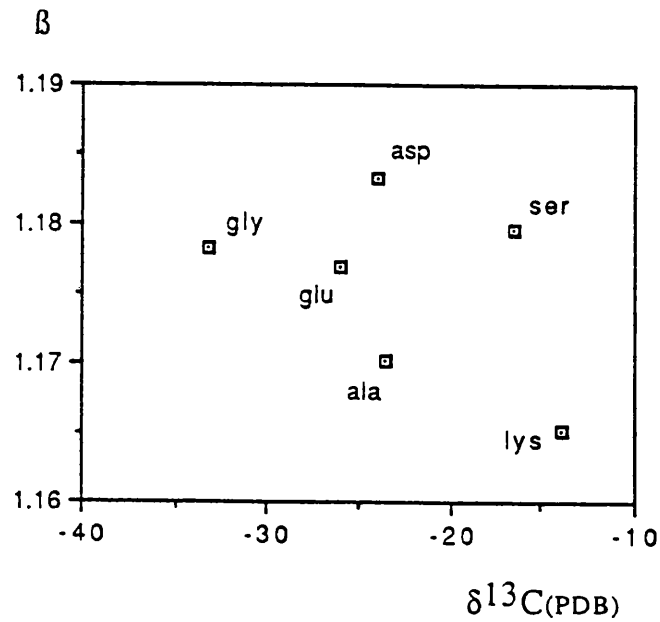

8.5 Discussion

The separation of individual amino acids using hplc was poor. The hplc column may be designed to separate mixtures of only a few compounds but natural samples consist of many more. During hplc, the sample mixture is transported by a mixture of two buffer solutions to the column, which contains beads with apolar surface properties which cause them to bind to the hydrophobic parts of molecules. The proportions of the two buffers are gradually changed until the polarity weakens. As the interaction between the beads and a particular molecule diminishes, that molecule is released. The sample mixture is therefore separated as a result of different components adhering to the beads to different extents. But the polar properties of underivatized amino acid molecules are so similar to each other that the process seems only to have been partially successful in this case.

Amino acid interactions with each other and with carbohydrates and other organic molecules within the intracrystalline organic matter may also be a problem. For instance, some amino acids may react with each other or with the buffer solutions at any stage in the process, sometimes producing other

amino acids in their place. The presence of carbohydrates has been shown to significantly speed up amino acid reactions (Vallentyne, 1964). Hence some ubiquitous amino acids such as glycine may have a multiple origin: some of it original and some of it appearing as reaction products of other amino acid interactions at some stage in the process. In preparing samples for carbon isotope analysis, isotope fractionation can also be a problem- the presence of organic solvents such as formalin has been shown to change the carbon isotope value by 1 or 2 per mil (Boutton, 1991). The effect of acetonitrile is unknown.

The large variability in $\delta^{13}C$ values for different standard bacterially produced amino acid samples may reflect different environments of production or may reflect biological fractionation effects. There is little or no correlation between experimental values and the ß factors calculated for each amino acid (fig. 8.2). However, a correlation would only be seen if the amino acids had originated from the same biological (in this case bacterial) system, such that isotope partitioning could occur freely between them. Such correlations have been shown using amino acids extracted from various organisms (e.g. fig. 8.3). If this is not assumed to be the case, the carbon isotope signatures would not be related in this way. Any relationship between experimental values and ß factors would be obscured by isotopic differences reflecting different environments of production, and the experimental values would reflect a combination of the $\delta^{13}C$ of the production environment and the effect of biological fractionation on the $\delta^{13}C$ of individual amino acids.

8.6 Conclusions

Separation of underivatized amino acids by hplc for carbon isotope analysis is less satisfactory than separation of derivatized amino acids and simultaneous isotope analysis using GCIRMS, even though the latter may involve some loss of accuracy due to the derivatization process. After separation by hplc, some amino acids show multiple peaks and most peaks partly overlap. Carbon isotope analysis of standard amino acid samples shows a high variability between individual amino acids. This may be due to a combination of different environments of production and biological fractionation effects.

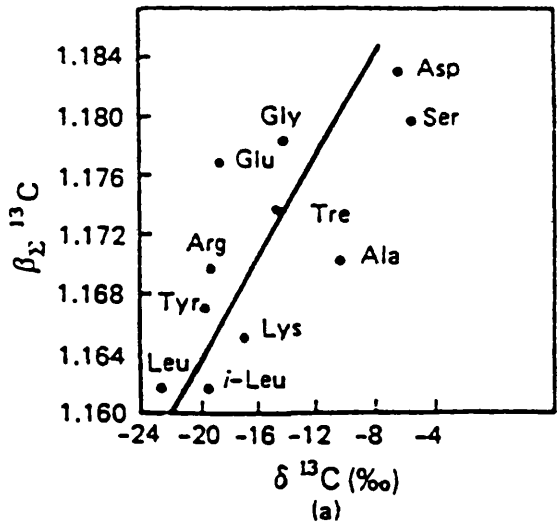

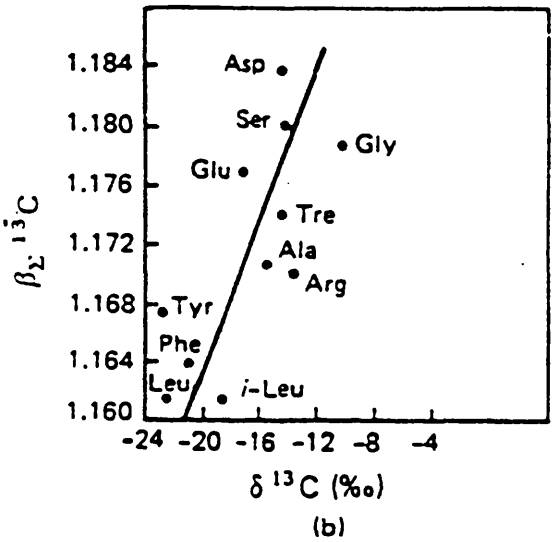

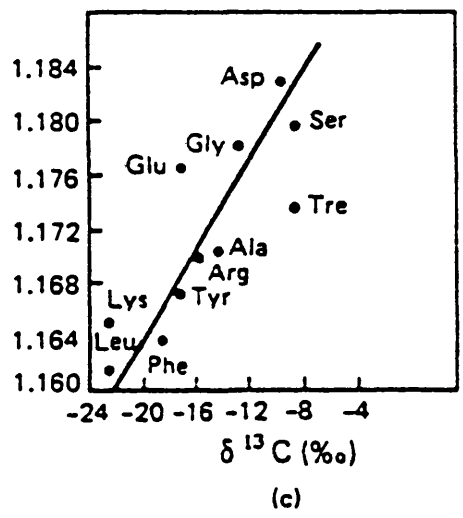

Fig 8.3 Comparison of values of $\delta^{13}C$ and $\beta_\Sigma{}^{13}C$ of the amino acids for various organisms. The graphs show the value of the correlation coefficients η and give the regression equation. (a) *Chlorella pyrenoidosa*, $\delta^{13}C_X = -15.3 + 0.58(\beta_X - 1.1715) \times 10^3$, and $\eta = 0.76$; (b) *Gracilaria* sp., $\delta^{13}C_X = -16.8 + 0.40(\beta_X - 1.1714) \times 10^3$, and $\eta = 0.74$; (c) *Euglena gracilis*, $\delta^{13}C_X - 15.3 + 0.60(\beta_X - 1.1717) \times 10^3$, and $\eta = 0.82$. From Galimov (1985)

CHAPTER 9

DISCUSSION AND CONCLUSIONS OF THESIS

9.1 Summary of Results

The bulk stable carbon and oxygen isotope analysis of fast growing mollusc shells may yield a range of values which show a strong linear correlation between $\delta^{18}O$ and $\delta^{13}C$. This is due to kinetic effects associated with the fast precipitation of carbonates which favour the lighter isotopes of both carbon and oxygen during the hydration and hydroxylation of CO_2. 'Fast' may be taken to mean a precipitation rate of anything above about 2 mm per year (McConnaughey 1989). Such growth rates are likely to be common in large mollusc shells. Care must be taken, therefore, with mollusc shells commonly used for environmental reconstruction. The range in values may be quite large as different parts of the shell structure may have different growth rates and yield different isotope results. For instance, shells of *Pecten maximus* from the west coast of Scotland yield oxygen isotope results from different parts of the shell which differ by up to 5‰: this could be interpreted as a temperature difference of 20°C. The highest $\delta^{18}O$ and $\delta^{13}C$ values are most likely to approach equilibrium, as departure from equilibrium is likely to be in the direction of the lighter isotopes. Non-equilibrium isotope results due to kinetic effects can be detected by the proportional variation in $\delta^{18}O$ and $\delta^{13}C$ within a shell. These results have implications for environmental analysis using isotope data from fast growing shells and may be applicable to any carbonate precipitating organism.

In order to reconstruct palaeotemperatures using oxygen isotope ratios from mollusc shells care was taken to avoid these problems. A significant enrichment is found in the $\delta^{18}O$ values from mollusc shells from interglacial shellbeds from Wanganui, New Zealand from about 1 My. This is thought to reflect a cooling of about 10°C in interglacial temperatures in this region which corresponds to a well documented change in the dominant global climate periodicity which also occurred at this time from a 41 ky to a 100 ky periodicity cycle. Further evidence for climatic change is provided by a significant molluscan extinction event between the New Zealand Nukumaruan and Castlecliffian stages and a positive excursion in the

strontium isotope ratio of seawater showing an increase in continental weathering.

Oxygen and carbon stable isotope profiles within individual shells can be related to both environment and ontogeny. Intracrystalline amino acid profiles of the New Zealand giant oyster *Crassostrea ingens* reflect both ontogeny and processes of amino acid diagenesis. Oxygen isotopes show a gradual increase in $\delta^{18}O$ from the umbo to the shell margin, levelling off about half way towards the margin. The $\delta^{13}C$ profile shows an initial sharp increase at the umbo, then a gradual decrease towards the shell margin. There is a progressive increase in the relative amounts of inorganic carbon to protein over the life of the oyster. Both isotope profiles and bulk intracrystalline amino acid profiles can be linked to the changing growth rate of the shell as it develops from a fast growing juvenile into a slower growing, sexually mature adult. The isotope data, therefore, do not reflect environmental factors alone: these results again show that care must be taken in environmental reconstruction using isotopic data from shell carbonates.

Bulk amino acid analysis of intracrystalline biomolecules from shell samples of different species and ages shows that there is a gradual decline in most intracrystalline amino acids through time as they decompose to other compounds. Alanine shows an increase (at least over the time scale of this study, 3.6 My) because it is a common product of other amino acid decomposition reactions. In recent shells, most amino acids are still peptide bound and the number of free amino acids is small. However, most of the peptide bonds are broken within the first 0.5 My. Free amino acids are therefore at a maximum at about 0.5-1 My after which there is a decline, except in alanine which continues to increase as other amino acids are broken down. Taxonomic relationships can still be inferred from intracrystalline amino acid compositions even after amino acid diagenesis reactions have taken place, as long as there is enough original amino acid left to give a taxonomic signal. The results of multivariate analysis of amino acid compositions tend to reinforce morphological taxonomy.

Separation of individual underivatized intracrystalline amino acids by hplc for carbon isotope analysis was not satisfactory. After separation by hplc, some amino acids show multiple peaks and most peaks partly overlap. Carbon isotope analysis of standard amino acid samples shows a high variability

between individual amino acids. This may be due to a combination of different environments of production and biological fractionation effects. It is suggested that in future amino acids are derivatized and separated by GCIRMS (gas chromatography isotope ratio mass spectrometry).

9.2 Suggestions for Further Work

Well known fast growing mollusc species should be further investigated to determine the extent of kinetic isotope disequilibrium effects in mollusc shells. Other carbonate precipitating organisms, particularly those used routinely in palaeoenvironmental reconstruction using stable oxygen isotope analysis (e.g. foraminifera) should also be investigated. The importance of this effect on the stable carbon isotope signature should be assessed.
Further isotopic analysis should be carried out on shells from the period 1.5-0.5 Ma from the Wanganui Basin. Different recent and fossil species should be rigorously analysed in order to determine and discard those which are not absolutely in equilibrium with their environments and which do not therefore reflect temperature alone. Further work should also concentrate on investigating the carbon isotope signatures of the shells in more detail and determining which major influences these reflect.
Now that fully automated equipment for the microsampling of carbonates for stable carbon and oxygen isotope analysis is available it is possible to determine isotope profiles in much more detail than ever before. Previous work involving several isotopic measurements per yearly growth increment has usually concentrated on oxygen isotope measurements interpreted as seasonal fluctuations (e.g. Dare and Deith, 1991). All too often corresponding carbon isotope data are ignored presumably because they are little understood. Rather than being a simple reflection of one main variable, the carbon isotope signature may reflect several influences at once and sorting out the relative importance of these is an important goal. There is still also much work to be done on carbon isotopes in organic matter. This is becoming easier with improvements in GCIRMS techniques and equipment. There is potential for the use of carbon isotopes in both inorganic and organic matter from a known environment to determine non-environmental influences on the signature. This work could lead to results relating to carbon fluxes and non-equilibrium partitioning effects between different carbon compounds which could then be used in the detailed investigation of aspects of the global carbon cycle.

REFERENCES

Abbott, S. T. & Carter, R. M. 1991. The sequence architecture of mid-Pleistocene (c.1.1-0.4 Ma) cyclothems from New Zealand: Facies development during a period of orbital control on sea level cyclicity. in Orbital Forcing and Cyclic Sequences, IAS Special Publication IX. (ed. P. L. de Boer & S. D. G.).

Abell, P. I. & Williams, M. A. J. 1989. Oxygen and carbon isotope ratios in gastropod shells as indicators of palaeoenvironments in the Afar region of Ethiopia. Palaeogeography, Palaeoclimatology, Palaeoecology **74**: 265-278.

Abelson, P. H. 1954. Organic constituents of fossils. Carnegie Inst. Wash. Yearb. **53**: 97-101.

Anderton, P. W. 1981. Structure and evolution of the South Wanganui Basin, New Zealand. New Zealand Journal of Geology and Geophysics **24**: 39-83.

Bada, J. L. 1991. Amino acid cosmogeochemistry. Phil. Trans. Roy. Soc. Lond., **333**: 349-358.

Bada, J. L. & Man, E. H. 1980. Amino acid analysis in Deep Sea Drilling Project Cores: kinetics and mechanisms of some reactions and their applications in geochronology and in paleotemperature and heat flow determinations. Earth Science Reviews **16**: 21-55.

Bada, J. L. & Miller, S. L. 1970. Kinetics and mechanism of the reversible non enzymatic deamination of aspartic acid. J. Am. Chem. Soc. **92**: 2774-2780.

Bada, J. L., Shou, M., Man, E. H. & Schroeder, R. A. 1978. Decomposition of hydroxy amino acids in foraminifera tests; kinetics, mechanism and geochronological implications. Earth. Planet. Sci. Lett. **41**: 67-76.

Belknap, D. F. & Wehmiller, J. F. 1980. Amino acid racemization in Quaternary molluscs: examples from Delaware, Maryland, and Virginia. in Biogeochemistry of Amino Acids. (ed. P. E. Hare, T. C. Hoering & K. King). New York, John Wiley and Sons.

Berger, W. H., Killingley, J. S. & Vincent, E. 1978. Stable isotopes in deep-sea carbonates: Box core ERDC-92, West Equatorial Pacific. Oceanol. Acta **1**: 203-216.

Beu, A. G. 1972. Molluscan evidence of warm sea temperatures in New Zealand during Kapitean (late Miocene) and Waipipian (middle Pliocene) time. New Zealand Journal of Geology and Geophysics **17**(2): 465-479.

Beu, A. G. 1987. Molluscan generic diversity of New Zealand late Neogene stages: extinction and biostratigraphic avents. Fourth International congress on Pacific Neogene Stratigraphy, Berkeley, California,

Beu, A. G. & Edwards, A. R. 1984. New Zealand Pleistocene and late Pliocene glacio-eustatic cycles. Palaeogeog. Palaeoclim. Palaeoecol. **46**: 119-142.

Beu, A. G., Grant-Taylor, T. L. & Hornibrook, N. de B. 1977. Nukumaruan records of the subantarctic scallop *Chlamys delicatula* (Hutton) and crab *Jacquinotia edwardsii* (Jacquinot) in central Hawkes Bay. New Zealand Journal of Geology and Geophysics **20**: 217-248.

Beu, A. G., Edwards, A. R. & Pillans, B. J. 1987. A review of New Zealand Pleistocene stratigraphy, with emphasis on the marine rocks. Proceedings of the First International Colloquium on Quaternary Stratigraphy of Asia and Pacific Area, Osaka. (ed. M. Itihara & T. Kamei). 250-269.

Beu, A. G. & Maxwell, P. A. 1990. Cenozoic Molluscs of New Zealand. New Zealand Geological Survey Palaeontological Bulletin **58**.

Boellstorff, J. D. & Te Punga, M. T. 1977. Fission-track ages and correlation of Middle and Lower Pleistocene sequences from Nebraska and New Zealand. New Zealand Journal of Geology and Geophysics **20**: 47-58.

Boutton, T. W. 1991. Stable carbon isotope ratios of natural materials: 1. Sample preparation and mass spectrometric analysis. In Carbon Isotope Techniques (ed. D. C. Coleman & B. Fry). Academic Press Ltd, London. 155-171.

Brigham, J. K. 1983. Intrashell variations in amino acid concentrations and isoleucine epimerization ratios in fossil *Hiatella artica*. Geology **11**: 509-513.

Buller, A. T. & McManus, J. 1979. Sediment sampling and analysis. in Estuarine Hydrography and Sedimentation. (ed. K. R. Dyer). Cambridge University Press. 87-130.

Bussell, M. R. 1988. Quaternary vegetational and climate changes recorded in cover beds of the South Wanganui Basin marine terraces, New Zealand. PhD thesis, ANU, Canberra.

Capo, R. C. & DePaolo, D. J. 1990. Seawater strontium isotopic variations from 2.5 million years ago to the present. Science 249: 51-55.

Clegg, H. 1993. Biomolecules in recent and fossil articulate brachiopods. PhD Thesis, Gasgow University.

Cochran, J. K., Rhy, D. M. & Landman, N. H. 1981. Growth rate and habitat of *Nautilus pompilius* inferred from radioactive and stable isotope studies. Palaeobiology 7: 469-480.

Collins, M., Muyzer, G., Curry, G. B., Sandberg, P. & Westbroek, P. 1991. Macromolecules in brachiopod shells: characterization and diagensis. Lethaia 24: 387-397.

Craig, H. 1965. The measurement of oxygen isotope palaeotemperatures. in Stable Isotopes in Oceanographic Studies and Palaeotemperatures. Pisa, Consiglio Nazionale delle Richerche, Laboratorio di Geologia Nucleare. 1-24.

Curry, G. B. 1993. Amino acids in water; an example from the Isle of Arran, Scotland. Water Pollution 2: 701-709.

Curry, G. B., Cusack, M., Endo, K., Walton, D. & Quinn, R. 1991. Intracrystalline molecules from brachiopods. in Mechanisms and Phylogeny of Mineralization in Biological Systems. (ed. S. Suga & H. Nakahara). Tokyo, Springer-Verlag. 35-39.

Curry, G. B., Cusack, M., Walton, D., Endo, K., Clegg, H., Abbott, G. & Armstrong, H. 1991b. Biogeochemistry of brachiopod intracrystalline molecules. Phil. Trans. Soc. Lond. B 333, 359-366.

Curry, G. B., Theng, B. K. G. & Zheng, H. 1994. Amino acid distribution in a loess-palaeosol sequence near Luochan, Loess Plateau, China. Organic Chemistry, in press.

Dare, P. J. & Deith, M. R. 1991. Age determination of scallops, *Pecten maximus* (Linnaeus, 1758), using stable isotope analysis, with some implications for fisheries management in British waters. in An International Compendium of Scallop Biology and Culture. (ed. S. E. Shumway & P. A. Sandifer). Baton Rouge, Lousiana, The World Aquiculture Society. 118-133.

Deines, P. 1980. The isotope composition of reduced organic carbon. In The Handbook of Environmental Isotope Geochemistry vol. 1A: The Terrestrial Environment. (ed P Fritz & J. C.-H. Fontes). Elsevier, Amsterdam. 329-406.

Deith, M. R. 1983. Molluscan callendars: the use of growth line analysis to establish seasonality of shellfish collection at the Mesolithic site of Morton, Fife. J. Archaeol. Sci. **10**: 423-440.

DePaolo, D. J. 1987. Correlating rocks with strontium isotopes. Geotimes (1987): 16-18.

Donner, O. & Nord, A. G. 1985. Carbon and oxygen stable isotope values in shells of *Mytilus edulis* and *Modiolus modiolus* from Holocene raised beaches at the outer coast of the Varanger Peninsula, North Norway. Palaeogeography, Palaeoclimatology, Palaeoecology **56**: 35-50.

Duplessy, J.-C., Blank, P.-L. & Be, A. W. H. 1981. Oxygen-18 enrichment of planktonic foraminifera due to gametogenic calcification below the euphotic zone. Science **213**: 1247-1250.

Dupont, D. R., Keim, P. S., Chui, A., Bello, R., Bozzini, M. & Wilson, K. J. 1989. A comprehensive approach to amino acid analysis. in Techniques in Protein Chemistry. (ed. T. E. Hugli). New York, Academic Press.

Eglington, G. & Logan, G. A. 1991. Molecular preservation. Phil. Trans. R. Soc. Lond. **333B**: 315-328.

Eichler, R. & Ristedt, H. 1966. Isotopic evidence on the early life hisory of *Nautilus pompilius* (Linne). Science **153**: 734-736.

Emiliani, C., Hudson, J. H., Shinn, E. A. & George, R. Y. 1978. Oxygen and carbon isotopic growth record in a reef coral from the Florida Keys and a deep-sea coral from Blake Plateau. Science **202**: 627-629.

Emiliani, C. & Shackleton, N. J. 1974. The Brunhes epoch: Isotopic palaeotemperatures and geochronology. Science **183**: 511-514.

Engel, M. H., Macko, S. A. & Silfer, J. A. 1990. Carbon isotope composition of individual amino acids in the Murchison meteorite. Nature **348**: 47-49.

Epstein, S., Buchsbaum, R., Lowenstam, H. A. & Urey, H. C. 1953. Revised carbonate-water isotopic temperature scale. Bull. Geol. Soc. Amer. **64**: 1315-1326.

Epstein, S. & Mayeda, T. K. 1953. Variation of 18O content of waters from natural sources. Geochim. Cosmochim. Acta **4**, 213-224.

Erez, J. 1977. Influence of symbiotic algae on the stable isotope composition of hermatypic corals: A radioactive tracer approach. Proc. 3rd Intl. Coral Reef Symp., Miami : 563-569.

Erez, J. 1978. Vital effect on stable isotope composition seen in foraminiferal and coral skeletons. Nature **273**: 199-202.

Erez, J. & Honjo, S. 1981. Comparison of isotopic composition of planktonic foraminifera in plankton tows, sediment traps, and sediments. Palaeogeography, Palaeoclimatology, Palaeoecology **33**: 129-156.

Fairbanks, R. G. & Dodge, R. E. 1979. Annual periodicity of the $^{18}O/^{16}O$ and $^{13}C/^{12}C$ ratios in the coral *Montastrea annularis*. Geochim. Cosmochim. Acta **43**: 1009-1020.

Faure, G. 1986. Principles of Isotope Geology. New York, John Wiley and Son. 2nd edition.

Fleming, C. A. 1944. Molluscan evidence of Pliocene climate change in New Zealand. Trans. Roy. Soc. New Zealand **74**: 207-220.

Fleming, C. A. 1953. The geology of the Wanganui Subdivision. Wellington, Department of Scientific and Industrial Research: New Zealand Geological Survey Bulletin **52**: 362 p.

Folk, R. L. 1974. Petrology of Sedimentary Rocks. Hemphill, Austin.

Fritz, P. & Fontes, J.-C. 1966. Fractionnement isotopique pendant l'attaque acide des carbonates naturels: role de la granulometrie. Compt. Rend. **263**: 1345-1348.

Galimov, E. M. 1985. The Biological Fractionation of Isotopes (English translation). London, Academic Press.

Gartner, S. 1977. Calcareous nannofossil biostratigraphy and revised zonation of the Pleistocene. Marine Micropalaeontology 2: 1-25.

Gonzalez, L. A. & Lohmann, K. C. 1985. Carbon and oxygen isotopic composition of Holocene reef carbonates. Geology **13**: 811-814.

Grossman, E. L., Betzer, P. R., Dudley, W. C. & Dunbar, R. B. 1986. Stable isotopic variation in pteropods and atantids from north Pacific sediment traps. Micropalaeontology **10**: 9-22.

Hare, P. E. & Abelson, P. H. 1965. Amino acid composition of some calcified proteins. Carnegie Inst. Wash. Year Book **64**: 223-232.

Hare, P. E. & Abelson, P. H. 1968. Racemization of amino acids in fossil shells. Carnegie Inst. Wash. Year Book **66**: 526-528.

Hays, J. D., Imbrie, J. & Shackleton, N. J. 1976. Variations in the earth's orbit: pacemaker of the ice ages. Science **194**: 1121-31.

Ho, T.-Y. 1966. Stratigraphic and palaeographic applications of water soluble fraction of residual shell proteins in fossil shells. Geol. Soc. Am. Bull. **77**: 375-392.

Hoefs, J. 1987. Stable-isotope geochemistry. Berlin and Heidelberg, Springer-Verlag. 3rd edition.

Horibe, Y. & Oba, T. 1972. Temperature scales of aragonite-water and calcite-water systems. Fossils **23/24**: 69-79.

Ikawa, M. & Snell, E. E. 1954. Oxidative deamination of amino acids by pyidoxal and metal salts. J. Am. Chem. Soc. **76**: 4900-4902.

Imbrie, J., Berger, A. & Shackleton, N. J. 1993. Role of orbital forcing: a two million year perspective. in Global Changes in the Perspective of the Past. (ed. J. A. Eddy & H. Oeschger). John Wiley and Sons Ltd.

Imbrie, J. & Imbrie, J. Z. 1980. Modeling the climatic response to orbital variations. Science **207**: 943-53.

Imbrie, J., McIntyre, A. & Mix, A. 1989. Oceanic response to orbital forcing in the late Quaternary: Observational and experimental strategies. Climate and Geosciences **285**: 121-164.

Jackson, M. L. 1979. Soil chemical analysis- advanced course (2nd edition). Jackson, M. L. (Published by the author).

Jones, D. S. 1980. Annual cycle of shell growth increment formation in two continental shelf bivalves and its palaeoecologic significance. Palaeobiology **6**: 331-340.

Jones, D. S., Williams, D. F. & Arthur, M. A. 1983. Growth history and ecology of the Atlantic surf clam *Spisula solidissima* (Dillwyn), as revealed by stable isotope and annual shell increments. J. Exp. Mar. Biol. Ecol. **73**: 225-242.

Jones, D. S., Williams, D. F. & Romanek, C. S. 1986. Life history of symbiont-bearing giant clams from stable isotope profiles. Science **231**: 46-48.

Jones, J. D. & Vallentyne, J. R. 1960. Biogeochemistry of organic matter-I. Geochim. Cosmochim. Acta. **21**: 1-34.

Kahn, D. & Still, W. C. 1988. Hydrolysis of a peptide bond in neutral water. J. Am. Chem. Soc. **110**: 7529-7534.

Kahn, M. I. 1979. Non-equilibrium oxygen and carbon isotopic fractionation in tests of living planktonic foraninifera. Oceanol. Acta **2**: 195-208.

Keith, M. L. & Weber, J. N. 1965. Systematic relationships between carbon and oxygen isotopes in carbonates deposited by modern corals and algae. Science **150**: 498-501.

Kennett, J. P. 1977. Cenozoic evolution of Antarctic glaciation, the circum-Antarctic ocean, and their impact on global palaeoceanography. J. Geophys. Res. **82**: 3843-59.

Krantz, D. E., Williams, D. F. & Jones, D. S. 1987. Ecological and palaeoenvironmental information using stable isotope profiles from living and fossil molluscs. Palaeogeography, Palaeoclimatology, Palaeoecology **58**: 249-266.

Krumbein, W. C. & Pettijohn, F. J. 1961. Manual of Sedimentary Petrography. New York, Appleton-Century-Crofts.

Land, L. S., Lang, J. C. & Barnes, D. J. 1985. Extension rate: A primary control on the isotopic composition of West Indian (Jamaican) scleractinian reef coral skeletons. Mar. Biol. **33**: 221-233.

Landman, N. H., Rye, D. M. & Shelton, K. L. 1983. Early ontogeny of *Eutrephoceras* compared to recent *Nautilus* and Mesozoic ammonites: evidence from shell morphology and light stable isotopes. Palaeobiology **9**: 269-279.

Le Treut, H. & Ghil, M. 1983. Orbital forcing, climatic interactions, and glaciation cycles. J. Geophys. Res. **88**: 5167-5190.

Lowenstam, H. A. & Weiner, S. 1989. On Biomineralization. New York, Oxford University Press.

McConnaughey, T. 1989. 13C and 18O isotopic disequilibrium in biological carbonates: 1. Patterns. Geochimica et Cosmochimica Acta **53**: 151-162.

McCrea, J. M. 1950. On the isotope chemistry of carbonates and a palaeotemperature scale. The Journal of Chemical Physics **18**(6): 849-857.

Miller, G. H. & Hare, P. E. 1980. Amino acid geochronology: Integrity of the carbonate matrix and potential of molluscan fossils. in Biogeochemistry of Amino Acids. (ed. P. E. Hare, T. C. Hoering & K. King). New York, John Wiley and Sons.

Mitchell, L., Fallick, A. E. & Curry, G. B. 1994. Stable carbon and oxygen isotope compositions of mollusc shells from Britain and New Zealand. Palaeogeography, Palaeoclimatology, Palaeoecology **111**: 207-216.

Muhs, D. R. & Kyser, T. K. 1987. Stable isotope compositions of fossil mollusks from southern California: Evidence for a cool last interglacial ocean. Geology **15**: 119-122.

Ostrom, P. H., Zonneveld, J.-P. & Robbins, L. L. 1994. Organic geochemistry of hard parts: Assessment of isotopic variability and indigeneity. Palaeogeography, Palaeoclimatology, Palaeoecology **107**, in press.

Pillans, B. 1983. Upper Quaternary marine terrace chronology and deformation, South Taranaki, New Zealand. Geology **11**: 292-297.

Pillans, B. 1990. Pleistocene marine terraces in New Zealand: a review. New Zealand Journal of Geology and Geophysics **33**: 219-231.

Pillans, B. 1990. Vertical displacement rates on Quaternary faults, Wanganui Basin. New Zealand Journal of Geology and Geophysics **33**: 271-275.

Pillans, B. & Kohn, B. P. 1981. Rangitawa Pumice: a widespread (?) Quaternary marker-bed in Taranaki-Wanganui. Publ. Geol. Dep., Vic. Univ. Wellington 20: 94-104.

Pisias, N. G. & Moore, T. C. 1981. The evolution of Pleistocene climate: A time series approach. Earth and Planet. Sci. Lett. **52**: 450-458.

Powell, A. W. B. 1931. Waitotaran faunules of the Wanganui System: and descriptions of new species of Mollusca from the New Zealand Pliocene. Records of the Auckland Institute and Museum 1: 85-112.

Powell, A. W. B. 1979. New Zealand Mollusca. Marine, Land and Freshwater Shells. Auckland, Collins.

Prell, W. L. 1983. Oxygen and carbon isotope stratigraphy for the Quaternary of hole 502B: Evidence for two modes of isotopic variability. in Init. Repts. DSDP 68. (ed. W. L. Prell & J. V. Gardner). Washington, U.S. Govt. Printing Office.

Risk, M. J. (1991). Organic matrix of bivalve shells; environmental and evolutionary data from stable isotopes and NMR. Geological Society of America, North-central section; 25th annual meeting, Toledo, OH, United States,

Rollins, H. B., Sandweiss, D. H., Brand, U. & Rollins, J. C. 1987. Growth increment and stable isotope analysis of marine bivalves: implications for the geoarchaeological record of El Nino. Geoarchaeology **2**: 181-197.

Romanek, C. S. & Grossman, E. L. 1989. Stable isotope profiles of *Tridacna maxima* as environmental indicators. Palaios **4**: 402-413.

Ruddiman, W. F., Raymo, M. & McIntyre, A. 1986. Matuyama 41,000-year cycles: North Atlantic Ocean and northern hemisphere ice sheets. Earth and Planet. Sci. Lett. **80**: 117-129.

Schifano, G. & Censi, P. 1983. Oxygen isotope composition and rate of growth of *Patella coerulea, Monodonta turbinata* and *M. articulata* shells from the western coast of Sicily. Palaeogeography, Palaeoclimatology, Palaeoecology **42**: 305-311.

Schroeder, R. A. & Bada, J. L. 1976. A review of the geochemical applications of the amino acid racemization reaction. Earth Sci. Rev. **12**: 347-391.

Seward, D. 1974. Age of New Zealand Pleistocene substages by fission-track dating of glass shards from tephra horizons. Earth Planet. Sci. Lett. **24**: 242-248.

Seward, D. 1976. Tephrostratigraphy of the Marine Sediments in the Wanganui Basin, New Zealand. New Zealand Journal of Geology and Geophysics **19**(1): 9-20.

Shackleton, N. J. 1968. Depth of pelagic foraminifera and isotopic changes in Pleistocene oceans. Nature **218**: 79-80.

Shackleton, N. J., Backman, J. & Zimmerman, H. 1984. Oxygen isotope calibration of the onset of ice-rafting and history of glaciation in the North Atlantic region. Nature **307**: 620.

Shackleton, N. J., Berger, A. & Peltier, W. R. 1990. An alternative astronomical calibration of the lower Pleistocene timescale based on ODP site 677. Trans. Roy. Soc. Edinburgh: Earth Sciences **81**: 251-261.

Shackleton, N. J. & Opdyke, N. D. 1977. Oxygen isotope and palaeomagnetic evidence for early Northern Hemisphere glaciation. Nature **270**: 216.

Simkiss, K. & Wilbur, K. M. 1989. Biomineralization. Academic Press, San Diego, California.

Sneath, P. H. A. & Sokal, R. R. 1973. Numerical Taxonomy. San Francisco, W.H. Freeman and Company.

Stevens, K. F. & Vella, P. 1981. Palaeoclimatic interpretation of stable isotope ratios in molluscan fossils from middle Pleistocene marine strata, Wanganui, New Zealand. Palaeogeography, Palaeoclimatology, Palaeoecology **34**: 257-265.

Swart, P. K. 1983. Carbon and oxygen isotope fractionation in scleractinian corals: a review. Earth Sci. Rev. **19**: 51-80.

Taylor, D. L. & Ward, P. D. 1983. Stable isotope studies of *Nautilus macromphalus sowerby* (New Caledonia) and *Nautilus pompilius* L. (Fiji). Palaeogeography, Palaeoclimatology, Palaeoecology **41**: 1-16.

Thierstein, H. R., Geitzenauer, K. R., Molfino, B. & Shackleton, N. J. 1977. Global synchroneity of late Quaternary coccolith datum levels: validation by oxygen isotopes. Geology 5: 400-404.

Towe, K. M. 1980. Preserved organic ultrastructure: an unreliable indicator for Palaeozoic amino acid biogeochemistry. in Biogeochemistry of the amino acids. (ed. P. E. Hare, T. C. Hoering & K. J. King). New York, John Wiley and Sons. 65-74.

Turner, G. M. & Kamp, P. J. J. 1990. Palaeomagnetic location of the Jaramillo Subchron and Brunhes-Matuyama transition in the Castlecliffian Stratotype section, Wanganui Basin, New Zealand. Earth Planet. Sci. Lett. **100**: 42-50.

Turner, J. V. 1982. Kinetic fractionation of carbon-13 during calcium carbonate precipitation. Geochim. et Cosmochim. Acta **46**: 1183-1191.

Urey, H. C. 1947. The thermodynamic properties of isotopic substances. J. Chem. Soc. **1947**: 562-581.

Vallentyne, J. R. 1964. Biogeochemistry of organic matter II: Thermal reaction kinetics and transformation products of amino compounds. Geochim. Cosmochim. Acta **28**: 157-188.

Vallentyne, J. R. 1968. Pyrolysis of proline, leucine, arginine and lysine in aqueous solution. Geochim. Cosmochim. Acta **32**: 1353-1356.

van Kleef, F. S. M., de Jong, W. W. & Hoenders, H. J. 1975. Stepwise degradations and deamidation of the eye lens protein a-crystallin in ageing. Nature **258**: 264-266.

Vergnaud Grazzini, C. 1976. Non-equilibrium isotopic compositions of shells of planktonic foraminifera in the Mediterranean Sea. Palaeogeography, Palaeoclimatology, Palaeoecology **20**: 263-276.

Vinot-Bertouille, A.-C. & Duplessy, J. C. 1973. Individual isotopic fractionation of carbon and oxygen in benthic foraminifera. Earth Planet. Sci. Lett. **18**: 247-252.

Wachter, E. A. & Hayes, J. M. 1985. Exchange of oxygen isotopes in carbon dioxide-phosphoric acid systems. Chemical Geology (Isotope Geoscience Section) **52**: 365-374.

Walton, D. & Curry, G. B. 1991. Amino acids from fossils, facies and fingers. Palaeontology **34**(4): 851-858.

Walton, D. I. 1992. Biogeochemistry of brachiopod intracrystalline proteins and amino acids. PhD Thesis, Glasgow University.

Weber, J. N. & Raup, D. M. 1966. Fractionation of the stable isotopes of carbon and oxygen in marine calcareous organisms- the Echinoida: 1. Variation of C-13 and O-18 within individuals. Geochim. Cosmochim. Acta **30**: 681-703.

Wefer, G. 1985. Die Verteilung stabiler isotope in kalkschalen mariner organismen. Geologisches Jahrbuch **Reihe A 82**: 3-111.

Weil, S. M., Buddemeier, R. W., Smith, S. V. & Kroopnick, P. M. 1981. The stable isotope composition of coral skeletons: Control by environmental variables. Geochim. Cosmochim. Acta **45**: 1147-1153.

Weiner, S. & Lowenstam, H. A. 1980. Well preserved mollusk shells: characterization of mild diagenetic processes. In Biogeochemistry of the Amino Acids. (ed. P. E. Hare, T. C. Hoering & K. King). New York, John Wiley and Sons. 95-114.

Williams, D. F., Moore, W. S. & Fillon, R. H. 1981. Role of glacial Arctic Ocean ice sheets in Pleistocene oxygen isotope and sea level records. Earth. Planet. Sci. Lett. **56**: 157-166.